CARBON DYNAMICS IN TEMPERATE FORESTS

CLIMATIC CONTROLS ON PHENOLOGY AND CARBON DYNAMICS IN TEMPERATE DECIDUOUS AND CONIFEROUS FORESTS

By

ERIC R. BEAMESDERFER

A Thesis

Submitted to the School of Graduate Studies

In Partial Fulfillment of the Requirements

For the Degree

Doctor of Philosophy

McMaster University

DOCTOR OF PHILOSOPHY (2019)
(Biogeosciences)

McMaster University
School of Geography
and Earth Sciences
Hamilton, Ontario, Canada

TITLE: Climatic controls on phenology and carbon dynamics in temperate deciduous and coniferous forests

AUTHOR: Eric R. Beamesderfer

SUPERVISOR: Professor M. Altaf Arain

NUMBER OF PAGES: xix, 247

ABSTRACT

Forests ecosystems cover about 30% of the Earth's land surface, corresponding to an area of roughly 42 million km^2 globally. Forests play an important role in the global carbon cycle by exchanging carbon dioxide (CO_2) with the atmosphere. Annually, forests act to effectively sequester large amounts of anthropogenically-emitted CO_2 from the atmosphere through photosynthetic processes. Through the unparalleled increase of CO_2 emissions over the past century and the subsequent climatic inconsistencies due to global climate change, the carbon sink-capacity of the world's forests remains uncertain. Furthermore, since increasing temperatures have been shown to extend the vegetative growing season in forests, phenological responses to this change are of particular interest. In an effort to effectively assess the future carbon sequestration potential of forests, a better understanding of the climatic controls on phenology, and its influence on carbon processes, is needed.

The eddy covariance (EC) technique is a stand-level, in-situ, method used widely to assess the net CO_2 exchange across the canopy-atmosphere interface. Together with meteorological data, the sequestration of CO_2 and the subsequent ecosystem productivity can be quantified over various time scales (half-hours to decades). This dissertation reports results from field observations of EC measured fluxes that were used to study the climatic impacts on forest phenology and the resulting carbon dynamics in southern Ontario, Canada. The study sites, part of the Turkey Point Observatory, consisted of two similarly-aged, temperate, North American forests growing under similar climatic and edaphic conditions: the 80-year old (in 2019) white pine plantation (coniferous evergreen) and 90+ year-old, naturally-regenerated, white oak (deciduous broadleaf) forest. These forests were studied from 2012 to 2017, using the EC technique, digital phenological cameras, and remote-sensing measurements.

At the deciduous broadleaf forest, mid-summer (July and August) meteorological conditions were the key period in determining the annual carbon sink-strength of the site, acting to regulate the interannual variability in carbon uptake. The forest experienced higher net ecosystem productivity (+NEP; carbon sink) when soil temperatures ranged from 15 to 20°C and vapor pressure deficit was 0.7 and 1.2 kPa. From 2012 to 2016, the forest remained a net annual sink, with mean NEP of 206 ± 92 g C m^{-2} yr^{-1}, similar to that of other North American deciduous forests.

Spring and autumn phenological transition dates were calculated for each year (2012 to 2017) from measured EC data and digital camera greenness indices. The timing of spring and autumn transition dates were impacted by seasonal changes in air temperature and other meteorological variables. Contrary to past studies, an earlier growing season start did not equate to increased annual carbon uptake. In autumn, a later end to the deciduous forest growing season negatively impacted the net carbon uptake of the forest, as ecosystem respiration (RE) outweighed the

gains of photosynthesis. The digital camera indices failed to capture the peak dates of photosynthesis, but accurately measured the spring and autumn transition dates, which may be useful in future remote sensing applications.

A comparison of the two forests from 2012 to 2017 found the coniferous forest to have higher but more variable annual NEP (218 ± 109 g C m^{-2} yr^{-1}) compared to that of the deciduous broadleaf forest (200 ± 83 g C m^{-2} yr^{-1}). Similarly, the mean annual evapotranspiration (ET) was higher (442 ± 33 mm yr^{-1}) at the coniferous forest compared to that of the broadleaf forest (388 ± 34 mm yr^{-1}). The greatest difference between years resulted from the response to heat and drought. During drought years, deciduous carbon and water fluxes were less sensitive to changes in temperature or water availability compared to the evergreen forest.

Carotenoid sensitive vegetative indices and the red-edge chlorophyll index were shown to effectively capture seasonal changes in photosynthesis phenology within both forests via proximal remote sensing measurements during the 2016 growing season. Satellite vegetative indices were highly correlated to EC photosynthesis, but significant interannual variability resulted from either meteorological inputs or the heterogeneous landscapes of the agriculturally-dominated study area.

This dissertation improved our understanding of the dynamics of carbon exchange within the northeastern North American deciduous forest ecozone, through the examination of climatic variability and its impact on carbon and phenology. This dissertation also contributed to efforts being made to better evaluate the impact of species composition on carbon dynamics in geographically similar forests. Moreover, the use of the digital phenological camera observations and remote sensing techniques to complement and better understand the fluxes observed with the EC method was innovative and may help other researchers in future studies.

ACKNOWLEDGEMENTS

I would like to thank my supervisor, Dr. Altaf Arain, for providing me with the opportunity and funding to pursue my PhD within his research group at McMaster University. I am grateful for his guidance, patience, and encouragement through the years, and I appreciate his advice and support in preparing me for my future.

I would also like to thank all the members of my PhD committees throughout my time at McMaster: Dr. Sean Carey, Dr. Mike Waddington, Dr. Howard Barker, and Dr. Jim Smith for their time, encouragement, and guidance. Advice from Dr. Alemu Gonsamo in regards to phenological studies is also acknowledged.

I would like to thank Dr. Nicholas Coops, Dr. Riccardo Tortini, and Shangrong Lin from the University of British Columbia Integrated Remote Sensing Studio for their assistance in AMSPEC-III deployment, data processing, and intellectual support. A special thank you to Zoran Nesic at the University of British Columbia for his countless hours of troubleshooting and technical support over the years.

Thank you to everyone from the McMaster Hydrometeorology and Climatology Research Group at McMaster University (Jung, Katey, Olivier, Stefan, Rizwan, Tariq, Nur, David, Dilanka, Bing, Shawn and Rob) for a memorable time over the years. Specifically, I would like to thank Felix Chan, Brandon Burns and Alanna Bodo for the valuable support in field work and data collection at Turkey Point. A special thanks to both Jay Brodeur and Myroslava Khomik for their assistance in data analysis and for their valuable guidance. Thank you to GWF technicians Keegan Smith and Ian Martin for their endless hours of assistance in maintaining the research sites and general technical support.

Thanks to Steve Williams from the Ontario Ministry of Natural Resources for his assistance, maintenance, and cooperation with studies conducted at Turkey Point.

A special thanks to all past and present School of Geography and Earth Sciences (SGES) graduate students who I have met and spent time with during my time at McMaster. Thank you to all SGES staff and faculty for their help and support.

A heartfelt thank you to my closest friends and family for their encouragement over the years and for helping me believe this was all possible. To my parents, thank you sending me to weather camp in middle school and for all your love.

Last, but certainly not least, an exceptionally special thank you to my loving wife Annalyssa. Thank you for believing in me, encouraging me, and supporting me through every step of the journey. I am forever grateful for your endless patience, love, and ability to make even the roughest days a little bit easier.

TABLE OF CONTENTS

LIST OF FIGURES

LIST OF TABLES

PREFACE

This dissertation consists of four individual manuscripts that have either been submitted or are ready for submission in peer-reviewed scientific journals. Results presented in this dissertation originated from research done within the Turkey Point Observatory. Naturally, there is some overlap in the information (i.e. description of study sites and methodology) and results presented in each chapter. However, each manuscript contains additional information specifically relevant to the respective study and the results of each chapter are distinct from one another. While all four of the main chapters present unique ideas and components of my PhD work, this thesis also represents a collaborative effort from a number of contributors. The specific contribution from the PhD candidate and the co-authors of the submitted manuscripts are described below.

Chapter 2

Title: How will the carbon fluxes within the northernmost temperate deciduous forests of North America fair under future climates?

Authorship: Eric R. Beamesderfer, M. Altaf Arain, Myroslava Khomik, Jason J. Brodeur

Status: Submitted to *Journal of Geophysical Research – Biogeosciences* in July 2019

Candidate's Contribution: Eric R. Beamesderfer (the PhD candidate) contributed to the collection and processing of flux and meteorological data, and to system and instrument maintenance at the deciduous forest (TPD) during the study period. The candidate had the lead role in data analysis, interpretations, and manuscript write up. Altaf Arain secured funding for the research, contributed to field work, and provided valuable editorial criticism during the writing of the manuscript. Myroslava Khomik provided extensive intellectual and editorial input throughout the writing process. Jason Brodeur contributed to the collection of meteorological and flux data as well as assistance in the processing of annual datasets.

Chapter 3

Title: The impact of spring and autumn seasons' timing and duration on the carbon uptake of a temperate deciduous forest in Eastern North America

Authorship: Eric R. Beamesderfer, M. Altaf Arain, Myroslava Khomik, Jason J. Brodeur, Alemu Gonsamo

Status: In review with *Agricultural and Forest Meteorology* since October 2019

Candidate's Contribution: Eric R. Beamesderfer (the PhD candidate) contributed to the collection and processing of flux and meteorological data, and to system and instrument maintenance at the deciduous forest (TPD) during the study period. The candidate had the lead role in data analysis, interpretations, and manuscript write up. Altaf Arain secured funding for the research, contributed to field work, and provided valuable editorial criticism during the writing of the manuscript. Myroslava Khomik provided extensive intellectual and editorial input throughout the writing process. Jason Brodeur contributed to the collection of meteorological and flux data, and aided in the processing and modeling of annual flux data. Alemu Gonsamo provided intellectual input and comments and assisted in the phenological modeling of flux data.

Chapter 4

Title: Response of carbon and water fluxes to environmental variability in two Eastern North American forests of similar-age but contrasting leaf-retention and shape strategies

Authorship: Eric R. Beamesderfer, M. Altaf Arain, Myroslava Khomik, Jason J. Brodeur, Brandon M. Burns

Status: Submitted to Biogeosciences (EGU) in November 2019

Candidate's Contribution: Eric R. Beamesderfer (the PhD candidate) contributed to the collection and processing of flux and meteorological data, and to system and instrument maintenance at both the deciduous (TPD) and coniferous (TP39) forests during the study period. The candidate had the lead role in data analysis, interpretations, and manuscript write up. Altaf Arain secured funding for the research, contributed to field work, and provided valuable editorial criticism during the writing of the manuscript. Myroslava Khomik provided extensive intellectual and editorial input throughout the writing process. Jason Brodeur contributed to the collection of meteorological and flux data, and aided in the processing and modeling of annual flux data. Brandon Burns assisted in data collection and instrument maintenance and provided editorial input on water fluxes.

Chapter 5

Title: Seasonal patterns of photosynthesis captured by remote sensing vegetation indices in a temperate coniferous evergreen and deciduous broadleaf forest

Authorship: Eric R. Beamesderfer, M. Altaf Arain, Nur Hussain, Shangrong Lin, Riccardo Tortini, Zoran Nesic, Nicholas Coops

Status: To be submitted to a peer-reviewed journal in December 2019 or January 2020

Candidate's Contribution: Eric R. Beamesderfer (the PhD candidate) contributed to the collection and processing of flux and meteorological data, and to system and instrument (EC and remote sensing) maintenance at both the deciduous (TPD) and coniferous (TP39) forests during the study period. The candidate had the lead role in data analysis, interpretations, and manuscript write up. Altaf Arain secured funding for the research, contributed to field work, and provided valuable editorial criticism during the writing of the manuscript. Nur Hussain obtained and corrected satellite data used in the analysis and provided assistance with GIS mapping. Dr. Nicholas Coops' group developed, installed, and operated the AMSPEC system to conduct canopy spectral measurements. Dr. Coops' group processed and analyzed the AMSPEC data, while the candidate helped in the operation of the AMSPEC system. The UBC members: Shangrong Lin, Riccardo Tortini, Zoran Nesic, and Nicholas Coops provided intellectual input and editorial comments on the manuscript.

CHAPTER 1:

INTRODUCTION

1.1 Changing Climate

Globally, surface temperatures have risen by 0.85°C over the past century, and are predicted to further increase by 2.0 to 4.5°C over the next century (IPCC, 2014). These increasing temperatures are correlated with increasing atmospheric greenhouse gas concentrations, such as carbon dioxide (CO_2), among others (Luthi et al., 2008; Solomon et al., 2009). Greenhouse gases and the global carbon cycle play an important role in Earth's climate, acting to trap long-wave radiation in the Earth's atmosphere, supporting further increases in global temperatures (Trenberth, 1996; Le Quere et al., 2018). The global mean atmospheric CO_2 concentration has increased from 280 parts per million (ppm) in 1750 to more than 405 ppm in 2017 (Joos and Spahni, 2008; Le Quere et al., 2018). Although, the global CO_2 cycle is coupled to natural climatological and biogeochemical processes (Falkowski et al., 2000), the current rapid and alarming increase in atmospheric CO_2 concentration is largely driven by human activities, such as the use of fossil fuels and changes in land use (IPCC, 2014). A portion of atmospheric CO_2 is subsequently stored in terrestrial biospheres and ocean reservoirs (Running and Coughlan, 1988). As a result, seasonal fluctuations in the variability of atmospheric CO_2 can be attributed to the seasonal cycling of CO_2 within terrestrial ecosystems, predominantly located in the northern hemisphere (Keeling et al.,

1996). Accordingly, greater interest has been focused on the role and controls of terrestrial ecosystems in the global carbon cycle, in order to further understand their impact in future climates (Dixon et al., 1994; Gough et al., 2008).

1.2 Terrestrial Ecosystems and Forests

Quantifying the role of terrestrial ecosystems in the global carbon cycle is increasingly difficult due to the complex biological processes underlying carbon storage and the heterogeneity of vegetation and soils (Schimel, 1995; Batin et al., 2009). Within the low- and mid-latitudes, terrestrial ecosystems store roughly 550 ± 100 Gt C, while the organic matter in soils is 2-3 times this amount (Houghton, 2007). Among terrestrial ecosystems, forests store a large amount of carbon and are a key component in the global carbon cycle. The world's forests cover ~42 million km^2, roughly 30% of the Earth's total land surface (Bonan, 2008). These forests store ~45% of terrestrial carbon, but they are estimated to contain ~80% of all aboveground carbon, and 40% of all belowground carbon (Wofsy et al., 1993; Dixon et al., 1994; Pan et al., 2013). Globally, the allocation of carbon between forests and soils differs by latitude, with the mid-latitudes of the northern hemisphere representing a significant sink of atmospheric CO_2 (Le Quere et al., 2018). Many mid-latitude forests in eastern North American were subject to large-scale deforestation near the start of the past century, releasing CO_2 to the atmosphere, and producing forest landscapes of different-aged natural and plantation forests (Niu & Duiker, 2006; Pan et al., 2011; Goetz et al., 2012). The

regrowth of forests and afforestation on former agricultural land in the US and Canada is responsible for a significant portion of the overall North American forest carbon sink (Dixon et al., 1994; Pacala et al., 2001). In recent years, the planting and management of forests has been proposed as a potential means to sequester atmospheric CO_2, in order to offset greenhouse gas emissions (IPCC, 2014; Watson and Noble, 2004). Such forests are increasingly important to the global carbon cycle, as many forests are relatively young, with the capability to accumulate carbon in future decades (Dixon et al., 1994; Barford et al., 2001). Therefore, continued research is needed into understanding the annual and seasonal carbon budgets of these forests, in order to accurately predict how they may respond to changes in climate and age.

1.3 Forest Carbon Exchange

The net carbon balance in forests consists of two major fluxes: CO_2 sequestered (sink) through photosynthesis and CO_2 emitted (source) from the forest through respiration processes. The assimilation of CO_2 by forests, in the form of gross primary or ecosystem productivity (GPP or GEP, respectively, where GEP is less autotrophic respiration), is the largest global terrestrial carbon flux, while the concurrent release of CO_2 to the atmosphere due to ecosystem respiration (RE) of live vegetation (autotrophic) and decomposition of organic matter (heterotrophic), accounts for a lesser global terrestrial CO_2 flux (Waring et al., 1998; Gower, 2003; Beer et al., 2010). A small portion of the net balance between these two

fluxes regulates the net gain or loss of CO_2, defined as net ecosystem productivity (NEP) (Chapin, 2006; Cole et al., 2007). However, the quantification of NEP in forests is challenging due to the underlying processes and feedbacks associated with climate, water, and nutrient cycling within forests (Fan et al., 1998; Band et al., 2001). Recent studies indicate major challenges for forest ecosystems due to human activity and natural causes such as: fires, droughts, heatwaves, insect infestation, deforestation, and land use changes (Attiwill et al., 1994; Amiro et al., 2010; Allen et al., 2010). Disturbance events may alter forest growth and the carbon sink strength, altering annual forest productivity (Cao and Woodward, 1998; Saxe et al., 2001; Hyvonen et al., 2007). Furthermore, periodic heat and drought events have the potential to reduce NEP in forest ecosystems (Ciais et al., 2005; Piao et al., 2008). While annually, the NEP of mature temperate forests typically ranges from 100-700 g C m^{-2}, uncertainty remains on how these forests will response to future climates (Law et al., 2002; Bonan, 2008). Consequently, there is a need to study the CO_2 cycling in forest ecosystems across the world in order to better understand how they will respond under future changes in climate.

1.4 Novel Aspects of Study

In Eastern North America, temperate deciduous forests are the dominant forest cover type, and at their peak coverage they occupied upwards of 2.5 million km^2 (Botkin et al., 1993; Barbour & Billings, 2000). Home to a diverse range of tree species, these forests are characterized by four distinct seasons (winter, spring,

summer, and fall), and a growing season ranging between 150-200 days (Mooney et al., 1996). The Carolinian forests of Canada represent the northernmost edge of the temperate deciduous forests ranging from the Carolinas in the United States northward to southern Ontario (Lauriault, 1989; Blouin, 2001; Johnston, 2009). Carolinian forests are largely secondary growth forests dominated by a number of hardwood species at the northernmost extent of their natural ranges (Richart & Hewitt, 2008). The climate of southern Ontario is unique to Canada, experiencing some of the longest growing seasons and warmest temperatures, home to many tree and plant species found nowhere else in the country. Within the deciduous forests of this region, leaf area (Neumann et al., 1989), canopy water (Price et al., 2003), tree growth (Goldblum and Rigg, 2005), and stemflow (Carlyle-Moses and Price, 2006) studies have been completed among many others, though to date, no studies have examined stand-level forest-atmosphere carbon exchange, providing researchers with a climatologically and geographically unique study area, with the exception of a mixedwood forest (Borden) further north in the boreal-temperate transition zone (Froelich et al., 2015).

1.5 Study Sites

Measurements supporting this dissertation were conducted at the Turkey Point Observatory, centrally located near the town of St. Williams, in close proximity to the northern shore of Lake Erie, in southern Ontario, Canada. The Turkey Point Observatory was established in 2002 by the Hydrometeorology and Climatology

Lab at McMaster University (Arain & Restrepo-Coupe, 2005). The study sites consist of an age-sequence of afforested, eastern white pine (*Pinus Strobus* L.) forest stands (17-, 45-, 80-years-old in 2019) which grow within 20 km of each other, under similar edaphic and climatic conditions. A fourth site was added to the Turkey Point Observatory in 2012, a 70-110 year-old naturally regrown but managed eastern (Carolinian) deciduous forest, located 3 km south of the 17-year old pine forest. Throughout this text, the study sites may be referred to by their shortened names, TP02, TP74, TP39, and TPD, respectively. The acronyms correspond to 'Turkey Point', followed by the year of the stand's establishment (i.e. 2002, 1974, 1939), with TPD (Turkey Point Deciduous) as an exception. The Turkey Point Observation is part of the Global Water Futures (GWF) program and Fluxnet – a global network of sites studying the exchanges of carbon, water, and energy across various ecosystems. In the global Fluxnet data archives and literature, the Turkey Point Observatory sites are referred to as CA-TP1, CA-TP3, CA-TP4, and CA-TPD for the 17-, 45-, 80-year old pine forests, and 70-110 year-old deciduous forest, respectively. Detailed descriptions of site characteristics, instrumentation, and measurements are included in the individual chapters.

1.6 Overview of Methodology

The fundamental measurements found within this dissertation were completed through the implementation of the eddy-covariance (EC) technique, an in-situ approach used to examine ecosystem-atmosphere gas exchange. Past efforts have

addressed the net ecosystem exchange of carbon through the quantification of temporal changes in soil carbon and biomass (Clark et al., 2001). While such measurements continue today, in recent decades, the EC technique has proven to be an alternative and important method used to quantify carbon exchange on the ecosystem scale (Running et al., 1999; Baldocchi, 2003). The principle concept driving the EC technique is derived from boundary layer turbulence, as turbulent motions of air (eddies) effectively transport trace gases within the lowest levels of the atmosphere (Swinbank, 1951; Schlichting & Gersten, 2016). EC systems used at the Turkey Point forest sites consisted of an infra-red gas analyzer (IRGA) combined with a three-dimensional sonic anemometer, mounted above the ecosystem of interest. High frequency (typically 10-20 Hz) measurements of the turbulent exchange of CO_2 and H_2O were combined with the changes in CO_2 storage below sensor height in order to provide an ecosystem-scale estimate of net ecosystem productivity (NEP). From NEP, gross ecosystem productivity (GEP) and ecosystem respiration (RE) were derived on half-hourly to annual time scales through flux partitioning procedures (Reichstein et al., 2005). To reduce uncertainties, EC systems are best suited over flat terrain, when environment conditions are steady, and when vegetation extends upwind (Baldocchi, 2003). The Turkey Point Observatory forests are spatially extensive and reside on flat or slightly undulating terrain. Within each forest, scaffold towers extend above the forest canopy containing EC instrumentation, effectively recording the continuous exchange of gases between the forest and atmosphere. In addition to EC

measurements, continuous half-hourly measurements of soil and meteorological variables were also conducted at each site, including: air temperature, relative humidity, wind speed and direction, photosynthetically active radiation, net radiation, and precipitation, above the forest canopy, as well as soil moisture, soil temperature, and soil heat flux across different soil depths.

1.7 Study Objectives

This study investigated the influence of changes in phenology and environmental variability on seasonal and annual fluxes of CO_2 in a temperate deciduous and coniferous forest in southern Ontario, Canada. The primary study objectives were:

(1) To determine the climatic, environmental, and latitudinal controls on carbon fluxes in the northernmost extent of deciduous forests

(2) To examine the influence of climate on phenology and photosynthesis, and assess the role of phenology on future carbon sequestration

(3) To investigate the responses of two climatically similar forest of differing dominant tree species to climate and extreme weather events

(4) To compare remote-sensing and satellite derived vegetation indices to photosynthesis across the all Turkey Point Observatory sites

Results presented in this dissertation should be of interest to the eddy covariance research community and those involved in the study of forests in future climates.

1.8 References

Allen, C.D., Macalady, A.K., Chenchouni, H., Bachelet, D., McDowell, N., Vennetier, M., Kitzberger, T., Rigling, A., Breshears, D.D., Hogg, E.T. and Gonzalez, P., 2010. A global overview of drought and heat-induced tree mortality reveals emerging climate change risks for forests. *Forest Ecology and Management*, 259(4), 660-684.

Amiro, B.D., Barr, A.G., Barr, J.G., Black, T.A., Bracho, R., Brown, M., Chen, J., Clark, K.L., Davis, K.J., Desai, A.R. and Dore, S., 2010. Ecosystem carbon dioxide fluxes after disturbance in forests of North America. *Journal of Geophysical Research: Biogeosciences*, 115(G4).

Arain, M.A. and Restrepo-Coupe, N., 2005. Net ecosystem production in a temperate pine plantation in southeastern Canada. *Agricultural and Forest Meteorology*, 128(3-4), 223-241.

Attiwill, P.M., 1994. The disturbance of forest ecosystems: the ecological basis for conservative management. *For. Ecol. Manag*., 63(2-3), 247-300.

Baldocchi, D.D., 2003. Assessing the eddy covariance technique for evaluating carbon dioxide exchange rates of ecosystems: past, present and future. *Global Change Biology*, 9(4), 479-492.

Band, L.E., Tague, C.L., Groffman, P. and Belt, K., 2001. Forest ecosystem processes at the watershed scale: hydrological and ecological controls of nitrogen export. *Hydrol. Proc*., 15: 2013–2028.

Barbour, M.G. & Billings, W.D. eds., 2000. North American terrestrial vegetation. Cambridge University Press.

Barford, C.C., Wofsy, S.C., Goulden, M.L., Munger, J.W., Pyle, E.H., Urbanski, S.P., Hutyra, L., Saleska, S.R., Fitzjarrald, D. and Moore, K., 2001. Factors controlling long-and short-term sequestration of atmospheric CO2 in a mid-latitude forest. *Science*, 294(5547), 1688-1691.

Battin, T.J., Luyssaert, S., Kaplan, L.A., Aufdenkampe, A.K., Richter, A. and Tranvik, L.J., 2009. The boundless carbon cycle. *Nat. Geosci*., 2(9), 598.

Beer, C., Reichstein, M., Tomelleri, E., Ciais, P., Jung, M., Carvalhais, N., Rödenbeck, C., Arain, M.A., Baldocchi, D., Bonan, G.B. and Bondeau, A., 2010. Terrestrial gross carbon dioxide uptake: global distribution and covariation with climate. *Science*, 329(5993), 834-838.

Blouin, G., 2001. An eclectic guide to trees east of the Rockies. Boston Mills Press. Erin, ON.

Bonan, G.B., 2008. Forests and climate change: forcings, feedbacks, and the climate benefits of forests. *Science*, 320(5882), 1444-1449.

Botkin, D.B., 1993. Forest dynamics: an ecological model. Oxford University Press on Demand.

Cao, M. and Woodward, F.I., 1998. Dynamic responses of terrestrial ecosystem carbon cycling to global climate change. *Nature*, *393*(6682), 249.

Carlyle-Moses, D.E. & Price, A.G., 2006. Growing-season stemflow production within a deciduous forest of southern Ontario. *Hydrologic Processes*, 20(17) 3651–3663.

Chapin, F.S., Woodwell, G.M., Randerson, J.T., Rastetter, E.B., Lovett, G.M., Baldocchi, D.D., Clark, D.A., Harmon, M.E., Schimel, D.S., Valentini, R. and Wirth, C., 2006. Reconciling carbon-cycle concepts, terminology, and methods. *Ecosystems*, 9(7), 1041-1050.

Ciais, P., Reichstein, M., Viovy, N., Granier, A., Ogée, J., Allard, V., Aubinet, M., Buchmann, N., Bernhofer, C., Carrara, A. and Chevallier, F., 2005. Europe-wide reduction in primary productivity caused by the heat and drought in 2003. *Nature*, 437(7058), 529.

Clark, D.A., Brown, S., Kicklighter, D.W., Chambers, J.Q., Thomlinson, J.R. and Ni, J., 2001. Measuring net primary production in forests: concepts and field methods. *Ecological Applications*, 11(2), 356-370.

Cole, J.J., Prairie, Y.T., Caraco, N.F., McDowell, W.H., Tranvik, L.J., Striegl, R.G., Duarte, C.M., Kortelainen, P., Downing, J.A., Middelburg, J.J. and Melack, J., 2007. Plumbing the global carbon cycle: integrating inland waters into the terrestrial carbon budget. *Ecosystems*, 10(1), 172-185.

Dixon, R.K., Solomon, A.M., Brown, S., Houghton, R.A., Trexier, M.C. and Wisniewski, J., 1994. Carbon pools and flux of global forest ecosystems. *Science*, 263(5144), 185-190.

Falkowski, P., Scholes, R.J., Boyle, E.E.A., Canadell, J., Canfield, D., Elser, J., Gruber, N., Hibbard, K., Högberg, P., Linder, S. and Mackenzie, F.T., 2000.The global carbon cycle: a test of our knowledge of earth as a system. *Science*, 290(5490), 291-296.

Fan, S., Gloor, M., Mahlman, J., Pacala, S., Sarmiento, J., Takahashi, T., and Tans, P., 1998. A Large Terrestrial Carbon Sink in North America Implied by Atmospheric and Oceanic Carbon Dioxide Data and Models. *Science*, 282: 442-446.

Froelich, N., Croft, H., Chen, J.M., Gonsamo, A. and Staebler, R.M., 2015. Trends of carbon fluxes and climate over a mixed temperate–boreal transition forest in southern Ontario, Canada. *Agricultural and Forest Meteorology*, 211, 72-84.

Goetz, S.J., Bond-Lamberty, B., Law, B.E., Hicke, J.A., Huang, C., Houghton, R.A., McNulty, S., O'Halloran, T., Harmon, M., Meddens, A.J.H. and Pfeifer, E.M., 2012. Observations and assessment of forest carbon dynamics following disturbance in North America. *Journal of Geophysical Research: Biogeosciences*, 117(G2).

Goldblum, D., & Rigg, L.S., 2005. Tree growth response to climate change at the deciduous-boreal forest ecotone, Ontario, Canada. *Canadian Journal of Forest Research*, 35:2709-2718.

Gough, C.M., Vogel, C.S., Schmid, H.P. & Curtis, P.S., 2008. Controls on annual forest carbon storage: lessons from the past and predictions for the future. *Bioscience*, *58*(7), 609-622.

Gower, S.T., 2003. Patterns and mechanisms of the forest carbon cycle. *Annual Review of Environment and Resources*, 28(1), 169-204.

Houghton, R.A., 2007. Balancing the global carbon budget. *Annual Review of Earth and Planetary Sciences*, 35, 313-347.

Hyvonen, R., Agren, G.I., Linder, S., Persson, T., Cotrufo, M.F., Ekblad, A., et al., 2007. The likely impact of elevated CO_2, nitrogen deposition, increased temperature and management on carbon sequestration in temperate and boreal forest ecosystems: a literature review. *New Phytologist*, 173: 463-480.

IPCC, 2014: Climate Change 2014: Synthesis Report. Contribution of Working Groups I, II & III to the Fifth Assessment Report of the Intergovernmental Panel on Climate Change [Core Writing Team, R.K. Pachauri and L.A. Meyer (eds.)]. *IPCC*, Geneva, Switzerland, 151.

Johnston, M., 2009. Vulnerability of Canada's tree species to climate change and management options for adaptation: An overview for policy makers and practitioners. Canadian Council of Forest Ministers.

Joos, F. & Spahni, R., 2008. Rates of change in natural and anthropogenic radiative forcing over the past 20,000 years. *Proceedings of the National Academy of Sciences*, *105*(5), 1425-1430.

Lauriault, J., 1989. Identification guide to the trees of Canada. National Museum of Natural Sciences. Fitzhenry & Whiteside. Markham, Ontario.

Law, B.E., Falge, E., Gu, L.V., Baldocchi, D.D., Bakwin, P., Berbigier, P., Davis, K., Dolman, A.J., Falk, M., Fuentes, J.D. and Goldstein, A., 2002. Environmental controls over carbon dioxide and water vapor exchange of terrestrial vegetation. *Agric. For. Meteorol*., 113(1-4), 97-120.

Le Quéré, C., Andrew, R.M., Friedlingstein, P., Sitch, S., Hauck, J., Pongratz, J., Pickers, P.A., Korsbakken, J.I., Peters, G.P., Canadell, J.G. and Arneth, A., 2018. Global carbon budget 2018. *Earth System Science Data*, 10(4).

Lüthi, D., Le Floch, M., Bereiter, B., Blunier, T., Barnola, J.M., Siegenthaler, U., Raynaud, D., Jouzel, J., Fischer, H., Kawamura, K. and Stocker, T.F., 2008. High-resolution carbon dioxide concentration record 650,000–800,000 years before present. *Nature*, 453(7193), 379.

Mooney, H.A., Cushman, J.H., Medina, E., Sala, O.E., and Schulze, E.-D. (Eds). 1996. Functional Roles of Biodiversity—A Global Perspective. Wiley, Chichester, UK.

Neumann, H.H., Hartog, G.D., and Shaw, R.H., 1989. Leaf area measurements based on hemispheric photographs and leaf-litter collection in a deciduous forest during autumn leaf-fall, *Agric. For. Meteorol*., 45(3–4), 325-345.

Niu, X. & Duiker, S.W., 2006. Carbon sequestration potential by afforestation of marginal agricultural land in the Midwestern US. *Forest Ecology and Management*, 223(1-3), 415-427.

Pacala, S.W., Hurtt, G.C., Baker, D., Peylin, P., Houghton, R.A., Birdsey, R.A., Heath, L., Sundquist, E.T., Stallard, R.F., Ciais, P. and Moorcroft, P., 2001. Consistent land-and atmosphere-based US carbon sink estimates. *Science*, 292(5525), 2316-2320.

Pan, Y., Chen, J.M., Birdsey, R., McCullough, K., He, L. and Deng, F., 2011. Age structure and disturbance legacy of North American forests. *Biogeosciences*. 8: 715-732., 8, 715-732.

Pan, Y., Birdsey, R.A., Phillips, O.L. and Jackson, R.B., 2013. The structure, distribution, and biomass of the world's forests. *Annual Review of Ecology, Evolution, and Systematics*, *44*, 593-622.

Piao, S., Ciais, P., Friedlingstein, P., Peylin, P., Reichstein, M., Luyssaert, S., Margolis, H., Fang, J., Barr, A., Chen, A. and Grelle, A., 2008. Net carbon dioxide losses of northern ecosystems in response to autumn warming. *Nature*, 451(7174), 49.

Price, A.G., & Carlyle-Moses, D.E., 2003. Measurement and modelling of growing-season canopy water fluxes in a mature mixed deciduous forest stand, southern Ontario, Canada. *Agric. For. Meteorol*., 119, 69-85.

Reichstein, M., Falge, E., Baldocchi, D., Papale, D., Aubinet, M., Berbigier, P., Bernhofer, C., Buchmann, N., Gilmanov, T., Granier, A. and Grünwald, T., 2005. On the separation of net ecosystem exchange into assimilation and ecosystem respiration: review and improved algorithm. Global *Change Biology*, 11(9), 1424-1439.

Richart, M., & Hewitt, N., 2008. Forest remnants in the Long Point region, Southern Ontario: Tree Species diversity and size structure. *Landscape and Urban Planning*, 86, 25-37.

Running, S.W. & Coughlan, J.C., 1988. A general model of forest ecosystem processes for regional applications I. Hydrologic balance, canopy gas exchange and primary production processes. *Ecol. Model.*, *42*(2), 125-154.

Running, S.W., Baldocchi, D.D., Turner, D.P., Gower, S.T., Bakwin, P.S. and Hibbard, K.A., 1999. A global terrestrial monitoring network integrating tower fluxes, flask sampling, ecosystem modeling and EOS satellite data. *Remote Sensing of Environment*, 70(1), 108-127.

Saxe, H., Cannell, M.G., Johnsen, Ø., Ryan, M.G. and Vourlitis, G., 2001. Tree and forest functioning in response to global warming. *New Phytologist*, 149(3), 369-399.

Schimel, D.S., 1995. Terrestrial ecosystems and the carbon cycle. *Global Change Biology*, *1*(1), 77-91.

Schlichting, H. & Gersten, K., 2016. Boundary-layer theory. Springer.

Solomon, S., Plattner, G.K., Knutti, R. and Friedlingstein, P., 2009. Irreversible climate change due to carbon dioxide emissions. *Proceedings of the National Academy of Sciences*, 106(6), 1704-1709.

Swinbank, W.C., 1951. The measurement of vertical transfer of heat and water vapor by eddies in the lower atmosphere. *Journal of Meteo*., 8(3):135-145.

Trenberth, K.E. and Hoar, T.J., 1996. The 1990–1995 El Niño-southern oscillation event: longest on record. *Geophys. Res. Lett*., 23(1), 57-60.

Waring, R.H., Landsberg, J.J. and Williams, M., 1998. Net primary production of forests: a constant fraction of gross primary production?. *Tree Physiology*, 18(2), 129-134.

Watson, R.T. & Noble, I.R., 2004. The global imperative and policy for carbon sequestration: the carbon balance of forest biomes. London: Garland Science/BIOS Scientific Publishers.

Wofsy, S.C., Goulden, M.L., Munger, J.W., Fan, S.M., Bakwin, P.S., Daube, B.C., Bassow, S.L. and Bazzaz, F.A., 1993. Net exchange of CO2 in a mid-latitude forest. *Science*, 260(5112), 1314-1317.

CHAPTER 2:

HOW WILL THE CARBON FLUXES WITHIN THE NORTHERNMOST TEMPERATE DECIDUOUS FORESTS OF NORTH AMERICA FAIR UNDER FUTURE CLIMATES?

2.1 Abstract

In the northern deciduous forests of Eastern North America, many tree species grow at the northernmost extent of their typical geographical ranges, where slight changes in environmental conditions could aid or impede their survival and advance further north. There is still uncertainty in how potential changes in environmental conditions, due to climate change, will impact the growth of these forests. One way to assess the growth of forests is to measure their ability to uptake carbon (C) from the atmosphere – a key building element of wood. The main goal of this study was to analyze the impact of seasonal and annual climate variations on the C sink capacity of a deciduous forest within the Great Lakes Region in Canada. We found that mid-summer (late July to early August) was the key period in determining the annual carbon sink-strength of the site, with meteorology and soil water status driving interannual variability in C uptake. Furthermore, the timing and duration of environmental impacts were important and greatly shaped the overall C dynamics of this forest over the study period (2012 – 2016). During summer, high evaporative demand, when air temperature (Ta) was > 20°C and vapour pressure deficit (VPD) > 1 kPa, caused seasonal soil

water deficits, which negatively impacted the forest C-sink capacity. The forest was most productive when soil temperature (Ts) ranged from 15 to 20°C and VPD was between 0.7 and 1.2 kPa. With increasing VPD past this point, the net C-uptake of the forest dropped considerably. While other studies have found that a positive spring Ta anomaly increases annual C-uptake, our study suggests that it is the mid-summer environmental conditions which determine the annual C-uptake in this forest. During the five years of this study, in all years, even during water-stressed conditions, the forest remained a net annual carbon sink, with mean net ecosystem productivity (NEP) of 206 ± 92 g C m-2 yr-1 that was well within the range observed in similar forest (69 – 459 g C m-2 yr-1) over the same period. Our study suggests that with increasing Ta and precipitation (P) variability under future climate conditions, frequent soil water deficits and heat-stressed periods may be observed in the Great Lakes Region that may impact the growth and carbon sequestration capabilities of local forests.

2.2 Introduction

Temperate forests occupy nearly 25% of the global forested land cover (~10.4 million km^2), primarily in Eastern North America, Europe, and Eastern Asia (Tyrrell et al., 2012; Settele et al., 2014). They store roughly 99 to 159 Pg of carbon (~11% of the global carbon stock) and account for up to 37% of the global forest carbon sink (Pan et al., 2011). Most of the temperate forests are deciduous stands, covering 7.8 million km^2 of the 10.4 million km^2 globally (i.e. 75%)

(Allaby, 2006; Vasseur, 2012). In Eastern North America, temperate deciduous forests are the dominant forest cover type and at their past peak-coverage they occupied upwards of 2.5 million km^2 (Botkin et al., 1993; Delcourt, 2000). These forests have been severely impacted by human activities over the last 100 years (Johnston, 2009; Gao et al., 2012). Widespread agricultural deforestation occurred during the early 1900's in the northeast, causing a drastic reduction in forest cover from 90% to 11% (Richart & Hewitt, 2008). Later in the mid-1900's, abandonment of agricultural land and forest regrowth initiatives led by the local government resulted in an increase of forested area (Richart and Hewitt, 2008; Hansen et al., 2013). Now secondary growth forests occupy 40% to 50% of their original cover in some regions (Tyrrell et al., 2012). Long-term regrowth and resiliency of these secondary growth forests has helped them to become an important carbon sink in North America (Birdsey et al., 2006).

The strength of this carbon sink remains uncertain under future climate projections. Carbon sequestration reflects the daily difference between gross ecosystem productivity (GEP) and ecosystem respiration (RE) (Goulden et al., 1996a). Seasonally, carbon budgets of temperate deciduous forests are unique due to their distinct patterns of carbon gain and carbon loss (Greco and Baldocchi, 1996). The production of leaves and foliage is necessary for photosynthesis in these forests, leading to fluxes within the first 4-5 months of each year being dominated by RE (Richardson et al., 2010). While photosynthesis begins much later in deciduous forests compared to evergreen forests, due to leaf-emergence

timing, deciduous trees exhibit higher rates of photosynthesis following leaf-out, sometimes twice as high as coniferous-evergreen stands (Gaumont-Guay et al., 2009). Changes in climate could alter the timing, frequency, and magnitude of extreme weather events, which could convert these forests from being a large carbon sink to a net carbon source over time (Vose et al., 2012).

Studies suggest that forest ecosystems within Eastern North America have already begun experiencing increases in the intensity and frequency of extreme heat and precipitation events in response to a changing climate (Iverson et al., 2008; Zhu et al., 2012). This is leading to warmer winters, greater winter precipitation (P), and higher annual rainfall, affecting both local and regional hydrologic cycles (USGCRP, 2017). Over the past 114 years (1901 – 2015), the air temperature (Ta) throughout the Great Lakes Basin has increased by 0.89°C (1.6°F), and over the next 30 years it is predicted to experience an increase of 1.5-2°C (3-3.3°F). Increasing Ta will not change uniformly, leading to winter Ta rising more than summer Ta, and average minimum Ta warming more than average maximum Ta (IPCC, 2013; USGCRP, 2017). The annual total P of the Great Lakes Basin has increased by 10% during the same time and is predicted to continue to increase by 4.5% over the next 30 years. However, while total annual P may increase overall, the distribution of this P during the year may vary. Regional water deficits are expected, as summer P is predicted to decrease by 5-15% by the end of the century (O'Gorman and Schneider, 2009; Byun and Hamlet, 2018). In future climates, this area is predicted to see a decrease in the

number of days below freezing, leading to an increase in the frost-free season and growing season length, which in turn may perturb the balance between photosynthesis and respiration, i.e. net ecosystem productivity (NEP) (Barr et al., 2002; Byun et al., 2018). Additionally, while higher Ta may promote longer growing seasons and enhanced carbon uptake in spring, late-season warming in the autumn could prolong respiratory losses, offsetting gains from extended photosynthetic uptake (Schimel, 1995; Piao et al., 2008; Richardson et al., 2010; Froelich et al., 2015). Any potential changes in environmental conditions can lead to changes in leaf-phenology (leaf emergence and senescence) or stand-composition, which could greatly impact the forest's carbon uptake and carbon budget in the long run (Aerts, 1995; Malhi et al., 1999; Curtis et al., 2002; Wilson and Baldocchi, 2000; Way and Oren, 2010; Fisichelli et al., 2013; Froelich et al., 2015), which highlights the importance of understanding the growth dynamics of such forests and their and environmental stresses.

The northernmost ecoregion of temperate forests in North America, known as Carolinian forests in Canada, range from southeastern Canada in the north to the Carolinas in the United States to the south (Lauriault, 1989; Blouin, 2001; Johnston, 2009). Forests in the area cover 18 to 25% of the land surface within the agricultural landscape. This region also has the highest percentage of temperate forest cover area in Canada (Arain and Restrepo-Coupe, 2005). In the Carolinian forests of Canada, many of the deciduous trees species are growing at the northern extent of their natural geographic range, these include: oak

(*Quercus*), beech (*Fagus*), and maple (*Acer*) (Solomon and Bartlein, 1992; Richart and Hewitt, 2008). The sandy, well-drained soils, around the northern edges of Lake Erie in southern Canada, often aid in the growth of red maple (*Acer rubrum*), white oak (*Quercus alba*), and red oak (*Quercus rubra*) tree species over other more common species (e.g. beech), typically seen throughout other eastern deciduous forests (Varga, 1985; Richart and Hewitt, 2008). Currently, the suppression of human-induced or natural disturbance events in these forests, through management or protection practices, has allowed red maple, a shade-tolerant species, to flourish while reducing less tolerant oak species (Abrams and Nowacki, 1992; Abrams, 1998). In the future, climate change may support more drought tolerant species, forcing a temporal transition in southern Canada deciduous forests.

The main goal of this study was to understand the impact of environmental drivers on the carbon sink or source capacity of a deciduous (Carolinian) forest within the Great Lakes Basin in Canada. No studies have previously examined the carbon sink capacity in this northernmost extent of Carolinian forests, or the sensitivity of C-uptake to climatic variables. The specific objectives were: (i) to examine the impacts of seasonal and interannual climate variability, including the occurrence of extreme weather events, on the forest's net ecosystem productivity using observations made over five years (2012 to 2016); and (ii) to compare the growth and productivity of this forest to other similar (i.e. geography, age, etc.) deciduous forests in eastern North America.

2.3 Methods

2.3.1 Site Description

The study site (42°38' 7"N, 80° 33' 28"W; elevation 265 m) is located north of Lake Erie near Long Point Provincial Park, roughly 5 km southwest of Walsingham in Norfolk County, Ontario, Canada (Table 2.1). The study site is part of the Turkey Point Observatory and Global Water Futures Program. The forest is known as Canadian Turkey Point Deciduous Forest (CA-TPD) in the global FLUXNET network. The Turkey Point Observatory is comprised of an age-sequence of three planted and managed white pine conifer forests (Peichl et al., 2010a), and this 70-110 year-old, naturally-regenerated, deciduous forest. The forest is growing on abandoned agricultural land, with nearby forest tracts subject to periodic timber extraction. The site is owned by the Ontario Ministry of Natural Resources and Forestry (OMNRF) and managed by the Long Point Region Conservation Authority (LPRCA) (Parsaud, 2013). Some key site characteristics are listed in Table 2.1 and described further below.

The site is predominantly comprised of hardwood species with a few scattered conifer species. White oak (*Quercus alba*) is the dominant tree species, while other tree species include: sugar (*Acer saccharum*) and red (*Acer rubrum*) maple, American beech (*Fagus grandifolia*), black (*Quercus velutina*) and red (*Quercus rubra*) oak, and white ash (*Fraxinus americana*), with white pine (*Pinus strobes*) comprising roughly 5% of the forests tree population. A sample of tree cores taken on site date the oak species back to 1942, while some pine species

appear to have begun growing around 1903 (Dr. Shawn McKenzie, personal communication). The extensive understory is made up of young deciduous trees as well as other plants including: Canada mayflower (*Maianthemum canadense)*, putty root (*Aplectrum hymale*), yellow mandarin (*Disporum lanuginosum*), red trillium (*Trillium erectum*), horsetail (*Equistum*) and other species. The forest is rich in biodiversity with a total of 573 tree and plant species (Elliot et al., 1999).

Biometric data was obtained in 2012 following National Forestry Inventory (NFI) protocol (Kula, 2013; Parsaud, 2013). The data showed that the mean tree height was 25.7 m, while the mean tree diameter at breast height (DBH = 1.3 m) was 23.1 cm. The mean stand basal area was 21.2 m^2 ha^{-1}, the mean stand density was 504 ± 181 trees ha^{-1}, and the stand volume was 381.4 m^3 ha^{-1} (Table 2.1). In 2012, the total carbon stored in aboveground biomass was 83.10 t C ha^{-1} (Kula, 2013). The maximum leaf area index (LAI), measured by a plant canopy analyzer (LAI-2000, LI-COR Inc.) and TRAC (Tracing Radiation and Architecture of Canopy, c.f. Chen, 1996), was 8.0 m^2 m^{-2} in 2012.

The site is located within the Southern Norfolk Sand Plains, an area defined by coarse-grained, sandy deposits from glacial melt water (Richart and Hewitt, 2008). The soil is predominantly sandy (Brunisolic gray brown luvisol, according to the Canadian Soil Classification Scheme) and is well drained, with a low-to-moderate water holding capacity. A regional soil analysis described similar soils in the area as having a 20 cm thick Ap horizon, followed by a 30 cm Bm1 horizon, and then a Bm2 horizon, reaching up to 80 cm (Presant and Acton,

1984). Site measurements in 2012 found a 5-10 cm thick litterfall and organic-rich loamy-sand layer (18% organic matter), while lower soil layers were comprised of over 90% sand and contained less than 2% organic matter. Additionally, the average bulk density of the sand was estimated to be 1.15 g cm^{-3}, with an average soil pH of 5 (Parsaud, 2013).

The climate of the region is humid temperate with warm, humid summers and cool winters (Meteorological Service of Canada). The moderating effect of nearby Lake Erie helps to regulate cold winter temperatures. Environment Canada climate records from the Delhi CDA weather station (25 km north of the site) found that on average (1981 – 2010), the area experiences 145 days of frost-free weather, a mean annual temperature of 8.0°C and 997 mm of total mean annual precipitation. Total precipitation is evenly distributed throughout the year, with 13% of that falling as snow (Environment and Climate Change Canada).

2.3.2 Eddy Covariance (EC) Flux Measurements

Half-hourly fluxes of momentum, latent heat (LE), sensible heat (H), and CO_2 (F_c) have been measured continuously using a closed-path eddy covariance system (CPEC), since January 2012. This study examines the first 5 years (2012 – 2016) of data recorded, while measurements are still ongoing today. The CPEC setup consists of an enclosed infrared gas analyzer (IRGA) (LI-7200, LI-COR Inc.) and a 3D sonic anemometer (CSAT3, Campbell Scientific Inc.). The IRGA and CSAT3 are mounted at 38 m height atop a walk-up scaffold tower. The

CSAT3 is installed and oriented west (270°), while a 1 m long intake tube immediately behind the CSAT3 delivers sampled air to the IRGA. A flow module (7200-101, LI-COR Inc.) helps to regulate and control the air flow rate through the IRGA. Air is drawn at a flow rate of 15 L/min, while maintaining turbulent flow. The IRGA is calibrated once a month using high purity nitrogen gas for the zero offset, and Environment Canada Greenhouse gas laboratory specified CO_2 gas concentrations for the CO_2 span check. Mid-canopy CO_2 concentrations are also measured at 16 m height, using an IRGA (LI-820, LI-COR Inc.) and used for calculating the two-level CO_2 storage flux, as described below. Fluxes measured by the EC system are sampled at 20 Hz frequency and averaged to half-hourly data using custom software created by the Biometeorology & Soil Physics Group at the University of British Columbia (British Columbia, Canada), installed on a desktop computer housed in a trailer at the site.

The CO_2 storage (S_{CO2}) within the column of air below the EC sensors is calculated by vertically integrating the difference between the current and previous half-hourly measured CO_2 concentrations. This calculation is performed using CO_2 concentration measurements made above the canopy at 38 m height and mid-canopy at 16 m height. At times when mid-canopy measurements are not available, the change in storage is calculated from the above-canopy measurements. CO_2 storage has been shown to generally increase at night, while decreasing in the morning (Goulden et al., 1996a).

Net ecosystem exchange (NEE, µmol m^{-2} s^{-1}) was calculated as the sum of the vertical CO_2 flux (F_c), and the change of CO_2 storage ($NEE = F_c + S_{CO2}$). Both vertical and horizontal advections were assumed to average to zero over long periods and were not considered. Net ecosystem productivity (NEP) was calculated as the opposite of NEE (NEP = -NEE), where positive NEP indicates net carbon uptake by the forest (sink), and negative NEP is carbon loss from the forest to the atmosphere (source).

2.3.3 Meteorological Measurements

Meteorological measurements have also been made simultaneously with EC measurements since January 2012. Relative humidity (RH) and Ta are measured (HMP155A, Campbell Scientific Inc.) at 38 m height. A compact aspirated shield (43502-L, R.M. Young Company) is used to mount the sensor, providing continuous ambient air over the sensor head, while also protecting it from solar radiation interference. Both wind speed and direction were recorded in the first three years of measurements using a Model 85000 anemometer (R.M. Young Company) that was replaced (Model 05103, R.M. Young Company) in 2015. Upward and downward photosynthetically active radiation (PAR, PQS1, Kipp & Zonen B.V.) and all four components of radiation (CNR4, Kipp & Zonen B.V.) are also measured at 36 m height.

Atmospheric pressure (61302V, R.M. Young Company), and snow depth (model SR50A, Campbell Scientific Inc.) are measured at the ground.

Precipitation (P) is measured in a small forest opening, 350 m southwest of the tower, using an all-season, heated tipping-bucket rain gauge (model CS700H, Campbell Scientific Inc.). The rain gauge is located at 1.5 m height and is protected by an Alter Wind Screen (260-953, Campbell Scientific Inc.). Precipitation data are cross-checked and gap-filled from an accumulation rain gauge data (T-200B, GEONOR Inc.), installed 15 km to the east, near the 80-year and 45-year old conifer sites of the Turkey Point Observatory. Soil temperature (Ts) and soil water content (θ) are measured using temperature (model 107, Campbell Scientific Inc.) and moisture probes (model CS650, Campbell Scientific Inc.) at 2, 5, 10, 20, 50, and 100 cm depth in two locations. Soil heat flux (G) measurements are made using four soil heat flux plates (model HFT3, Campbell Scientific Inc.) buried 3 cm below the surface at two locations. All meteorological, soil, and precipitation data are sampled and recorded using two data loggers (met/soil – CR3000; precipitation – CR10X, Campbell Scientific Inc.). Automated data downloads occur half-hourly within the desktop computer.

2.3.4 Leaf-Phenology Measurements

Phenological imagery is acquired at half-hourly temporal resolution using a PhenoCam (Richardson et al., 2007a; Richardson et al., 2009) located facing north on top of the flux tower at 36 m height. The start and end dates of the growing season were estimated using phenological transition dates (phenophases) calculated by the greenness chromatic coordinate (GCC) derived by the

PhenoCam. From the GCC minima and maxima, dates identifying the 10%, 25%, and 50% amplitude of greenness rising and greenness falling stages were then identified (Richardson et al., 2018). A range of transition dates (10% - 50%) were used in this analysis to identify the start and end of the growing season. All GCC data retrieval and post-processing analysis of the PhenoCam transition dates was done using the PHENOCAMR R package (Hufkens et al., 2018). These dates were only used for the purpose of identifying key seasonal transition periods within this study. In this study seasons were defined as spring (March, April, May), summer (June, July, August), fall (September, October, November) and winter (December, January, February).

2.3.5 Data Processing, Gap-Filling, and Statistical Analysis

The flux and meteorological data were filtered, cleaned (threshold and point cleaned), and gap-filled using the Biometeorological Analysis, Collection, and Organizational Node (BACON) software following protocols designed by the AmeriFlux Network (Brodeur, 2014). Outliers in the data were identified and removed. Small gaps (hours) within meteorological data were linearly interpolated, while larger gaps (hours to days) were filled using linear regression-model fitted values from other Turkey Point Observatory sites. Overall, the mean flux recovery was 89% (from 83 to 94%) over the 5-years of data collection.

During periods of low turbulence, typically at night within a stable nocturnal boundary layer, EC measurements may underestimate fluxes. To

resolve this underestimation, threshold passing methods were incorporated in the data processing. First, a footprint model, following Kljun et al. (2004), was applied to exclude fluxes when greater than 10% of the flux footprint extended outside of the forest boundary. To further remove unrepresentative measurements, a friction-velocity, u-star threshold (u^{*Th}), was applied to all nocturnal NEE measurements (Barr et al., 2013; Papale et al., 2006). Half-hourly NEE values were removed from the dataset when the measured u* was below thresholds estimated using the Moving Point Test u^{*Th} determination method (Reichstein et al., 2005). This method estimated u^{*Th} from the relationship between nighttime NEE and u^* (Papale et al., 2006). An average, site specific, u^{*Th} of 0.40 m s^{-1} was determined, where nighttime NEE values below this threshold were removed. These data were filled using exponential relationships between sufficiently turbulent (u* > 0.4 m s^{-1}) nighttime NEE and Ts at 2 cm depth. Following the aforementioned threshold passing methods, the mean capture for non-gap filled NEE was 49% (from 46% to 53%) annually.

Ecosystem respiration (RE) was modeled as a function of Ts_{5cm} and $\theta_{0\text{-}30cm}$ (Brodeur, 2014) using fitted temperature response parameters (R_{10} & Q_{10}) to describe the relationship between RE and Ts_{5cm}, modified by a soil moisture function, as shown:

$$RE = R_{10} \times Q_{10}^{\frac{(Ts_{5\,cm} - 10)}{10}} \times \frac{1}{[1 + \exp(a_1 - a_2\,\theta_{0-30\,cm})]} \quad (1)$$

Here a_1 and a_2 are fitted parameters as a function of the independent variable, $\theta_{0\text{-}30cm}$, acting to scale the Ts_{5cm} – RE relationship. The gross ecosystem productivity (GEP) was estimated by adding measured NEP and daytime modeled RE. During periods where there were gaps in NEP data, GEP was modelled using a rectangular hyperbolic function:

$$GEP = \frac{\alpha PARd\ A_{max}}{\alpha PARd + A_{max}} \times \int(T_s) \times \int(VPD) \times \int(\theta_{0\text{-}30cm}) \quad (2)$$

The first term defines a relationship between PAR and GEP. The remaining terms are scaling responses of GEP to T_s, vapor pressure deficit (VPD), and $\theta_{0\text{-}30cm}$, respectively (Brodeur, 2014). Where meteorological data was missing to compute RE and GEP, gaps were filled using a non-linear regression approach and a marginal distribution sampling approach (Reichstein et al., 2005; Brodeur, 2014). Gaps in NEP, due to instrumentation errors, maintenance, calibrations, and power outages, were filled as the difference between the modeled GEP and modeled RE.

Additionally, in order to determine the most significant environmental controls on half-hourly and daily NEE within the deciduous forest, a multivariate regression model was fit to the data using incident PAR, VPD, Ts_{5cm} and $\theta_{0\text{-}30cm}$ as explanatory variables. These variables were chosen due to their usage in the aforementioned gap-filling methods. The analysis was restricted to daytime (PAR > 1000 μmol m^{-2} s^{-1}) growing season data. Variables included in the model were significant at $\alpha < 0.05$, while the model fit was determined using the residual

analysis of the coefficient of variation (R^2). In order to accurately determine the relative contribution or explanatory power of the environmental variables derived from the model, a residual analysis was completed (Lindeman et al., 1980; Skubel et al., 2015). Each variables contribution to the model R^2 was determined by the differences in fit between the total model (i.e. all variables) and the model without individual variables, resulting in a percentage of total model R^2. All data processing and analyses were completed using MatLab (*The MathWorks Inc*.).

2.3.6 Regional Analysis

We identified available studies in the peer-reviewed scientific literature of the past 20 years, which reported annual NEE or NEP values measured by EC systems. The ISI Web of Science was searched for the following specific terms: "eddy covariance", "net ecosystem productivity", "eastern deciduous", "temperate forest", "North America". These searches yielded numerous results, highlighting the work that has been done on carbon fluxes within eastern deciduous forests. To be included in our analysis, studies had: (1) to report annual NEE values from EC measurements for the majority (3+ yrs) of 2012 to 2016 study; and (2) although temperate deciduous forests reside around the globe, this study only considered forests within North America. In an attempt to expand the study, we also considered research sites within the initial search containing past peer-reviewed annual NEE measurements, even if such studies did not publish data within the period of study. In three such cases, the authors were contacted for unpublished

data, or requested to confirm the accuracy of data downloaded from AmeriFlux [*http://ameriflux.lbl.gov*]. The reporting of standard deviations was not essential as flux errors are often not reported in the literature. Forest age, annual mean Ta and annual total P were taken from the cited study or AmeriFlux database, when not readily available. Ultimately, if no recent data could be found on the ISI Web of Science or validated from external sources, sites were not included in this study. Consequently, a total of 5 study sites (including our forest) encompassing 23 years of data from 2012 to 2016 were analyzed in this study.

2.4 Results

2.4.1 Environmental Variability

The mean annual Ta between January 1, 2012 and December 31, 2016 was 9.76 ± 1.5°C, at our study site, while the mean total annual precipitation (P) for the same measurement period was 881 ± 102 mm. In comparison, the 30-year mean Ta and P from 1981 to 2010, measured at the nearby Environment Canada Weather Station in Delhi, Ontario, were 8.0 ± 1.6°C and 997 ± 145 mm, respectively. The 5-year mean annual Ta at our site exceeded the 30-year mean Ta by 1.7°C, with most years indicating warmer conditions than the 30-year mean. The highest mean annual Ta was in 2012 (11.8°C) and the lowest in 2014 (8.0°C). The highest annual P sum was observed in 2014 (991 mm), while the lowest annual P was observed in 2015 (750 mm). None of the five years experienced annual P greater

than the 30-year mean; however, three years (2013, 2014, and 2016) saw annual precipitation within the 30-year normal range of 852 to 1142 mm.

Figure 2.1 illustrates the monthly mean Ta and cumulative P sum measured at the site. The corresponding 30-year means (Delhi) are also shown. The Ta followed a similar annual trend over all 5 years, reaching a minimum in January and February, and a maximum in late summer, primarily in July and August. From April to October the mean monthly temperature remained above 10°C in all years. The coldest month was February 2015 (-11.4°C), however 2015 ended the year with the highest mean December Ta (5.3°C). In 2012, the mean monthly Ta was the warmest of all 5 years for the period from January through July, leading to a summer drought. Furthermore, late growing season warming was experienced in 2016, with unusually warm mean monthly Ta in August (23.6°C) and September (20°C), which was 3.6°C and 4.5°C above the 30-year mean, respectively (Figure 2.1a). Late growing season warming was evident in all years with the 5-year mean fall Ta being 2°C (Figure 2.2a; Table 2.2) warmer than the 30-year mean. Fall was the only season where mean seasonal Ta was higher in all years compared to the 30-year mean.

During 2012, total annual P (801 mm) was 50 mm below the 30-year P-range (852 – 1142 mm), with the lowest spring P, and an evident absence of P from May through July. In 2016, mean annual P was 908 mm, with sufficient P seasonally, except during the summer (Figure 2.2a; Table 2.2). Following a wet March and April, 2016 experienced the lowest summer P (144 mm) of the 5-

years, though similar to the dry summer of 2012 (159 mm). On average (1981 to 2010), 64 days per year receive P greater than 5 mm (0.2 in). During the 30-year mean, extreme P events in excess of 25 mm day^{-1} were measured 7 days per year, while July and September saw the largest mean days per month (1 day). Extreme daily P events (> 25 mm day^{-1}) were measured in 2013 (8 days) and 2014 (9 days), while 2016 saw fewer extreme P days (4 days), but the most consistent and frequent P (Figure 2.1b) out of the five years (53 days greater than 5 mm).

Daily downward PAR followed similar patterns year-to-year, however, slight deviations between the years were typically experienced during the summer months (Figure 2.3a). Mean June PAR yielded a maximum in 2016 (522 μmol m^{-2} $month^{-1}$), but a clear decrease in June PAR was present in 2013 (417 μmol m^{-2} $month^{-1}$) and 2015 (416 μmol m^{-2} $month^{-1}$). Large declines in PAR are often associated with increased cloudiness or P events, seen in 2013 and 2015 (Figure 2.3d). With decreased PAR, Ta and therefore VPD may also decrease. This was evident in 2013 and 2015, which experienced the lowest mean summer VPDs of 0.75 kPa and 0.77 kPa, respectively (Figure 2.3b; Table 2.2). The highest daily PAR typically occurred at the same time as the highest VPD, leading to the warmest years of 2012 and 2016 having the highest summer and annual VPD. The difference between these years was that in 2012 the daily summer mean VPD (1.33 kPa) peaked in July, while in 2016, the summer VPD (1.01 kPa) peak was reached in June, due largely in part to the difference in the timing of peak summer Ta (Figure 2.1a).

Soil temperature (Ts) followed Ta closely (R^2 = 0.88) at our site (c.f. Figure 2.1a and Figure 2.3c). While maximum Ts_{5cm} occurred during the summer months, the timing of the maximum Ts varied year to year, often occuring during prolonged periods of decreased P or volumetric soil water content (θ). The mean daily θ (Figure 2.3d) ranged from a minimum of 0.023 m^3 m^{-3} in August of 2016, to a maximum of 0.196 m^3 m^{-3} in December of 2013. The 5-year mean $\theta_{0\text{-}30cm}$ was 0.104 m^3 m^{-3}. Deep declines in θ were observed during summer months characterized by high Ta and little to no P (i.e. 2012, 2014, and 2016). In 2012, a significant decrease in $\theta_{0\text{-}30cm}$ occurred over a 63 day period (June – July), before substantial rain (> 25 mm) was received. Similarly in 2016, a near three month (May – July) decrease in $\theta_{0\text{-}30cm}$ reached a 5-year low. In all years, θ was the highest in the spring (after snowmelt, before declining with the onset of photosynthetic activity at the start of the growing season. The depletion of θ typically lasted the majority of the summer, before being replenished near the end of the growing season following decreased atmospheric and physiological water demand and increased P. During winter, mean $\theta_{0\text{-}30cm}$ values typically ranged between 0.1 and 0.15 m^3 m^{-3}.

2.4.2 Deciduous Forest Carbon Fluxes

On average, the source-sink transition date, defined here as the growing-season, began near the beginning of May (day 127) at our site, and continued into mid-October (day 292). This was due in part to the deciduous nature of the forest, as

well as the latitude. Many long days (~13 hours of sunlight and carbon uptake) of positive half-hourly NEP comprised a large portion of the growing-season. As the summer progressed, daily NEP values decreased with the shortening of the length of the days (decreased photoperiod) before the growing season came to an end. During the night and leafless periods following the conclusion of the growing season, our site was a source of carbon. The start and end of the growing-season varied from year to year by up to 12 days.

Half-hourly flux data indicating the diurnal and annual variations in NEP are shown in Figure 2.4. Cool, blue colors symbolize a carbon-source (i.e negative NEP, carbon released by the forest), and warmer yellow, orange, and red colors represent carbon uptake by the forest (i.e. positive NEP). In 2012 (Figure 2.4a), non-growing season NEP remained near zero, acting as a slight source of carbon. Following the onset of leaf-out (day 121), mid-day NEP values exceeded 0.5 g C m^{-2} hhr^{-1}, with a few measurements near 1 g C m^{-2} hhr^{-1}. The low cumulative NEP recorded in both 2013 and 2015 (Figure 2.4b & 2.4d) was defined by high growing-season RE. In 2014, (Figure 2.4c), the same diurnal pattern of negative NEP at night (RE) and positive NEP during the day (GEP outweighing RE) was observed. Interestingly, in 2014 the growing season began much later than in other years (day 133, almost two weeks later). Despite the late start to the growing season, the year had the largest carbon uptake (highest NEP) of all years. In June and July (days 160 – 200) of 2016 (Figure 2.4e), the site was a carbon sink, the strength of which slowly decreased throughout the remainder of the year. Higher

nighttime RE resulted in lower daily NEP, but the extended length of the growing season (approaching day 300) allowed moderate NEP (0.5 g C m^{-2} hhr^{-1}) to be measured well into October 2016.

Daily (Figure 2.5) and cumulative (Figure 2.6) carbon fluxes (NEP, GEP, and RE) were also examined. At the beginning of each year (Figure 2.5), the forest was a slight carbon source (negative NEP), due to the absence of leaves on trees (no GEP), as well low daily Ta leading to relatively low repiration (RE) efflux. Following leaf-out, through much of the early growing-season, increasing PAR combined with cooler daily Ta helped photosynthetic fluxes to outweigh respiratory fluxes. Peak daily NEP (max carbon sink) was reached at this time, in May and June of each year (Figure 2.5a). Low PAR in June of 2013 and 2015 (Figure 2.3a) resulted in more frequent decreases in daily GEP sums (~5 g C m^{-2} day^{-1}) in comparison to other years (Figure 2.5b). Competing processes (high PAR and high VPD) took place at this time to limit the overall GEP measured. The year with the highest VPD (2012) resulted in the lowest summer GEP values. Overall, daily GEP sums reached a maximum (15 g C m^{-2} day^{-1}) in the middle of summer (July), when PAR was at a maximum. The maximum daily RE (Figure 2.5c) was measured during the middle of summer (July) in all years, at the point when Ta and Ts were highest (c.f. Figure 2.1a and Figure 2.3c). During the second half of each summer, NEP steadily declined until leaf senescense occurred and the growing season ended, a period when NEP returned to negative daily values and the site became a source of carbon once more.

The highest annual NEP occurred in 2014 (305 g C m^{-2} yr^{-1}), followed closely by 2012 (292 g C m^{-2} yr^{-1}). The remaining three years had annual NEP values less than 200 g C m^{-2} yr^{-1}, with 2015 being the lowest at 90 g C m^{-2} yr^{-1} (Figure 2.6a). The spring of 2016 experienced a delayed start to the growing season similar to 2014 (Figure 2.4), the year with the highest NEP, however the annual carbon sink strength of 2016 (185 g C m^{-2} yr^{-1}) was just over half of 2014. Following a delayed onset of spring warming and growth, the annual NEP in 2016 fell short of the warmest (2012) and wettest (2014) years, due in large part to warm summer and fall Ta conditions. The fall of 2016 experienced the warmest and most productive (highest GEP) fall in the five years of measurements, though this also led to the highest fall RE (389 g C m^2) within the measurement period, quickly decreasing daily and cumulative NEP (Table 2.2).

2.4.3 Statistical Analysis and Environmental Controls

A multivariate linear regression analysis was performed between carbon fluxes and meteorological explanatory variables (i.e. gap-filling methods) at half-hourly and daily time scales for daytime, growing season measurements. The individual contribution of each of these variables (PAR, VPD, Ts_{5cm}, and $\theta_{0\text{-}30cm}$) was compared to model R^2 in an attempt to quantify the relative explanatory power of the meteorological data (Table 2.3). NEP, GEP, and RE residuals had normal distributions at our forest. Overall, model explanatory power was highest for RE at both time scales (R^2~0.8). NEP was the only flux to have higher R^2 for the

daily model when compared to the half-hourly model (Table 2.3). Ts_{5cm} explained most of the variability in RE and GEP at both time scales. Ts is able to best predict the fluxes in the deciduous forest as it captures the soil freeze/thaw and seasonal phenological effects within the deciduous forest. Ts_{5cm} explained more variability in NEP at the daily time scale, however, it was the secondary explanatory variable on the half-hourly time scale, behind PAR. PAR ranked next in explanatory power for GEP, although, it explained no variability in RE. $\theta_{0\text{-}30cm}$ contributed to RE at both time scales, though it failed to explain GEP and NEP. Additionally, VPD was found to have a significant effect on NEP and GEP at the half-hourly time scale, although it was not significant at the daily time scale. Overall, during the five years of the study, the key meteorological controls on carbon fluxes at our site were calculated to be Ts_{5cm} and PAR.

Half-hourly bin-averaged daytime, growing season, NEP (non gap-filled), GEP, and RE, plotted against the significant meteorological variables (Ts_{5cm}, VPD, PAR, and $\theta_{0\text{-}30cm}$) are shown in Figure 2.7. All years experienced a steady rise in NEP (Figure 2.7a) and GEP (Figure 2.7e) following an increase in Ts_{5cm} up to 15-20°C. Past this range of Ts, NEP and GEP began to plateau or even decrease with increasing Ts. An exponential increase in RE (Figure 2.7i) with increasing Ts_{5cm} was seen in all years. During 2014, the year with the highest annual NEP, maximum half-hourly NEP reached nealy 17 μmol C m^{-2} hhr^{-1} when Ts_{5cm} was 20°C, considerably higher than other years. Even within the ideal range of Ts, NEP and GEP may be limited through stomatal restrictions related to VPD

or water limitations (Table 2.3). As Ts_{5cm} increases, $\theta_{0\text{-}30cm}$ decreases illustrating how Ts and θ are highly correlated here. The years with the highest GEP and NEP at maximum Ts_{5cm} values, were also the wettest, especially during the summer (2013 & 2014). While all years saw a decrease in NEP (Figure 2.7b) and GEP (Figure 2.7f) with increasing $\theta_{0\text{-}30cm}$, GEP was sustained at higher $\theta_{0\text{-}30cm}$ values in 2013 and 2014. The hot and dry years (2012 and 2016) saw a dramatic decrease in GEP at moderate $\theta_{0\text{-}30cm}$ as water availability controlled stomatal restrictions.

Binned VPD plotted against NEP and GEP illustrates that fluxes are typically low at very low VPD (< 0.5 kPa) and considerably higher VPD (> 1.5 kPa). These conditions represent sufficiently wet and dry atmospheric conditions, respectively. Maximum NEP (16 μmol C m^{-2} hhr^{-1}) and GEP (21 μmol C m^{-2} hhr^{-1}) were shown to occur within a VPD range of 0.7 to 1.2 kPa (c.f. Figure 2.7c and Figure 2.7g). In 2012, high Ts and very high, year-long VPD led to considerable deviation from other years, with the maximum photosynthetic fluxes being reached near a VPD of 1.5 kPa while extending above 3 kPa. For wet years (2013 and 2014), the annual maximum VPD (2 – 2.5 kPa) resulted in near zero GEP and negative NEP. In all years, RE saw nearly constant values at all ranges of VPD (Figure 2.7k), though a localized maximum respiratory flux was observed around a VPD of 2 kPa. Lastly, bin-averaged PAR and NEP (Figure 2.7d), GEP (Figure 2.7h), and RE (Figure 2.7l) was examined. GEP was gap-filled with PAR, so a highly correlated parabolic curve is observed, with increasing GEP and NEP with increasing PAR. All years but 2012 experienced similar patterns of GEP and

PAR, while the environmental conditions in 2012 (high Ta, high VPD) may have limited leaf stomata from efficiently utlizing PAR.

2.4.4 North American Regional Analysis

Annual values of carbon fluxes measured at our site were compared to fluxes from 4 other Eastern North American temperate deciduous forests for the time period from 2012 to 2016. Initially, a fifth site, Silas Little – New Jersey (US-Slt), was considered. However, a major insect defoliation event in 2007 resulted in the site being a carbon source for two years after and a decrease in site NEP to only 22% of pre-distrubance values from 2009 to 2016 (Clark et al., 2018). Consequently, this study was excluded in order to only consider non-disturbed, old-growth deciduous forests. Annual values of NEP, GEP, and RE, and other meteorological and characteristic information are given in Table 2.4. The forests' age ranged from 70 to 130 years old, with the youngest being Harvard Forest in Petersham, Massachusetts (Urbanski et al., 2007) and the oldest being the Bartlett Experimental Forest in Durham, New Hampshire (Lee et al., 2018). For all forests, mean annual Ta and P calculated from available data, ranged from 5.2 to 14.5°C and 560 to 2384 mm, respectively. On an annual basis, the forests were sinks of carbon with NEP ranging from 69 to 459 g C m^2 $year^{-1}$, GEP from 1180 to 1684 g C m^2 $year^{-1}$, and RE from 954 to 1406 g C m^2 $year^{-1}$. The five year mean values of NEP (206 g C m^2 $year^{-1}$), GEP (1343 g C m^2 $year^{-1}$), and RE

(1171 g C m^2 $year^{-1}$) at our site fell just slightly below the mean values for all sites but within the range of standard deviations (Table 2.4).

Carbon fluxes (NEP, GEP, and RE) were plotted against individual site characteristics, including forest age, mean annual Ta, and total annual P in Figure 2.8. No significant relationship between annual fluxes and latitude was found. This was illustrated by the similarities in annual NEP, GEP, and RE values between the Coweeta forest (35°N) and Harvard forest (42.5°N), even though site Ta and P varied considerably (Table 2.4). Forest age (Figure 2.8a; 2.8d; 2.8g) was shown to be negatively correlated to NEP and GEP. The 5-year mean fit found that an increase of 10 years in a forests age decreased annual NEP by 56 g C m^2 $year^{-1}$, with a similar decrease experienced in GEP (73 g C m^2 $year^{-1}$) for these mature forest stands. Mean annual Ta (Figure 2.8b) and total P (Figure 2.8c) had little influence on annual NEP, largely varying between individual years. Interestingly, the driest and warmest years (2012, 2015, and 2016) experienced decreases in NEP with increasing Ta and P. In all years, annual GEP increased with increasing mean annual Ta (Figure 2.8e) and total annual P (Figure 2.8f). The 5-year mean fit found an increase of 2°C and 200 mm to result in an increase in GEP of 50 g C m^2 $year^{-1}$ and 30 g C m^2 $year^{-1}$, respectively. No significant relationships were found between RE and forest age (Figure 2.8g) and mean annual Ta (Figure 2.8h), though annual RE was shown to increase with increasing total annual P (Figure 2.8i).

2.5 Discussion

2.5.1 Carbon Fluxes

Carbon budgets of temperate deciduous forests are unique due to their distinct seasonal patterns of carbon gain and loss over the course of a year driven largely by leaf-phenology and seasonal meteorological conditions (Greco and Baldocchi, 1996). At our site, photosynthesis (GEP) was initiated between the end of April and mid-May (days 105 to 121) before ending in early to mid-November (days 300 to 314). Seasonally, the site was a small but consistent carbon source through winter (i.e. consistently negative NEP) due to small respiratory fluxes and no photosynthesis (Table 2.2). During that time, daily NEP values averaged between negative 1-2 g C m^{-2} day^{-1}. Similar winter NEP values have been observed at other deciduous forests (Bolstad et al., 2004; Curtis et al., 2002). Following the winter and into early spring until leaf-out, the site becomes a strong C source. NEP values continue to decrease with increasing Ta. Following leaf-out, however, NEP rapidly increased and the site became a carbon sink. At our site, the spring of 2012 (Table 2.2) had the highest spring Ta (11.7°C), ~ 3°C higher than any other year, leading to the earliest growing season start and highest spring NEP (-17 g C m^{-2}), similar to that conditions described by Richardson et al. (2010). Ultimately, this early start to the 2012 growing season aided the year in having the second highest annual NEP. Variability in summer NEP is likely driven by changes in GEP (Figure 2.7). Though $\theta_{0\text{-}30cm}$ was not shown to significantly contribute to GEP (Table 2.3) at our site, others have shown that with sufficient water

availability, radiation is the limiting factor in GEP (Wu et al., 2013). During each summer, rising Ts produced an overall negative impact on NEP. The inhibition of GEP at higher Ts (Figure 2.7d), and increasing RE due to both increasing Ts and biomass (Figure 2.7g), led to a decrease in NEP for the remainder of the year.

The key period which determined the overall annual NEP at our site occurred during mid-summer (late July, early August) – what happened in these months would determine the strength of the carbon sink at our site on an annual basis. In all years, this period acted to prolong or inhibit forest productivity. In 2013 and 2015, the two years with the lowest annual NEP values, fluxes began with nearly identical growing season starts and carbon uptake until mid-July (Figure 2.6a). These two years had the lowest summer NEP, PAR, VPD, and Ta (Table 2.2), but very different seasonal and annual P patterns. In 2015, $\theta_{0\text{-}30cm}$ (Figure 2.3d) approached a summer minimum at the end of July; while in 2013 it did not, leading to different carbon uptake for the remainder of the year. In 2014 and 2016, the two highest annual NEP years on record, the growing season start varied by three weeks, but both years experienced similar carbon uptake until July (Figure 2.6a). A drought and lull in P (Figure 2.1b) from May to July occurred in 2012, but was replenished by ample P in late July. While the NEP of both years continued similarly after this point, the timing and severity of the heat and lack of P in 2012 produced lower photosynthetic uptake for the remainder of the growing season as compared to 2014. Furthermore, 2016 and 2014 had similar growing season starts but experienced a large deviation in carbon uptake following a

decrease in $\theta_{0\text{-}30cm}$ similar to 2012. Overall, it appears that mid-summer meteorology and soil water status greatly impacted forest carbon uptake. More importantly, the timing and duration of these meteorological responses greatly shaped overall NEP dynamics in this forest over the study period.

2.5.2 Environmental Controls

At our site, the variation in carbon fluxes was strongly influenced by the onset of photosynthetic activity in spring to begin the growing season, as well as senescense in the autumn. During the summer, high Ta (>20°C) and high VPD (>1 kPa) caused seasonal soil water (θ) deficits, highlighting the importance of $\theta_{0\text{-}30cm}$ and its correlation to Ts_{5cm}. In the summers of 2012, 2014, and 2016, daily $\theta_{0\text{-}30cm}$ dropped well below average conditions (0.104 m^3 m^{-3}), reaching 0.05 m^3 m^{-3} on different occasions. The forest however always recovered later in the year, typically following a large P event (Figure 2.3d). Daily NEP peaked in the early growing season (May – July), but after this time and during water stressed periods (low θ or high VPD), NEP often dropped considerably. Warm spring Ta can help enhance GEP through the lengthening of the growing season (Richardson et al., 2009b). However, increased heat or water stressed conditions and high summer Ta may reduce GEP, while warmer soils enhance RE (Barr et al., 2002). Our forest experienced two faint peaks in RE, one in mid-summer (June and July) and one in early-autumn (August-September), similar to Black et al. (2000). In the autumn, RE was high when leaves were senescing but Ts remained high. This was

illustrated in 2016, when late season warming caused a slight rise in NEP in late September. However, even with supporting environmental conditions, limitations from light or nutrients could not sustain carbon uptake that late into the season.

With continued warming later in the year, high fall Ta may lead to a lengthening of the growing season through October, predicted to cause an asymmetry in the carbon fluxes of deciduous forests (Barr et al., 2002). Often though, as seen at our site, late season warming leads to a reduction of the carbon storage through increased RE. The resulting late season carbon losses prior to leaf senescence are likely to outweigh the gains from prolonged photosynthesis (Schimel, 1995; Piao et al., 2008; Richardson et al., 2010; Froelich et al., 2015). In all years, even in water-stressed conditions, our site remained a net annual carbon sink. However, in the future, with more extreme Ta and more variable P, extending an already hot and dry growing season could further promote carbon loss, affecting the annual sink/source status of these forests.

2.5.3 Regional Analysis

Without human disturbances, deciduous forests would be the dominant forest type in the temperate climate region across eastern North America (Curtis et al., 2002). These forests are estimated to sequester an average of 1.0 to 2.4 Mg C ha^{-1} yr^{-1} or 100 to 240 g C m^{-2} yr^{-1} (Birdsey, 1992). Annual measurements of carbon storage and driving factors were compared to other North American temperate deciduous forests. For forests included in our study with similar latitude, stand age, and

vegetation types, the mean annual carbon sequestration was 213 ± 102 g C m^{-2} yr^{-1} (Table 2.4). The lowest NEP estimates, included in the analysis, were found in northern locations of the United States (Michigan and New Hampshire) and southern Ontario Canada.

Although not included in our regional analysis due to the availability of recent data, a maple dominated deciduous forest in Borden, Ontario (44°N) had an average NEP of 177 g C m^{-2} yr^{-1} over 17 years (1996-2013) of measurements, with the forest being a weak carbon source for two years during the measurement period (Froelich et al., 2015). Higher NEP was measured further south at the Walker Branch deciduous forest in Oak Ridge, Tennessee (35°N), averaging 574 g C m^{-2} yr^{-1} during 5 years (1995-1999) of measurements (Wilson and Baldocchi, 2001). While the more southern forest in our analysis (e.g. Coweeta) had high annual NEP, we found no relationship between latitude and annual NEP.

The University of Michigan Biological Station (UMBS) forest in Northern Michigan lies within the transition zone between mixed hardwood forests and boreal forests and has similar stand age, soil characteristics, tree species and latitude as our site (Gough et al., 2013). At their site the NEP ranged from 70 to 170 g C m^{-2} yr^{-1} over a 3-year period from 1998 to 2001 (Curtis et al., 2002; Schmid et al., 2003). However, in recent years (2012-2016), their site NEP ranged from 172 to 331 g C m^{-2} yr^{-1} (Table 2.4). At our site, NEP ranged from 90 to 305 C m^{-2} yr^{-1}, well within the range of similar forests. These similar sites yielded a

negative correlation (R^2 ~ 0.5) between forest age and annual NEP, though other site variables could not help explain NEP.

Eastern deciduous forests are typically a moderate carbon sink, but their carbon sink capacity varies due to meteorological conditions. The studies at the Oak Openings forest in northwestern Ohio suggested that seasonal GEP was determined by Ta, θ, and VPD, while year-to-year differences were explained by changes in LAI. Additionally, RE was most sensitive to Ta and θ, while the θ effect on RE may have been facilitated by GEP (Noormets et al., 2008, Xie et al., 2014). The Borden forest found that total annual NEP was most strongly correlated with mean annual PAR (Froelich et al., 2015). The main meteorological factors driving variability in the fluxes at our site were due to Ts (driven by Ta) and PAR. While no significant contribution from θ was found for NEP and GEP, we do recognize its close relationship with Ts. As Ts increased, θ tended to decrease. RE in our forest was sensitive to θ. Theses seasonal and phenological influences on meteorological controls appear to influence most temperate deciduous forests across eastern North America.

2.6 Conclusions

Seasonal and annual dynamics of carbon fluxes were studied for five years (2012 to 2016) at a mature temperate deciduous forest in the Great Lakes region of southern Ontario, Canada. On average, the forest was an annual carbon sink of 206 ± 92 g C m^{-2} yr^{-1} over this period and was within the range of NEP values

from other Carolinian forests. Mid-summer meteorological conditions greatly impacted annual NEP. Heat (Ta and Ts) and moisture conditions (P, VPD, and θ) during the summer largely defined the direction of the annual carbon sequestration. The inter-annual variability of temperature was the dominant control on the length of the growing season and the timing of the carbon fluxes. However, seasonal anomalies suggest that even during years with shorter periods of leaf-cover, larger-scale meteorological processes (i.e. temperature and light intensity) determine the overall carbon sequestration of the forest. The forest was an overall annual carbon sink even in years with increased heat and moisture stress. With an increase in these heat and drought events, despite an extension of the growing season predicted under future climates, autumn late-season warming and respiratory losses may significantly impact the strength of annual carbon sequestration at our site. Finally, our findings suggest that even under future warming, our oak dominated forest, at the northernmost extent of deciduous forests in North America, will continue to be a viable option for reforestation practices, due to its continued carbon sink capability even during droughts.

2.7 Acknowledgements

This study was funded by Natural Sciences and Engineering Research Council (NSERC), Global Water Futures Program (GWF) and Ontario Ministry of Environment and Climate Change (MOECC). Funding from the Canadian Foundation of Innovation (CFI) through the New Opportunity and Leaders

Opportunity Fund and Ontario Research Fund of the Ministry of Research and Innovation is also acknowledged. In kind support from the Ontario Ministry of Natural Resources and Forestry (OMNRF) and the Long Point Region Conservation Authority (LPRCA) is acknowledged. We acknowledge support from Zoran Nesic at the University of British Columbia (Dr. T.A Black's group) in assistance with flux measurements at our site. We are grateful members of the Hydrometeorology and Climatology lab for their support in field work and data collection. We acknowledge Dr. Andrew Richardson (Bartlett), Dr. Chris Gough (UMBS), Dr. Gil Bohrer (UMBS), and Dr. Bill Munger (Harvard) for their assistance and guidance with site data used in the regional analysis.

2.8 References

Abrams, M.D., 1998. The red maple paradox. *BioScience*, 48(5), 355-364.

Abrams, M., & Nowacki, G., 1992. Historical Variation in Fire, Oak Recruitment, and Post-Logging Accelerated Succession in Central Pennsylvania. *Bulletin of the Torrey Botanical Club*, 119(1), 19-28.

Aerts, R., 1995. The advantages of being evergreen. *Trends in Ecology & Evolution,* 10(10), 402-407.

Allaby, M., 2006. Biomes of the Earth: Temperate Forests. New York, NY: Chelsea House.

Arain, M.A., & Restrepo-Coupe, N., 2005. Net ecosystem production in a temperate pine plantation in southeastern Canada. *Agricultural and Forest Meteorology*, 128, 223-241.

Barr, A. G., Griffis, T. J., Black, T. A., Lee, X., Staebler, R. M., Fuentes, J. D., Chen, Z., and Morgenstern, K., 2002. Comparing the carbon budgets of boreal and temperate deciduous forest stands. *Canadian Journal of Forest Research*, 32: 813-822.

Barr, A.G., Richardson, A.D., Hollinger, D.Y., Papale, D., Arain, M.A., Black, T.A., Bohrer, G., Dragoni, D., Fischer, M.L., Gu, L., Law, B.E., Margolis, H.A., Mccaughey, J.H., Munger, J.W., Oechel, W., Schaeffer, K., 2013. Use of change-point detection for friction-velocity threshold evaluation in eddy-covariance studies. *Ag. For. Met*., 31–45.

Birdsey, R.A., 1992. Carbon storage and accumulation in United States forest ecosystems. United States Department of Agriculture Forest Service, Gen Technical Report W0-59.

Birdsey, R., Pregitzer, K., Lucier, A. 2006. Forest carbon management in the United States: 1600–2100. *J. Environ. Qual.,* 35:1461–1469.

Black, T.A., Chen, W.J., Barr, A.G., Arain, M.A., Chen, Z., Nesic, Z., Hogg, E.H., Neumann, H.H., and Yang, P.C., 2000. Increased carbon sequestration by a boreal deciduous forest in years with a warm spring. *Geophysical Research Letters*, 27, 1271-1274.

Blouin, G., 2001. An eclectic guide to trees east of the Rockies. Boston Mills Press. Erin, ON.

Bolstad, P.V., Davis, K.J., Cook, B.D., and Wang, W., 2004. Component and whole-system respiration fluxes in northern deciduous forests. *Tree Physiol*., 24 (5), 493-504.

Botkin, D.B., Simpson, L.G., and Nisbet, R.A., 1993. Biomass and carbon storage of the North American deciduous forest. *Biogeochemistry,* 20: 1-17.

Brodeur, J.J., 2014. Data-driven approaches for sustainable operation and defensible results in a long-term, multi-site ecosystem flux measurement program. McMaster University.

Byun, K. & Hamlet, A.F., 2018. Projected changes in future climate over the Midwest and Great Lakes region using downscaled CMIP5 ensembles. *Int. J. Climatol*., 38, e531-e553.

Byun, K., Chiu, C.M., & Hamlet, A.F., 2018. Effects of 21st century climate change on seasonal flow regimes and hydrologic extremes over the Midwest and Great Lakes region of the US. *Science of the Total Environment*, 650, 1261-1277.

Chan, F.C.C., Arain, M.A., Khomik, M., Brodeur, J.J., Peichl, M., Restrepo-Coupe, N., Thorne, R., Beamesderfer, E., McKenzie, S., Xu, B., Croft, H., Pejam, M., Trant, J., Kula, M., and Skubel, R., 2018. Carbon, water

and energy exchange dynamics of a young pine plantation forest during the initial fourteen years of growth. *For Ecol Manag,* 410, 12-26.

Chen, J.M., 1996. Canopy architecture and remote sensing of the fraction of photosynthetically active radiation absorbed by boreal conifer forests. *IEEE Transactions on Geoscience and Remote Sensing*, 34(6), 1353-1368.

Clark, K.L., Skowronski, N. and Hom, J., 2010. Invasive insects impact forest carbon dynamics. *Global Change Biology*, 16(1), 88-101.

Curtis, P.S., Hanson, P.J., Bolstad, P., 2002. Biometric and eddy covariance based estimates of annual carbon storage in five eastern North American deciduous forests. *Agricultural and Forest Meteorology*, 113, 3–19.

Delcourt, H.R., 2000. Eastern deciduous forests. *North American terrestrial vegetation*. 2nd edition. Cambridge University Press, Cambridge, UK.

Elliott, K., McCracken, J.D. and Couturier, A., 1999. A Management Strategy for South Walsingham Sand Ridges/Big Creek Floodplain Forest. Ont. Min. Nat. Resources. London, Ontario. 54.

Fisichelli, N. A., Frelich, L. E. Reich, P. B., 2013. Climate and interrelated tree regeneration drivers in mixed temperate–boreal forests. *Landscape Ecol*., 28 (1), 149-159.

Froelich, N., Croft, H., Chen, J.M., Gonsamo, A., Staebler, R.M., 2015. Trends of carbon fluxes and climate over a mixed temperate-boreal transition forest in southern Ontario, Canada. *Agric. Forest Meteorol*., 211–212, 72–84.

Gao, C., McAndrews, J.H., Wang, X., Menzies, J., Turton, C.L., et al., 2012. Glaciation of North America in the James Bay Lowland, Canada, 3.5 Ma. *Geology*, 40(11), 975-978.

Gaumont-Guay, D., Black, T.A., McCaughey, H., Barr, A.G., Krishnan, P., Jassal, R.S., and Nesic, Z., 2009. Soil CO2 efflux in contrasting boreal deciduous and coniferous stands and its contribution to the ecosystem carbon balance. *Glob. Chang. Biol*., 15: 1302–1319.

Gough, C.M., Hardiman, B.S., Nave, L.E., Bohrer, G., Maurer, K.D., Vogel, C.S., Nadelhoffer, K.J. and Curtis, P.S., 2013. Sustained carbon uptake and storage following moderate disturbance in a Great Lakes forest. *Ecological Applications*, 23(5), 1202-1215.

Goulden, M.L., Munger, J.W., Fan, S.M., Daube, B.C., and Wofsy, S.C., 1996a. Measurements of carbon sequestration by long-term eddy covariance: Methods and a critical evaluation of accuracy. *Global Change Biol.*, 2, 169–182.

Greco, S. & Baldocchi, D.D., 1996. Seasonal variations of CO2 and water vapour exchange rates over a temperate deciduous forest. *Global Change Biology*, 2: 183–197.

Hansen, M.C., Potapov, P.V., Moore, R., Hancher, M., Turubanova, S.A., Tyukavina, A., Thau, D., Stehman, S.V., Goetz, S.J., Loveland, T.R. and Kommareddy, A., 2013. High-resolution global maps of 21st-century forest cover change. *Science*, 342(6160), 850-853.

Hufkens, K., Basler, D., Milliman, T., Melaas, E.K. and Richardson, A.D., 2018. An integrated phenology modelling framework in R. *Methods Ecol Evol*, 9(5), 1276-1285.

IPCC, 2013: Climate Change 2013: The Physical Science Basis. Contribution of Working Group I to the Fifth Assessment Report of the Intergovernmental Panel on Climate Change [Stocker, T.F., D. Qin, G.-K. Plattner, M. Tignor, S.K. Allen, J. Boschung, A. Nauels, Y. Xia, V. Bex and P.M. Midgley (eds.)]. Cambridge University Press, Cambridge, United Kingdom and New York, NY, USA, 1535.

Iverson, L.R., Prasad, A.M., Matthews, S.N. & Peters, M., 2008. Estimating potential habitat for 134 eastern US tree species under six climate scenarios. *Forest Ecology and Management*, 254(3), 390-406.

Johnston, M., 2009. Vulnerability of Canada's tree species to climate change and management options for adaptation: An overview for policy makers and practitioners. Canadian Council of Forest Ministers.

Kljun, N., Calanca, P., Rotach, M.W., Schmid, H.P., 2004. A simple parametrization for flux footprint predictions. *Boundary-Layer Meteorol*. 112, 503–523.

Kula, M. 2013. Determining the effects of climate variability and forest thinning on above ground carbon in temperate forests. McMaster University, School of Geography and Earth Sciences, Master of Science Thesis.

Lauriault, J., 1989. Identification guide to the trees of Canada. National Museum of Natural Sciences. Fitzhenry & Whiteside. Markham, Ontario.

Lee, M.S., Hollinger, D.Y., Keenan, T.F., Ouimette, A.P., Ollinger, S.V. and Richardson, A.D., 2018. Model-based analysis of the impact of diffuse radiation on CO2 exchange in a temperate deciduous forest. Agricultural and Forest Meteorology, 249, 377-389.

Lindeman, R.H., Merenda, P.F., Gold, R.Z., 1980. Introduction to Bivariate and Multivariate Analysis. Glenview, IL: Scott, Foresman and Company.

Malhi, Y., Baldocchi, D.D., and Jarvis, P.G., 1999. The carbon balance of tropical, temperate and boreal forests. *Plant, Cell and Environment*, 22, 715-740.

Munger W., S. Wofsy. 2017. Canopy-Atmosphere Exchange of Carbon, Water and Energy at Harvard Forest EMS Tower since 1991. Environmental Data Initiative. *https://doi.org/10.6073/pasta/dd9351a3ab5316c844848 c3505a8149d*. Dataset accessed 6/06/2019.

Noormets, A., McNulty, S. G., DeForest, J. L., Sun, G., Li, Q. and Chen, J., 2008. Drought during canopy development has lasting effect on annual carbon balance in a deciduous temperate forest. *New Phytologist*, 179: 818–828.

Novick, K.A., Walker, J., Chan, W.S., Schmidt, A., Sobek, C. and Vose, J.M., 2013. Eddy covariance measurements with a new fast-response, enclosed-path analyzer: Spectral characteristics and cross-system comparisons. *Ag. For. Met.*, 181, 17-32.

O'Gorman, P.A. and Schneider, T., 2009. The physical basis for increases in precipitation extremes in simulations of 21st-century climate change. *Proceedings of the National Academy of Sciences*, 106(35), 14773-14777.

Oishi, A.C., Miniat, C.F., Novick, K.A., Brantley, S.T., Vose, J.M. and Walker, J.T., 2018. Warmer temperatures reduce net carbon uptake, but do not affect water use, in a mature southern Appalachian forest. *Agricultural and Forest Meteorology*, 252, 269-282.

Pan, Y., Birdsey, R.A., Fang, J., Houghton, R., Kauppi, P.E., Kurz, W.A., Phillips, O.L., Shvidenko, A., Lewis, S.L., Canadell, J.G. and Ciais, P., 2011. A large and persistent carbon sink in the world's forests. *Science*, 333, 988-993.

Papale, D., Reichstein, M., Aubinet, M., Canfora, E., Bernhofer, C., Kutsch, W., Longdoz, B., Rambal, S., Valentini, R., Vesala, T., Yakir, D., 2006. Towards a standardized processing of Net Ecosystem Exchange measured

with eddy covariance technique: algorithms and uncertainty estimation. *Biogeosciences,* 3, 571–583.

Parsaud, A. 2013. Carbon exchange in a temperate deciduous forest in Southern Ontario. McMaster University, School of Geography and Earth Sciences, M.Sc. Thesis.

Peichl, M., Arain, M.A., Brodeur, J.J., 2010a. Age effects on carbon fluxes in temperate pine forests. *Ag. For. Met*., 150, 1090-1101.

Piao, S. L. et al., 2008. Net carbon dioxide losses of northern ecosystems in response to autumn warming. *Nature*, 451, 49–52.

Presant, E.W. & Acton, C.J., 1984. The Soils of the Regional Municipality of Haldimand-Norfolk. Ontario Institute of Pedology, Ontario Ministry of Agriculture and Food. Report No.57, Vol 2.

Reichstein, M., Falge, E., Baldocchi, D., Papale, D., Aubinet, M., et al., 2005. On the separation of net ecosystem exchange into assimilation and ecosystem respiration: review and improved algorithm. *Glob. Chang. Biol*., 11, 1424–1439.

Richardson, A. D., Jenkins, J.P., Braswell, B.H., Hollinger, D.Y., Ollinger, S.V., and Smith, M.L., 2007a. Use of digital webcam images to track spring green-up in a deciduous broadleaf forest. *Oecologia*, 152: 323–334.

Richardson, A.D., Braswell, B.H., Hollinger, D.Y., Jenkins, J.P., and Ollinger, S.V., 2009. Near- surface remote sensing of spatial and temporal variation in canopy phenology. *Ecological Applications*, 19(6): 1417 – 1428.

Richardson, A.D., Hollinger, D.Y., Dail, D.B., Lee, J.T., Munger, J.W. and O'keefe, J., 2009b. Influence of spring phenology on seasonal and annual carbon balance in two contrasting New England forests. *Tree physiology*, 29(3), 321-331.

Richardson, A.D., Black, T.A., Ciais, P., Delbart, N., Friedl, M.A., Gobron, N., Hollinger, D.Y., Kutsch, W.L., Longdoz, B., Luyssaert, S., et al., 2010. Influence of spring and autumn phenological transitions on forest ecosystem productivity. *Philosophical Transactions of the Royal Society B-Biological Sciences*, 365: 3227–3246.

Richardson, A.D., Hufkens, K., Milliman, T., Aubrecht, D.M., Chen, M., Gray, J.M., Johnston, M.R., Keenan, T.F., Klosterman, S.T., Kosmala, M. and

Melaas, E.K., 2018. Tracking vegetation phenology across diverse North American biomes using PhenoCam imagery. *Scientific Data*, 5, 180028.

Richart, M., and Hewitt, N., 2008. Forest remnants in the Long Point region, Southern Ontario: Tree Species diversity and size structure. *Landscape and Urban Planning*, 86, 25-37.

Schimel, D. S., 1995. Terrestrial ecosystems and the carbon cycle. *Glob Change Biol*, 1: 77–91.

Schmid, H.P., Su, H.-B., Vogel, C.S., and Curtis, P.S., 2003. Ecosystem-atmosphere exchange of carbon dioxide over a mixed hardwood forest in northern lower Michigan, *J. Geophys. Res*., 108(D14), 4417.

Settele, J., R. Scholes, R. Betts, S. Bunn, P. Leadley, D. Nepstad, J.T. Overpeck, and M.A. Taboada, 2014: Terrestrial and inland water systems. In: Climate Change 2014: Impacts, Adaptation, and Vulnerability. Part A: Global and Sectoral Aspects. Contribution of Working Group II to the Fifth Assessment Report of the Intergovernmental Panel on Climate Change [Field, C.B., V.R. Barros, D.J. Dokken, K.J. Mach, M.D. Mastrandrea, T.E. Bilir, M. Chatterjee, K.L. Ebi, Y.O. Estrada, R.C. Genova, B. Girma, E.S. Kissel, A.N. Levy, S. MacCracken, P.R. Mastrandrea, and L.L. White (Eds.)]. Cambridge University Press, Cambridge, United Kingdom and New York, NY, USA, 271-359.

Skubel, R., Arain, M.A., Peichl, M., Brodeur, J.J., Khomik, M., Thorne, R., Trant, J. and Kula, M., 2015. Age effects on the water-use efficiency and water-use dynamics of temperate pine plantation forests. *Hydrological Processes*, 29(18), 4100-4113.

Solomon, A.M. & Bartlein, P.J.,1992. Past and future climate change: response by mixed deciduous-coniferous forest ecosystems in northern Michigan. *Canadian Journal of Forest Research*, 22:1727-1738.

Tyrrell, M. L., Ross, J., & Kelty, M., 2012. Carbon dynamics in the temperate forest. In: Ashton, M. S., Tyrrell, M. L., Spalding, D., & Gentry, B. (Eds.). Managing Forest Carbon in a Changing Climate. *Springer Science & Business Media*, 77-107.

Urbanski, S., Barford, C., Wofsy, S., Kucharik, C., Pyle, E., Budney, J., McKain, K., Fitzjarrald, D., Czikowsky, M. and Munger, J.W., 2007. Factors controlling CO2 exchange on timescales from hourly to decadal at Harvard Forest. *JGR: Biogeosciences*, 112(G2).

U.S. Global Change Research Program (USGCRP), 2017. Climate Science Special Report: Fourth National Climate Assessment, Volume I, [Wuebbles, D.J., Fahey, D.W., Hibbard, K.A., Dokken, D.J., Stewart, B.C., and Maycock, T.K. (eds.)]. Washington, DC, USA.

Varga, S., 1985. Vegetation Inventory of Backus Woods: Report submitted to the Backus Group. Ontario Heritage Foundation and Ontario Ministry of Natural Resources.

Vasseur, L., 2012. Restoration of Deciduous Forests. *Nature Education Knowledge*, 3(12):1.

Vose, J.M., Peterson, D.L. and Patel-Weynand, T., 2012. Effects of climatic variability and change on forest ecosystems: a comprehensive science synthesis for the US. Gen. Tech. Rep. PNW-GTR-870. Portland, OR: US Department of Agriculture, Forest Service, Pacific Northwest Research Station, 265, 870.

Way, D.A. & Oren, R., 2010. Differential responses to changes in growth temperature between trees from different functional groups and biomes: a review and synthesis of data. *Tree Physiology*, 30(6), 669-688.

Wilson, K.B. & Baldocchi, D.D., 2000. Seasonal and interannual variability of energy fluxes over a broadleaved temperate deciduous forest in North America. *Agricultural and Forest Meteorology*, 100(1), 1-18.

Xie, J., Chen, J., Sun, G., Chu, H., Noormets, A., Ouyang, Z., John, R., Wan, S. and Guan, W., 2014. Long-term variability and environmental control of the carbon cycle in an oak-dominated temperate forest. *Forest Ecology and Management*, 313, 319-328.

Zhu, K., Woodall, C.W., & Clark, J.S., 2012. Failure to migrate: lack of tree range expansion in response to climate change. *Global Change Biology*, 18(3), 1042-1052.

Table 2.1: Turkey Point Deciduous (TPD) site characteristics

Stand Parameter	**Condition**
Location	42˚ 38’ 7.124’’ N 80˚ 33’ 27.222’’ W
Stand Age	70 – 110 years
Ground Elevation above Sea Level	210.6 m
Dominant Overstory Species	White Oak (*Quercus alba*)
Secondary Overstory Species	Red Oak (*Quercus rubra*) Sugar Maple (*Acer saccharum*) White Pine (*Pinus strobus*) Red Maple (*Acer rubrum*) American Beech (*Fagus grandifolia*) Yellow Birch (*Betula alleghaniensis*)
Understory Species	Putty Root (*Aplectrum hyemale*) Yellow Mandarin (*Disporum lanuginosum)* Canada Mayflower (*Maianthemum canadense)* Red Trillium (*Trillium erectum*) Black Cherry (*Prunus serotina*) Horsetail (*Equistum*) Wood Violet (*Viola palmata*)
Maximum Leaf Area Index (LAI)	8.0 m^2 m^{-2}
Mean Diameter at Breast Height (DBH)[a]	23.14 ± 14.05 cm
Mean Tree Height [a]	25.7 ± 7.44 m
Stem Density [a]	504 ± 181 ha^{-1}
Mean Tree Basal Area [a]	0.06 ± 0.02 m^2

[a] Kula (2013)

Table 2.2: Seasonal sums of carbon fluxes (NEP, GEP, and RE), sum of precipitation (P), and mean seasonal air temperature (Ta) and vapor pressure deficit (VPD) values are shown. Winter calculations for each year used December values from the previous year. 5-year seasonal means are also shown. Mean values in brackets (Ta and P) are measured 30-year means from the Environment Canada Delhi CDA weather station (Environment and Climate Change Canada).

	Season	2012	2013	2014	2015	2016	Mean
NEP sum ($g\ C\ m^{-2}$)	Spring	-17	-23	-58	-32	-71	-40
	Summer	379	287	448	265	373	350
	Fall	8	-50	-16	-65	-30	-31
	Winter	-50	-60	-61	-66	-98	-67
GEP sum ($g\ C\ m^{-2}$)	Spring	179	153	100	159	117	142
	Summer	787	936	980	907	945	911
	Fall	232	280	303	281	357	291
	Winter	--	--	--	--	--	--
RE sum ($g\ C\ m^{-2}$)	Spring	214	182	173	205	204	196
	Summer	408	648	531	638	570	559
	Fall	234	339	323	351	389	327
	Winter	60	90	78	74	108	82
P sum (mm)	Spring	115	214	233	190	231	197 (266)
	Summer	159	267	244	206	144	204 (236)
	Fall	311	256	373	218	311	294 (255)
	Winter	143	206	188	104	189	166 (218)
Ta avg. (°C)	Spring	11.7	7.50	5.66	7.20	7.89	7.99 (6.87)
	Summer	22.9	20.3	20.1	19.9	22.0	21.0 (20.0)
	Fall	11.4	10.8	10.7	13.1	13.6	11.9 (9.90)
	Winter	0.27	-0.14	-5.56	-5.40	0.49	-2.07 (-3.85)
VPD avg. (kPa)	Spring	0.85	0.54	0.43	0.50	0.54	0.57
	Summer	1.33	0.75	0.79	0.77	1.01	0.93
	Fall	0.61	0.45	0.47	0.55	0.52	0.52
	Winter	0.23	0.41	0.26	0.29	0.38	0.31

Table 2.3: Relative linear-fit calculated contribution of the individual explantaory variables to the multivariate models of daytime, growing season net ecosystem productivity (NEP), gross ecosystem productivity (GEP), and ecosystem respiration (RE), as well as model performance. Variables included in the model were PAR, VPD, Ts_{5cm} and $\theta_{0\text{-}30cm}$. Analysis was performed at daily and half-hourly time scales. NS indicates that a variable was not significant in the model.

	Daily			***Half-Hourly***		
	NEP	GEP	RE	NEP	GEP	RE
PAR *(% r^2)*	18.5	8.89	NS	58.5	41.3	0.17
VPD *(% r^2)*	NS	1.93	3.69	11.1	11.0	1.83
Ts $_{5cm}$ *(% r^2)*	32.2	68.3	95.3	24.3	43.2	97.1
$\theta_{0\text{-}30cm}$ *(% r^2)*	2.20	0.49	9.32	0.58	NS	12.9
Model r^2	0.32	0.70	0.82	0.47	0.61	0.81
F-statistic *($\alpha < 0.001$)*	94	462	886	4.03E3	7.02E3	1.93E4

Table 2.4: Summary of site characteristics (i.e. location & dominant tree species), mean annual Ta (°C), total annual P (mm), and fluxes (NEP, GEP, RE in g C m^{-2} yr^{-1}) of Eastern North American deciduous forests, from 2012 to 2016.

Site	Location	Species	Ta (°C)	P (mm)	Year	Age	NEP	GEP	RE	Site Reference
Coweeta (US-Cwt)	35.0592; -83.4275	Tulip Poplar, White Oak, Black Birch, Red Maple	13	1495	2012	81	194	1563	1369	Novick et al. (2013) Oishi et al. (2018)
					2013	82	364	1602	1238	
					2014	83	315	1552	1237	
					2015	84	147	1463	1316	
Harvard Forest (US-Ha1)	42.5369; -72.1725	Red Oak, Red Maple, Eastern Hemlock	6.6	1071	2012	74	339	1684	1345	Urbanski et al. (2007) Munger et al. (2017)
					2013	75	218	1495	1277	
					2014	76	459	1557	1098	
					2015	77	194	1600	1406	
Turkey Point Deciduous (CA-TPD)	42.6353; -80.5577	White Oak, Sugar Maple, Red Maple, American Beech	8	1036	2012	90*****	292	1198	954	This Study
					2013	91*****	156	1369	1250	
					2014	92*****	305	1382	1110	
					2015	93*****	90	1347	1283	
					2016	94*****	185	1420	1260	
Bartlett (US-Bar)	44.0639; -71.2874	Red Maple, Sugar Maple Paper Birch, American Beech	6.6	1300	2012	110*****	114	1291	1177	Lee et al. (2018)
					2013	111*****	120	1309	1189	
					2014	112*****	102	1314	1200	
					2015	113*****	110	1268	1166	
					2016	114*****	69	1378	1269	
University of Michigan Biological Station (US-UMB)	45.5598, -84.7138	Red Oak, Sugar Maple, Red Maple, Bigtooth Aspen	5.5	817	2012	89	331	1309	978	Gough et al. (2013)
					2013	90	214	1180	966	
					2014	91	172	1299	1127	
					2015	92	229	1315	1081	
					2016	93	182	1318	1131	
Mean			**7.94**	**1144**			**213±102**	**1401±138**	**1192±124**	

*Mean forest age used in analysis. CA-TPD: 70 – 110 years; US-Bar: 90 – 130 years.

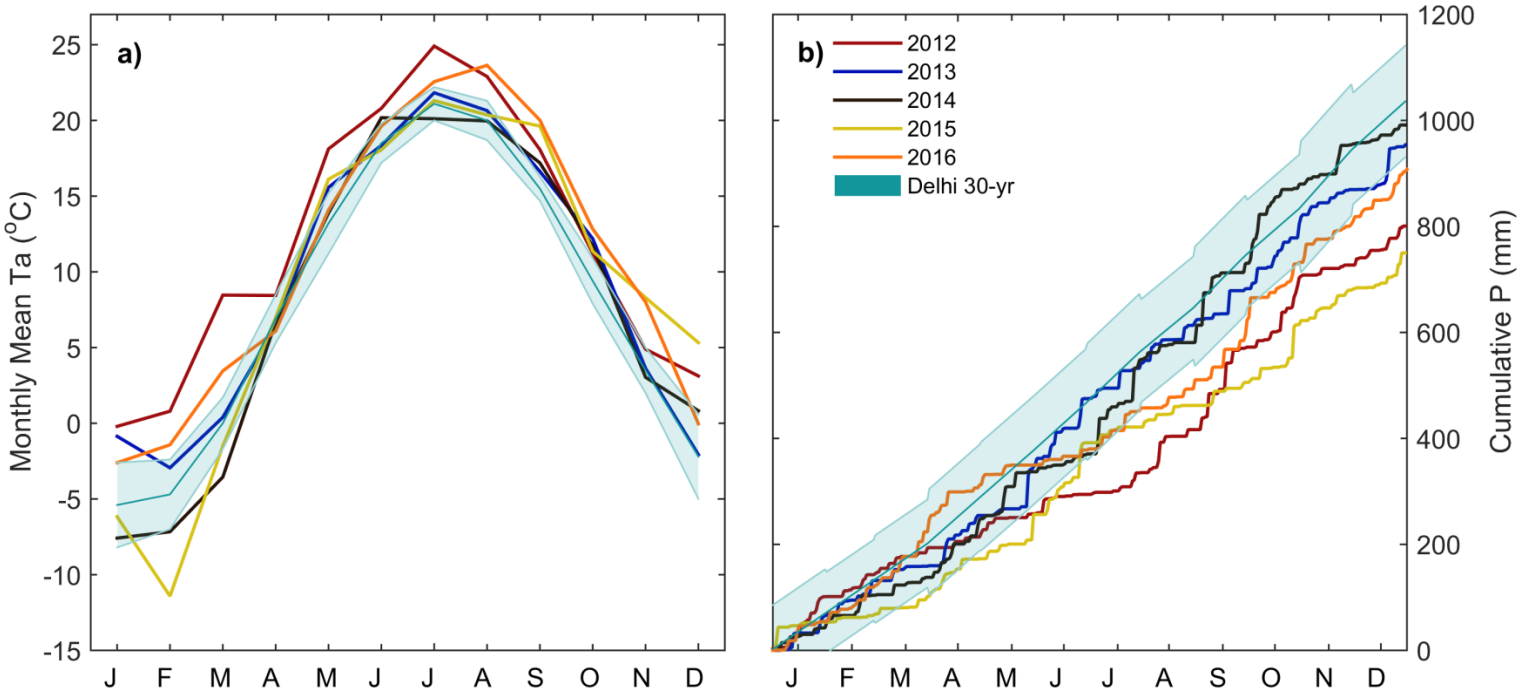

Figure 2.1: Monthly mean (a) air temperature (Ta) and (b) cumulative precipitation (P) from 2012 to 2016. The Environment Canada Delhi CDA weather station measured 30-year mean Ta and P values are plotted in teal, with the monthly standard deviation shaded.

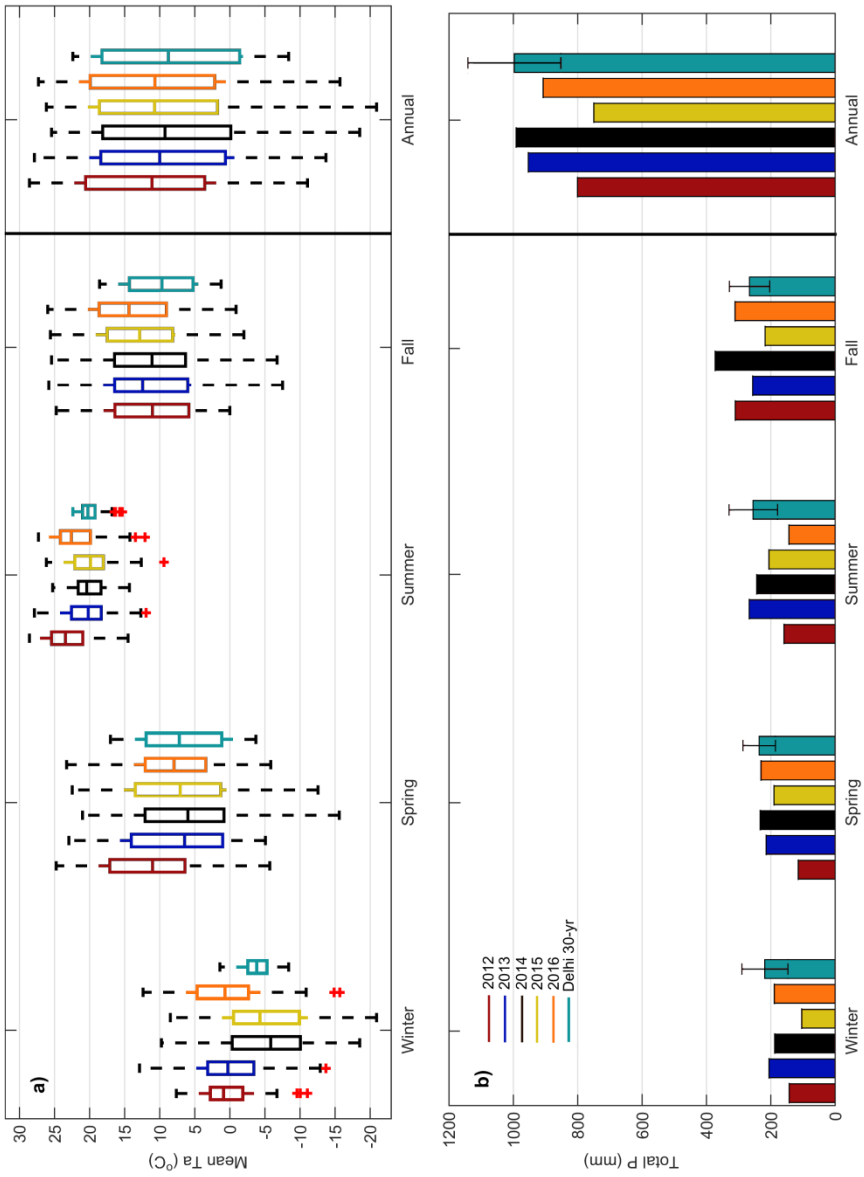

Figure 2.2: (a) Box plot of seasonal (i.e. winter, spring, summer, fall) and annual mean air temperature (Ta) from 2012-2016 including the Environment Canada Delhi 30-year mean Ta (teal), and (b) the total sum of seasonal and annual precipitation (P), including 30-year mean P with standard deviation.

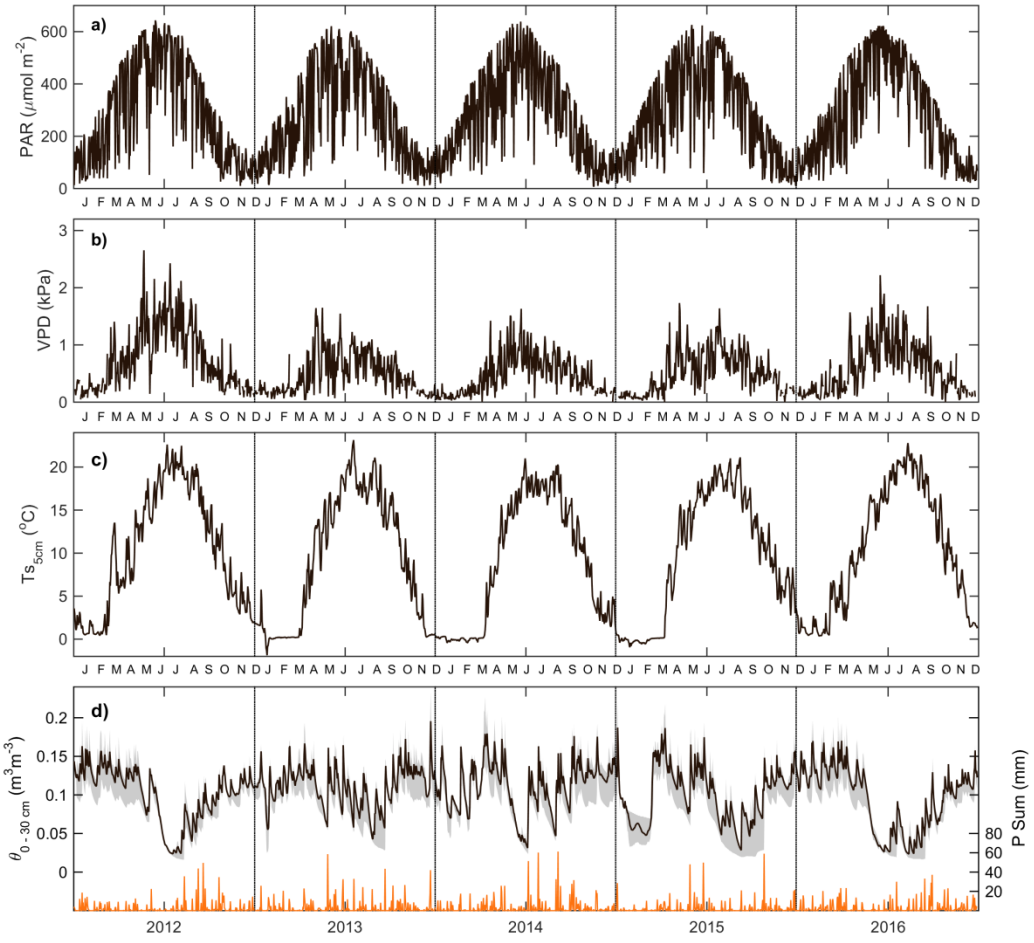

Figure 2.3: Daily time series from 2012-2016 of the mean (a) photosynthetically active radiation (PAR), (b) vapor pressure deficit (VPD), (c) soil temperature at 5 cm depth (Ts_{5cm}), (d; left) the mean volumetric water content (θ) between 0 and 30 cm depths, and (d; right) daily sum of P. Grey shading (d) includes the range (5 – 50 cm) of θ within the mean 0 – 30 cm column of soil.

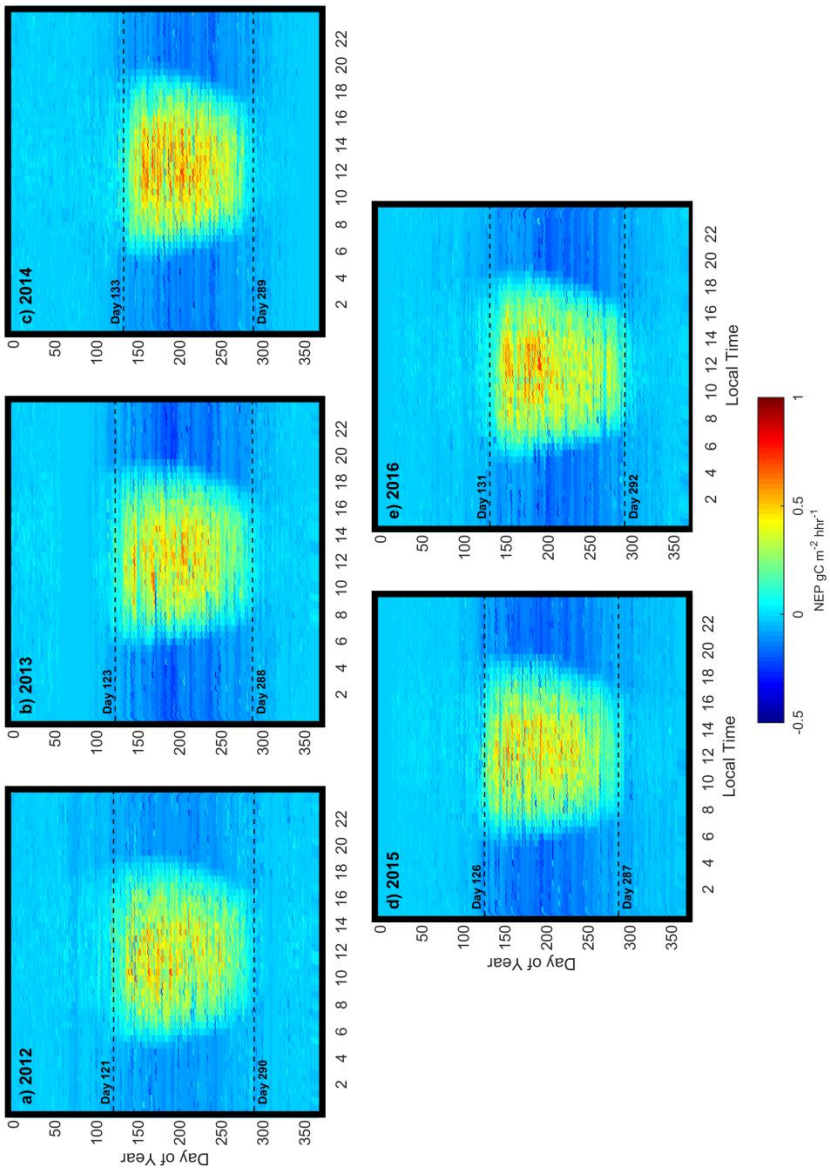

Figure 2.4: (a – e) Gap-filled half-hourly net ecosystem productivity (NEP, g C m^{-2} hr^{-1}) plotted each half hour of the day (local time, x-axis) and day of year (y-axis) from 2012 to 2016. The timing of leaf-out and leaf-fall determined by transitions in PhenoCam greenness chromatic coordinate (GCC) values are labeled annually by horizontal dashed lines.

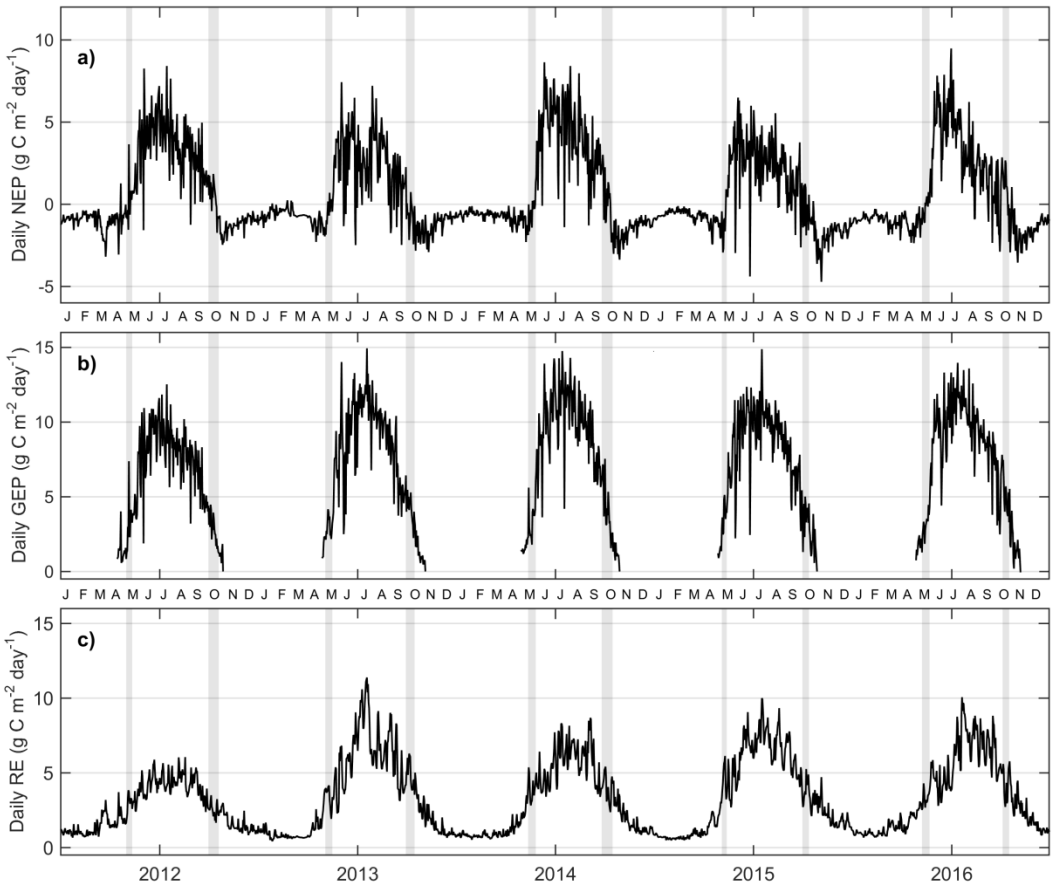

Figure 2.5: Daily sums of (a) net ecosystem productivity (NEP), (b) gross ecosystem productivity (GEP), and (c) ecosystem respiration (RE) from 2012-2016. Grey shading illustrates the 10% to 50% range of transition dates derived from PhenoCam GCC measurements. Note: NEP (a) y-axis (i.e. -5 to 10 g C m^{-2} day^{-1}) is not the same as GEP (b) and RE (c) (i.e. 0 to 15 g C m^{-2} day^{-1}).

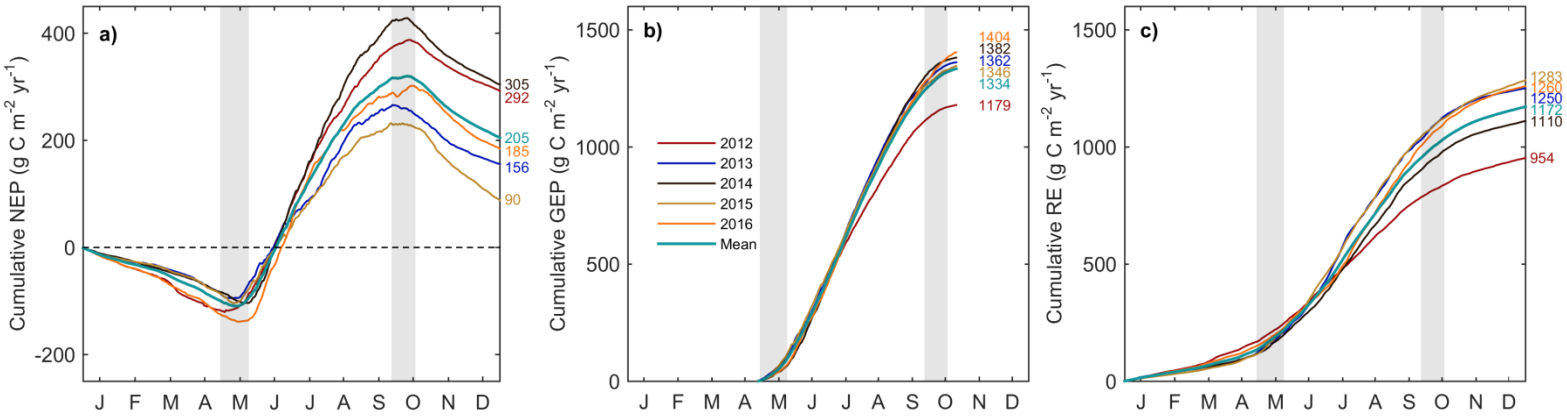

Figure 2.6: Annual (a) cumulative daily sums of NEP, (b) GEP (from days 119 to 300, encompassing all years), and (c) RE, from 2012-2016. Grey shading (same as Figure 2.5) covers the entire range of growing season transition dates for the five years of data. Cumulative annual sums values also shown on the right of each figure (g C m^{-2} yr^{-1}).

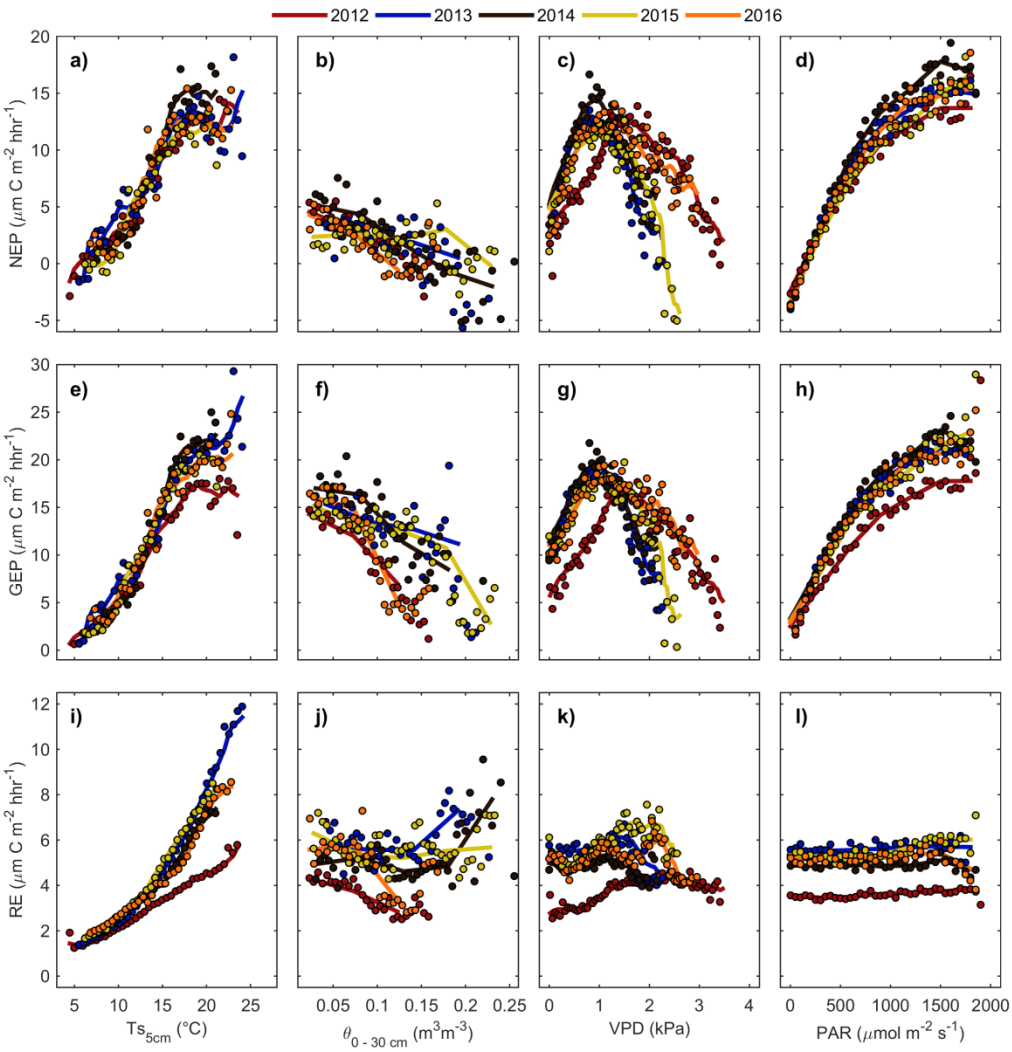

Figure 2.7: (a) Non-gapfilled growing season net ecosystem productivity (NEP) versus bin averaged 5 cm soil temperature (Ts_{5cm}, bin size of 0.5°C), (b) bin averaged 0 to 30 cm volumetric water content ($\theta_{0\text{-}30cm}$, bin size of 0.005 m^3 m^{-3}), (c) bin averaged vapour pressure deficit (VPD, bin sizes of 0.05 kPa), and bin averaged photosynthetically active radiation (PAR, bin sizes of 50 µmol m^{-2} s^{-1}). (e-h) Same analysis for gross ecosystem productivity (GEP) and (i-l) ecosystem respiration (RE) also shown. Solid lines are annual moving average fits.

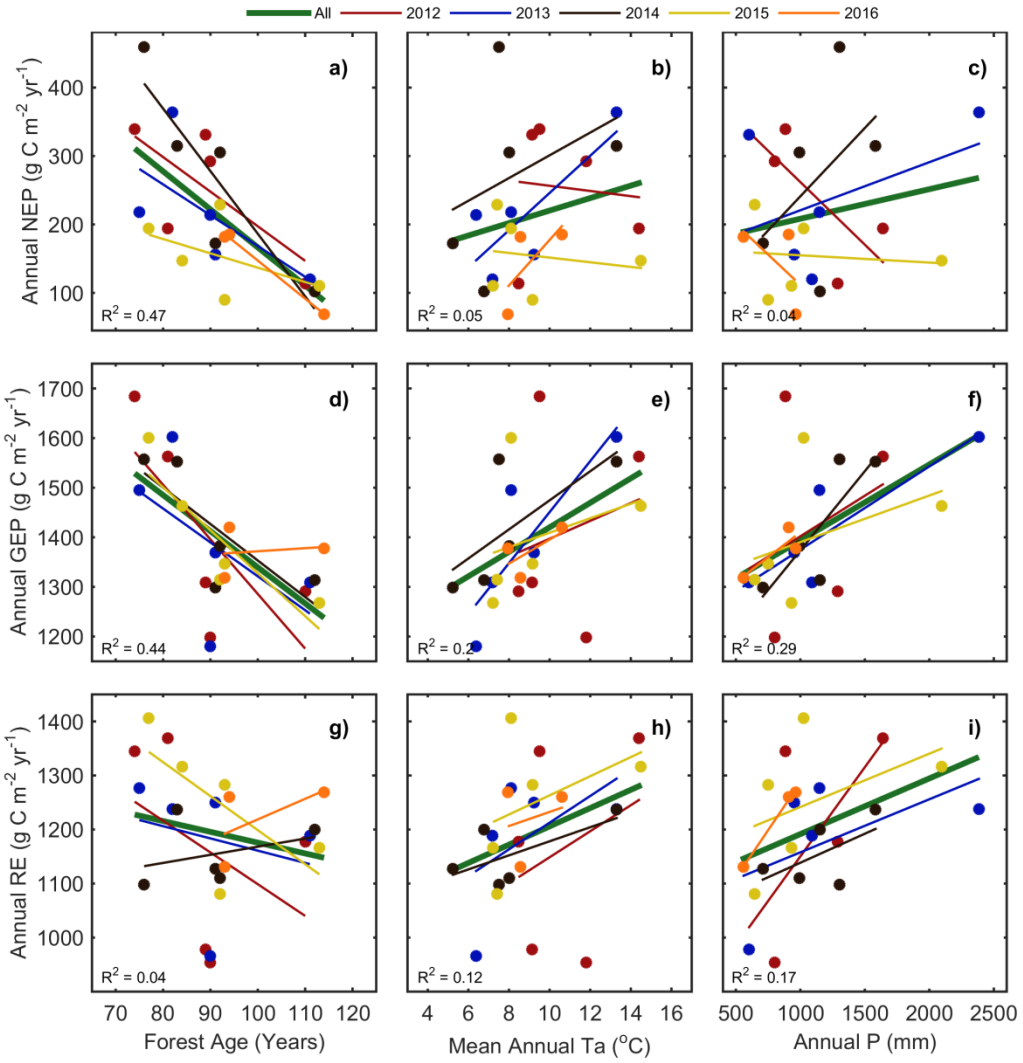

Figure 2.8: Linear relationships from 2012-2016 between (a-c) annual NEP, (d-f) GEP, and (g-i) RE, and site characteristics of North American deciduous forest research sites included in the regional analysis, including: (a, d, g) forest age, (b, e, h) mean annual air temperature (Ta), and (c, f, i) total annual P. The fit of each year is color coded, while the listed R^2 value is for all data (dark green line).

CHAPTER 3:

THE IMPACT OF SPRING AND AUTUMN SEASONS' TIMING AND DURATION ON THE CARBON UPTAKE OF A TEMPERATE DECIDUOUS FOREST IN EASTERN NORTH AMERICA

3.1 Abstract

Within the temperate deciduous forests of North America, phenology plays an important role in determining the timing and length of the growing season, ultimately affecting annual rates of carbon uptake. This is especially true of phenology during the shoulder seasons, such as spring and autumn. While many studies have analyzed the impact of the onset of early spring on forest carbon dynamics, few have analyzed the impact of an extended autumn season. This study examined the interaction of carbon emissions, phenology, and climate during six years (2012 – 2017) in a deciduous forest in the Great Lakes Region of southern Ontario, Canada. Spring and autumn phenological transition dates were calculated for each year from measured carbon flux data as well as from digital camera greenness indices (GCC). The calculated phenological transition dates were then compared to various climatic drivers. We show that the timing of both spring and autumn transition dates were impacted by seasonal changes in air temperature and other meteorological variables. In general, years with warm early-May conditions saw an advanced start to the growing season in the study region, while years with warm October and November conditions saw a

prolonged autumn season and prolonged growing season end dates. In contrast to results of past studies, we show that an earlier start to the growing season in spring, and the resulting extended growing season length, does not necessarily translate into an increased annual carbon uptake by the forest. The two years with the latest growing season starts and shortest growing season lengths were the largest annual sinks of carbon in our study. We also found that the variability in autumn phenological dates was greater than that of spring dates. Prolonged autumns negatively impacted the overall annual carbon uptake of the forest, because the steady carbon emissions by ecosystem respiration outweighed the reducing carbon uptake by photosynthesis, when warm temperatures persisted and daylight length (photoperiod) shortened. Our results suggest that if the growing season extends and phenological transition dates shift, due to warming in the autumn shoulder season, this may negatively impact the overall annual carbon uptake of deciduous forests in eastern North America. Finally, in our analysis we found that while GCC data could not capture peak photosynthesis dates, it was able to accurately capture key changes in photosynthesis associated with spring and autumn transition dates, which may be useful in remote sensing applications.

3.2 Introduction

The variability of carbon uptake within temperate deciduous forests is governed by numerous meteorological variables, including surface phenology (Froelich et al., 2015). Studies have shown phenology to be primarily driven by air

temperature, leading to annual differences in the timing and duration of the growing season within deciduous forests (Richardson et al., 2010, Vitasse et al., 2011; Barichivich et al., 2013; Shao et al., 2015). Recent increases in temperature, due to global climate warming, especially in northern latitudes, have impacted the timing of phenological stages by advancing leaf emergence in the spring and delaying leaf senescence in the autumn (Richardson et al., 2013; Fu et al., 2014; Piao et al., 2019). While phenology within temperate deciduous forests is flexible and congruent to local meteorological and climatological conditions, the timing of emergence and senescence, marking the photosynthetic season, can have significant effects on seasonal variations of surface-atmosphere interactions and carbon uptake (Baldocchi et al., 2005; Polgar & Primack, 2011). Earlier spring leaf emergence may promote increased photosynthetic gains and enhanced carbon uptake due to greater precipitation and/or radiation interception within a forest canopy (White et al., 1999; Richardson et al., 2010). However, increased canopy uptake may also negatively impact the temperature, moisture, and energy profiles of understory vegetation and soil, dependent on typical early non-growing season conditions (Wilson and Baldocchi, 2001; Morisette et al., 2009). Furthermore, increased spring warming may lead trees to experience an increased risk of freezing temperatures or frost damage following leaf emergence (Cannell & Smith, 1986; Polgar & Primack, 2011). In the autumn, the carbon uptake potential of many tree species is shown to decrease due to light limitations from low irradiance and the shortening of the daily photoperiod (Morecroft et al., 2003;

Froelich et al., 2015). Therefore, higher autumn temperatures, acting to extend the growing season, may lead to respiratory losses which exceed photosynthetic gains experienced earlier in the spring, leading to a possible reduction in forest carbon uptake (Dunn et al., 2007; Piao et al., 2008).

Globally, predicted increases in temperatures and variability in the timing and frequency of precipitation will put the future of forest carbon and water cycles and stores at risk, as they have been reported to be sensitive to changes in climate (Bonan, 2008; Allen et al., 2010; Vose et al., 2012; Reichstein et al., 2013; Pachauri et al., 2014). Within the Great Lakes Basin of Eastern North America, a region containing extensive temperate mixed and deciduous broadleaf forests (Wolter et al., 2006; Danz et al., 2007), accelerated climate change conditions are expected by the end of the 21st century (IPCC, 2013; USGCRP, 2017). In this region, predicted increases in mean winter (3 – 7°C) and summer temperatures (3 – 11°C) may lead to increases in growing season length as well as shifts in the composition, range, structure, and diversity of tree species within these forests (Kling et al. 2003; Iverson et al., 2008; Scheller et al., 2008; Zhu et al., 2012; IPCC, 2013; Duveneck et al., 2014). Changes in the local phenology and meteorology may also promote the migration of trees to higher latitudes, with evidence suggesting strong northward shifts of 10 to 15 km per decade in many northern hardwood forests around the Great Lakes (Iverson et al., 2004; Bertin, 2008; Woodall et al., 2009; Lafleur et al., 2010; Vitasse et al., 2011). Such modifications to forest diversity and structure may lead to changes in a forests

resilience or resistance to changing meteorological conditions, ultimately shaping forest carbon uptake (Chapin et al., 1998; Erskine et al., 2006; Paquette and Messier, 2010). Earlier emergence from certain species in the spring with minimal temperature or light requirements (i.e. chilling, photoperiod, shade-tolerance, etc.), could alter the leaf emergence timing and carbon uptake of an entire forest (Goulden et al., 1996; Morecroft et al., 2003). Conversely, a delay in the response of tree species to these phenological changes may lead to species mortality and decreases in ecosystem-scale resilience and carbon uptake capacity (Soja et al. 2007, Scheller et al. 2008, Frelich and Reich 2010). Overall, the degree at which changes in phenology and climate will affect carbon sequestration within temperate forests remains uncertain (Grace & Rayment, 2000; Barr et al., 2002; Polgar & Primack 2011). Therefore, the evaluation of the interaction between forest climate, phenology, and carbon sequestration requires continued exploration.

Of particular importance to the phenology of temperate deciduous forests are the transition or shoulder seasons (Monson et al., 2005; Garrity et al., 2011; Wu et al., 2012; Wu et al., 2013), loosely defined as the periods of rapid leaf growth and decay, outside of the period of maximum photosynthetic uptake. The shoulders, beginning with the start of the growing season to the end of leaf emergence/bud burst in the spring, and the initiation of leaf senescence to the end of the growing season in the autumn, will likely have a greater control on carbon balances of temperate deciduous forests under future climates, as compared to the

peak growing season (Kramer et al., 2000; Richardson et al., 2009b; Kwit et al., 2010; Desai, 2010). This study: (i) examined the climatic controls on spring and autumn phenology in a temperate deciduous forest at the northern extent of North American deciduous forests, (ii) analyzed how these controls influenced annual carbon sequestration as the result of variability in shoulder season lengths and duration, and (iii) outlined the implications of climate-phenology interactions on forest carbon uptake capacity in the area, under predicted future climate warming.

3.3 Methods

3.3.1 Site Description

This study was conducted at the Turkey Point Deciduous (TPD) forest (42°38'7"N, 80°33'28"W; elevation 265 m), located approximately 10 km northwest of Long Point Provincial Park on the northern shore of Lake Erie in southern Ontario, Canada. The study site is part of the Turkey Point Observatory, Global Water Futures Program, and global FLUXNET network. The site is a naturally grown eastern deciduous (Carolinian) forest, with small portions of forested land regenerated from abandoned agricultural land and natural sandy terrain. The site is located on lightly undulating terrain within the Southern Norfolk Sand Plains, containing predominantly sandy (Brunisolic gray brown luvisol, following the Canadian Soil Classification Scheme) well drained soil, with a low-to-moderate water holding capacity. The dominant tree species is white oak (*Quercus alba*), with other hardwood species including: black and red

oak (*Q. velutina, Q. rubra*), sugar and red maple (*Acer saccharum, A. rubrum*), American beech (*Fagus grandifolia*), white ash (*Fraxinus americana*) and yellow birch (*Betula alleghaniensis*). Scattered white pines (*Pinus strobus*) make up less than 5% of the tree population. Tree cores estimate the forest to be 70 – 110 years old, with some pine species likely dating back to the early 1900s (personal communication, Dr. Shawn McKenzie, McMaster University). The climate of the region is defined as humid cool-temperate with warm summers and cool winters (Meteorological Service of Canada). Climate records from the Delhi CDA weather station (25 km) north of the site found the 30-year (1981 – 2010) mean annual air temperature and annual precipitation to be 8.0°C and 997 mm, respectively. Further site details can be found in Beamesderfer et al., (2019a).

3.3.2 Meteorological Measurements

Meteorological measurements have been conducted at this site since January 2012 and are presently ongoing. Air temperature (Ta), relative humidity (RH), wind speed and direction, upward (PARup) and downward (PARdn) photosynthetically active radiation, and upward and downward shortwave (SW) and longwave (LW) radiation are measured at 36 m height atop a walk-up scaffold tower. Soil temperature (Ts) and soil volumetric water content (θ) are measured at five depths (2, 5, 10, 20, 50, and 100 cm) at two soil pit locations near the scaffold tower and are averaged for a more spatially representative value. Shallow rooting zone θ ($\theta_{0\text{-}30cm}$) was calculated using depth-weighted averages following McLaren et al.

(2008). Precipitation (P) is measured in a small forest opening, 350 m southwest of the tower. All data (meteorological, soil, and precipitation) are sampled and recorded using data loggers with automated data downloads occurring every half hour on a desktop computer in a trailer at the base of the tower.

3.3.3 Flux Measurements and Calculations

Half-hourly fluxes of momentum, sensible heat (Hs), latent heat (LE) and CO_2 (F_c) have been measured continuously using a closed-path eddy covariance (CPEC) system, since January 2012. This study examines the first 6 years (2012 – 2017) of data recorded, while measurements are still ongoing today. The CPEC setup consists of an enclosed infrared gas analyzer (IRGA) (LI-7200, LI-COR Inc.) and a 3D sonic anemometer (CSAT3, Campbell Scientific Inc.) mounted atop a walk-up scaffold tower, oriented west at 36 m height. Eddy covariance (EC) fluxes are sampled at 20 Hz frequency and averaged half-hourly on site, using custom software developed by the Biometeorology & Soil Physics Group at the University of British Columbia, Canada.

The CO_2 storage (S_{CO2}) within the column of air below the EC sensors is calculated by vertically integrating the difference between the current and previous half-hourly measured CO_2 concentrations above the canopy at 36 m height and mid-canopy at 16 m height. Net ecosystem exchange (NEE, µmol m^{-2} s^{-1}) is then calculated as the sum of the vertical CO_2 flux (F_c), and the change of CO_2 storage ($NEE = F_c + S_{CO2}$). Both vertical and horizontal advections are

assumed to average to zero over long periods and were not considered. Net ecosystem productivity (NEP) is defined as the opposite of NEE (NEP = - NEE), where positive NEP (-NEE) indicates carbon uptake (sink) by the forest, and negative NEP (+NEE) is carbon loss (source) from the forest to the atmosphere. All EC flux and meteorological data were cleaned and gap-filled (if necessary) using custom software implemented by Brodeur (2014), following protocols designed by the AmeriFlux Network. Further threshold passing methods (i.e. footprint model and u-star [friction-velocity] threshold) were incorporated into the data processing to remove unrepresentative data (Kljun et al., 2004; Brodeur, 2014; Beamesderfer et al., 2019a).

Ecosystem respiration (RE) was modeled as a function of Ts_{5cm} and $\theta_{0\text{-}30cm}$ (Brodeur, 2014) using fitted temperature response parameters (R_{10} & Q_{10}) in order to accurately describe the relationship between RE and $Ts_{5cm.}$ Large gaps in Ts_{5cm} were gapfilled using a relationship with Ta for the site. Each half-hourly point was then scaled by the same ΔTa or ΔTs_{5cm}. Gross ecosystem productivity (GEP) was estimated by subtracting measured NEE from daytime modeled RE. During periods where there were gaps in NEE data, GEP was modelled using a rectangular hyperbolic function defined by the relationship between GEP and PAR, and scaling responses of GEP to Ts, vapor pressure deficit (VPD) and $\theta_{0\text{-}30cm}$ (Brodeur, 2014; Beamesderfer et al., 2019a). Gaps in NEE due to instrumentation errors, calibrations, and power failure were filled as the difference between modeled GEP and RE.

3.3.4 Phenological Calculations

Daily maximum photosynthetic uptake (GEP_{Max}) was calculated using half-hourly non-gapfilled GEP. This was done to remove potential biases of meteorological responses to GEP found from using site specific gapfilling equations, which can be found in Beamesderfer et al. (2019a). GEP_{Max} was calculated daily and fit using a double logistic function described by Gonsamo et al. (2013). Following the initial fit, a Grubb's test was conducted to statistically ($p < 0.01$) remove outliers in GEP_{Max} data using the approach outlined by Gu et al. (2009). With outliers removed, the function was fit once more. The Gonsamo et al. (2013) approach allows transition dates, and therefore phenological events, to be identified using first, second, and third derivatives of the logistics curves. The second derivatives effectively estimate the end of greenup (EOG), the length of canopy closure (LOCC), and the start of browndown (SOB), while the third derivatives calculated the start of the growing season (SOS), and the end of the growing season (EOS). SOS marks the end of winter dormancy, and the beginning of the photosynthetic season in spring. The phenologically defined spring season is defined as the period from SOS to EOG. Phenologically defined summer or peak carbon uptake period is defined as the entire LOCC period from the day of EOG to day of SOB, bound by spring and autumn shoulder seasons. LOCC also corresponds to the period between the onset and end of maximum leaf area index (LAI). Finally, the resulting phenologically defined autumn season is from SOB date to EOS date. EOS date marks the end of photosynthetic activity in

autumn. The length of the overall growing season (LOS) was calculated as the number of days between SOS and EOS (Gonsamo et al., 2013).

Phenological imagery and greenness values were downloaded every half hour using a PhenoCam web camera (StarDot NetCam SC) installed at 36m height on top of the scaffold walk-up tower, as part of the PhenoCam network (Richardson et al., 2007a; Richardson et al., 2009a), which provides near-surface, automated remote sensing of canopy phenology at flux towers across North America. Supplementary to the main phenological date calculations, key growing season dates (phenophases) were calculated by changes in the greenness chromatic coordinate (GCC), calculated from the PhenoCam imagery, using the PHENOCAM R package (Richardson et al., 2007a; Toomey et al., 2015; Hufkens et al., 2018). Dates identifying the 10%, 25%, and 50% amplitudes from seasonal GCC minima at the start and end of the growing season were used in this analysis (Richardson et al., 2018). These dates were used for comparison to the modeled phenology dates using photosynthesis (GEP).

Lastly, the impact of climate on phenology was examined by the use of growing degree days (GDD) and cooling degree days (CDD), in order to understand the thermal response of the forest. In the spring, GDD accumulation occurred during periods where the mean daily Ta was greater than 10°C. In the autumn, cooling degree days were calculated using the daily mean Ta below a base Ta of 20°C (Richardson et al., 2006; Gill et al., 2015). Both the cumulative

degrees and number of days matching the growing or cooling criteria were considered in the analysis.

3.3.5 Modelling the Impact of Fluctuating Temperatures on Carbon Fluxes

In an attempt to better understand future changes in forest productivity due to climate, sums of predicted GEP, RE, and NEP (GEP – RE) were created each year to provide a baseline estimate (i.e. change in air temperature (ΔTa) = 0). Then ten scenarios were calculated, by adding ΔTa to the original Ta time series, by increments of 0.1°C from -0.5°C to 0.5°C (i.e. ΔTa: -0.5:0.1:0.5). For each scenario, the original Ta and Ts values were substituted by Ta + ΔTa or Ts + ΔTs in estimates of RE and GEP, using previously parameterized models used in flux data gapfilling and partitioning as described above. Modified annual sums were then calculated to estimate the effects a 1°C Ta change could potentially have on fluxes. All data processing, analyses and figures were completed using MatLab software (The MathWorks Inc.).

3.4 Results

3.4.1 Climate Influences on Phenology

Figure 3.1 illustrates the seasonal and annual variations in key meteorological variables from 2012 to 2017. The timing and shape of total daily incoming photosynthetically active radiation (PAR_{dn}) was consistent each year, though decreased summer PAR_{dn} was measured during both 2013 and 2015 (Figure 3.1a).

Decreases in total daily PAR_{dn} can be attributed to cloudy or wet conditions. Daily mean air temperature (Ta) varied from -20°C in the winter up to 30°C in the summer (Figure 3.1b). In all years, except for 2014 (8.0°C), mean annual Ta exceeded the 30-year (Environmental Canada) mean (8.0°C). A more detailed analysis of Ta anomalies in comparison to the 30-year norms is shown in Figure 3.2. The daily mean vapor pressure deficit (VPD) was consistent for most years, with a peak present in the early to-mid summer, before decreasing later in the year (Figure 3.1c). An apparent outlier in daily VPD was found in 2012, when extreme heat and dry conditions throughout much of the year led to heightened VPD exceeding all other years of measurements. With increased VPD and Ta, most years experienced significant decreases in soil volumetric water content (θ) at near-surface (0 – 30 cm) and deep (100 cm) soil depths (Figure 3.1d). The timing and magnitude of Ta and P events throughout the year led to differences in the response and duration of decreases in θ. Most notable were the decreases in θ at both depths in both 2012 and 2016. Total precipitation (P) was typical for southern Ontario, Canada, with moderate P experienced at all times, although the magnitude of extreme events (P > 25 mm) was greatest in summer (Figure 3.1e). No year within the period of study exceeded the 30-year mean P (997 mm).

Meteorological and climatic conditions influenced the timing and duration of key phenological dates and events shown in Table 3.1 and Figure 3.2. Unseasonably warm Ta in winter and spring of 2012 did not influence an earlier start of to the spring season (SOS, Figure 3.2a). This year ended up having the

longest summer (LOCC, 112 days) of all years, but also the lowest annual GEP (Table 3.4). The SOS in 2013 was the earliest (Day 116) of all years (Figure 3.2b), but unfavorable conditions (i.e. low PAR), following leaf-emergence, led 2013 to have the shortest summer (94 days, Figure 3.2b, Tables 3.1 & 3.2). The shortest overall growing season (180 days) was observed in 2014, which was also the coolest and wettest year on record during the study period (Table 3.2). This year was also the one with the highest net carbon uptake of all years (305 g C m^{-2} yr^{-1}, Table 3.4). A warm spring in 2015 advanced the SOS (Day 118), followed by one of the earliest EOG (Day 146), just behind the warm spring of 2012 (Day 145). Therefore, the spring season was not unusually long, but it was the spring with the lowest net carbon uptake (4 g C m^{-2} $season^{-1}$, Table 3.4). Both 2016 and 2017 had similar starts to the growing season (SOS) and length of summer (LOCC), despite largely different meteorological conditions for most of the year (Figures 3.2e & 3.2f). Warmer spring time temperatures allowed leaf-out to complete sooner in 2016 compared to 2017, so EOG came a few days earlier, however both years experienced nearly identical starts of autumn (SOB, Table 3.1 & Figure 3.2). Both of these years also experienced the latest EOS (Days 328 & 318, respectively), ultimately promoted by above average October mean Ta (Figure 3.2). These two years experienced the highest net carbon losses in the autumn season (Table 3.4).

In all years, with 2017 being the exception, the SOS began at the same time as a positive Ta anomaly, immediately following a negative Ta anomaly

(Figure 3.2). In the case of 2017, the SOS began during a prolonged period of unseasonably cold Ta (Figure 3.2f), likely highlighting physiological or photoperiod responses driving SOS outside of just responses due to temperature. The SOS of 2012 (Day 120) and 2015 (Day 118) began near the same time, but the winter and early spring conditions were largely different (Figure 3.2a & 3.2d). Furthermore, cold conditions in 2014 (Figure 3.2c) were similar to 2015 prior to SOS, but in these years the SOS differed by 9 days. The same could be said about autumn Ta, where late-growing season Ta anomalies often extended the EOS (i.e. 2016 & 2017), though other years (2015) saw less of an impact of anomalous Ta on EOS timing. Lastly, significant decreases in θ during 2012 and 2016 (Figure 3.1d), were driven by positive Ta anomalies occurring the majority of each year.

To help quantify the relationship between Ta, cumulative growing degree days (GDD), and the number of cooling degree days (CDD), and the timing and duration of key phenological dates and periods, we plotted the various variables against each other (Figure 3.3). The timing of the SOS was compared to the mean Ta (Figure 3.3a) and cumulative GDD (Figure 3.3b), calculated using Ta data from day of year 117 to day of year 127 (which corresponded to the 6-yearm mean SOS ± standard deviation). Our results showed a strong correlation between SOS, Ta, and GDD ($R^2 = 0.95$). A 0.6°C and 5.45 degree-day increase in mean Ta and cumulative GDD, respectively, led to an advancement of the SOS by 1 day. However, after the SOS and the initiation of leaf-out, it was the degree of cooling (CDD) that largely controlled the length of the spring shoulder season and

therefore also the timing of the EOG (Figure 3.3c). In this case, fewer cold days following SOS (2012) allowed trees to more quickly reach EOG (Figure 3.2a), shortening the length of the spring shoulder (25 days, Table 3.1). Increasing cold Ta anomalies by just 1.05 CDD following SOS, led to a 1-day prolongation of the spring shoulder period, delaying the timing of EOG and start of summer/peak uptake period (i.e. 2013: 39 day spring shoulder).

Further, while the relationship between mean uptake Ta and LOCC length was strongly positive (see supplementary Table S3.1, $R^2 = 0.69$), the influence of cool periods outside of the peak uptake period had a large control on LOCC length. Therefore, the Ta and GDD within a larger time period, from the mid of greenup (MOG) to the mid of browndown (MOB), was found to positively impact the overall length of summer (LOCC, Figure 3.3d & 3.3e). A mean Ta increase of 0.13°C and 23.6 cumulative GDD during this period led to a 1-day prolonging of LOCC, highlighting that years with the warmest summers (2012 and 2016) had the longest LOCC (Table 3.1 & Table 3.2). Similarly, the initiation of autumn (SOB) at the end of the LOCC period was found to be highly negatively correlated to mean summer $\theta_{0\text{-}30cm}$ ($R^2 = 0.87$), where the years (2013 & 2015) with the highest summer $\theta_{0\text{-}30cm}$ ultimately had the earliest SOB (Table 3.2, Table S3.1). Here it can be assumed that higher summer $\theta_{0\text{-}30cm}$ would likely coincide with cooler conditions (i.e. low Ta, low PAR, high P etc.) supporting an earlier end to the LOCC. Once senescence (SOB) had begun, the length of autumn continued to be driven by Ta. The cumulative CDD between days 210 and 290,

following Hwang et al. (2014) and Oishi et al. (2018), was shown to have a large positive correlation (R^2 = 0.93) with the end of the growing season (EOS, Figure 3.3f). For this period, roughly from the peak of the growing season to the mid of browndown (August to October), every 5.18 cumulative CDD led to an advancement of the EOS by 1 day. As such, late growing season warming (2016 & 2017) was important in delaying the timing of senescence as these two years had the latest SOB and EOS (Table 3.1). Conversely, the years with the highest CDD in this time (2012 & 2014) had the earliest EOS and shortest autumn shoulder, highlighting the acceleration of senescence and the response to temperature and climate.

3.4.2 Canopy Greenness from Digital Cameras in Relation to Phenology

Capturing phenological transition dates with eddy covariance data can be logistically and financially challenging. Employing relatively simple and far more affordable digital cameras may be more practical and also useful in remote sensing applications. The PhenoCam installed on top of the scaffold tower in our forest tracks seasonal changes in the color of the forest canopy beneath. Generally, the timing and trends of daily GEP_{Max} from the EC tower were captured by mean GCC indices derived from PhenoCam data (Figure 3.4a). In every year, a nearly constant baseline mean GCC value marked the non-growing season, when trees in the forest remained leafless and photosynthesis (GEP) was not occurring (Figure 3.4a). Following the SOS and initiation of greenup in

spring, a rapid rise in GCC was seen, before reaching peak greenness, and gradually declining for the remainder of the summer. Following the beginning of browndown (senescence) in autumn, a similar decline in GCC was present, before reaching an annual minimum and returning to the non-growing season baseline values (Figure 3.4a).

The PhenoCam transition dates (Table 3.3) calculated from mean GCC, following Hufkens et al. (2018) and Richardson et al. (2018), were compared to phenology dates calculated from the eddy covariance (EC) data (Table 3.1). The PhenoCam 10% transition in spring GCC was able to effectively capture (R^2 = 0.73) the start of the EC defined growing season (SOS). In four of the six years, the 10% spring GCC transition was reached 8 to 9 days following the SOS calculated from EC-data. In 2016, it only took 5 days, while in 2012 the 10% transition was reached 2 days after the EC-derived SOS. While the PhenoCam was unable to capture the annual timing of peak photosynthesis (GEP_{Max}) measured by the flux tower during the middle of summer, the camera could identify the timing of the day of the most rapid (maximum) increase in GEP (i.e. MOG) during spring (Figure 3.4b). We then considered the same for autumn, as senescence (browndown) should also be captured by the PhenoCam during the most rapid decrease in GEP (i.e. MOB data computed from EC-data). While the 50% autumn GCC transition was closer to the actual date of the EC MOB in most years (Tables 3.1 & 3.3), we found that the 25% autumn GCC transition was highly correlated to MOB, except during 2016 (Figure 3.4c), a year with late

season warming extending the EOS (Figure 3.2e). Due to the unfortunate timing of PhenoCam GCC data-loss at our site during the autumn of 2016, it is possible the estimated GCC transition date could in fact be later, leading to a better fit. A brief regional comparison of mean GCC from PhenoCams within deciduous broadleaf forests across Wisconsin, Michigan, Pennsylvania, and Ontario, during the autumn of 2016, showed a consistent rise in GCC during the period of concern (Figure 3.4f). If data were available during that period for our site, it is possible the calculation of the timing of the transition dates could shift later, similar to the other warm autumn years, such at 2017 (Figure 3.4e). These results demonstrate that EC-based phenology dates appear to have the ability to be recorded by the timing of certain seasonal PhenoCam-based GCC phenology dates.

3.4.3 Phenology Impact on Fluxes

Total GEP, RE, and NEP sums within the spring shoulder, peak uptake, and autumn shoulder are shown in Table 3.4. The three years (2013, 2014, & 2015) with the coldest early non-growing season mean Ta (Figure 3.2), began the year leading up to the SOS with the least carbon losses (i.e. lowest ecosystem respiration, RE), roughly 30 to 50 g C m^{-2} less than in the other years. Although these years ultimately experienced very different cumulative annual net carbon uptake (i.e. annual NEP values), in general, colder Ta resulted in higher seasonal NEP at the SOS (Table 3.4). The years with the latest SOS (2014, 2016, & 2017) had the longest summer periods (i.e. LOCC) and greatest annual photosynthetic

carbon uptake (GEP). However, following the SOS, GEP varied noticeably regardless of the spring shoulder length, due to the climate during that period (i.e. Ta, PAR, P). As Ta began to increase, an increased spring shoulder length led to greater RE losses between SOS and EOG. The peak summer/uptake total GEP was similar across all years (± 58 g C m^{-2}), while RE varied much more (± 83 g C m^{-2}), largely due to 2012. Extended heat and water stress conditions during the summer of 2012 greatly reduced RE, with extreme conditions leading to decreased $\theta_{0\text{-}30cm}$ (Figure 3.1d), which in turn negatively affected soil carbon release through decomposition. This reduction in RE was beneficial to the forest in terms of NEP, as less RE during typical mid-summer water-stressed periods led to the second highest annual NEP (only behind 2014). In the autumn, RE was highest in the years with the longest autumn shoulders seasons and latest end of seasons (EOS). Near the EOS, decreased GEP following seasonal limitations (i.e. PAR & photoperiod), and enhanced RE due to higher Ta and Ts, caused greater carbon losses (negative NEP) than the years with the earliest EOS (2012 and 2014). Higher total NEP in both 2012 (292 g C m^{-2}) and 2014 (305 g C m^{-2}) was measured due to decreased RE, but for largely different reasons. With cooler Ta, low VPD, sufficient P and θ, and the most 'normal' (30-year mean) conditions at all times throughout the year (Figure 3.2; Table 3.2), NEP in 2014 was the highest of all the years despite the shortest growing season (i.e. latest SOS, earliest EOS, and shortest LOCC of all 6 years). Under future climate warming, our study region may experience warmer springs and autumns, which may effectively

prolong the growing season. If the prolonged growing season is due to an early spring, then deciduous forests in the area may benefit in terms of carbon uptake. However, if the prolonged growing season is due to a longer autumn, then the forests of the area may lose more carbon on an annual basis.

3.4.4 Modeling Impacts of Changing Climate on Carbon Fluxes

To further explore the effects of increasing temperatures on carbon, a constant increasing trend in Ta (and equivalent increase in Ts) was examined to examine the impact on carbon fluxes. Modelled annual sums of GEP, RE, and NEP were created for ten different scenarios with Ta varying by 0.1°C from -0.5°C to 0.5°C (Figure 3.5). A constant 1°C increase in Ta had very little effect (2.3 g C m^{-2} yr^{-1}) on annual GEP (Figure 3.5a), but it had a modest effect (54.5 g C m^{-2} yr^{-1}) on annual RE (Figure 3.5b), leading to an overall reduction of 52.2 g C m^{-2} yr^{-1} (Figure 3.5c) in annual NEP. While the results are not realistic of an actual change in Ta, due to irregular deviations in Ta (similar to Figure 3.2), and secondary effects caused by increasing Ta (i.e. increasing VPD or decreasing θ; as occurred in 2012), they provide insight into the Ta controls on overall site productivity. Under future warming, given sufficient seasonal P and θ, increasing Ta could lead to decreased NEP through respirative losses exceeding photosynthetic gains.

3.5 Discussion

3.5.1 Climate Driving Phenology

The growing season of a deciduous forest is defined by the phenological dates: bud-burst (SOS) and full leaf-out (EOG) in the spring and start of senescence (SOB) and abscission (EOS) in the autumn. These events directly impact the overall longevity of canopy cover and summer season (LOCC), and affect the amount of light (PAR), energy, and water (P) the forest intercepts and ultimately forest-atmosphere interactions (Kramer et al., 2000; Morisette et al., 2009; Noormets, 2009). It is widely understood that annual leaf development is sensitive to changes in Ta (Polgar & Primack, 2011; Richardson et al., 2013). In spring, the SOS is driven by winter chilling requirements, and after a certain time, increasing Ta and increasing photoperiod in temperate deciduous forests (Korner & Basler, 2010; Fu et al., 2014). These factors, along with there being a strong genetic control among different tree species for when bud-burst will begin, cause forests to work to maximize the trade-off between increased photosynthetic gains and the risk of damage due to late spring frosts (Sanz-Perez et al., 2009; Kramer et al., 2010; Polgar & Primack, 2011). At our site, regardless of winter chilling and mean Ta prior to leaf-out, on average, the SOS began on Day 122 ± 5 days, with a maximum difference of 11 days between all years (Table 3.1). The SOS also occurred on similar day of year (122 ± 5 days) as the last day when daily mean Ta in the forest remained below the annual mean Ta (Table 3.2). Baldocchi et al. (2005) suggested that the probability of frost becomes low once the mean daily Ta

exceeds the annual mean Ta. At our site, the later SOS or slow development could be reflective of the tree species composition being dominated by oak species. Ring-porous species, such as oak, suffer more damage from winter freezing which often leads to a later SOS for those trees compared to the coexisting diffuse porous species, such as maple or birch (Barbaroux & Breda, 2002; Morecroft et al., 2003; Caffarra & Donnelly, 2011; Polgar & Primack, 2011).

Once the growing season had begun, competing meteorological variables (i.e. PAR, Ta, P, etc.) shaped the spring shoulder length: i.e. the time between SOS and EOG. During this time, PAR continued to increase each day, so to no surprise, the years (2013, 2014, and 2017) with the longest spring shoulder season had the highest total PAR. However, years with the longest spring shoulder season also had the most total P and the most CDD days (Figure 3.3c) in that period (Table 3.2), suggesting that cool, wet days led to an extension of the spring shoulder season. This in turn influenced the timing of peak photosynthesis. For example, the two years with the latest SOS and the two longest springs (i.e. 2014 & 2017), experienced shorter overall summer periods. In all years, the length of the spring season had a negative effect on the length of summer. Slow leaf development has been found in many Quercus species. In a mixed deciduous forest in Tennessee, it took *Quercus alba* leaves roughly 40 to 50 days to reach maximum photosynthetic capacity, others 60 to 80 days (Wilson et al., 2000; Morecroft et al., 2003). At our site, we saw a consistent average of 79 ± 3 days from the SOS to peak photosynthesis, with the timing of the peak varying by a

maximum of only nine days. Overall, the length of the phenologically defined summer and the timing of maximum photosynthetic capacity in summer appeared to be driven by Ta during the time from mid of greenup (MOG) to mid of browndown (MOB) (Figures 3.3d & 3.3e).

After this time, a combination of unfavorable meteorological conditions (i.e. decreasing day length and/or decreasing Ta) controlled the onset and duration of senescence (Richardson et al., 2006; Vitasse et al., 2011; Travers & Eldridge, 2013; Fu et al., 2014). Studies have shown that warming during the summer and autumn delays the timing of senescence, acting to postpone the end of the growing season (EOS) in forests (Ibanez et al., 2010; Gallinat et al., 2015; Liu et al., 2016; Fu et al., 2017). This was also the case in our study, where the two years with late season warming (Figure 3.2: 2016 & 2017) and lowest CDD (Figure 3.3f) experienced that latest EOS. The EOS for these two years (323 ± 7) was roughly 1 to 2 weeks later than for the other four years (309 ± 4). For the 'normal' year of 2014, the EOS (Day 307) was earlier than all years, with the exception of year 2012. Our results support data on plant physiology, where *Quercus* species have been found to be flexible to Ta changes, and typically hold senescing leaves longer than other genera (Kuster et al., 2014; Gill et al., 2015).

3.5.2 Comparison of PhenoCam derived Phenology Dates Flux-Derived Dates

Photography derived indices such as the greenness chromatic coordinate (GCC) have been found to be closely related to photosynthesis (GEP) in deciduous

forests (Wingate et al., 2015). Recent scientific efforts (Hufkens et al., 2016; Bowling et al., 2018) have attempted to model the relationship between photosynthesis (GEP) and GCC to fill-in the gaps between automated satellite measurements and field based measurements (Misra et al., 2016; Matiu et al., 2017). Our study expanded on this research by examining the seasonality of photosynthesis and GCC within the northernmost extent of temperate deciduous forests. In all years, fluctuations in both GEP and GCC were typical of deciduous forests, with low values in the inactive winter season, and high values during the photosynthetically active period (Toomey et al., 2015).

In spring, there was very little difference between the SOS dates computed from EC-flux data (Table 3.1) and those from PhenoCam data (Table 3.3), varying on average by 0 ± 2 days. After the SOS, an abrupt increase in GCC took a consistent mean time of 29 ± 2 days to reach peak GCC. However, this spring peak in GCC occurred well before the summer peak in GEP (Figure S3.1). Past studies have found that maximum GCC within deciduous forests precede maximum GEP by several weeks to two months (Richardson et al., 2009a; Sonnentag et al., 2012). Our site was at the later end of that estimate, with a mean difference of 49 ± 2 days between peak GCC and peak GEP. While studies have concluded the limitations of using GCC as a predictor of GEP due to this difference in timing, we found the peak GCC to be positively correlated (R^2 = 0.94) to GEP on the day corresponding to mid greenup (MOG) computed from EC-data. Peak GCC in spring is a product of seasonal variations in foliage

pigments (Sims and Gamon, 2002). As a result, the quickest increase in photosynthetic greenup (MOG) was able to be accurately captured by the PhenoCam through peak GCC. Toomey et al. (2015) found similar results, concluding that strong correlations were found in the 'middle of spring' for GCC and GEP. Little to no relationship was seen between GEP and GCC throughout summer due to differences in timing and controls. Following the GCC peak in the spring, GCC gradually declined for the remainder of the summer at our site. GEP on the other hand, driven by variations in local meteorological (PAR, VPD, Ta, etc.), steadily increased before reaching a peak mid-July (Day 201 ± 5 days), and decreasing for the remainder of the year. These peak uptake meteorological controls had little impact on detectable canopy greenness (Toomey et al., 2015).

Nearing the end of summer, senescence begins in deciduous forests, marking the end of the growing season, as forests progress towards the leafless winter period. Autumn phenology plays an important role in the annual biogeochemistry of temperate deciduous forests, yet this period remains relatively neglected in many phenological studies due to the complexity and nature of autumn climate and meteorological drivers (Richardson et al., 2010; Klosterman et al., 2014; Gallinat et al., 2015; Liu et al., 2016). Further, the definitions of autumn phenology timing vary from spring in that spring leaf-out is rapid and able to be observed, while senescence ranges from the first change in leaf color to the date of leaf abscission (Soolanayakanahally et al., 2013; Gallinat et al., 2015).

Using phenological dates derived from daily observed photosynthesis rates

(Table 3.1) we attempted to compare the autumn shoulder period to PhenoCam greenness (GCC). The average initiation of senescence (SOB) began in mid-September (Day 255 ± 6) at our site, prior to the dramatic decrease in GCC. The magnitude of seasonal GCC varied from year to year, illustrating the impacts of meteorological conditions on both leaf color and leaf longevity (Richardson et al., 2010; Archetti, et al., 2013). The two years (2016 & 2017) with the warmest autumn Ta experienced the latest SOB and the latest 50% autumn transition in GCC. These two years also saw decreased GCC at the start of senescence, unlike in other years, possibly due to the lowest observed deep soil moisture (i.e. θ_{100cm}: 0.04 & 0.05 m^3 m^{-3} in 2016 & 2017, respectively). It has been suggested that years with low, deep θ experience sharp declines in GCC, primarily due to accelerated leaf aging (Hanan et al., 2002; Noormets et al., 2008). Even with accelerated aging and annual differences in the timing and duration of autumn phenology, both photosynthetic phenological dates and PhenoCam GCC derived dates were able to capture senescence. Past research found weak correlations between autumn GCC and GEP (Richardson et al., 2010; Toomey et al., 2015). We found the date of the 25% autumn transition in GCC to be positively correlated to MOB derived from GEP, illustrating that the most rapid decrease in photosynthesis was seen by GCC. Following MOB, 2016 and 2017 had the latest EOS and minimum GCC values, both marking a delay in leaf abscission and EOS. While an initial acceleration of leaf aging may have occurred at the start of senescence for these years, the prolonged GCC later into the season can be

attributed to a delay in leaf color from autumn warming (Gunderson et al., 2012; Archetti et al., 2013; Gallinat et al., 2015; Liu et al., 2016). Lastly, higher CDD values were shown to be a good indicator for EOS (Dragoni and Rahman, 2012), which we observed.

3.5.3 Carbon Fluxes and Implications

The timing of leaf-out (SOS) in the spring and the end of senescence (EOS) in autumn have been shown to alter ecosystem processes within deciduous forests, affecting the forest-atmosphere exchange of carbon dioxide and other greenhouse gases (Chapin et al., 2000; Noormets, 2009; Richardson et al., 2010). These phenological dates ultimately shape the annual carbon exchange, which may be impacted under future climates. Long-term data sets have shown increasing air temperatures are expected to lengthen growing seasons of temperate ecosystems within the northern hemisphere, leading to an earlier start in the spring and later end in autumn (White & Nemani, 2003; Richardson et al., 2010; Settele et al., 2014; Duveneck & Thompson, 2017; Oishi et al., 2018). While warmer temperatures and longer growing seasons may benefit some ecosystems, we attempted to examine how a North American deciduous forest at the northern edge of the natural range would be impacted by increasing air temperatures.

In the future, as mean winter Ta is expected to increase by 3 – 7°C in this area (USGCRP, 2017), greater RE losses can be expected, causing the forest to begin the SOS at lower cumulative NEP. It has been suggested that winter and

early spring warming may advance the SOS (Wolf et al., 2013; Jin et al., 2017; Oishi et al., 2018), although the response and extent of this advancement within our forest remains uncertain. In all years, even during the extremely anomalous spring Ta of 2012 (Figure 3.3a), the SOS only varied by 11 days (Table 3.1), suggesting *Quercus* tree trigger is based on photoperiod and Ta conditions only after a certain time of the year (Caffarra & Donnelly, 2011). However, studies suggest that the late budbreak and slow development of *Quercus* trees may give way to other species with minimal photoperiod and Ta requirements, allowing these species to increase in abundance, possibly becoming the dominant species over time (Morecroft et al., 2003; Morin et al., 2009; Polgar & Primack, 2011).

Even if SOS is advanced due to higher Ta, seasonal PAR will remain low in our area due to the latitude, limiting overall photosynthesis. In future climates, an increase in NEP is expected following the SOS due to greater rates of productivity as warmer Ta has a greater positive effect on photosynthesis in the spring versus autumn (Piao et al., 2008; Duveneck & Thompson, 2017; Oishi et al., 2018). Furthermore, while studies examining deciduous forest phenology have found that a positive spring Ta anomaly increases annual NEP, our results suggest differently. In our study, the year (2014) with the lowest spring Ta and latest SOS produced the highest annual NEP (305 g C m^{-2} yr^{-1}), while the two years with the earliest SOS (2013 & 2015), had the lowest cumulative NEP of all years. Additionally, a number of past studies have shown that longer growing seasons lead to enhanced carbon uptake (Goulden et al., 1996; Desai, 2010; Dragoni et al.,

2011). We found the most productive (highest NEP) years had the two shortest growing season lengths (i.e. 2012 & 2014). An extremely warm year 2012, with seasonal water deficits, led to decreases in both annual GEP and RE, which shortened the growing season length. The suppression of photosynthesis and respiration has been suggested to occur in deciduous forests during extreme years (Davidson et al., 1998; Palmroth et al., 2005; Novick et al., 2015). Conversely, in 2014, the shortest and most productive year, cool and wet conditions dominated all year. The contrast in the two most productive years creates difficulty in predicting how changes in climate may affect fluxes, but growing season length and earlier SOS did not appear to have any positive influences on annual carbon exchange. In contrast, autumn may play a key role. Oishi et al. (2018) found that for an Appalachian deciduous forest in North Carolina, years with the lowest annual NEE showed the earliest declines in autumn $GEP_{Max.}$ We saw similar results at our site for 2013 (156 g C m^{-2} yr^{-1}) and 2015 (90 g C m^{-2} yr^{-1}), the two years with the lowest total NEP. Both of these years had the earliest SOB dates (Day 249), marking the initiation of autumn senescence and the decline in GEP_{Max}. These years had two of the longest autumn seasons, so while senescence had begun, late season warming prolonged the end of the growing season (EOS). In every case, years with longer autumn shoulder seasons and later EOS had increased net carbon loss (i.e. negative NEP in that period), while those with the shortest autumns and earliest EOS had increased net carbon uptake (i.e. positive NEP, seen in years 2012 & 2014). The autumn decline in NEP was the result of

RE increasing more strongly with Ta than photosynthesis, making the potential for carbon gain small (Kramer et al., 2000; Nemani et al., 2002; Dunn et al., 2007; Piao et al., 2008; Wu et al., 2013; Gallinat et al., 2015).

Similar to other studies, these results suggest that an earlier SOS would benefit forest productivity, as rising early season photosynthesis (GEP) would outweigh RE. The degree of SOS advancement remains uncertain due to the physiological constraints controlling the timing of budburst for *Quercus* species, the dominant tree species in the forest. During the growing season, less variation was seen in GEP as compared to RE on an annual basis, implying that increasing Ta would have little impact on overall growing season GEP. Conversely, increasing Ta will increase RE, although heat and drought stress (i.e. 2012) could suppress the RE losses. Late season warming was shown to prolong the growing season later into November, when GEP gains were diminished by reducing photoperiod and senescing leaves. RE during this time outweighed photosynthesis every year. Under continued warming expected in the future, less of a positive impact on overall forest carbon uptake may be seen due to earlier springs, when the forest would benefit from added days of photosynthesis. Instead, an extension of the growing season in autumn could be detrimental to carbon uptake, as RE losses during that time exceed the gains in GEP. However, during this study, despite the differences in the timing and duration of various phenological seasons, our forest study site remained an annual sink of carbon (200 ± 83 g C m^{-2}), with

interannual variability (50 – 100 g C m^{-2}) typical of other midlatitude deciduous forests (Yuan et al., 2009; Desai, 2010).

3.6 Conclusions

The influence of phenology on photosynthesis was studied for six years (2012 to 2017) within a temperate deciduous forest in southeastern Canada. Seasonal air temperatures were shown to have a control on phenological dates during the spring, summer, and autumn. In the spring, warmer Ta advanced the growing season, while cooler conditions prolonged the period from the start of the growing season to peak summer uptake. After this time, the overall length of canopy closure and peak photosynthetically active period were further driven by Ta. In autumn, late season warming prolonged the growing season later into the year. In contrast to results of some past studies, we show that an earlier start to the growing season in spring, and the resulting extended growing season length, does not necessarily translate into increased annual carbon uptake by the forest. The two years with the latest growing season starts and shortest growing season lengths were the largest annual sinks of carbon in our study. We also found that the variability in autumn phenological dates was greater than that of spring dates. Prolonged autumns negatively impacted the overall annual carbon uptake of the forest, as the steady carbon emissions by ecosystem respiration outweighed the reducing carbon uptake by photosynthesis, when warm temperatures persisted and daylight length (photoperiod) shortened. Our results suggest that if the growing

season extends and phenological transition dates shift, due to warming in the autumn shoulder season, this may negatively impact the overall annual carbon uptake of deciduous forests in eastern North America. Finally, in our analysis we found that key phenological periods derived from eddy-covariance based flux measurements (i.e. mid of greenup & mid of browndown at the start and end of the growing season, respectively) were captured by changes in canopy greenness detected by digital cameras. These results could benefit future researchers, especially in remote sensing applications.

3.7 Acknowledgements

This study was funded by the Natural Sciences and Engineering Research Council (NSERC), the Global Water Futures Program (GWF), and the Ontario Ministry of Environment, Conservation and Parks (MOECP). Funding from the Canadian Foundation of Innovation (CFI) through New Opportunity and Leaders Opportunity Fund and Ontario Research Fund of the Ministry of Research and Innovation is also acknowledged. In kind support from the Ontario Ministry of Natural Resources and Forestry (OMNRF) and the Long Point Region Conservation Authority (LPRCA) is also acknowledged. We acknowledge support from Zoran Nesic at the University of British Columbia in assistance with flux measurements at our site. The PhenoCam development has been supported by the Northeastern States Research Cooperative, NSF's Macrosystems Biology program (award EF-1065029), DOE's Regional and Global Climate Modeling

program (award DE-SC0016011), and the US National Park Service Inventory and Monitoring Program and the USA National Phenology Network (grant number G10AP00129 from the United States Geological Survey). PhenoCam collaborators, including site PIs and technicians, are thanked for their efforts in support of PhenoCam data.

3.8 References

Allen, C.D., Macalady, A.K., Chenchouni, H., Bachelet, D., McDowell, N., Vennetier, M., Kitzberger, T., Rigling, A., Breshears, D.D., Hogg, E.T. and Gonzalez, P., 2010. A global overview of drought and heat-induced tree mortality reveals emerging climate change risks for forests. *Forest Ecology and Management*, 259(4), 660-684.

Archetti, M., Richardson, A.D., O'Keefe, J. and Delpierre, N., 2013. Predicting climate change impacts on the amount and duration of autumn colors in a New England forest. *PLoS One*, 8(3), 57373.

Baldocchi, D.D., Black, T.A., Curtis, P.S., Falge, E., Fuentes, J.D., Granier, A., Gu, L., Knohl, A., Pilegaard, K., Schmid, H.P. and Valentini, R., 2005. Predicting the onset of net carbon uptake by deciduous forests with soil temperature and climate data: a synthesis of FLUXNET data. *Int. J. Biometeorol.*, 49(6), 377-387.

Barbaroux, C. & Bréda, N., 2002. Contrasting distribution and seasonal dynamics of carbohydrate reserves in stem wood of adult ring-porous sessile oak and diffuse-porous beech trees. *Tree Physiology*, 22(17), 1201-1210.

Barichivich, J., Briffa, K.R., Myneni, R.B., Osborn, T.J., Melvin, T.M., Ciais, P., Piao, S. and Tucker, C., 2013. Large-scale variations in the vegetation growing season and annual cycle of atmospheric CO2 at high northern latitudes from 1950 to 2011. *Global change Biology*, 19(10), 3167-3183.

Barr, A. G., Griffis, T. J., Black, T. A., Lee, X., Staebler, R. M., Fuentes, J. D., Chen, Z., and Morgenstern, K., 2002. Comparing the carbon budgets of boreal and temperate deciduous forest stands. *Canadian Journal of Forest Research*, 32: 813-822.

Beamesderfer, E.R., Arain, M.A., Khomik, M., and Brodeur, J.J., 2019a. How will the carbon fluxes within the northernmost temperate deciduous forests of North America fair under future climates?. *Journal of Geophysical Research: Biogeosciences*.

Bertin, R.I., 2008. Plant phenology and distribution in relation to recent climate change. *The Journal of the Torrey Botanical Society*, 135(1), 126-147.

Bowling, D.R., Logan, B.A., Hufkens, K., Aubrecht, D.M., Richardson, A.D., Burns, S.P., Anderegg, W.R., Blanken, P.D. and Eiriksson, D.P., 2018. Limitations to winter and spring photosynthesis of a Rocky Mountain subalpine forest. *Agricultural and Forest Meteorology*, 252, 241-255.

Brodeur, J.J., 2014. Data-driven approaches for sustainable operation and defensible results in a long-term, multi-site ecosystem flux measurement program. *McMaster University*.

Caffarra, A. and Donnelly, A., 2011. The ecological significance of phenology in four different tree species: effects of light and temperature on bud burst. *International Journal of Biometeorology*, 55(5), 711-721.

Cannell, M.G.R. and Smith, R.I., 1986. Climatic warming, spring budburst and forest damage on trees. *Journal of Applied Ecology*, 177-191.

Chapin III, F.S., Sala, O.E., Burke, I.C., Grime, J.P., Hooper, D.U., Lauenroth, W.K., Lombard, A., Mooney, H.A., Mosier, A.R., Naeem, S. and Pacala, S.W., 1998. Ecosystem consequences of changing biodiversity. *Bioscience*, 48(1), 45-52.

Chapin III, F.S., Zavaleta, E.S., Eviner, V.T., Naylor, R.L., Vitousek, P.M., Reynolds, H.L., Hooper, D.U., Lavorel, S., Sala, O.E., Hobbie, S.E. and Mack, M.C., 2000. Consequences of changing biodiversity. *Nature*, 405(6783), 234-242.

Danz, N.P., Niemi, G.J., Regal, R.R. et al., 2007. Integrated Measures of Anthropogenic Stress in the U.S. Great Lakes Basin. *Environmental Management*, 39(5), 631-647.

Davidson, E.A., Belk, E., Boone, R.D., 1998. Soil water content and temperature as independent or confounding factors controlling soil respiration in a temperate mixed hardwood forest. *Global Change Biol*., 4, 217–227.

Desai, A.R., 2010. Climatic and phenological controls on coherent regional interannual variability of carbon dioxide flux in a heterogeneous landscape. *Journal of Geophysical Research: Biogeosciences*, 115(G3).

Dragoni, D., Schmid, H.P., Wayson, C.A., Potter, H., Grimmond, C.S.B. and Randolph, J.C., 2011. Evidence of increased net ecosystem productivity associated with a longer vegetated season in a deciduous forest in south-central Indiana, USA. *Global Change Biology*, 17(2), 886-897.

Dragoni, D. and Rahman, A.F., 2012. Trends in fall phenology across the deciduous forests of the Eastern USA. *Agricultural and Forest Meteorology*, 157, 96-105.

Dunn, A.L., Barford, C.C., Wofsy, S.C., Goulden, M.L. and Daube, B.C., 2007. A long-term record of carbon exchange in a boreal black spruce forest: Means, responses to interannual variability, and decadal trends. *Global Change Biology*, 13(3), 577-590.

Duveneck, M. J., R. M. Scheller, M. A. White, S. D. Handler, and C. Ravenscroft. 2014. Climate change effects on northern Great Lake (USA) forests: A case for preserving diversity. *Ecosphere* 5(2), 1-26.

Duveneck, M.J. and Thompson, J.R., 2017. Climate change imposes phenological trade-offs on forest net primary productivity. *Journal of Geophysical Research: Biogeosciences*, 122(9), 2298-2313.

Erskine, P.D., Lamb, D. and Bristow, M., 2006. Tree species diversity and ecosystem function: can tropical multi-species plantations generate greater productivity?. *Forest Ecology and Management*, 233(2-3), 205-210.

Frelich, L.E. and Reich, P.B., 2010. Will environmental changes reinforce the impact of global warming on the prairie–forest border of central North America?. *Frontiers in Ecology and the Environment*, 8(7), 371-378.

Froelich, N., Croft, H., Chen, J.M., Gonsamo, A. and Staebler, R.M., 2015. Trends of carbon fluxes and climate over a mixed temperate–boreal transition forest in southern Ontario, Canada. *Agricultural and Forest Meteorology*, 211, 72-84.

Fu, Y.S., Campioli, M., Vitasse, Y., De Boeck, H.J., Van den Berge, J., AbdElgawad, H., Asard, H., Piao, S., Deckmyn, G. and Janssens, I.A., 2014. Variation in leaf flushing date influences autumnal senescence and next year's flushing date in two temperate tree species. *Proceedings of the National Academy of Sciences*, 111(20), 7355-7360.

Gallinat, A.S., Primack, R.B. and Wagner, D.L., 2015. Autumn, the neglected season in climate change research. *Trends Ecol. Evol.*, 30(3), 169-176.

Garrity, S.R., Bohrer, G., Maurer, K.D., Mueller, K.L., Vogel, C.S. and Curtis, P.S., 2011. A comparison of multiple phenology data sources for estimating seasonal transitions in deciduous forest carbon exchange. *Agric. For. Meteorol.*, 151(12), 1741-1752.

Gill, A.L., Gallinat, A.S., Sanders-DeMott, R., Rigden, A.J., Short Gianotti, D.J., et al., 2015. Changes in autumn senescence in northern hemisphere deciduous trees: a meta-analysis of autumn phenology studies. *Annals of Botany*, 116(6), 875-888.

Gonsamo, A., Chen, J.M. and D'Odorico, P., 2013. Deriving land surface phenology indicators from CO_2 eddy covariance measurements. *Ecological Indicators*, 29, 203-207.

Goulden, M.L., Munger, J.W., Fan, S.M., Daube, B.C. and Wofsy, S.C., 1996. Exchange of carbon dioxide by a deciduous forest: response to interannual climate variability. *Science*, 271(5255), 1576-1578.

Grace, J. & Rayment, M., 2000. Respiration in the balance. *Nature*, 404, 819.

Gu, L., Post, W.M., Baldocchi, D.D., Black, T.A., Suyker, A.E., Verma, S.B., Vesala, T. and Wofsy, S.C., 2009. Characterizing the seasonal dynamics of plant community photosynthesis across a range of vegetation types. In Phenology of Ecosystem Processes (35-58). *Springer*, New York, NY.

Gunderson, C.A., Edwards, N.T., Walker, A.V., O'Hara, K.H., Campion, C.M., Hanson, P.J., 2012. Forest phenology and a warmer climate–growing season extension in relation to climatic provenance. *Global Change Biology*, 18, 2008–2025.

Hanan, N.P., Burba, G., Verma, S.B., Berry, J.A., Suyker, A. and Walter-Shea, E.A., 2002. Inversion of net ecosystem CO2 flux measurements for estimation of canopy PAR absorption. *Glob. Change Biol.*, 8(6), 563-574.

Hufkens, K., Keenan, T.F., Flanagan, L.B., Scott, R.L., Bernacchi, C.J., Joo, E., Brunsell, N.A., Verfaillie, J. and Richardson, A.D., 2016. Productivity of North American grasslands is increased under future climate scenarios despite rising aridity. *Nature Climate Change*, 6(7), 710.

Hufkens, K., Basler, D., Milliman, T., Melaas, E.K. and Richardson, A.D., 2018. An integrated phenology modelling framework in R. *Methods Ecol Evol*, 9(5), 1276-1285.

Hwang, T., Band, L.E., Miniat, C.F., Song, C., Bolstad, P.V., Vose, J.M. and Love, J.P., 2014. Divergent phenological response to hydroclimate variability in forested mountain watersheds. *Global Change Biology*, 20(8), 2580-2595.

Ibáñez, I., Primack, R.B., Miller-Rushing, A.J., Ellwood, E., Higuchi, H., Lee, S.D., Kobori, H. and Silander, J.A., 2010. Forecasting phenology under global warming. *Philosophical Transactions of the Royal Society B: Biological Sciences*, 365(1555), 3247-3260.

IPCC, 2013: Climate Change 2013: The Physical Science Basis. Contribution of Working Group I to the Fifth Assessment Report of the Intergovernmental Panel on Climate Change [Stocker, T.F., D. Qin, G.-K. Plattner, M. Tignor, S.K. Allen, J. Boschung, A. Nauels, Y. Xia, V. Bex and P.M. Midgley (eds.)]. Cambridge University Press, Cambridge, United Kingdom and New York, NY, USA, 1535.

Iverson, L.R., Schwartz, M.W. and Prasad, A.M., 2004. How fast and far might tree species migrate in the eastern United States due to climate change?. *Global Ecology and Biogeography*, 13(3), 209-219.

Iverson, L.R., Prasad, A.M., Matthews, S.N. & Peters, M., 2008. Estimating potential habitat for 134 eastern US tree species under six climate scenarios. *Forest Ecology and Management*, 254(3), 390-406.

Jin, J., Zhan, W., Wang, Y., Gu, B., Wang, W., Jiang, H., Lu, X. and Zhang, X., 2017. Water use efficiency in response to interannual variations in flux-based photosynthetic onset in temperate deciduous broadleaf forests. *Ecological Indicators*, 79, 122-127.

Keenan, T.F., Darby, B., Felts, E., Sonnentag, O., Friedl, M.A., Hufkens, K., O'Keefe, J., Klosterman, S., Munger, J.W., Toomey, M. and Richardson, A.D., 2014. Tracking forest phenology and seasonal physiology using digital repeat photography: a critical assessment. *Ecological Applications*, 24(6), 1478-1489.

Kling, G. W., K. Hayhoe, L. B. Johnson, J. J. Magnuson, S. Polasky, S. K. Robinson, B. J. Shuter, M. M. Wander, D. J. Wuebbles, and D. R. Zak. 2003. Confronting climate change in the Great Lakes Region: impacts on

our communities and ecosystems. *Ecological Society of America*, Washington, D.C., USA.

Kljun, N., Calanca, P., Rotach, M.W., Schmid, H.P., 2004. A simple parametrization for flux footprint predictions. *Boundary-Layer Meteorology*, 112, 503–523.

Klosterman, S., Hufkens, K., Gray, J.M., Melaas, E., Sonnentag, O., Lavine, I., Mitchell, L., Norman, R., Friedl, M.A. and Richardson, A., 2014. Evaluating remote sensing of deciduous forest phenology at multiple spatial scales using PhenoCam imagery. *Biogeosciences Discussions*, 11(2), 2305-2342.

Körner, C. & Basler, D., 2010. Phenology under global warming. *Science*, 327, 1461-1462.

Kramer, K., Leinonen, I. and Loustau, D., 2000. The importance of phenology for the evaluation of impact of climate change on growth of boreal, temperate and Mediterranean forests ecosystems: an overview. *International Journal of Biometeorology*, 44(2), 67-75.

Kramer, K., Degen, B., Buschbom, J., Hickler, T., Thuiller, W., Sykes, M.T. and de Winter, W., 2010. Modelling exploration of the future of European beech (Fagussylvatica L.) under climate change—Range, abundance, genetic diversity and adaptive response. *Forest Ecology and Management*, 259(11), 2213-2222.

Kuster, T.M., Dobbertin, M., Günthardt-Goerg, M.S., Schaub, M. and Arend, M., 2014. A phenological timetable of oak growth under experimental drought and air warming. *PLoS One*, 9(2), 89724.

Kwit, M.C., Rigg, L.S. and Goldblum, D., 2010. Sugar maple seedling carbon assimilation at the northern limit of its range: the importance of seasonal light. *Canadian Journal of Forest Research*, 40(2), 385-393.

Lafleur, B., Pare, D., Munson, A.D. and Bergeron, Y., 2010. Response of northeastern North American forests to climate change: Will soil conditions constrain tree species migration?. *Environmental Reviews*, 18(NA), 279-289.

Liu, Q., Fu, Y.H., Zhu, Z., Liu, Y., Liu, Z., Huang, M., Janssens, I.A. and Piao, S., 2016. Delayed autumn phenology in the Northern Hemisphere is related to change in both climate and spring phenology. *Global Change Biology*, 22(11), 3702-3711.

Matiu, M., Bothmann, L., Steinbrecher, R. and Menzel, A., 2017. Monitoring succession after a non-cleared windthrow in a Norway spruce mountain forest using webcam, satellite vegetation indices and turbulent CO2 exchange. *Agric. For. Meteorol*., 244, 72-81.

McLaren, J.D., Arain, M.A., Khomik, M., Peichl, M. and Brodeur, J., 2008. Water flux components and soil water-atmospheric controls in a temperate pine forest growing in a well-drained sandy soil. *Journal of Geophysical Research: Biogeosciences*, 113(G4).

Misra, G., Buras, A. and Menzel, A., 2016. Effects of Different Methods on the Comparison between Land Surface and Ground Phenology—A methodological case study from south-western Germany. *Remote Sensing*, 8(9), 753.

Monson, R.K., Sparks, J.P., Rosenstiel, T.N., Scott-Denton, L.E., Huxman, T.E., Harley, P.C., Turnipseed, A.A., Burns, S.P., Backlund, B. and Hu, J., 2005. Climatic influences on net ecosystem CO 2 exchange during the transition from wintertime carbon source to springtime carbon sink in a high-elevation, subalpine forest. *Oecologia*, 146(1), 130-147.

Morecroft, M.D., Stokes, V.J. and Morison, J.I.L., 2003. Seasonal changes in the photosynthetic capacity of canopy oak (Quercus robur) leaves: the impact of slow development on annual carbon uptake. *International Journal of Biometeorology*, 47(4), 221-226.

Morin, X., Lechowicz, M.J., Augspurger, C., O' Keefe, J., Viner, D., Chuine, I., 2009. Leaf phenology in 22 North American tree species during the 21st century. *Global Change Biology*, 15: 961–975.

Morisette, J.T., Richardson, A.D., Knapp, A.K., Fisher, J.I., Graham, E.A., Abatzoglou, J., Wilson, B.E., Breshears, D.D., Henebry, G.M., Hanes, J.M. and Liang, L., 2009. Tracking the rhythm of the seasons in the face of global change: phenological research in the 21st century. *Frontiers in Ecology and the Environment*, 7(5), 253-260.

Nemani, R., White, M., Thornton, P., Nishida, K., Reddy, S., Jenkins, J. and Running, S., 2002. Recent trends in hydrologic balance have enhanced the terrestrial carbon sink in the United States. *Geophysical Research Letters*, 29(10), 106-1.

Noormets, A., McNulty, S.G., DeForest, J.L., Sun, G., Li, Q. and Chen, J., 2008. Drought during canopy development has lasting effect on annual carbon balance in a deciduous temperate forest. *New Phytologist*, 179, 818-828.

Noormets, A. ed., 2009. Phenology of Ecosystem Processes: Applications in Global Change Research. *Springer Science & Business Media*.

Novick, K.A., Oishi, A.C., Ward, E.J., Siqueira, M.B.S., Juang, J.Y., Stoy, P.C., 2015. On the difference in the net ecosystem exchange of CO2 between deciduous and evergreen forests in the southeastern United States. *Global Change Biol*., 21, 827–842.

Oishi, A.C., Miniat, C.F., Novick, K.A., Brantley, S.T., Vose, J.M. and Walker, J.T., 2018. Warmer temperatures reduce net carbon uptake, but do not affect water use, in a mature southern Appalachian forest. *Agricultural and Forest Meteorology*, 252, 269-282.

Pachauri, R.K., Allen, M.R., Barros, V.R., Broome, J., Cramer, W., Christ, R., Church, J.A., Clarke, L., Dahe, Q., Dasgupta, P. and Dubash, N.K., 2014. Climate change 2014: synthesis report. Contribution of Working Groups I, II and III to the fifth assessment report of the Intergovernmental Panel on Climate Change (p. 151). IPCC.

Palmroth, S., Maier, C.A., McCarthy, H.R., Oishi, A.C., Kim, H.S., Johnsen, K.H., et al., 2005. Contrasting responses to drought of forest floor CO2 efflux in a loblolly pine plantation and a nearby oak-hickory forest. *Global Change Biol*., 11, 421–434.

Paquette, A. and Messier, C., 2011. The effect of biodiversity on tree productivity: from temperate to boreal forests. *Global Ecology and Biogeography*, 20(1), 170-180.

Piao, S., Ciais, P., Friedlingstein, P., Peylin, P., Reichstein, M., Luyssaert, S., Margolis, H., Fang, J., Barr, A., Chen, A. and Grelle, A., 2008. Net carbon dioxide losses of northern ecosystems in response to autumn warming. *Nature*, 451(7174), 49.

Piao, S., Liu, Q., Chen, A., Janssens, I.A., Fu, Y., Dai, J., Liu, L., Lian, X., Shen, M. and Zhu, X., 2019. Plant phenology and global climate change: Current progresses and challenges. *Global Change Biology*, 25(6), 1922-1940.

Polgar, C.A. and Primack, R.B., 2011. Leaf-out phenology of temperate woody plants: from trees to ecosystems. *New Phytologist*, 191(4), 926-941.

Reichstein, M., Bahn, M., Ciais, P., Frank, D., Mahecha, M.D., Seneviratne, S.I., Zscheischler, J., Beer, C., Buchmann, N., Frank, D.C. and Papale, D., 2013. Climate extremes and the carbon cycle. *Nature*, 500(7462), 287.

Richardson, A.D., Bailey, A.S., Denny, E.G., Martin, C.W. and O'keefe, J., 2006. Phenology of a northern hardwood forest canopy. *Global Change Biology*, 12(7), 1174-1188.

Richardson, A. D., Jenkins, J.P., Braswell, B.H., Hollinger, D.Y., Ollinger, S.V., and Smith, M.L., 2007a. Use of digital webcam images to track spring green-up in a deciduous broadleaf forest. *Oecologia*, 152: 323–334.

Richardson, A. D., B. H. Braswell, D. Y. Hollinger, J. P. Jenkins, and S. V. Ollinger. 2009a. Near-surface remote sensing of spatial and temporal variation in canopy phenology. *Ecological Applications*, 19:1417–1428.

Richardson, A.D., Hollinger, D.Y., Dail, D.B., Lee, J.T., Munger, J.W. and O'keefe, J., 2009b. Influence of spring phenology on seasonal and annual carbon balance in two contrasting New England forests. *Tree physiology*, 29(3), 321-331.

Richardson, A.D., Black, T.A., Ciais, P., Delbart, N., Friedl, M.A., Gobron, N., Hollinger, D.Y., Kutsch, W.L., Longdoz, B., Luyssaert, S. and Migliavacca, M., 2010. Influence of spring and autumn phenological transitions on forest ecosystem productivity. *Philos. Trans. Royal Soc. B*, 365(1555), 3227-3246.

Richardson, A.D., Keenan, T.F., Migliavacca, M., Ryu, Y., Sonnentag, O. and Toomey, M., 2013. Climate change, phenology, and phenological control of vegetation feedbacks to the climate system. *Agricultural and Forest Meteorology*, 169, 156-173.

Richardson, A.D., Hufkens, K., Milliman, T., Aubrecht, D.M., Chen, M., Gray, J.M., Johnston, M.R., Keenan, T.F., Klosterman, S.T., Kosmala, M. and Melaas, E.K., 2018. Tracking vegetation phenology across diverse North American biomes using PhenoCam imagery. *Scientific Data*, 5, 180028.

Sanz-Pérez, V., Castro-Díez, P. and Valladares, F., 2009. Differential and interactive effects of temperature and photoperiod on budburst and carbon reserves in two co-occurring Mediterranean oaks. *Plant Biol.*, 11, 142-151.

Scheller, R.M. and Mladenoff, D.J., 2008. Simulated effects of climate change, fragmentation, and inter-specific competition on tree species migration in northern Wisconsin, USA. *Climate Research*, 36(3), 191-202.

Settele, J., R. Scholes, R. Betts, S. Bunn, P. Leadley, D. Nepstad, J.T. Overpeck, and M.A. Taboada, 2014: Terrestrial and inland water systems. Climate Change 2014: Impacts, Adaptation, and Vulnerability. Part A: Global and

Sectoral Aspects. Contribution of Working Group II to the Fifth Assessment Report of the Intergovernmental Panel on Climate Change [Field, C.B., V.R. Barros, D.J. Dokken, K.J. Mach, M.D. Mastrandrea, T.E. Bilir, M. Chatterjee, K.L. Ebi, Y.O. Estrada, R.C. Genova, B. Girma, E.S. Kissel, A.N. Levy, S. MacCracken, P.R. Mastrandrea, and L.L.White (eds.)]. Cambridge University Press, Cambridge, United Kingdom and New York, NY, USA, 271-359.

Shao, J., Zhou, X., Luo, Y., Li, B., Aurela, M., Billesbach, D., Blanken, P.D., Bracho, R., et al., 2015. Biotic and climatic controls on interannual variability in carbon fluxes across terrestrial ecosystems. *Agricultural and Forest Meteorology*, 205, 11-22.

Sims, D. A., and J. A. Gamon. 2002. Relationship between leaf pigment content and spectral reflectance across a range of species, leaf structures and developmental stages. *Remote Sensing of Environment*, 81:337–354.

Soja, A.J., Tchebakova, N.M., French, N.H., Flannigan, M.D., Shugart, H.H., Stocks, B.J., Sukhinin, A.I., Parfenova, E.I., Chapin III, F.S. and Stackhouse Jr, P.W., 2007. Climate- induced boreal forest change: predictions versus current observations. *Global and Planetary Change*, 56(3-4), 274-296.

Sonnentag, O., K. Hufkens, C. Teshera-Sterne, A.M. Young, M. Friedl, B.H. Braswell, T. Milliman, O'Keefe, J., and Richardson, A.D., 2012. Digital repeat photography for phenological research in forest ecosystems. *Agricultural and Forest Meteorology*, *1*52:159–177.

Soolanayakanahally, R.Y., Guy, R.D., Silim, S.N. and Song, M., 2013. Timing of photoperiodic competency causes phenological mismatch in balsam poplar (Populus balsamifera L.). *Plant, Cell & Environment*, 36(1), 116-127.

Toomey, M., Friedl, M.A., Frolking, S., Hufkens, K., Klosterman, S., Sonnentag, O., Baldocchi, D.D., Bernacchi, C.J., Biraud, S.C., Bohrer, G. and Brzostek, E., 2015. Greenness indices from digital cameras predict the timing and seasonal dynamics of canopy-scale photosynthesis. *Ecological Applications*, 25(1), 99-115.

Travers, S.K. and Eldridge, D.J., 2013. Increased rainfall frequency triggers an increase in litter fall rates of reproductive structures in an arid eucalypt woodland. *Austral Ecology*, 38(7), 820-830.

U.S. Global Change Research Program (USGCRP), 2017. Climate Science Special Report: Fourth National Climate Assessment, Volume I,

[Wuebbles, D.J., Fahey, D.W., Hibbard, K.A., Dokken, D.J., Stewart, B.C., and Maycock, T.K. (eds.)]. Washington, DC, USA.

Vitasse, Y., François, C., Delpierre, N., Dufrêne, E., Kremer, A., Chuine, I. and Delzon, S., 2011. Assessing the effects of climate change on the phenology of European temperate trees. *Agricultural and Forest Meteorology*, 151(7), 969-980.

Vose, J.M., Peterson, D.L. and Patel-Weynand, T., 2012. Effects of climatic variability and change on forest ecosystems: a comprehensive science synthesis for the US. *Gen. Tech. Rep. PNW-GTR-870. Portland, OR: US Department of Agriculture, Forest Service, Pacific Northwest Research Station*, 265, 870.

White, M.A. and Nemani, R.R., 2003. Canopy duration has little influence on annual carbon storage in the deciduous broad leaf forest. *Global Change Biology*, 9(7), 967-972.

White, M.A., Running, S.W. and Thornton, P.E., 1999. The impact of growing-season length variability on carbon assimilation and evapotranspiration over 88 years in the eastern US deciduous forest. *International Journal of Biometeorology*, 42(3), 139-145.

Wilson, K.B., Baldocchi, D.D. and Hanson, P.J., 2000. Spatial and seasonal variability of photosynthetic parameters and their relationship to leaf nitrogen in a deciduous forest. *Tree Physiology*, 20(9), 565-578.

Wilson, K.B. and Baldocchi, D.D., 2001. Comparing independent estimates of carbon dioxide exchange over 5 years at a deciduous forest in the southeastern United States. *Journal of Geophysical Research: Atmospheres*, 106(D24), 34167-34178.

Wolf, S., Eugster, W., Ammann, C., Häni, M., Zielis, S., Hiller, R., Stieger, J., Imer, D., Merbold, L. and Buchmann, N., 2013. Contrasting response of grassland versus forest carbon and water fluxes to spring drought in Switzerland. *Environmental Research Letters*, 8(3), 035007.

Wolter, P.T., Johnston, C.A. and Niemi, G.J., 2006. Land use land cover change in the US Great Lakes basin 1992 to 2001. *Journal of Great Lakes Research*, 32(3), 607-628.

Woodall, C.W., Oswalt, C.M., Westfall, J.A., Perry, C.H., Nelson, M.D. and Finley, A.O., 2009. An indicator of tree migration in forests of the eastern United States. *Forest Ecology and Management*, 257(5), 1434-1444.

Wu, C., Chen, J.M., Gonsamo, A., Price, D.T., Black, T.A. and Kurz, W.A., 2012. Interannual variability of carbon sequestration is determined by the lag between ends of net uptake and photosynthesis: evidence from long records of two contrasting forest sands. *Agric. For. Meteorol.*, 164, 29–38.

Wu, C., Chen, J.M., Black, T.A., Price, D.T., Kurz, W.A., Desai, A.R., Gonsamo, A., Jassal, R.S., Gough, C.M., Bohrer, G. and Dragoni, D., 2013. Interannual variability of net ecosystem productivity in forests is explained by carbon flux phenology in autumn. *Global Ecology and Biogeography*, 22(8), 994-1006.

Yuan, W., Luo, Y., Richardson, A.D., Oren, R.A.M., Luyssaert, S., Janssens, I.A., Ceulemans, R., Zhou, X., Grünwald, T., Aubinet, M. and Berhofer, C., 2009. Latitudinal patterns of magnitude and interannual variability in net ecosystem exchange regulated by biological and environmental variables. *Global Change Biology*, 15(12), 2905-2920.

Zhu, K., Woodall, C.W., & Clark, J.S., 2012. Failure to migrate: lack of tree range expansion in response to climate change. *Global Change Biology*, 18(3), 1042-1052.

Table 3.1: Annual calculated phenological dates, reported as day of year, from 2012 to 2017, are shown in the upper portion of the table. Dates were calculated following Gonsamo et al. (2013) from eddy covariance (EC) measured GEP_{Max} data. The six-year mean values and standard deviations are included in the final column. The resulting phenological periods and their duration in days are also shown, in the lower portion of the table.

Phenology Transition Dates	**2012**	**2013**	**2014**	**2015**	**2016**	**2017**	**Mean**
Start of Season (SOS, bud-break)	120	116	127	118	126	125	122 ± 5
Mid of Greenup (MOG, fastest green-up)	136	141	148	136	144	147	142 ± 5
End of Greenup (EOG, end of leaf-out)	145	155	160	146	154	159	153 ± 6
Start of Browndown (SOB, start of senescence)	257	249	255	249	262	261	255 ± 6
Mid of Browndown (MOB, fastest senescence)	275	273	274	271	286	282	277 ± 6
End of Season (EOS)	306	314	307	309	328	318	314 ± 8
Phenologically-Defined Seasons	**2012**	**2013**	**2014**	**2015**	**2016**	**2017**	**Mean**
Spring (EOG – SOS)	25	39	34	28	28	34	31 ± 5
Summer (SOB – EOG) (LOCC, Length of Canopy Closure)	112	94	95	103	107	102	102 ± 7
Autumn (EOS – SOB)	49	65	52	61	67	57	58 ± 7
Length of Growing Season (LOS)	186	198	180	191	202	193	192 ± 8

Table 3.2: Seasonal and annual means and totals of key site meteorological parameters from 2012 to 2017, summarized by phenologically defined seasons (see Table 3.1 for more details). The six year mean values, standard deviations, and the day of year when daily mean Ta at the start of the growing season exceeded the annual mean Ta are also included. Values in parentheses represent the 30-year Environment Canada (Delhi, Ontario, weather station) mean Ta and annual P.

	Time Period	2012	2013	2014	2015	2016	2017	Mean
PAR Sum (μmol m^{-2})	Spring (SOS to EOG)	1077	1541	1291	1091	1148	1289	1240 ± 175
	Summer (EOG to SOB)	4442	3402	3506	3911	4287	3783	3889 ± 415
	Autumn (SOB to EOS)	898	1246	1046	1324	1188	1056	1127 ± 155
	Annual	9071	8408	8845	8994	9088	8530	8823 ± 290
Ta Mean (^{o}C)	DOY daily Ta < annual Ta	121	116	125	118	124	130	122 ± 5
	Spring (SOS to EOG)	16.6	15.1	16.1	15.1	15.6	14.0	15.4 ± 0.9
	Summer (EOG to SOB)	22.8	20.3	20.2	20.1	21.8	20.3	20.9 ± 1.1
	Autumn (SOB to EOS)	12.4	12.9	12.5	14.7	12.4	13.6	13.1 ± 0.9
	Annual	11.8	9.2	8.0	9.2	10.6	10.0	9.8 ± 1.3 (8.0 ± 1.6)
VPD Mean (kPa)	Spring (SOS to EOG)	0.93	0.66	0.59	0.61	0.71	0.51	0.67 ± 0.15
	Summer (EOG to SOB)	1.00	0.53	0.53	0.55	0.72	0.57	0.65 ± 0.19
	Autumn (SOB to EOS)	0.41	0.34	0.34	0.43	0.35	0.41	0.38 ± 0.04
	Annual	0.57	0.35	0.33	0.35	0.42	0.36	0.40 ± 0.09
$\theta_{0\text{-}30cm}$ (m^3 m^{-3})	Spring (SOS to EOG)	0.12	0.10	0.12	0.11	0.10	0.12	0.11 ± 0.15
	Summer (EOG to SOB)	0.06	0.10	0.09	0.10	0.04	0.07	0.08 ± 0.19
	Autumn (SOB to EOS)	0.10	0.11	0.12	0.08	0.09	0.09	0.10 ± 0.04
	Annual	0.10	0.11	0.11	0.10	0.10	0.10	0.10 ± 0.09
θ_{100cm} (m^3 m^{-3})	Spring (SOS to EOG)	0.09	0.10	0.11	0.10	0.09	0.11	0.10 ± 0.01
	Summer (EOG to SOB)	0.06	0.08	0.08	0.07	0.04	0.05	0.06 ± 0.02
	Autumn (SOB to EOS)	0.09	0.06	0.10	0.04	0.08	0.07	0.07 ± 0.02
	Annual	0.09	0.09	0.10	0.08	0.08	0.09	0.09 ± 0.01
P Sum (mm)	Spring (SOS to EOG)	37	123	93	28	19	71	62 ± 41
	Summer (EOG to SOB)	234	263	357	262	217	148	247 ± 69
	Autumn (SOB to EOS)	224	213	176	160	225	200	200 ± 27
	Annual	801	954	991	750	908	795	866 ± 98 (997)

Table 3.3: Mean greenness chromatic coordinate (GCC) dates (day of year) from 2012 to 2017, calculated from annual GCC transition thresholds (10%, 25%, and 50%) from the site's digital camera (PhenoCam), installed at 36 m height. Also included are the timing of seasonal smoothed GCC maximum (spring peak) and minimum (autumn EOS) dates.

Greenness Transition Dates	**2012**	**2013**	**2014**	**2015**	**2016**	**2017**
Spring Transition 10%	122	124	136	127	131	133
Spring Transition 25%	125	128	142	130	138	136
Spring Transition 50%	131	135	146	134	144	140
GCC_{Smooth} Maximum	147	149	156	148	154	155
Autumn Transition 50%	275	274	279	276	281	288
Autumn Transition 25%	286	284	286	282	288	295
Autumn Transition 10%	289	287	289	286	291	--
GCC_{Smooth} Minimum (EOS)	298	309	303	300	309	316

Table 3.4: Seasonal and annual sums of eddy covariance (EC) flux measurements from 2012 to 2017, calculated using the timing of key phenological dates included in Table 3.1. The six-year mean and standard deviations are also included.

	Season	2012	2013	2014	2015	2016	2017	Mean
GEP Sum	Jan 1 to SOS	--	--	--	--	--	--	--
	Spring (SOS to EOG)	104	197	165	117	129	174	148 ± 36
	Summer (EOG to SOB)	942	949	1023	1006	1084	1070	1012 ± 59
	Autumn (SOB to EOS)	147	239	200	240	219	213	210 ± 34
	EOS to Dec 31	--	--	--	--	--	--	--
	Annual	1198	1369	1382	1347	1420	1447	1360 ± 87
RE Sum	Jan 1 to SOS	167	107	129	109	163	170	141 ± 30
	Spring (SOS to EOG)	78	151	133	109	109	144	121 ± 27
	Summer (EOG to SOB)	500	672	581	714	684	700	642 ± 84
	Autumn (SOB to EOS)	138	269	196	259	266	252	230 ± 52
	EOS to Dec 31	82	64	84	110	55	65	77 ± 20
	Annual	954	1250	1110	1283	1260	1317	1196 ± 138
NEP Sum	Jan 1 to SOS	-117	-79	-88	-82	-129	-130	-104 ± 24
	Spring (SOS to EOG)	25	45	30	4	18	29	25 ± 14
	Summer (EOG to SOB)	442	276	441	288	398	371	369 ± 73
	Autumn (SOB to EOS)	16	-26	4	-18	-46	-37	-18 ± 24
	EOS to Dec 31	-68	-56	-79	-103	-51	-58	-69 ± 19
	Annual	292	156	305	90	185	169	200 ± 83

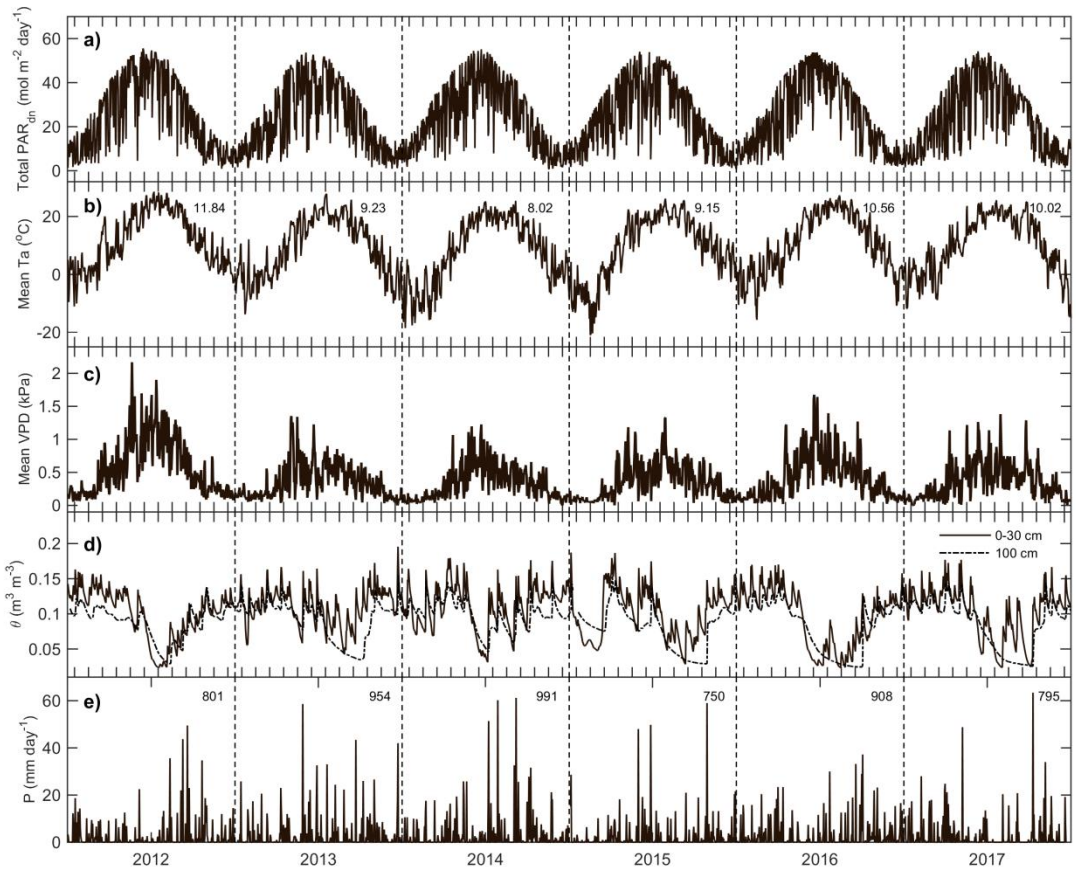

Figure 3.1: Daily time series from 2012 to 2017 of (a) total photosynthetically active radiation (PAR, mol m^{-2}), (b) mean air temperature (Ta, °C), (c) vapor pressure deficit (VPD, kPa), and volumetric water content (θ, m^3 m^{-3}) at 0-30 cm and 1 m depths, and total precipitation (P, mm). Annual mean Ta and annual total P are also included for each year, with 8.0°C and 997 mm corresponding to the 30-year (1981 – 2010) Environment Canada Delhi CDA weather station (located 25 km north of sites) mean annual Ta and P, respectively.

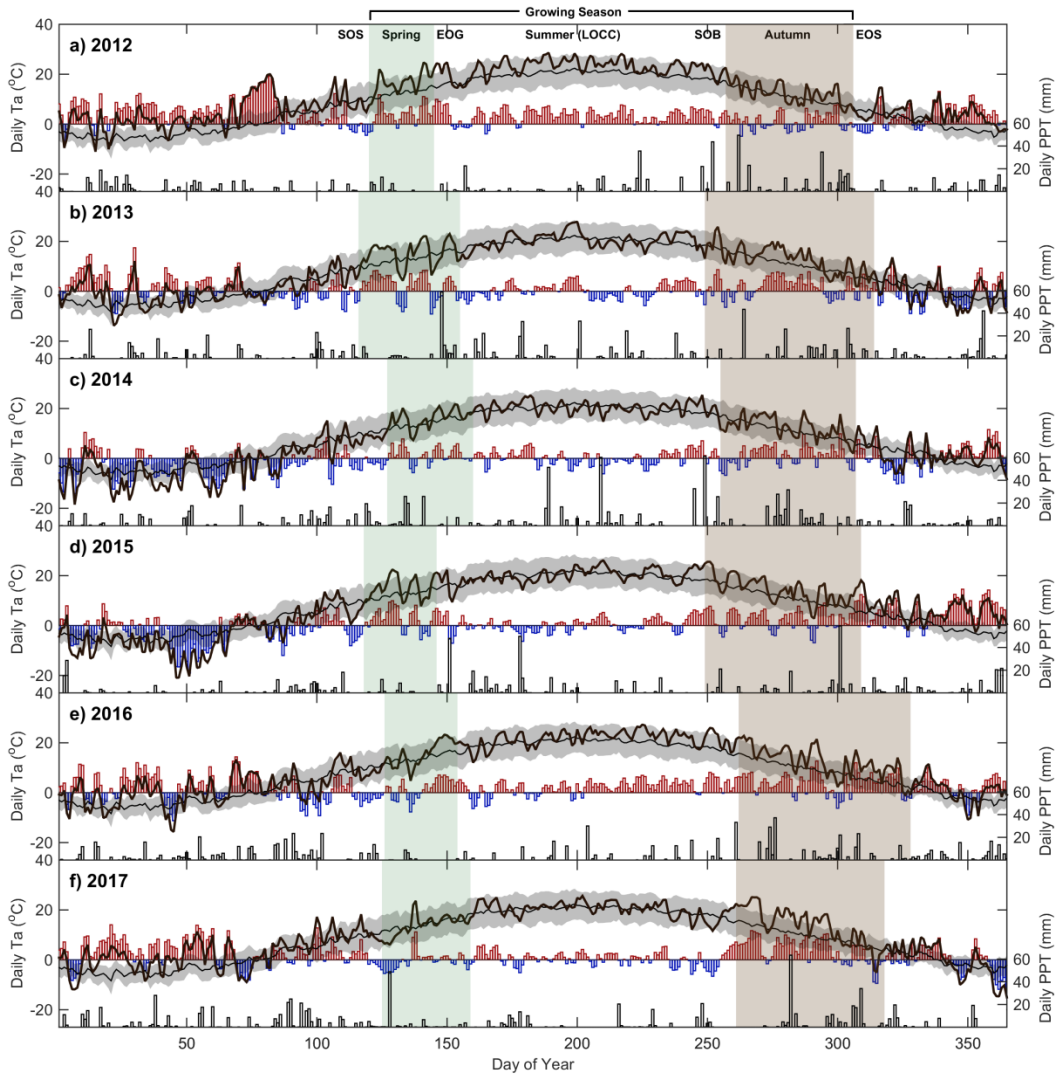

Figure 3.2: Bar plots of the anomalies of daily mean air temperature (Ta, °C) within the forest compared to the 30-year Environment Canada mean Ta (left axis), and daily precipitation (P, mm) on the right axis, from 2012 to 2017 (a – f). Grey shade about the 30-year mean-curve represents the range of 30-year mean Ta (thin line). The bold black lines represent the measured forest Ta, used for the calculation of the bars. Vertical green and brown shaded regions cover the annual ranges of dates from SOS to EOG and SOB to the EOS, respectively (Table 3.1).

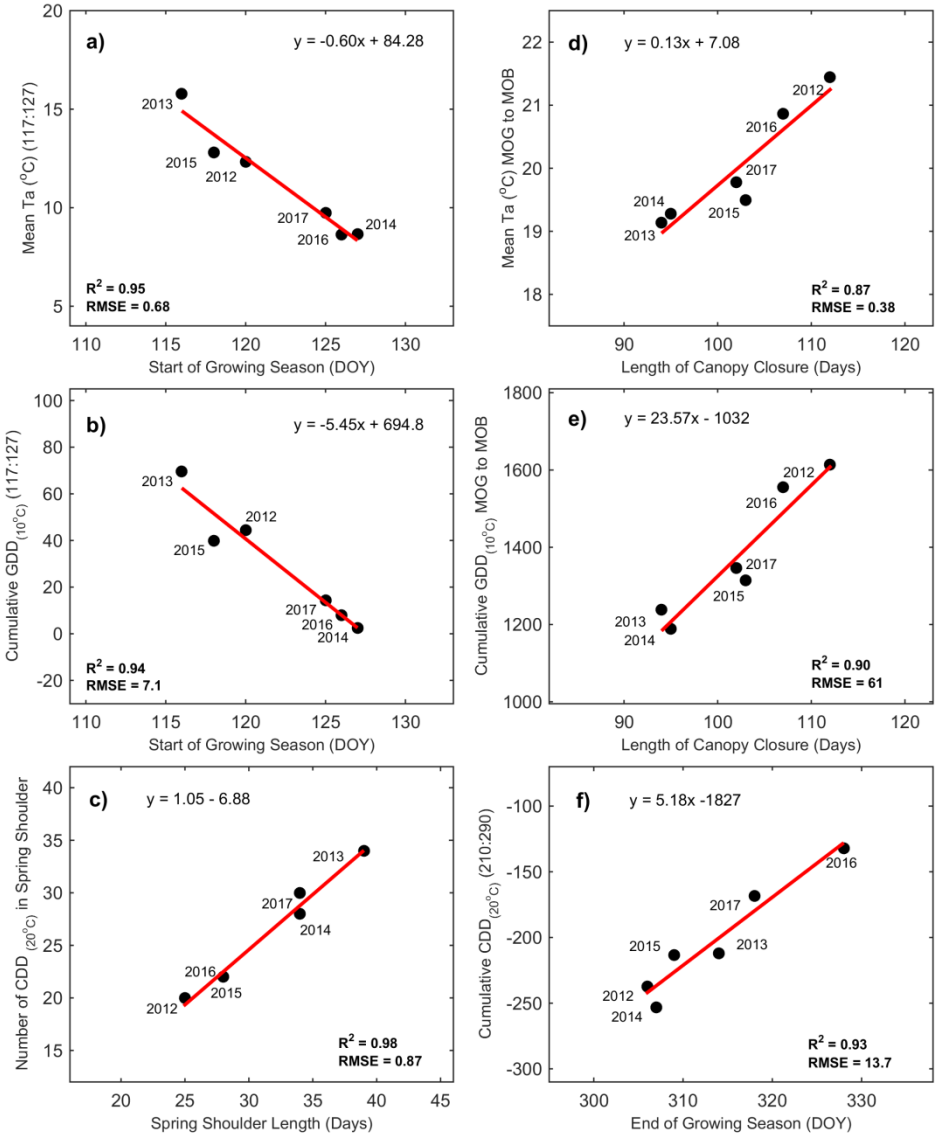

Figure 3.3: Correlations between key environmental drivers and phenological dates and phenological periods: a) seasonal mean air temperature (Ta) and start of growing season (SOS); b) cummulative seasonal growing degree days (GDD) and SOS; c) cooling degree days (CDD) and length of the phenological spring season; d) seasonal mean Ta and the length of canopy closure (LOCC) or phenological summer season; e) GDD and LOCC; and (f) CDD and end of the growing season (EOS). Linear fit equations, R^2, and RMSE included for each correlation.

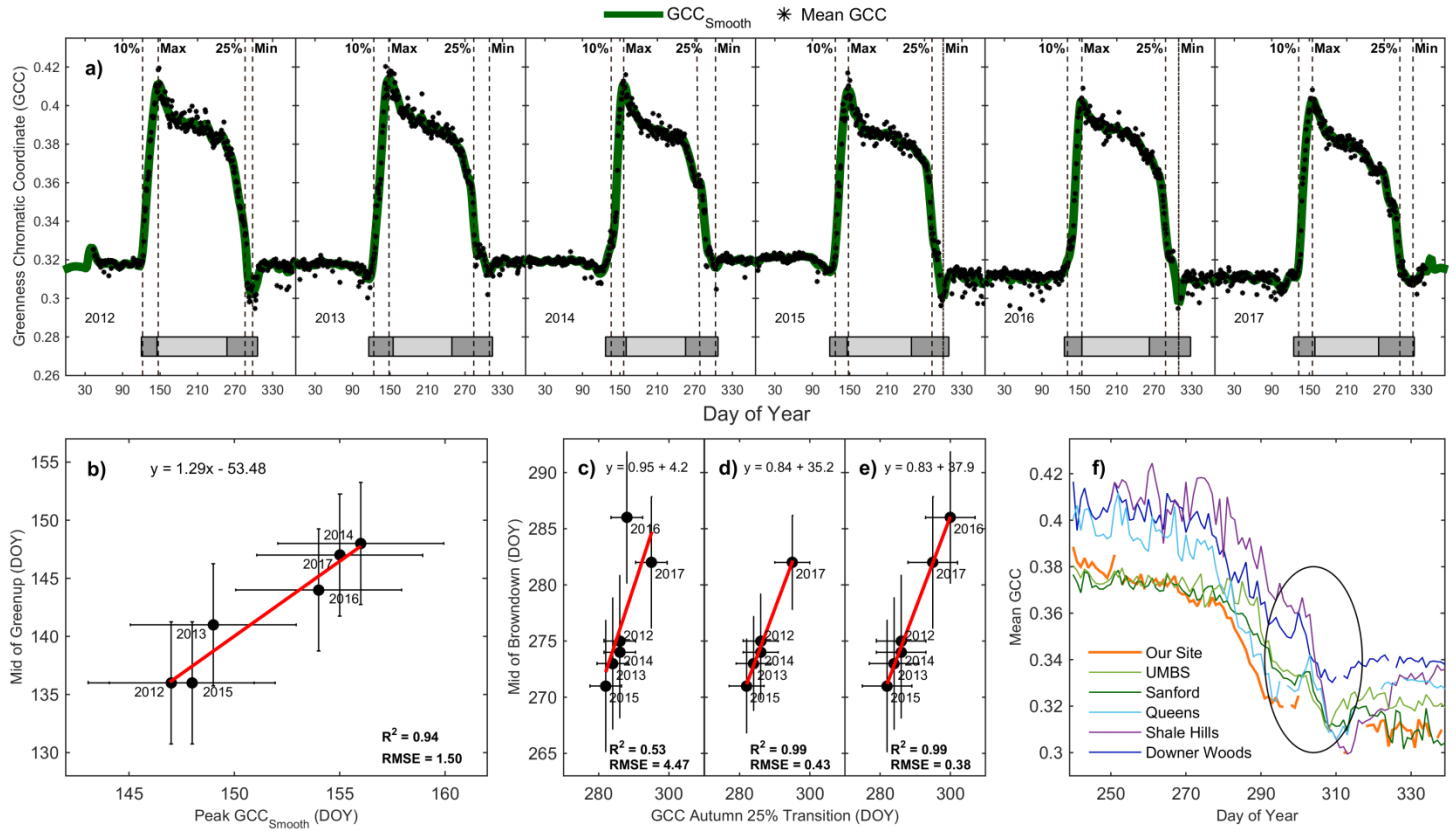

Figure 3.4: (a) Annual time series of mean greenness chromatic coordinate (GCC) and smoothed GCC derived from the PhenoCam installed at 36 m height. Vertical lines represent the dates of the 10% spring GCC transition, maximum GCC, 25% autumn GCC transition, and minimum GCC, respectively (Table 3.3). Dark grey shading illustrates the spring and autumn seasons derived from EC-data, while light grey in between represents summer. Also shown are the annual relationships between (b) peak GCC and mid of greenup (MOG), and the (c) GCC 25% autumn transition date and mid of browndown (MOB). For the 25% autumn GCC transition dates and MOB, 2016 was removed (d), and (e) estimated using (f) mean autumn GCC data from regional PhenoCams at deciduous forests in nearby study sites.

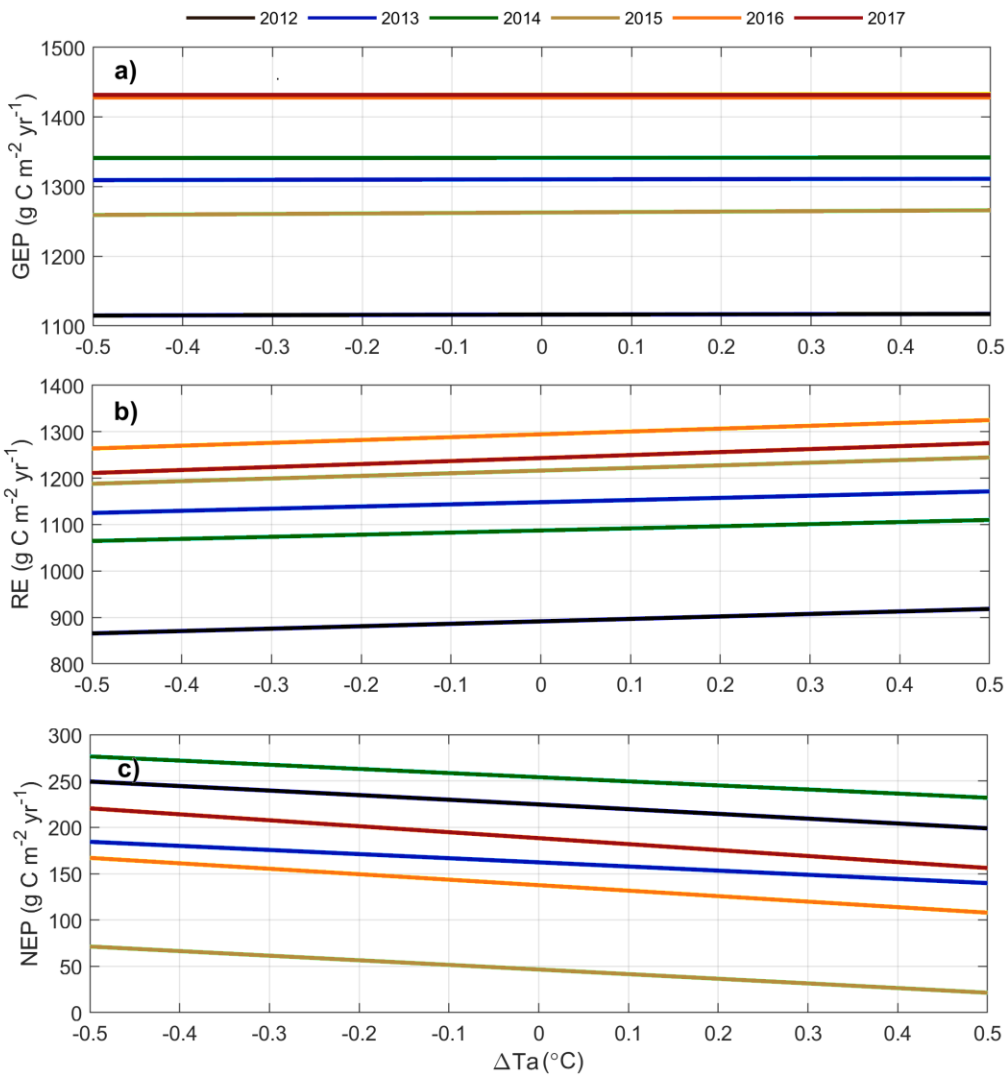

Figure 3.5: Annual total (a) gross ecosystem productivity (GEP), (b) ecosystem respiration (RE), and (c) net ecosystem productivity (NEP) using modified (increasing & decreasing) mean daily air temperature (Ta). The range of ΔTa chosen represents an effective 1°C increase in Ta.

Table S3.1: R^2 and root mean square errors (RMSE, in parentheses) of linear regressions between seasonal meteorological variables (PAR, Ta, VPD, $\theta_{0\text{-}30cm}$, P, GDD, and CDD) and EC-derived phenological dates for the spring, summer and autumn seasons from 2012-2017, highlighting the variables driving phenology.

	Start of Season	**Spring Length**	**End of Greenup**	**Summer Length**	**Start of Browndown**	**Autumn Length**	**End of Season**
Spring PAR	0.04 (191)	0.94 (48.0)	0.40 (152)	0.69 (110)	0.10 (185)	0.10 (186)	0.01 (195)
Spring Ta	0.00 (1.00)	0.25 (0.87)	0.17 (0.92)	0.12 (0.94)	0.00 (1.00)	0.20 (0.90)	0.16 (0.92)
Spring VPD	0.08 (0.16)	0.37 (0.13)	0.47 (0.12)	0.45 (0.12)	0.00 (0.16)	0.08 (0.15)	0.04 (0.16)
Spring $\theta_{0\text{-}30cm}$	0.15 (0.01)	0.03 (0.01)	0.01 (0.01)	0.03 (0.01)	0.08 (0.01)	0.79 (0.00)	0.29 (0.01)
Spring P	0.03 (44.9)	0.87 (16.7)	0.37 (36.4)	0.73 (23.9)	0.16 (41.9)	0.00 (45.7)	0.06 (44.3)
Spring GDD	0.04 (35.5)	0.54 (24.6)	0.18 (32.9)	0.56 (24.1)	0.21 (32.2)	0.00 (36.2)	0.06 (35.1)
Spring CDD	0.21 (4.28)	0.21 (4.27)	0.45 (3.58)	0.21 (4.27)	0.02 (4.75)	0.22 (4.25)	0.07 (4.64)
Summer PAR	0.02 (441)	0.86 (165)	0.41 (343)	0.95 (104)	0.26 (383)	0.02 (441)	0.04 (436)
Summer Ta	0.00 (1.24)	0.50 (0.88)	0.26 (1.07)	0.69 (0.69)	0.21 (1.10)	0.08 (1.19)	0.00 (1.24)
Summer VPD	0.00 (0.21)	0.54 (0.14)	0.36 (0.17)	0.73 (0.11)	0.15 (0.19)	0.19 (0.19)	0.01 (0.21)
Summer $\theta_{0\text{-}30cm}$	0.31 (0.02)	0.29 (0.02)	0.00 (0.02)	0.51 (0.02)	0.81 (0.01)	0.00 (0.02)	0.38 (0.02)
Summer P	0.00 (76.5)	0.02 (75.6)	0.01 (76.3)	0.24 (66.8)	0.27 (65.6)	0.05 (74.6)	0.29 (64.6)
Summer GDD	0.00 (210)	0.67 (121)	0.37 (167)	0.87 (74.3)	0.23 (184)	0.08 (202)	0.01 (209)
Summer CDD	0.00 (111)	0.51 (78.2)	0.33 (91.3)	0.74 (57.2)	0.18 (101)	0.09 (106)	0.00 (111)
Autumn PAR	0.16 (160)	0.07 (168)	0.00 (174)	0.16 (159)	0.29 (147)	0.68 (98)	0.09 (166)
Autumn Ta	0.15 (0.94)	0.00 (1.02)	0.07 (0.98)	0.00 (1.02)	0.20 (0.92)	0.04 (1.00)	0.02 (1.01)
Autumn VPD	0.09 (0.04)	0.29 (0.04)	0.39 (0.03)	0.31 (0.04)	0.00 (0.04)	0.11 (0.04)	0.11 (0.04)
Autumn $\theta_{0\text{-}30cm}$	0.02 (0.02)	0.32 (0.02)	0.27 (0.02)	0.38 (0.01)	0.03 (0.02)	0.05 (0.02)	0.07 (0.02)
Autumn P	0.00 (29.7)	0.01 (29.6)	0.01 (29.7)	0.18 (26.9)	0.27 (25.5)	0.02 (29.4)	0.23 (26.1)
Autumn GDD	0.07 (72.2)	0.07 (72.1)	0.00 (74.6)	0.04 (73.2)	0.03 (73.7)	0.49 (53.4)	0.21 (66.7)
Autumn CDD	0.02 (15.9)	0.02 (15.8)	0.00 (16.0)	0.00 (16.0)	0.00 (16.0)	0.00 (16.0)	0.10 (15.1)

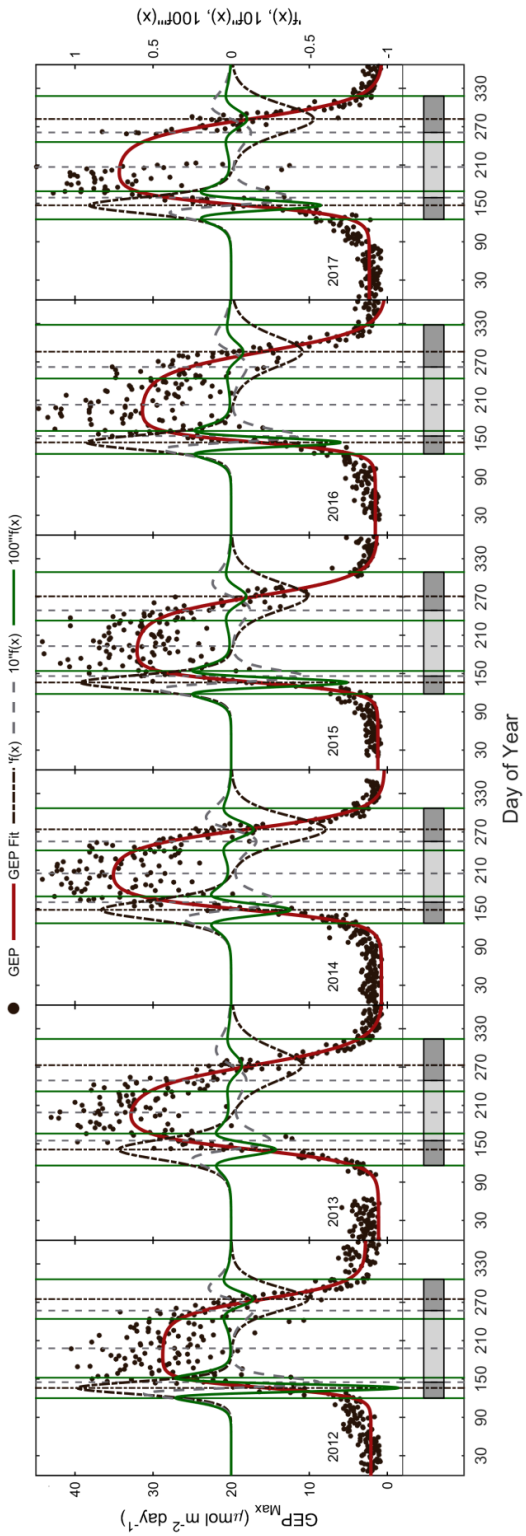

Figure S3.1: The seasonal course of gross ecosystem productivity (GEP), and phenological dates (vertical lines) found in Table 3.1, defined by the maxima and minima of the first (f'(x)), second (f''(x)), and third (f'''(x)) derivatives (right) of the fitted logistic curve. Dark grey shading represents the shoulder seasons (i.e. spring and autumn), while the lighter grey shading represents the summer (peak uptake) period.

CHAPTER 4:

RESPONSE OF CARBON AND WATER FLUXES TO ENVIRONMENTAL VARIABILITY IN TWO EASTERN NORTH AMERICAN FORESTS OF SIMILAR-AGE BUT CONTRASTING LEAF-RETNETION AND SHAPE STRATEGIES

4.1 Abstract

The annual carbon and water dynamics of two Eastern North American forests were compared over a six year period from 2012 to 2017. The geographic location, forest age, soil, and climate were similar between the sites, however, the species composition varied: one was a broadleaf deciduous forest, while the other an evergreen needleleaf forest. During the 6-year study period, the mean annual net ecosystem productivity (NEP) of the coniferous forest was slightly higher and more variable (218 ± 109 g C m^{-2} yr^{-1}) compared to that of the deciduous broadleaf forest NEP of 200 ± 83 g C m^{-2} yr^{-1}. Similarly, the mean annual evapotranspiration (ET) of the conifer forest over the 6-year study period was higher (442 ± 33 mm yr^{-1}) compared to that of the broadleaf forest (388 ± 34 mm yr^{-1}), but with similar interannual variability. Significant disagreements in fluxes were measured between sites during drought years. Summer meteorology greatly impacted fluxes at both sites, but to varying degrees and with varying responses. In general, warm temperatures caused higher ecosystem respiration (RE), resulting in reduced mean annual NEP values – an impact that was more

pronounced at the broadleaf deciduous forest compared to the evergreen needle-leaf forest. However, during drought years, the evergreen forest saw greater annual reduction in carbon sequestration compared to the deciduous forest. In the evergreen conifer forest, variability of summer meteorology greatly controlled the forest's annual carbon sink-source strength. Annual ET at both forests was driven by changes in air temperature (Ta), with the largest annual ET measured in the warmest years in the deciduous forest. Additionally, prolonged dry periods with increased Ta, greatly reduced ET. During drought years, the carbon and water fluxes of the deciduous forest were less sensitive to changes in temperature or water availability compared to the evergreen forest. If longer periods of increased temperatures and larger precipitation variability during summer months are to be expected under future climates, our findings suggest the carbon sink capacity of the deciduous forest will continue, while that of the conifer forest remains uncertain in the study region.

4.2 Introduction

Temperate forests play a significant role in the global carbon and water cycles, through their photosynthetic absorption of CO_2 emissions, and through their evapotranspiration (ET) processes (Huntington, 2006; Houghton et al., 2007). In Eastern North America, temperate forests are significant for future climate mitigation strategies, as they are impacted by warming and disturbance events (Bonan, 2008; Cubasch et al., 2013; Weed et al., 2013). These areas were a large

source of carbon, due to land clearing for agricultural purposes, at the start of the 20th century (Bonan, 2008; Richart & Hewitt, 2008). With the rise of industrial development and movement of agriculture into western states, many of these agricultural areas were abandoned and reforested through natural regrowth and afforestation practices (Canadell & Raupach, 2008). Within the mixed wood plains ecozone in the Great Lakes region of Canada and the USA, much of the current forested area is comprised of plantation or managed forests in different stages of growth (Wiken et al., 2011).

Recent increases in extreme weather, such as drought and heat stress, or the absence of winter snow or freezing events, may directly impact the abilities of forests to sequester carbon, adversely impacting regional forest-atmosphere interactions (Allen et al., 2010; Teskey et al., 2015). Furthermore, forests have the ability to dampen or deepen the effects of warming, acting as climate feedback systems (Bonan, 2008). With continued extreme weather and insufficient water availability, due to more frequent intermittent drought events, carbon assimilation and ET in forests could be hindered, leading to positive feedbacks of continued warming and decreased water availability (Bréda et al., 2006; Choat et al., 2012; Wu et al., 2013). Given the uncertainty of the duration and timing of future extreme weather events, it is necessary to further improve our understanding of the controls and limitations of carbon and water cycles under changing climates.

The result of a shifting climate may lead to different impacts on deciduous broadleaf and evergreen needleleaf ecosystems, as regions once dominated by

needle-leaved conifers may yield way to more deciduous broad-leaved species (Givnish, 2002; Bonan 2008). Such a shift could disturb carbon and water cycles, as deciduous broadleaf forests typically experience higher rates of photosynthesis when compared to evergreen conifers. Some deciduous forests have also been shown to reduce transpiration and ecosystem respiration during drought events (Givnish, 2002; Cias et al., 2005). Conversely, evergreen conifer forests routinely experience a longer photosynthetic season than deciduous forests, albeit at lower rates (Barr et al., 2002). Even for climatically and geographically similar forests, differences in the timing of photosynthesis and respiration would lead to asymmetries in the partitioning of the resulting fluxes, as well as overall forest productivity and longevity.

While many studies have examined the annual carbon and water fluxes within specific land use and forest types, to date, only a handful of studies have compared these fluxes among similar-age deciduous broadleaf and evergreen coniferous forest stands growing in close proximity, in similar climatic and edaphic conditions (Gaumont-Guay et al., 2009; Baldocchi et al., 2010; Novick et al., 2015; Wagle et al., 2016). Even fewer studies have the ability to conduct such research over sufficiently long time scales (multiple years). Such a study would help to evaluate how differing forest types will respond to meteorological forcings annually and interannually, helping to investigate the long-term impacts on carbon and water exchanges (Granier et al., 2007; Novick et al., 2015). In order to understand the benefits of deciduous broadleaf and evergreen coniferous forests to

terrestrial-atmosphere gas exchange and identify the factors driving that exchange, long-term comparison studies are needed.

The Turkey Point Observatory in southern Ontario, Canada is located near Lake Erie Lowlands at the northernmost extent of temperate deciduous forests in Eastern North America, just south of the Great Lakes – St. Lawrence forest ecotone (Liu, 1990). Forests in the area contain numerous North American temperate species (e.g. white oak [*Quercus Alba*], red maple [*Acer Rubrum*], eastern white pine [*Pinus Strobus L.*], and red pine [*Pinus Resinosa*]), many at the northern extent of their natural climatic ranges (Richart & Hewitt, 2008; Froelich et al., 2015). Four sites make up the Observatory, three white pine plantation forests of various ages and a mixed-wood broadleaf deciduous forest.

Previous carbon and water studies conducted within the conifer forests of the Turkey Point Observatory have been reported in literature (i.e. Arain & Restrepo-Coupe, 2005; Peichl & Arain, 2007; McLaren et al., 2008; Peichl et al., 2010a; MacKay et al., 2012; Skubel et al., 2015; Chan et al., 2018). Other studies have written about variability in carbon and water fluxes of the broadleaf deciduous forest (Beamesderfer et al., 2019). This study examines the carbon and water exchanges between two forests of similar ages within the Turkey Point Observatory: the 80-year old (as of 2019) managed white pine plantation, and the naturally regenerated, mixed-wood, white oak-dominated forest that is roughly 90-years old. The objectives of this study are to: (1) examine seasonal and interannual dynamics of carbon and water exchanges in the two forests growing

under similar climatic and edaphic conditions, but of differing tree species composition, (2) compare controls on overall forest productivity between the two forests, and (3) identify the responses of the forests to meteorological events during extreme years (heat and drought). Six years of data, collected congruently at the two sites, from 2012 through 2017, will be used in this study.

4.3 Methods

4.3.1 Study Sites

The two forests are located within 20 km of each other, situated on the northern edge of Lake Erie, near St. Williams in Norfolk County, Ontario, Canada (Table 4.1). Monoculture pine plantations and mixed-wood deciduous forests cover only a small fraction of the agriculturally dominated landscape of southern Ontario. The deciduous broadleaf forest (from here on abbreviated and referred to as, Turkey Point Deciduous, TPD) was naturally regenerated in the early 1900s from abandoned agricultural land-use on natural sandy terrain. The forest is classified as an uneven aged (70 – 110 years-old with a mean age of roughly 90-years) oak-dominated forest. The stand is dominated by white oak (*Quercus Alba*), with secondary hardwood species including: red maple (*Acer Rubrum*), sugar maple (*Acer Saccharum*), black oak (*Quercus Velutina*), red oak (*Quercus Rubra*), white ash (*Fraxinus Americana*), yellow birch (*Betula alleghaniensis),* and American beech (*Fagus Grandifolia*). Conifer species make up a minor component (~5%) of the total tree population (Kula, 2014). The understory is made up of young

deciduous trees as well as Canadian mayflower (*Maianthemum canadense),* putty root (*Aplectrum hymale*), yellow mandarin (*Disporum lanuginosum*), red trillium (*Trillium erectum*), and horsetail (*Equistum*).

The white pine plantation in this study, referred to as Turkey Point 39 (TP39 from here on), was planted in 1939 on cleared oak-savanna lands. The dominant tree species in the 80-year old (as of 2019) site are white pine (*Pinus Strobus* L.) and balsam fir (*Abies balsamifera* L. Mill), making up 82% and 11% of the tree population, respectively. The remaining 7% of trees are typical native eastern North American forest species, which include: white oak, black oak, red maple, wild black cherry (*Prunus serotina* Ehrh.) and white birch (*Betula papyrifera*). The understory consists of young white pines, oak, balsam fir, and black cherry trees, as well as other ground vegetation, including: bracken fern (*Pteridium aquilinum*), blackberry (*Rubus spp.*), poison ivy *(Rhus radicans*), moss (*Polytrichum spp.*), and Canada Mayflower. The conifer forest has been managed on two occasions in the past (i.e. 1983 & 2012). In the early winter of 2012, the stand was thinned by harvesting one third of the trees, which reduced the stand density (Table 4.1). We acknowledge this disturbance at the beginning of our comparison period at the conifer site, though the objectives of this study were not to examine the impacts of this disturbance.

The two forests differ in vegetation cover and canopy structure, but experience nearly identical edaphic and climatic conditions. Both sites are located within the Southern Norfolk Sand Plains, historically defined by coarse-grained,

sandy deposits from glacial melt water (Richart and Hewitt, 2008). The soils at each forest are predominantly sandy (greater than 90% sand), classified by the Canadian Soil Classification Scheme as Brunisolic grey-brown luvisol (Present & Acton, 1984). They are both well-drained with a low-to-moderate water holding capacity (McLaren et al., 2008). Further soil and site details can be found in Arain & Restrepo-Coupe (2005), Peichl et al. (2010a), and Beamesderfer et al. (2019a). The climate of the region is humid temperate with warm, humid summers and cool winters. The moderating effect of Lake Erie helps to control cold winter temperatures. The 30-year (from 1981 to 2010) mean annual air temperature and total precipitation measured at the Environment Canada Delhi CDA weather station (25 km north of sites) were 8.0°C and 997 mm, respectively. Total precipitation is normally evenly distributed throughout the year, with 13% of that falling as snow (Environment and Climate Change Canada). The data presented from these forest sites are readily available following the global FluxNet and AmeriFlux initiatives, known as CA-TPD (TPD) and CA-TP4 (TP39).

4.3.2 Eddy Covariance and Meteorological Measurements

Half-hourly fluxes of momentum, energy, water vapor, and CO_2 (Fc) have been measured continuously at TP39 and TPD using closed-path eddy covariance (EC) systems since 2003 and 2012, respectively. This study examines the first 6 years (2012 to 2017) of recorded data at the deciduous forest, and the corresponding period for the conifer forest, though measurements at both sites are still ongoing

today. The closed-path EC systems consist of a 3D sonic anemometer (CSAT3, Campbell Scientific Inc.) and an infrared gas analyzer (IRGA); an LI-7000 (LI-COR Inc.) at TP39 and an LI-7200 (LI-COR Inc.) at TPD. The specific details of the two EC systems are outlined in the supplementary Table S4.1. At both sites, IRGAs are calibrated monthly using high purity N_2 gas for the zero offset, and Environment Canada Greenhouse gas specified CO_2 gas for the CO_2 span.

The CO_2 storage (S_{CO2}) in the air column below the EC sensors is calculated by vertically integrating the half-hourly difference in CO_2 concentrations. This calculation is completed for both the canopy and mid-canopy gas analyzers (Table S4.1). Half-hourly net ecosystem exchange (NEE, µmol m^{-2} s^{-1}) is calculated as the sum of the vertical CO_2 flux (F_c), and the rate of CO_2 storage (S_{CO2}) change in the air column below each IRGA ($NEE = F_c + S_{CO2}$). Horizontal and vertical advections were assumed to average to zero over long periods and were not considered. Half-hourly net ecosystem productivity (NEP) was calculated as the opposite of NEE (NEP = -NEE), where positive NEP (-NEE) indicates net carbon uptake by the forest (sink), and negative NEP (+NEE) is carbon loss from the forest to the atmosphere (source).

Meteorological measurements have been conducted alongside EC measurements during the entire measurement period at both sites. Air temperature (Ta), relative humidity (RH), wind speed and direction, downward and upward photosynthetically active radiation (PAR), and the four-components of radiation (Rn) are measured at the specified EC sampling heights for both sites (Table

S4.1). Soil temperature (Ts) and soil water content (θ) are measured at 2, 5, 10, 20, 50, and 100 cm depths in two soil pit locations at both sites. At TPD, precipitation (P) is measured in a small forest opening, 350 m southwest of the tower. Precipitation data are cross-checked and gapfilled from data collected by the Environment Canada Delhi CDA weather station as well as from an accumulation rain gauge (GEONOR), installed 1 km south of TP39. This analysis will focus on P data from the accumulation rain gauge. Lastly, all meteorological, soil, and P data were recorded using data loggers with automated data downloads occurring every half hour on desktop computers located at the base of the scaffold walk-up towers located at each site.

Following an AmeriFlux visit to TP39 for an instrument and data comparison (in 2019; post-processing), the downward PAR sensor at that site was found to be identical to the AmeriFlux measurements. Consequently, downward PAR at TPD was thus underestimating (likely due to sensor differences [i.e. PAR-Lite vs PQSI] and their coefficients) actual PAR values, leading to a correction factor of 1.22 (slope between sites) being applied to daily data for each year.

4.3.3 Eddy Covariance Data Processing

All meteorological and flux data were quality controlled, filtered, and cleaned (threshold and point cleaning) on lab-developed software following the FluxNet Canada Research Network (FCRN) guidelines (Brodeur, 2014). Data was frequently cross-checked with the AmeriFlux Network, before submission to

publicly available datasets. Outliers in the data were identified and removed, while missing data was gapfilled. Small gaps in the data (hours) due to instrument malfunctions, power failures, or instrument calibration, were filled by linear interpolation, while larger gaps (hours to days) were filled using linear regression-model fitted values from other Turkey Point Observatory sites. Overall, the mean flux recovery was 91% (from 83% to 94%) at TPD and 88% (from 79% to 94%) at TP39 over the 6-years of data collection. The data initially recovered and quality controlled was then subject to footprint threshold and friction velocity (u*) threshold (u^{*Th}) passing methods. For every half-hourly measurement, a footprint model (Kljun et al., 2004) was applied to exclude fluxes when greater than 10% of the flux footprint extended outside of the defined forest boundary (Brodeur, 2014). Following the footprint passing method, the remaining flux data recovery was 59% (from 54% to 64%) at TPD and 72% (from 67% to 77%) at TP39. Moreover, during periods of low turbulence, EC systems often underestimate fluxes. As a result, inaccurate measurements captured during periods of low turbulence were removed when measured u* was below thresholds estimated using a u^{*Th} Moving Point Test determination method (Reichstein et al., 2005; Papale et al., 2006; Barr et al., 2013). A mean, site specific, u^{*Th} of 0.40 m s^{-1} (TPD) and 0.49 m s^{-1} (TP39) was calculated, where daytime and nighttime NEE values with u* below this threshold were removed. These data were filled using exponential relationships between sufficiently turbulent ($u^* > u^{*Th}$) NEE and Ts at 2 cm depth. The final mean annual flux recovery following both threshold passing

methods was 49% (from 46% to 53%) at TPD and 53% (from 48% to 57%) at TP39 during the 6-years of measurements. The random flux error, referring to the variability among averaging periods and sample size (Loescher et al., 2006), was previously estimated at TP39 (35 g C m^{-2} $year^{-1}$; Brodeur, 2014), with similar variability in the random uncertainty expected between the two forest sites.

Gaps in ecosystem respiration (RE) were modelled similarly for both sites, as a function of Ts_{5cm} and $\theta_{0\text{-}30cm}$ (average from measurements made at 5, 10, 20, & 50 cm depths) using fitted ordinary least square non-linear regression models applied to half-hourly nighttime NEE. This was done in order to describe the relationship between RE and Ts_{5cm}, representing the diurnal variation in Ta, modified by a soil moisture (θ) function as shown (Brodeur, 2014):

$$RE = R_{10} \times Q_{10}^{\frac{(Ts_{\,5\,cm} - 10)}{10}} \times \frac{1}{[1 + \exp(a_1 - a_2\,\theta_{0-30\,cm})]} \quad (1)$$

where R_{10} and Q_{10} are fitted temperature response parameters describing the RE and Ts_{5cm} relationship, while a_1 and a_2 are fitted parameters ranging from 0 to 1, as a function of the independent variable, $\theta_{0\text{-}30cm}$, acting to scale the RE relationship. Modeled daytime RE was then added to measured NEP to estimate the gross ecosystem productivity (GEP). When half-hourly periods existed with gaps in NEP, GEP was modeled using a rectangular hyperbolic function:

$$GEP = \frac{\alpha PARd\ A_{max}}{\alpha PARd + A_{max}} \times f(T_s) \times f(VPD) \times f(\theta_{0\text{-}30cm}) \quad (2)$$

where the first term defines the relationship between PAR and GEP, through the calculation of the photosynthetic flux per quanta (α, quantum yield) and the light-saturated rate of CO_2 fixation (A_{max}). The remaining terms describe sigmoidal scales (ranging from 0 to 1) responses of GEP to Ts, vapor pressure deficit (VPD), and $\theta_{0\text{-}30cm}$, respectively. During half-hourly periods where meteorological data were missing, gaps in RE and GEP were filled using a non-linear regression approach and a marginal distribution sampling approach (Reichstein et al., 2005; Brodeur, 2014). Missing NEP data due to instrumentation errors, maintenance, calibrations, and power outages, were filled as the difference between the modeled RE and modeled GEP.

These gapfilling methods were further used to explore relationships between each sites component fluxes (RE and GEP) and controlling meteorological and edaphic variables using residual analyses. RE and GEP gapfilling models (see above) were parameterized using pooled data from the phenologically-derived summer months (end of greenup to start of browndown, defined in the next section) for all years (2012 to 2017). Furthermore, much like other temperate forests, due to the influence of canopy cover and optimal growing conditions, summer was identified as a key period for carbon uptake at both sites. Based on the functional models used to estimate fluxes (see above), controlling meteorological variables were separated into 'driving' (Ts_{5cm} for RE; PAR for GEP) and 'scaling' ($\theta_{0\text{-}30cm}$ for RE; Ta, $\theta_{0\text{-}30cm}$, VPD for GEP) variables. In this approach, the functional form for the driving variables defines a theoretical

maximum flux for a given value of driving variable, while the scaling variables modify the magnitude of the flux by a normalized factor (between 0 and 1) depending on its value. The influence of each 'scaling' variable on component fluxes was examined by removing one from the model, re-parameterizing, and regressing the model residuals (predicted - modeled flux) as a function of the removed variable. This approach provided a measure of the removed variable's influence on component fluxes as a function of its magnitude. The relationships derived using this approach were used in conjunction with the functional relationships derived during parameterization using all available variables to characterize the nature of effects, and quantify the total effect of a given variable during a particular season.

While the ultimate focus of this study was to compare differences in carbon fluxes between the two forests, the flux of water vapor was also essential to the analysis and necessary for the calculation of key variables. Following the aforementioned threshold and point cleaning, gaps in the latent heat flux (LE), and therefore the mass equivalent evapotranspiration (ET), were filled using an artificial neural network which utilized net radiation (Rn), wind speed, Ts_{5cm}, VPD, and $\theta_{0\text{-}30cm}$ (Brodeur, 2014). Following the approach outlined by Amiro et al. (2006), any remaining gaps in LE data were filled using a moving window linear regression method. Past studies examining the relationships between ET and meteorological variables for the forests of the Turkey Point Observatory have found Ta to largely drive ET, with smaller secondary effects driven by VPD and

$\theta_{0\text{-}30cm}$ during water or heat stressed periods (McLaren et al., 2008; MacKay et al., 2012; Skubel et al., 2015; Burns, 2017).

Lastly, we implemented the analysis of variance (ANOVA) and multivariate analysis of variance (MANOVA) techniques to evaluate statistical differences between groups (deciduous [TPD] versus coniferous [TP39]) on a set of dependent variables (i.e. GEP, RE, NEP, and ET) as well as differences in slopes of environmental response functions (i.e. resource efficiencies discussed in the next section). For all EC and meteorological data, processing and analyses were completed using MatLab R2014b software (The MathWorks Inc.).

4.3.4 Definitions of key climatic and plant-physiological variables

In this study, we define the term drought similar to Wolf et al. (2013), in that drought periods are related to deficits in precipitation, which impose either plant physiological stress due to decreased soil moisture (θ) or impose stress due to stomatal closures in response to high VPD.

Two resource efficiencies were calculated at both forests to compare the links between productivity and resource supply in order to reveal differences in their responses to changing climatic conditions. The amount of carbon fixed through photosynthesis per unit of absorbed solar radiation, described as the photosynthetic light use efficiency (LUE) was calculated as:

$$\mathrm{LUE} = \frac{\mathrm{GEP}}{\mathrm{APAR}} \tag{3}$$

where GEP is equivalent to the carbon fixed through photosynthesis, and APAR is the portion of photosynthetically active radiation (PAR) that is absorbed (Jenkins et al., 2007; Liu et al., 2019). The forest canopy radiation budget used in the calculation of APAR is described as:

$$APAR = PARdn - PARup - PARground \quad (4)$$

where PARdn is the incident PAR measured by PAR sensors mounted at the top of each tower facing skyward, PARup is measured as reflected PAR by instruments mounted at the same height as the PARdn sensor, but facing downward towards the forest canopy. PARground is the PAR transmitted through the canopy to a ground sensor located at 2 m height. Furthermore, the forest-level water-use efficiency (WUE), describing the carbon fixed through photosynthesis per water lost, was calculated as the ratio of GEP to ET (Keenan et al., 2013).

Using the methods of Gonsamo et al. (2013), we calculated phenologically-derived seasons for each year for each site. From half-hourly non-gapfilled data, the maximum daily photosynthetic uptake (GEP_{Max}) was calculated and fit using a double logistic function described by Gonsamo et al. (2013). From the initial fit, a Grubb's test was conducted to statistically ($p < 0.01$) remove outliers in GEP_{Max} data using the approach outlined by Gu et al. (2009). With outliers removed, the function was fit once more. This approach calculated photosynthetic transition dates, hereafter described as phenological dates, using

first, second, and third derivatives of the logistics curves. The second derivatives estimated the end of greenup (EOG), the length of canopy closure (LOCC), and the start of browndown (SOB), while the third derivatives calculated the start of the growing season (SOS), and the end of the growing season (EOS). The start of the growing season (SOS) marked the end of winter dormancy and the beginning of the spring season, leaf emergence/greenup. The phenologically defined spring season is defined as the period from SOS to EOG. The phenologically defined summer or peak carbon uptake period is defined as the entire LOCC period from the final day of greenup (EOG) to the initiation of leaf senescence (SOB), bound by spring and autumn shoulder seasons. Finally, the resulting phenologically defined autumn season is from SOB date to EOS date, with EOS marking leaf abscission and the end of photosynthetic activity in autumn. The length of the growing season (LOS) was calculated as the days between SOS and EOS.

Lastly, the impact of climate on phenology was examined by the use of growing degree days (GDD) and cooling degree days (CDD), in order to understand the thermal response of each forest. GDD acumulation was defined to occur when the mean daily Ta was greater than 0°C, while CDD were calculated using the daily mean Ta below a base Ta of 20°C (Richardson et al., 2006; Gill et al., 2015). Cumulative GDD and CDD were briefly considered in this analysis.

4.4 Results

4.4.1 Meteorological Variability

Air temperature (Ta) measurements conducted above the canopies at both sites showed that the daily mean values of Ta at TP39 (Figure 4.1a) and TPD (Figure 4.1b) responded similarly (Figure 4.1c) over the study period. All years experienced annual mean Ta greater than the 30-year mean (8.0°C). Record warm Ta conditions were measured throughout the majority of the year in 2012 and during the summer of 2016. Cooler conditions dominated 2013 and 2014, while these years had a higher magnitude of extreme cold days in winter, acting to decrease mean annual Ta. In 2015, 2016, and 2017, autumn warming was observed, with record Ta outside of the normal peak summer period. Overall, Ta at both sites was almost identical (Figure 4.1c), highlighting the similar climate both sites were growing in during the study period.

Meteorological conditions between the sites were further examined, beginning with the amount of photosynthetically active radiation absorbed by the forest canopy (APAR, Figure 4.2a). The use of different sensors (Table S4.1) and corresponding coefficients needed for the calculation of incoming PARdn, likely led to some of the discrepancies in the total magnitudes of APAR (outlined in the methods). The shapes of annual APAR provide insight on the seasonal PAR absorbed by the canopy of each forest. At TP39, APAR was similar throughout the year due to the continuous presence of a dense canopy, with a nearly constant fraction (FPAR) of PARdn being absorbed. At TPD, APAR showed lower values

in the winter seasons when the forest was leafless. The timing of the peak APAR at TPD was similar to TP39, though it varied each year based on the annual timing of canopy development. Daily reductions in PAR often coincided with cloudy conditions and precipitation (P) events (Figure 4.2a, right).

Fewer P events were measured during the first half of 2012, and most of 2015, 2016, and the late-summer of 2017, as the latter three years had annual P less than the 30-year mean (997 mm). Autumn P in 2012 helped the forests to recover from the record heat and water deficits, while 2013 and 2014 experienced consistent rain throughout much of the year.

Heightened daily vapor pressure deficit (VPD, Figure 4.2b) was experienced throughout 2012 by both sites, with seasonal maximum values measured during warm and dry conditions. In all years, except for 2012 and the autumn of 2016, daily VPD at TP39 was higher than at TPD Figure 4.2c). Annually, mean VPD was on average about 0.04 kPa higher at TP39 than TPD, with 2012 being the obvious exception (Figure 4.2c).

Soil temperatures (Ts) at 5 cm soil depths followed closely to Ta (Figure 4.1) with dampening effects evident at deeper (100 cm) soil layers (Figure 4.2d). The differences in Ts_{5cm} were explained by the species compositions of the two forests (Figure 4.2e). At TPD, when the deciduous forest was leafless in winter and spring, Ts_{5cm} was higher than at TP39 as the soil received more direct radiation. However, during the summer and autumn of each year, Ts_{5cm} at TP39 exceeded that of TPD.

Lastly, the volumetric water content from 0-30 cm depths ($\theta_{0\text{-}30cm}$) followed similar patterns between sites, with prolonged summer θ deficits in 2012, 2016, and 2017 (Figure 4.2f). The magnitudes again were different, but each forest experienced similar declining θ and the subsequent recharging θ analogous to local P events. In the summer θ was typically lower at TPD than TP39, while all other times of the year TP39 was higher (Figure 4.2g).

4.4.2 Phenological Variability

The meteorological conditions had a significant impact on the timing and duration of key phenological events, although ultimately the response was governed by different leaf-strategies of the various dominant tree species in each forest. The phenological transition dates and seasons calculated from EC-flux data are shown in Table 4.2 and Figure 4.3. The start of the growing season (SOS) varied considerably between the two forests, with the SOS at the evergreen forest, TP39, beginning on average 38 ± 14 days earlier than at the deciduous forest, TPD. TP39 experienced a larger variation in SOS dates, spanning a period of 26 days between the earliest (10 March 2012; day 70) and latest (6 April 2014; day 96) years, while TPD varied by 11 days between years.

Growing degree days (GDD) are a proxy used to assess the amount of heat the ecosystem has absorbed, as a result of increasing air temperatures. The response of the forests to changes in GDD was considered as a trigger for the SOS. The cumulative GDD from the start of the year (January 1st, day 1) to 6-year

mean day of season growth (25 March; day 84), was found to be highly correlated to SOS at TP39 (R^2 = 0.81), but not at TPD (Figures 4.4a & 4.4b). However, the cumulative heat absorbed around the time of the start of greenup, which we calculated as GDD for days of year 117-127 (27 April to 7 May; which represented the range of 6-year mean SOS data ± one standard deviation) was found to significantly influence the SOS at TPD (R^2 = 0.95), with a weaker influence at TP39 (days 73-95; R^2 = 0.76). This difference likely reflects the different leaf-strategies, in that evergreen trees are ready to start photosynthesizing as soon as conditions are favorable, while the deciduous trees still need to grow their leaves once conditions are favorable, before comparable rates of photosynthesis can start. Spring, defined as the period from SOS to the end of greenup (EOG), was more than double the length (69 ± 14 days) at TP39 when compared to TPD (31 ±5 days). However, even with largely different SOS and spring lengths, the peak summer period, defined as the period between the end of greenup (EOG) in spring and the start of browndown (SOB) in autumn, was essentially identical between the forests (Figure 4.3). This period, spanning June, July, and August, was found to be a key contributor to the net annual productivity of each forest (discussed in sections further below).

With similar peak summer lengths, the forests began senescence at similar times, though the length of autumn, the period from the SOB to the end of the growing season (EOS), varied considerably between the forests, due to differences in the timing of the EOS (Figure 4.3). Drought conditions in the

summer of 2012 led both sites to have the shortest autumns and earliest EOS (Figures 4.2f & 4.3). Conversely, the late season warming in the autumns of 2016 and 2017 helped to prolong the growing season at both sites, but the impacts of late season warming in 2015 were not as evident in shaping the timing of EOS (Figures 4.1 & 4.3; Table 4.2).

Ultimately, the timing of the end of the growing season (EOS) was found to be influenced by a certain degree of cooling (i.e. cooling degree days, CDD). At both sites, the cumulative CDD from days 230 to 290 (mid-August to mid-October), were found to be highly correlated to the EOS at TP39 ($R^2 = 0.84$) and TPD ($R^2 = 0.95$) (Figures 4.4e & 4.4f). Temperature responses in both the spring (i.e. GDD) and autumn (i.e. CDD) were much higher for TPD than TP39 (Figure 4.4), likely due to the deciduous nature of the forest. These results suggest that warmer winter and early spring (i.e. January to April) conditions will lead to an advancement of the SOS in the conifer forest, but the same cannot be said for the deciduous forest, whose SOS dates were heavily dependent on late-April, early-May growing conditions. To a certain degree, both forests responded similarly in autumn, however physiological constraints of the different tree leaf-strategies defined the overall differences in growing season lengths.

4.4.3 Carbon and Water Fluxes

The water (evapotranspiration) and carbon (photosynthesis and respiration) fluxes were analyzed in both forests from 2012 to 2017, with the daily patterns of these

fluxes illustrated in Figure 4.3 and expanded upon in Table 4.3. At first glance, each forest responded similarly between years, but significant seasonal irregularities existed, governing annual fluxes.

Annual photosynthesis (GEP) within the conifer forest (TP39) was the highest in 2017 (1709 g C m^2 yr^{-1}) and 2015 (1701 g C m^2 yr^{-1}), while the lowest annual GEP was measured in 2012 (1452 g C m^2 yr^{-1}) and 2013 (1501 g C m^2 yr^{-1}). GEP reductions during these years were due to opposing influences, with 2012 experiencing heat and drought conditions for most of the year, and 2013 experiencing cooler Ta and the highest annual P (1266 mm), reducing PAR and therefore GEP (Figure 4.3a). At the deciduous forest (TPD), similar GEP reductions were captured in 2012 (1198 g C m^2 yr^{-1}), but not in 2013 (1369 g C m^2 yr^{-1}) due to high photosynthetic gains, outside of the 2013 peak growing season (i.e. in the early spring and autumn periods). The highest annual GEP at TPD was found in 2016 (1420 g C m^2 yr^{-1}) and 2017 (1447 g C m^2 yr^{-1}) due to warm summer conditions (Figure 4.3b). Although 2014 had one of the shortest summers and the shortest overall growing season length of all years, high daily GEP rates were sustained through the summer, resulting in the year having above average annual GEP (1382 g C m^2 yr^{-1}). In all 6-years, spring was the only season when daily GEP was similar between the forests, as the advancement of SOS at TP39 did not greatly benefit the forest due to prevailing meteorological conditions (i.e. low PAR, Ta, etc.). However, summer and autumn daily GEP was higher at TPD when compared to TP39 across the 6-years ($p < 0.01$). Within individual

years, the 2016 summer was the only period where seasonal GEP at TPD was sufficiently greater than at TP39 ($p < 0.01$). In all years, TP39 annual GEP was greater than TPD because of longer growing season lengths.

Ecosystem respiration (RE) of the conifer forest was highly variable in all years, with significant daily minimums and maximums measured throughout each summer (Figure 4.3a). At TP39, the greatest annual total RE was measured in 2016 (1492 g C m^2 yr^{-1}) and 2017 (1525 g C m^2 yr^{-1}). The annual RE during these years was about 100 to 200 g C m^2 yr^{-1} greater than during the other years. Cooler spring Ta and reductions in RE during the summer of 2013, led the year to have the lowest annual RE (1282 g C m^2 yr^{-1}) of the 6-years. While 2012 encountered reduced ET and GEP during the summer, RE was largely unaffected, leading the year to have the third highest annual RE (1386 g C m^2 yr^{-1}). Conversely, the 2012 RE within the deciduous forest was greatly reduced, leading to an apparent outlier in annual RE at that site (954 g C m^2 yr^{-1}). Similar to TP39, but to a lesser degree, the annual RE at TPD during 2017 was the greatest of the 6-years (1317 g C m^2 yr^{-1}). Annually, the RE at both forests responded similarly, with 2012 being the exception (Figure 4.3b). The highest daily rates of RE at both sites were measured during the summer of 2013, coinciding with similar maximums in ET. In both cases, maximum rates of RE and ET occurred between precipitation events, as the soil was sufficiently wet and Ta was the highest. In all years, the spring and autumn RE was higher at TPD ($p < 0.01$), resulting from shorter spring and autumn periods at the deciduous forest. The summer RE though was higher at

TP39 in all years and when comparing individual years, with 2013 and 2015 being the exceptions. In these years, the RE at both sites was comparable, shaping the resulting seasonal and annual differences between the two sites.

The resulting balance between photosynthesis (GEP) and ecosystem respiration (RE), net ecosystem productivity (NEP), was found to be largely irregular between sites during individual years due to site-specific differences in the timing, magnitude, and duration of daily fluctuations in GEP and RE. The trajectory of growing season NEP was strikingly different between sites (Figure 4.3a & 4.3b). TPD (deciduous) captured consistently positive daily NEP (sink), while TP39 (conifer) was highly variable, with negative daily NEP (source) often occurring throughout the growing season. The NEP in the conifer forest was the lowest in 2012 (76 g C m^2 yr^{-1}) and 2016 (139 g C m^2 yr^{-1}), coinciding with heat and drought stress in both years (Figure 4.5a). At TP39, July 2012 was the only month during the 6-years of measurements where the peak summer growing season monthly NEP for either site was negative (source). The most productive years (largest annual sink) at the conifer site were 2015 (395 g C m^2 yr^{-1}) and 2014 (263 g C m^2 yr^{-1}). While 2014 (305 g C m^2 yr^{-1}) was simultaneously the most productive year at the deciduous forest, 2015 (90 g C m^2 yr^{-1}) was the lowest annual sink, highlighting the differences between sites (Figure 4.5b). Similarly, the least productive year at TP39 (2012) was the second most productive year at TPD (292 g C m^2 yr^{-1}). The cumulative site differences in NEP were analyzed to focus on seasonal differences (Figure 4.5c). With earlier SOS at TP39, the conifer

site quickly became a sink in spring, while the growing season had not yet begun at TPD. In all years except 2015, the NEP at TPD following the SOS exceeded TP39 ($p < 0.01$). In the autumn, there was no statistical difference between sites, although as photosynthesis ceased at TPD with leaf abscission, the cumulative difference in NEP between sites benefited the extended photosynthesis measured at TP39 (Figure 4.5c).

Within the evergreen conifer forest (TP39), annual evapotranspiration (ET) was the highest in 2012 (495 mm yr^{-1}) and 2013 (468 mm yr^{-1}). Warm Ta throughout much of the year and high summer VPD caused 2012 to have the highest annual ET, while continuous spring and summer P (Figure 4.2a) allowed 2013 to sustain higher daily rates of ET (Figure 4.3a). Cooler Ta during all of 2014 (421 mm yr^{-1}) and cooler Ta in the phenological spring of 2016 (409 mm yr^{-1}), combined with the lowest annual P (in 2016), caused these years to have the lowest ET for the conifer forest (Table 4.3). Within the deciduous forest (TPD), 2012 (428 mm yr^{-1}), 2016 (417 mm yr^{-1}), and 2017 (403 mm yr^{-1}), had the greatest annual ET, coinciding with the years with the highest annual Ta (Figure 4.1b). In 2014, the coolest year during the 6-years of measurements, annual ET (350 mm yr^{-1}) was greatly reduced at TPD. While the ET of each forest ultimately responded differently to the local meteorological forcings, on a few occasions, similar daily ET rates were measured, coinciding with significant P events. In the summer of 2013 (May 30 to July 19 or days 150 to 200), high daily ET was measured at both sites, immediately following multiple daily P events exceeding

40 mm of rain (Figures 4.2a, 4.4a & 4.4b). Additionally, in 2015 (June 20 to July 10 or days 180 to 200), increased ET was measured at both sites following steady P events. Considering the 6-years as a whole, phenological autumn was the only season where ET significantly differed between the sites. While the mean autumn ET was greater at TP39, the shorter duration of autumn (Table 4.2) led rates of daily ET to be higher at TPD as compared to TP39 ($p < 0.01$). In this case, the phenological autumn at TPD occurred when Ta remained high, while at TP39 autumn stretched later into the year when Ta and daily ET were reduced. Both forests experienced similar annual deviations in ET (± 33 & 34 mm), and in all years except for 2016, the conifer forest ET exceeded that of the deciduous forest.

4.4.4 Forest Light and Water Use Efficiencies

The specific forest resource efficiencies (i.e. water use efficiency [WUE] & light use efficiency [LUE]) were examined to understand the relationships between forest carbon uptake and site resources (i.e. water & light), illustrated in Figure 4.6. Each year, WUE varied between sites due to different forest responses to meteorological controls driving overall GEP and ET. At TP39, WUE was the highest in the spring of 2016, the summers of 2014 and 2017, autumns of 2015, 2016, and 2017 (Figure 4.6a). In 2016, the SOS began early (March 15; day 74) promoting prompt increases in spring GEP, when Ta and ET remained low. In autumn, the years with extended growing seasons, saw GEP increase later in the year as ET decreased, leading to higher forest WUE. At TPD, WUE was lowest in

the warm years (i.e. 2012, 2016, & 2017) due to increased annual ET, while the cool and highly productive year of 2014 experienced the highest summer and autumn WUE (Figure 4.6b). In the 6-years of measurements, highly significant ($p < 0.01$) linear relationships of the ratio of monthly ET and GEP (calculating WUE) were measured at both sites, with monthly WUE remaining relatively constant (Figure 4.6c; $R^2 = 0.92$). While monthly WUE was similar between forests (Figure 4.6c), WUE was higher at TPD (4.70 g C kg^{-1} H2O) when compared to that of TP39 (3.82 g C kg^{-1} H2O).

The general light use efficiency (LUE) trends and deviations were statistically comparable between the two forests. At both sites, 2014 and 2017 had the highest summer LUE, while reduced GEP at both sites during the summers of 2012 and 2016 yielded the lowest summer LUE (Figures 4.6d & 4.6e). Across all years, the monthly linear relationships between GEP and APAR yielded similar results, with larger variation ($R^2 = 0.70$) and slightly lower LUE at TP39 when compared to TPD (Figure 4.6f; $R^2 = 0.82$). Similarly, TPD had higher annual and summer LUE ($p < 0.01$), although spring and autumn was similar at both sites.

4.4.5 Meteorological Controls on Fluxes

To better understand and the water and carbon fluxes within each forest ecosystem, the roles of various meteorological variables (i.e. Ta, PAR, θ, etc.) were analysed during the study period. When first considering annual values, ET at the deciduous (TPD) forest was found to be highly correlated ($R^2 = 0.84$) to

annual mean Ta. A smaller secondary effect on ET (R^2 = 0.83; Table 4.4) was found for winter and early spring (January 1st to SOS) $\theta_{0\text{-}30cm}$, which helped to explain the impact of winter soil water storage and seasonal water availability at the start of each year. At TPD, higher winter $\theta_{0\text{-}30cm}$ was measured in the years with the greatest annual ET. At the conifer (TP39) forest, no strong relationships were found between annual ET values and seasonal or annual meteorological variables. However, monthly linear relationships of Ta and VPD to ET were significant at both sites (Figure 4.7). The evergreen conifer and deciduous broadleaf forests experienced similar increases in monthly ET, with increasing monthly mean Ta (Figure 4.7a). While the evergreen forest saw higher ET rates compared to the deciduous forest, the correlation of ET to Ta was greater for the deciduous forest (R^2 = 0.95 vs R^2 = 0.89; for TPD and TP39, respectively). Similar responses between monthly ET and monthly VPD were measured, although the difference between the sites was much smaller, as a mean monthly VPD of 1kPa corresponded to a monthly total ET of 104 mm and 97 mm at TP39 and TPD, respectively (Figure 4.7b). Overall, the correlation of ET to increasing VPD was greater for the evergreen forest (R^2 = 0.82 vs R^2 = 0.74; for TPD and TP39, respectively).

Following similar annual time scales used in the ET comparison, photosynthesis (GEP), respiration (RE), and net ecosystem productivity (NEP) were compared to meteorological measurements for each site and season (Table 4.4). In both forests, no significant relationships were found between

meteorological variables and annual GEP. In terms of RE at TP39, the years with the highest annual RE (i.e. 2016 & 2017) resulted from summer drought conditions, as evident through prolonged reductions in mean summer $\theta_{0\text{-}30cm}$ (R^2 = 0.89). The years with the lowest annual RE (i.e. 2013 & 2015) were ultimately the most productive (largest annual carbon sink) and both measured the highest mean summer $\theta_{0\text{-}30cm}$. The annual NEP was correlated to the length of spring (R^2 = 0.75), the mean summer Ta (R^2 = 0.73), and most importantly, summer NEP (R^2 = 0.99). For the evergreen conifer site, a shorter phenologic spring period due to rapid photosynthetic development was seen in years with the highest annual NEP. Higher summer Ta decreased annual NEP, highlighting the influence of limitations due to heat stress. Lastly, summer NEP at TP39 was nearly identical to the annual NEP, stressing the importance of this period (roughly June, July & August) in shaping the annual carbon sink status of the forest.

At the deciduous forest, the relationship between RE and spring Ta (R^2 = 0.77) suggested that warmer springs generally acted to decrease annual RE. Annual NEP at the conifer forest was shown to be correlated to summer RE (R^2 = 0.80; Table 4.4). Within the deciduous forest, the years with lower summer RE (i.e. 2012, 2014) were the largest annual carbon sinks. Lastly, the smallest annual NEP (2015) was observed when summer RE was highest (714 g C m^{-2}). Ultimately, on annual time scales, both sites emphasized the importance of summer meteorological conditions on annual productivity.

Based on the importance of summer outlined above, the flux parameterizations were further examined to understand the dominant meteorological factors during each summer. At the deciduous broadleaf forest, $\theta_{0\text{-}30cm}$ was shown to have no impact on GEP, while Ta, VPD, and PAR contributed to the summer photosynthesis each year (Table 4.5). Based on meteorological conditions experienced in each year, 2016 and 2014 were the most favorable for summer GEP, while 2012 was the least favorable. Similar results were found for the evergreen conifer forest, though at that site, low $\theta_{0\text{-}30cm}$ was shown to influence GEP. Therefore, years with lower $\theta_{0\text{-}30cm}$ or higher VPD did not experience the same beneficial meteorological inputs necessary for optimal summer GEP. Outside of Ts_{5cm}, $\theta_{0\text{-}30cm}$ impacted summer RE at both sites. At TPD, the years with the highest summer $\theta_{0\text{-}30cm}$ (i.e. 2013 & 2015) experienced optimal conditions for enhanced RE, while 2012 and 2016 saw less favorable RE. Similar responses were also found at TP39. Overall, the annual fluxes were a product of the season length and predicted daily rate that were in turn influenced by variability in meteorological variables.

4.5 Discussion

4.5.1 Meteorological and Phenological Variability

The meteorological conditions experienced by both sites during the study period were similar and typical of temperate North American ecosystems, characterized by four distinct seasons, with cold winters and warm summers. The close

proximity between the two forests (~20 km apart at the same latitude) led them to experience similar synoptic scale weather conditions during each year, and therefore nearly identical air temperature (Ta). Even with similar climatic forcings (i.e. Ta) seasonal deviations in 5 cm soil temperature (Ts_{5cm}) were found, suggesting certain differences were primarily influenced by forest canopy characteristics (Palmroth et al., 2005; Stoy et al., 2006). In this case, soil temperature was linked to the proportion of incoming radiation penetrating the forest canopy, reaching the forest floor. In all years, Ts_{5cm} at the conifer forest was higher during each summer, but lower than that of the deciduous forest during the rest of the year. In the conifer forest, branches and needles were highly clumped while the canopy remained relatively open, leading to minor annual variations in incoming radiation absorbed (APAR) by the forest canopy and soil, in line with Brummer et al. (2012). In the deciduous forest, Ts_{5cm} was higher when leaves were absent and incoming radiation was directly absorbed by the soil. Following the development and closure of the forest canopy in spring, deciduous Ts_{5cm} was lower than the conifer forest in our study, which was in line with other similar studies (i.e. Lee et al., 2010; Augusto et al., 2015).

In general, both forests had similar trends VPD in all years and TP39 had somewhat higher VPD compared to TPD, except in the record warm year of 2012. The higher VPD at the deciduous forest in 2012 could be due to the relative unresponsiveness of stomata to higher VPD typical of broadleaved species, or the suggested larger leaf boundary layers in deciduous trees, where VPD measured

above a canopy can be greater than what leaves experience (Kelliher et al., 1993; Baldocchi & Vogel, 1996; Baldocchi et al., 2002; Stokes et al., 2006). Ultimately, minor meteorological variations between the forests led to similar forcings during the study period, though species specific responses shaped the timing of phenological events in each forest.

The response of leaf phenology in temperate forests to changes in temperature has been shown throughout much of the Northern Hemisphere (Jeong et al., 2011; Settele et al., 2014). In future climates, rising Ta is predicted to lead to an earlier start, later end, and prolonged duration of the growing season, though ecosystem-level responses are expected to vary as there is a strong genetic control among plant species on the timing of phenological events (Vitasse et al., 2011; Sanz-Perez et al., 2009; Polgar & Primack, 2011; Oishi et al., 2018). In locations such as ours where different tree species face similar climates, the relative advantage of conifer species is seen as the start of the growing season (SOS) may often precede spring frost events (Givnish, 2002; Augusto et al., 2015). On the other hand, deciduous species (such as *Quercus*) often delay leaf-out to decrease the probability of frost damage (Kramer, 2010; Polgar & Primack, 2011), which was seen at our sites. The mean SOS for our conifer (*Pinus Strobus* L.) forest began over a month (38 days) earlier than the deciduous (*Quercus Alba*) forest, with much greater variability seen in the conifer forest especially in years with warm spring conditions. The timing of the deciduous SOS (2 May; day 122 ± 5 days) was consistent with similar North American deciduous forests; such as

Harvard Forest (4 May; day 124 ± 14 days; in Gonsamo et al., 2015) and Morgan Monroe Forest (28 April; day 118 ± 4 days; in Dragoni et al., 2011).

In the autumn, the onset of senescence and end of the growing season (EOS) has been reported to be advanced by high soil moisture (θ) deficits, and delayed with increased warming (Kramer, 2010, Warren et al., 2011; Liu et al., 2016). The relationship between summer θ deficits and the timing of senescence were insignificant at the conifer forest, although both forests experienced later senescence dates with decreased θ (although likely due to increased Ta), opposite to previous studies. For the conifer forest, the two years (i.e. 2012 & 2016) with continued heat and drought stress saw the latest dates of senescence, while at the deciduous forest, greater mean summer θ led to earlier senescence in all years but decreased θ extended senescence. Instead, we found that the late-summer (August to October) degree of cooling had a significant impact on the EOS as well as overall growing season length. This response has been confirmed by long term observational data, which has shown strong positive correlations between Ta and EOS, helping to postpone EOS for many forest ecosystems (Ibanez et al., 2010; Dragoni & Rahman, 2012; Gallinat et al., 2015; Liu et al., 2016). More cold days promoted earlier EOS and shorter seasons, while less cooling (greater warming) extended the season and phenologic autumn period at both sites. However, the degree of extension was much different between sites, similar to the response in spring. The mean EOS (10 November; day 314 ± 8 days) in the deciduous site occurred a month (31 days) before that of the evergreen coniferous site (11

December; day 345 ± 17 days). There was much greater variability in EOS experienced at the conifer forest compared to the deciduous broadleaf forest. Based on these findings, in future climates, evergreen conifer forests in the region may expect earlier springs, later autumns, and longer growing seasons, while the deciduous broadleaf forests will likely see greater gains in growing season length from prolonged autumns, only limited by their specific leaf-strategy.

4.5.2 Meteorological Impacts on Carbon Fluxes

Changes in local meteorology (and climate) have been recognized as a primary factor driving the interannual variability of carbon fluxes within forests (Bonan, 2008; Desai, 2010; Coursolle et al., 2012). Ta anomalies and seasonal fluctuations in water availability (θ) over a predictable course of the year were shown to strongly determine the carbon sequestered in many forests (Ciais et al., 2005; Sun et al., 2011; Xie et al., 2014). Conceptually, higher Ta will promote longer growing seasons and greater photosynthesis (GEP), though drawbacks due to increased respiration (RE) are expected (White & Nemani, 2003; Noormets et al., 2015). In this study, the differing forests responses to meteorological conditions led to significant divergences in annual GEP, RE, and NEP. At both sites, the overall growing season length in 2012 was the second shortest (behind 2014), despite record Ta experienced throughout much of the year. If this year is excluded, both the conifer and deciduous forests experienced longer growing season lengths with increased annual Ta. Annual GEP reductions were also

experienced in each forest during the heat and drought year of 2012. GEP reductions at our conifer site may also be associated with the reduction in canopy size, due to thinning performed at the site in the early winter of 2012 (see more discussion in the following section). Additionally, higher Ta and low θ acted to enhance RE in the conifer forest, but significantly reduced RE in the deciduous forest. The suppression of RE has been previously reported for other deciduous forests during warm and dry periods (Davidson et al., 1998; Palmroth et al., 2005; Novick et al., 2015; Darenova & Cater, 2018). Overall, these reductions in both the growing season length and the magnitude of carbon fluxes highlighted the forests sensitivities to heat and drought events, though it ultimately varied between sites. Contrasting studies have shown varying results on the overall drought tolerance of conifer forests. Some studies suggest that conifer species, especially those in resource-poor locations, may be less responsive to seasonal climate anomalies (Aerts et al., 1995; Way & Oren, 2010; Wolf et al., 2013). Others have found that conifer (i.e. *Pinus*) forests are highly coupled to atmospheric demand and drought sensitivities (Griffis et al., 2003; Stoy et al., 2006). The two years (i.e. 2012 & 2016) with the lowest annual carbon sequestration (NEP) in our conifer forest were found during hot and dry years with high atmospheric demand (i.e. high VPD). These years measured the lowest summer light use efficiency (LUE, due to decreased GEP) and the lowest summer NEP, consistent with past studies (Griffis et al., 2003; Vargas et al., 2013). Similar LUE reductions were measured at the deciduous forest during the

summers of 2012 and 2016, though annual NEP was drastically different due to comparable decreases in summer and annual RE, not experienced in the conifer forest. Instead, the two drought years were some of the largest annual carbon sinks (greater positive NEP) during the six years of measurements at the deciduous forest. Similar to this study, other research has shown deciduous oak (*Quercus*) forests to be more resilient to drought than their conifer counterparts (Elliot et al., 2015; Wang et al., 2016). Studies have suggested that warm (drought) conditions may lead to reduced carbon uptake or even carbon release (White & Nemani, 2003; Grant et al., 2009; Vargas et al., 2013). Based on our findings, reductions in NEP during expected future intermittent drought conditions in the area could be projected in the evergreen conifer forest, but not in the deciduous broadleaf forest.

Over the measurement period, both forests experienced similar interannual variability in all carbon fluxes (~100 g C m^{-2} yr^{-1}) to that expected in midlatitude forests (Yuan et al., 2009; Desai 2010). In all years the magnitude of GEP and RE were greater in the conifer forest, however, analogous increases at the deciduous forest led the two forests to have very similar annual NEP. While evergreen conifer forests have been shown to have lower photosynthetic capacities than deciduous broadleaf forests (Reich et al., 1995; Baldocchi et al., 2010), the longer growing seasons led the conifer forest in this study to have a greater magnitude of annual NEP in most years, with drought years being the exceptions. Even in drought years, both the conifer forest and the deciduous forest

in our study experienced annual NEP similar to past studies conducted in the temperate region of North America (Barford et al., 2001; Arain & Restrepo-Coupe, 2005; Gough et al., 2013; Xie et al., 2014; Dymond et al., 2016; Oishi et al., 2018). In the coolest year of this study (i.e. 2014), which was closest to the 30-year norm for the area in terms of its mean annual Ta, the two forests experienced similar seasonal and annual carbon uptake and some of the highest rates over the 6-year study. This suggests that both forests (especially the deciduous forest), favor meteorologically "normal" years, similar to the conclusion of Griffis et al. (2003) and Gonsamo et al. (2015). Therefore, under future climates, which are predicted to be warmer than the current 30-year norm for the area, the carbon sequestration capacity of both forests may be reduced.

4.5.3 Meteorological Impacts on Water Fluxes

The annual carbon uptake measured within each forest would not be possible without the availability and use of water (Baldocchi et al., 2001). With insufficient water availability annual tree growth and productivity may be limited (Nemani et al., 2003; Augusto et al., 2015). Hence, it is important to understand the efficiency of water use (WUE) and the corresponding release of water vapor (evapotranspiration, ET) to the atmosphere on seasonal and annual time scales. On average, our conifer forest had greater annual ET and less variability than the deciduous forest. However, we found conflicting results between sites in regards to annual ET during drought years. At both sites, ET was shown to be strongly

driven by air temperature (Ta). ET in 2012 was the highest of all years following amplified Ta for most of the year. Much like RE, ET responds year-round, so warmer spring or autumn periods often lead to annual increases in ET (Schwartz et al., 2006; Taylor et al., 2008).

Similarly, in the deciduous forest, annual ET was heightened during the hot and dry year of 2016. The characteristic amplification of both Ta and VPD during warm drought years led the years with the lowest mean summer $\theta_{0\text{-}30cm}$ and highest summer Ta (or VPD) to experience increased annual ET at the deciduous forest. An opposing ET response was measured in the coniferous forest, as 2016 had the lowest annual ET, the only year where the annual conifer ET was lower than that of the deciduous forest ET.

Typically, transpiration is beneficial to plants, helping to cool leaves and thereby reducing respiration (Rambal et al., 2003; Baldocchi et al., 2010; Brummer et al., 2012). In our case, high summer Ta, the lowest $\theta_{0\text{-}30cm}$, and very little summer and annual P removed most of the water from the system, significantly reducing ET, while RE continued to rise. At the conifer forest, the timing of summer P appeared to greatly influence ET (i.e. 2013), as the availability of rainfall during the physiological summer led to the greatest demand for water. Ultimately, it is likely that the differing response between sites was due to the ability of each forest to access deep soil water. Studies have shown oak (*Quercus*) forests to be less sensitive and more resilient to drought, due to more efficient access to deeper soil water, than conifer forests (Breda et al., 2006;

Bonan et al., 2008; Wang et al., 2016; Matheny et al., 2017). Evergreen conifer forests may have roots extending just as deep as deciduous broadleaf forests, but they are not as effective at obtaining water as broadleaf trees (Oren & Pataki, 2001). With higher atmospheric demand during dry periods often leading to greater ET across many forest types (Meinzer et al., 2013; Wu et al., 2013; Tang et al., 2014), the access and availability of water in deep soil layers allowed the deciduous forest to sustain high ET, even in drought years.

We found annual WUE of both forests to respond similarly across all years, though variations in GEP and ET between the forests led to seasonal WUE differences due to the aforementioned responses of both fluxes. The WUE at the conifer forest was consistent with previously reported values for that location (Brummer et al., 2012; Skubel et al., 2015), while the deciduous forest WUE was found to be higher than an oak forest in Ohio (Xie et al., 2016). Assuming similar carbon assimilation, this implies a higher evapotranspiration flux at the conifer forest (Augusto et al., 2015), which we saw.

4.5.3 Forest Management and Future Climate Impacts

Forest age, management practices, and historical land-use have been shown to impact annual carbon fluxes within forests (Wofsy et al., 1993; Song & Woodcock, 2003). While our forests are of relatively similar age (~80-90 years), they have experienced slightly different management practices over their lifetime so far, with the conifer forest being a planted forest that underwent low density

partial thinning in 1983 and 2012, while the deciduous broadleaf forest was naturally regenerated with periodic selective harvesting occurring in the past (most recent events occurring in the early 1990s). The difference in carbon uptake over the forest's life will be influenced by management treatments (Herbst et al., 2015). Some studies (Zha et al., 2009; Dore et al., 2012; Skubel et al., 2017) have suggested that overall forest carbon and water fluxes recover rapidly post-disturbance. Furthermore, some studies have found a positive correlation between species number and productivity in temperate forests (Morin et al., 2011). Similarly, mixed forests are generally assumed to be more resilient to extreme weather events and disturbance events than mono-specific forest stands (Pretzsch, 2014; Herbst et al., 2015). With a greater number of species in our deciduous broadleaf forest (500+ tree & plant species, as per Elliot et al., 1999), and the resistance to heat and drought induced carbon losses shown in this study, it is likely that the deciduous broadleaf forests will remain a carbon sink well into the future. Even following increased RE losses expected with warmer late-summer and autumn conditions (Dunn et al., 2007; Piao et al., 2008), such as those experienced in 2016 and 2017 at our site, the conclusions remain the same.

For similar forest types, the annual responses of GEP and RE to local meteorology will affect natural and managed forests similarly, however it has been proposed that many managed forests may already be maximized for a given Ta regime, leaving less room for adaptability or acclimation in the future (Litton & Giardina, 2008; Chen et al., 2014; Noormets et al., 2015). With RE shown to be

higher in managed forests compared to natural forests (Arain & Restrepo-Coupe, 2005), it is possible that our conifer forest (most recently managed) may see limitations in the annual carbon sequestration capability in the future. With considerable daily RE losses experienced following summer precipitation events (i.e. 2013 & 2014), enough hot periods with intermittent heavy rains in the future could cause forest RE to exceed in the conifer forest. As the climate continues to change, management practices and responses to meteorological conditions will determine the relative carbon sink or source strength in many temperate forests.

4.6 Conclusions

The annual carbon and water dynamics were compared between two forests of different leaf-strategy in the Great Lakes region of southern Ontario, Canada, over a six year period from 2012 to 2017. The geographic location, forest age, soil, and climate were similar between sites, but one was an evergreen needle-leaf monoculture plantation, while the other was a mixed-wood deciduous broadleaf naturally regenerated forest. On average, the evergreen conifer forest was a greater carbon sink (218 ± 109 g C m^{-2} yr^{-1}) with higher annual ET (442 ± 33 mm yr^{-1}) than the deciduous broadleaf forest (200 ± 83 g C m^{-2} yr^{-1} and 388 ± 34 mm yr^{-1}, respectively). While mean annual fluxes were similar in magnitude and variation, significant abnormalities were measured between sites, especially during drought years. Summer meteorology was shown to greatly impact fluxes at both sites, though to varying degrees with varying responses. Annual NEP was

reduced at the deciduous forest during years with increased summer RE. Similarly, annual deciduous forest ET was driven by changes in Ta, with the largest annual ET measured in the warmest years. During droughts, the carbon and water fluxes of the deciduous forest were less sensitive to changes in temperature or water availability. Conversely, annual NEP at the conifer forest was the result of competing influences of both GEP and RE, though ultimately, summer NEP determined annual NEP. The significant response of the conifer forest to heat and drought events led the summer months in all years to greatly control the forests annual carbon sink-source status. Additionally, prolonged dry periods with increased Ta were shown to greatly reduce ET (i.e. 2016). Both sites saw average ET, but increased NEP during 'normal' years, but only the conifer forest saw annual reductions in carbon sequestration during drought years. If longer summer periods of increased temperatures and larger variability in precipitation are to be expected in future climates, these findings suggest that the deciduous forest will continue to be a net carbon sink, while the response of the conifer forest remains uncertain. Given our findings, drought-induced RE increases or GEP decreases may hurt the conifer carbon uptake.

4.7 Acknowledgements

This study was funded by the Natural Sciences and Engineering Research Council (NSERC), the Global Water Futures Program (GWF), and the Ontario Ministry of Environment, Conservation and Parks (MOECP). Funding from the Canadian

Foundation of Innovation (CFI) through New Opportunity and Leaders Opportunity Fund and Ontario Research Fund of the Ministry of Research and Innovation is also acknowledged. In kind support from the Ontario Ministry of Natural Resources and Forestry (OMNRF). The St. Williams Conservation Reserve Community Council and the Long Point Region Conservation Authority (LPRCA) are also acknowledged. We acknowledge support from Zoran Nesic at the University of British Columbia in assistance with flux measurements at our site, and members of the Hydrometeorology and Climatology lab at McMaster University for their continued support at both study sites.

4.8 References

Abrams, Marc D.; Downs, Julie A. 1990. Successional replacement of old-growth white oak by mixed mesophytic hardwoods in southwestern Pennsylvania. *Canadian Journal of Forest Research*. 20(12), 1864-1870.

Aerts, R., 1995. The advantages of being evergreen. *Trends in Ecology & Evolution*, 10(10), 402-407.

Allen, C.D., Macalady, A.K., Chenchouni, H., Bachelet, D., McDowell, N., Vennetier, M., Kitzberger, T., Rigling, A., Breshears, D.D., Hogg, E.T. and Gonzalez, P., 2010. A global overview of drought and heat-induced tree mortality reveals emerging climate change risks for forests. *Forest Ecology and Management*, 259(4), 660-684.

Amiro, B.D., Barr, A.G., Black, T.A., Iwashita, H., Kljun, N., McCaughey, J.H., Morgenstern, K., Murayama, S., Nesic, Z., Orchansky, A.L. and Saigusa, N., 2006. Carbon, energy and water fluxes at mature and disturbed forest sites, Saskatchewan, Canada. *Agricultural and Forest Meteorology*, 136(3-4), 237-251.

Arain, M.A., & Restrepo-Coupe, N., 2005. Net ecosystem production in a temperate pine plantation in southeastern Canada. *Agricultural and Forest Meteorology*, 128, 223-241.

Augusto, L., De Schrijver, A., Vesterdal, L., Smolander, A., Prescott, C. and Ranger, J., 2015. Influences of evergreen gymnosperm and deciduous angiosperm tree species on the functioning of temperate and boreal forests. *Biological Reviews*, 90(2), 444-466.

Baldocchi, D.D. & Vogel, C.A., 1996. Energy and CO2 flux densities above and below a temperate broad-leaved forest and a boreal pine forest. *Tree Physiology*, 16(1-2), 5-16.

Baldocchi, D., Falge, E., Gu, L., Olson, R., Hollinger, D., Running, S., Anthoni, P., Bernhofer, C., Davis, K., Evans, R. and Fuentes, J., 2001. FLUXNET: A new tool to study the temporal and spatial variability of ecosystem-scale carbon dioxide, water vapor, and energy flux densities. *Bull. Amer. Meteor. Soc.*, 82(11), 2415-2434.

Baldocchi, D.D., Wilson, K.B. and Gu, L., 2002. How the environment, canopy structure and canopy physiological functioning influence carbon, water and energy fluxes of a temperate broad-leaved deciduous forest—an assessment with the biophysical model CANOAK. *Tree Physiology*, *22*(15-16), 1065-1077.

Baldocchi, D.D., Ma, S., Rambal, S., Misson, L., Ourcival, J.M., Limousin, J.M., Pereira, J. and Papale, D., 2010. On the differential advantages of evergreenness and deciduousness in Mediterranean oak woodlands: a flux perspective. *Ecol. Appl.*, 20(6), 1583-1597.

Barr, A.G., Griffis, T.J., Black, T.A., Lee, X., Staebler, R.M., Fuentes, J.D., Chen, Z. and Morgenstern, K., 2002. Comparing the carbon budgets of boreal and temperate deciduous forest stands. *Canadian Journal of Forest Research*, *32*(5), 813-822.

Barr, A.G., Richardson, A.D., Hollinger, D.Y., Papale, D., Arain, M.A., Black, T.A., Bohrer, G., Dragoni, D., Fischer, M.L., Gu, L., Law, B.E., Margolis, H.A., Mccaughey, J.H., Munger, J.W., Oechel, W., Schaeffer, K., 2013. Use of change-point detection for friction-velocity threshold evaluation in eddy-covariance studies. *Agricultural and Forest Meteorology*, 31–45.

Barford, C.C., Wofsy, S.C., Goulden, M.L., Munger, J.W., Pyle, E.H., Urbanski, S.P., et al., 2001. Factors controlling long-and short-term sequestration of atmospheric CO2 in a mid-latitude forest. *Science*, 294(5547), 1688-1691.

Beamesderfer, E.R., Arain, M.A., Khomik, M., and Brodeur, J.J., 2019. How will the carbon fluxes within the northernmost temperate deciduous forests of

North America fair under future climates?. *Journal of Geophysical Research: Biogeosciences*.

Bonan, G.B., 2008. Forests and climate change: forcings, feedbacks, and the climate benefits of forests. S*cience*, 320(5882), 1444-1449.

Bréda, N., Huc, R., Granier, A., and Dreyer, E., 2006. Temperate forest trees and stands under severe drought: a review of ecophysiological responses, adaptation processes and long-term consequences. *Annals of Forest Science*, *63*(6), 625-644.

Brodeur, J.J., 2014. Data-driven approaches for sustainable operation and defensible results in a long-term, multi-site ecosystem flux measurement program. McMaster University.

Brümmer, C., Black, T.A., Jassal, R.S., Grant, N.J., Spittlehouse, D.L., Chen, B., Nesic, Z., Amiro, B.D., Arain, M.A., Barr, A.G. and Bourque, C.P.A., 2012. How climate and vegetation type influence evapotranspiration and water use efficiency in Canadian forest, peatland and grassland ecosystems. *Agricultural and Forest Meteorology*, 153, 14-30.

Burns, B., 2017. Response of Ecosystem Evapotranspiration to Water-Stress in a Temperate Deciduous Forest in southern Ontario. McMaster University.

Canadell, J.G. & Raupach, M.R., 2008. Managing forests for climate change mitigation. *Science*, 320(5882), 1456-1457.

Chan, F.C., Arain, M.A., Khomik, M., Brodeur, J.J., Peichl, M., Restrepo-Coupe, N., Thorne, R., Beamesderfer, E., McKenzie, S., Xu, B. and Croft, H., 2018. Carbon, water and energy exchange dynamics of a young pine plantation forest during the initial fourteen years of growth. *Forest Ecology and Management*, 410, 12-26.

Chen, G., Yang, Y. and Robinson, D., 2014. Allometric constraints on, and trade-offs in, belowground carbon allocation and their control of soil respiration across global forest ecosystems. *Glob. Change Biol.*, 20(5), 1674-1684.

Choat, B., Jansen, S., Brodribb, T. J., Cochard, H., Delzon, S., Bhaskar, R., et al., 2012. Global convergence in the vulnerability of forests to drought. *Nature*, 491(7426), 752-755.

Ciais, P., Reichstein, M., Viovy, N., Granier, A., Ogée, J., Allard, V., Aubinet, M., Buchmann, N., Bernhofer, C., Carrara, A. and Chevallier, F., 2005.

Europe-wide reduction in primary productivity caused by the heat and drought in 2003. *Nature*, 437(7058), 529-533.

Coursolle, C., Margolis, H.A., Giasson, M.A., Bernier, P.Y., Amiro, B.D., Arain, M.A., Barr, A.G., Black, T.A., Goulden, M.L., McCaughey, J.H. and Chen, J.M., 2012. Influence of stand age on the magnitude and seasonality of carbon fluxes in Canadian forests. *Agricultural and Forest Meteorology*, 165, 136-148.

Cubasch, U., D. Wuebbles, D. Chen, M.C. Facchini, D. Frame, N. Mahowald, and J.-G. Winther, 2013: Introduction. In: Climate Change 2013: The Physical Science Basis. Contribution of Working Group I to the Fifth Assessment Report of the Intergovernmental Panel on Climate Change [Stocker, T.F., D. Qin, G.-K. Plattner, M. Tignor, S.K. Allen, J. Boschung, A. Nauels, Y. Xia, V. Bex and P.M. Midgley (eds.)]. Cambridge University Press, Cambridge, United Kingdom and New York, NY, USA.

Darenova, E. & Čater, M., 2018. Different structure of sessile oak stands affects soil moisture and soil CO2 efflux. *Forest Science*, 64(3), 340-348.

Davidson, E.A., Belk, E. and Boone, R.D., 1998. Soil water content and temperature as independent or confounded factors controlling soil respiration in a temperate mixed hardwood forest. *Global Change Biology*, 4(2), 217-227.

Desai, A.R., 2010. Climatic and phenological controls on coherent regional interannual variability of carbon dioxide flux in a heterogeneous landscape. *J. Geophys. Res. G: Biogeosci*., 115(G3).

Dore, S., Montes-Helu, M., Hart, S.C., Hungate, B.A., Koch, G.W., Moon, J.B., Finkral, A.J. and Kolb, T.E., 2012. Recovery of ponderosa pine ecosystem carbon and water fluxes from thinning and stand-replacing fire. *Global Change Biology*, *18*(10), 3171-3185.

Dragoni, D. & Rahman, A.F., 2012. Trends in fall phenology across the deciduous forests of the Eastern USA. *Agricultural and Forest Meteorology*, *157*, 96-105.

Dragoni, D., Schmid, H.P., Wayson, C.A., Potter, H., Grimmond, C.S.B. and Randolph, J.C., 2011. Evidence of increased net ecosystem productivity associated with a longer vegetated season in a deciduous forest in south-central Indiana, USA. *Global Change Biology*, 17(2), 886-897.

Dunn, A.L., Barford, C.C., Wofsy, S.C., Goulden, M.L. and Daube, B.C., 2007. A long-term record of carbon exchange in a boreal black spruce forest: Means, responses to interannual variability, and decadal trends. *Global Change Biol*., 13(3), 577-590.

Dymond, C.C., Beukema, S., Nitschke, C.R., Coates, K.D. and Scheller, R.M., 2016. Carbon sequestration in managed temperate coniferous forests under climate change. *Biogeosciences*, 13, 1933-1947.

Elliott, K., McCracken, J.D. and Couturier, A., 1999. A Management Strategy for South Walsingham Sand Ridges/Big Creek Floodplain Forest. Ont. Min. Nat. Resources. London, Ontario. 54.

Elliott, K.J., Vose, J.M., Knoepp, J.D., Clinton, B.D. and Kloeppel, B.D., 2015. Functional role of the herbaceous layer in eastern deciduous forest ecosystems. *Ecosystems*, 18, 221-236.

Froelich, N., Croft, H., Chen, J.M., Gonsamo, A. and Staebler, R.M., 2015. Trends of carbon fluxes and climate over a mixed temperate–boreal transition forest in southern Ontario, Canada. *Agricultural and Forest Meteorology*, 211, 72-84.

Gallinat, A.S., Primack, R.B. and Wagner, D.L., 2015. Autumn, the neglected season in climate change research. *Trends in Ecology & Evolution*, *30*(3), 169-176.

Gaumont-Guay, D., Black, T.A., McCaughey, H., Barr, A.G., Krishnan, P., Jassal, R.S. and Nesic, Z., 2009. Soil CO_2 efflux in contrasting boreal deciduous and coniferous stands and its contribution to the ecosystem carbon balance. *Glob. Change Biol*., 15, 1302-1319.

Givnish, T.J., 2002. Adaptive significance of evergreen vs. deciduous leaves: solving the triple paradox. *Silva Fennica*, 36(3), 703-743.

Gonsamo, A., Chen, J.M. and D'Odorico, P., 2013. Deriving land surface phenology indicators from CO_2 eddy covariance measurements. *Ecological Indicators*, 29, 203-207.

Gonsamo, A., Croft, H., Chen, J.M., Wu, C., Froelich, N. and Staebler, R.M., 2015. Radiation contributed more than temperature to increased decadal autumn and annual carbon uptake of two eastern North America mature forests. *Agricultural and Forest Meteorology*, 201, 8-16.

Gough, C.M., Hardiman, B.S., Nave, L.E., Bohrer, G., Maurer, K.D., Vogel, C.S., Nadelhoffer, K.J. and Curtis, P.S., 2013. Sustained carbon uptake and storage following moderate disturbance in a Great Lakes forest. *Ecological Applications*, 23(5), 1202-1215.

Granier, A., Reichstein, M., Bréda, N., Janssens, I.A., Falge, E., Ciais, P., Grünwald, T., Aubinet, M., Berbigier, P., Bernhofer, C. and Buchmann, N., 2007. Evidence for soil water control on carbon and water dynamics in European forests during the extremely dry year: 2003. *Agricultural and Forest Meteorology*, 143(1-2), 123-145.

Grant, R.F., Barr, A.G., Black, T.A., Margolis, H.A., Dunn, A.L., Metsaranta, J., Wang, S., McCaughey, J.H. and Bourque, C.A., 2009. Interannual variation in net ecosystem productivity of Canadian forests as affected by regional weather patterns–A Fluxnet-Canada synthesis. *Agricultural and Forest Meteorology*, *149*(11), 2022-2039.

Griffis, T.J., Black, T.A., Morgenstern, K., Barr, A.G., Nesic, Z., Drewitt, G.B., Gaumont-Guay, D. and McCaughey, J.H., 2003. Ecophysiological controls on the carbon balances of three southern boreal forests. *Agricultural and Forest Meteorology*, 117(1-2), 53-71.

Gu, L., Post, W.M., Baldocchi, D.D., Black, T.A., Suyker, A.E., Verma, S.B., Vesala, T. and Wofsy, S.C., 2009. Characterizing the seasonal dynamics of plant community photosynthesis across a range of vegetation types. In Phenology of Ecosystem Processes (35-58). *Springer*, New York, NY.

Herbst, M., Mund, M., Tamrakar, R. and Knohl, A., 2015. Differences in carbon uptake and water use between a managed and an unmanaged beech forest in central Germany. *Forest Ecology and Management*, 355, 101-108.

Houghton, R.A., 2007. Balancing the global carbon budget. *Annual Review of Earth and Planetary Sciences*, 35, 313-347.

Huntington, T.G., 2006. Evidence for intensification of the global water cycle: review and synthesis. *Journal of Hydrology*, 319(1-4), 83-95.

Ibáñez, I., Primack, R.B., Miller-Rushing, A.J., Ellwood, E., Higuchi, H., Lee, S.D., Kobori, H. and Silander, J.A., 2010. Forecasting phenology under global warming. *Philos. Trans. R. Soc. London B*, 365(1555), 3247-3260.

Jenkins, J.P., Richardson, A.D., Braswell, B.H., Ollinger, S.V., Hollinger, D.Y. and Smith, M.L., 2007. Refining light-use efficiency calculations for a

deciduous forest canopy using simultaneous tower-based carbon flux and radiometric measurements. *Agric. For. Meteorol.*, 143(1-2), 64-79.

Jeong, S.J., Ho, C.H., Gim, H.J. and Brown, M.E., 2011. Phenology shifts at start vs. end of growing season in temperate vegetation over the Northern Hemisphere for the period 1982–2008. *Global Change Biology*, *17*(7), 2385-2399.

Keenan, T.F., Hollinger, D.Y., Bohrer, G., Dragoni, D., Munger, J.W., Schmid, H.P. and Richardson, A.D., 2013. Increase in forest water-use efficiency as atmospheric carbon dioxide concentrations rise. *Nature*, 499, 324.

Kelliher, F.M., Leuning, R. and Schulze, E.D., 1993. Evaporation and canopy characteristics of coniferous forests and grasslands. *Oecologia*, 95(2), 153-163.

Kljun, N., Calanca, P., Rotach, M.W., Schmid, H.P., 2004. A simple parametrization for flux footprint predictions. *Boundary-Layer Meteorology*. 112, 503–523.

Kramer, K., Degen, B., Buschbom, J., Hickler, T., Thuiller, W., Sykes, M.T. and de Winter, W., 2010. Modelling explorationa of the future of European beech (Fagussylvatica L.) under climate change—Range, abundance, genetic diversity and adaptive response. *Forest Ecology & Management*, 259(11), 2213-2222.

Kula, M.V., 2014. Biometric-based carbon estimates and environmental controls within an age-sequence of temperate forests (Doctoral Dissertation), McMaster University.

Lee, N.Y., Koo, J.W., Noh, N.J., Kim, J. and Son, Y., 2010. Seasonal variations in soil CO_2 efflux in evergreen coniferous and broad-leaved deciduous forests in a cool-temperate forest, central Korea. *Ecological Research*, 25, 609– 617.

Litton, C.M. & Giardina, C.P., 2008. Below-ground carbon flux and partitioning: Global patterns and response to temperature. *Functional Ecology*, 22(6), 941-954.

Liu, K.B., 1990. Holocene paleoecology of the boreal forest and Great Lakes-St. Lawrence forest in northern Ontario. *Ecol. Monorg.*, 60(2), 179-212.

Liu, P., Black, T.A., Jassal, R.S., Zha, T., Nesic, Z., Barr, A.G., Helgason, W.D., Jia, X., Tian, Y., Stephens, J.J. and Ma, J., 2019. Divergent long-term

trends and interannual variation in ecosystem resource use efficiencies of a southern boreal old black spruce forest 1999–2017. *Global Change Biology*, 25: 3056-3069.

Liu, Q., Fu, Y.H., Zhu, Z., Liu, Y., Liu, Z., Huang, M., Janssens, I.A. and Piao, S., 2016. Delayed autumn phenology in the Northern Hemisphere is related to change in both climate and spring phenology. *Global Change Biology*, *22*(11), 3702-3711.

Loescher, H.W., Law, B.E., Mahrt, L., Hollinger, D.Y., Campbell, J. and Wofsy, S.C., 2006. Uncertainties in, and interpretation of, carbon flux estimates using the eddy covariance technique. *Journal of Geophysical Research: Atmospheres*, 111(D21).

MacKay, S.L., Arain, M.A., Khomik, M., Brodeur, J.J., Schumacher, J., Hartmann, H. and Peichl, M., 2012. The impact of induced drought on transpiration and growth in a temperate pine plantation forest. *Hydrological Processes*, 26(12), 1779-1791.

Matheny, A.M., Fiorella, R.P., Bohrer, G., Poulsen, C.J., Morin, T.H., Wunderlich, A., Vogel, C.S. and Curtis, P.S., 2017. Contrasting strategies of hydraulic control in two codominant temperate tree species. *Ecohydrology*, 10(3), 1815.

McLaren, J.D., Arain, M.A., Khomik, M., Peichl, M. and Brodeur, J., 2008. Water flux components and soil water-atmospheric controls in a temperate pine forest growing in a well-drained sandy soil. *Journal of Geophysical Research: Biogeosciences*, 113(G4).

Meinzer, F.C., Woodruff, D.R., Eissenstat, D.M., Lin, H.S., Adams, T.S. and McCulloh, K.A., 2013. Above-and belowground controls on water use by trees of different wood types in an eastern US deciduous forest. *Tree Physiology*, 33(4), 345-356.

Morin, X., Fahse, L., Scherer-Lorenzen, M. and Bugmann, H., 2011. Tree species richness promotes productivity in temperate forests through strong complementarity between species. *Ecology Letters*, 14(12), 1211-1219.

Nemani, R.R., Keeling, C.D., Hashimoto, H., Jolly, W.M., Piper, S.C., Tucker, C.J., Myneni, R.B. and Running, S.W., 2003. Climate-driven increases in global terrestrial net primary production from 1982 to 1999. *Science*, 300(5625), 1560-1563.

Noormets, A., Epron, D., Domec, J.C., McNulty, S.G., Fox, T., Sun, G. and King, J.S., 2015. Effects of forest management on productivity and carbon sequestration: A review and hypothesis. *Forest Ecology and Management*, 355, 124-140.

Novick, K.A., Oishi, A.C., Ward, E.J., Siqueira, M.B., Juang, J.Y. and Stoy, P.C., 2015. On the difference in the net ecosystem exchange of CO 2 between deciduous and evergreen forests in the southeastern United States. Global Change Biology, 21(2), 827-842.

Oishi, A.C., Miniat, C.F., Novick, K.A., Brantley, S.T., Vose, J.M. and Walker, J.T., 2018. Warmer temperatures reduce net carbon uptake, but do not affect water use, in a mature southern Appalachian forest. *Agricultural and Forest Meteorology*, *252*, 269-282.

Oren, R. & Pataki, D.E., 2001. Transpiration in response to variation in microclimate and soil moisture in southeastern deciduous forests. *Oecologia*, 127(4), 549-559.

Palmroth, S., Maier, C.A., McCarthy, H.R., Oishi, A.C., Kim, H.S., Johnsen, K.H., Katul, G.G. and Oren, R., 2005. Contrasting responses to drought of forest floor CO2 efflux in a loblolly pine plantation and a nearby oak-hickory forest. *Global Change Biology*, *11*(3), 421-434.

Papale, D., Reichstein, M., Aubinet, M., Canfora, E., Bernhofer, C., Kutsch, W., Longdoz, B., Rambal, S., Valentini, R., Vesala, T., Yakir, D., 2006. Towards a standardized processing of Net Ecosystem Exchange measured with eddy covariance technique: algorithms and uncertainty estimation. *Biogeosciences,* 3, 571–583.

Peichl, M. and Arain, M.A., 2007. Allometry and partitioning of above-and belowground tree biomass in an age-sequence of white pine forests. *For. Ecol. Manag*., 253(1-3), 68-80.

Peichl, M., Arain, M.A. and Brodeur, J.J., 2010. Age effects on carbon fluxes in temperate pine forests. *Agric. Forest Meteorol.*, *150*(7-8), 1090-1101.

Piao, S., Ciais, P., Friedlingstein, P., Peylin, P., Reichstein, M., Luyssaert, S., Margolis, H., Fang, J., Barr, A., Chen, A. and Grelle, A., 2008. Net carbon dioxide losses of northern ecosystems in response to autumn warming. *Nature*, 451(7174), 49.

Pretzsch, H., 2014. Canopy space filling and tree crown morphology in mixed-species stands compared with monocultures. *Forest Ecology and Management*, 327, 251-264.

Polgar, C.A. & Primack, R.B., 2011. Leaf-out phenology of temperate woody plants: from trees to ecosystems. *New Phytologist*, *191*(4), 926-941.

Rambal, S., Ourcival, J.M., Joffre, R., Mouillot, F., Nouvellon, Y., Reichstein, M. and Rocheteau, A., 2003. Drought controls over conductance and assimilation of a Mediterranean evergreen ecosystem: scaling from leaf to canopy. *Global Change Biology*, 9(12), 1813-1824.

Reich, P.B., Walters, M.B., Kloeppel, B.D. and Ellsworth, D.S., 1995. Different photosynthesis-nitrogen relations in deciduous hardwood and evergreen coniferous tree species. *Oecologia*, 104(1), 24-30.

Reichstein, M., Falge, E., Baldocchi, D., Papale, D., Aubinet, M., et al., 2005. On the separation of net ecosystem exchange into assimilation and ecosystem respiration: review and improved algorithm. *Global Change Biology*, 11, 1424–1439.

Richart, M. and Hewitt, N., 2008. Forest remnants in the Long Point region, Southern Ontario: Tree species diversity and size structure. *Landscape and Urban Planning*, 86(1), 25-37.

Sanz-Pérez, V., Castro-Díez, P. and Valladares, F., 2009. Differential and interactive effects of temperature and photoperiod on budburst and carbon reserves in two co-occurring Mediterranean oaks. *Plant Biology*, *11*(2), 142-151.

Schwartz, M.D., Ahas, R. and Aasa, A., 2006. Onset of spring starting earlier across the Northern Hemisphere. *Global Change Biology*, 12(2), 343-351.

Settele, J., R. Scholes, R. Betts, S. Bunn, P. Leadley, D. Nepstad, J.T. Overpeck, and M.A. Taboada, 2014: Terrestrial and inland water systems. Climate Change 2014: Impacts, Adaptation, and Vulnerability. Part A: Global and Sectoral Aspects. Contribution of Working Group II to the Fifth Assessment Report of the Intergovernmental Panel on Climate Change [Field, C.B., V.R. Barros, D.J. Dokken, K.J. Mach, M.D. Mastrandrea, T.E. Bilir, et al (eds.)]. Cambridge University Press, Cambridge, UK & New York, NY, USA, 271-359.

Skubel, R., Arain, M.A., Peichl, M., Brodeur, J.J., Khomik, M., Thorne, R., Trant, J. and Kula, M., 2015. Age effects on the water-use efficiency and water-

use dynamics of temperate pine plantation forests. *Hydrological Processes*, 29(18), 4100-4113.

Skubel, R.A., Khomik, M., Brodeur, J.J., Thorne, R. and Arain, M.A., 2017. Short-term selective thinning effects on hydraulic functionality of a temperate pine forest in eastern Canada. *Ecohydrology*, *10*(1), p.e1780.

Song, C. & Woodcock, C.E., 2003. A regional forest ecosystem carbon budget model: impacts of forest age structure and landuse history. *Ecological Modelling*, 164(1), 33-47.

Stokes, V.J., Morecroft, M.D. and Morison, J.I., 2006. Boundary layer conductance for contrasting leaf shapes in a deciduous broadleaved forest canopy. *Agricultural and Forest Meteorology*, 139(1-2), 40-54.

Stoy, P.C., Katul, G.G., Siqueira, M.B., Juang, J.Y., Novick, K.A., McCarthy, H.R., Oishi, A.C., Uebelherr, J.M., Kim, H.S. and Oren, R.A.M., 2006. Separating the effects of climate and vegetation on evapotranspiration along a successional chronosequence in the southeastern US. *Global Change Biology*, 12(11), 2115-2135.

Sun, G., Caldwell, P., Noormets, A., McNulty, S.G., Cohen, E., Moore Myers, J., Domec, J.C., Treasure, E., Mu, Q., Xiao, J. and John, R., 2011. Upscaling key ecosystem functions across the conterminous United States by a water-centric ecosystem model. *Journal of Geophysical Research: Biogeosciences*, 116(G3).

Tang, Y., Wen, X., Sun, X., Zhang, X. and Wang, H., 2014. The limiting effect of deep soilwater on evapotranspiration of a subtropical coniferous plantation subjected to seasonal drought. *Adv. Atmospheric Sci.*, 31(2), 385-395.

Taylor, G., Tallis, M.J., Giardina, C.P., Percy, K.E., Miglietta, F., Gupta, P.S., Gioli, B., Calfapietra, C., Gielen, B., Kubiske, M.E. and Scarascia-Mugnozza, G.E., 2008. Future atmospheric CO_2 leads to delayed autumnal senescence. *Glob. Change Biol*, 14, 264-275.

Teskey, R., Wertin, T., Bauweraerts, I., Ameye, M., McGuire, M.A. and Steppe, K., 2015. Responses of tree species to heat waves and extreme heat events. *Plant, Cell & Environment*, 38(9), 1699-1712.

Vargas, R., Sonnentag, O., Abramowitz, G., Carrara, A., Chen, J.M., Ciais, P., Correia, A., Keenan, T.F., Kobayashi, H., Ourcival, J.M. and Papale, D., 2013. Drought influences the accuracy of simulated ecosystem fluxes: a

model-data meta-analysis for Mediterranean oak woodlands. *Ecosystems*, 16(5), 749-764.

Vitasse, Y., François, C., Delpierre, N., Dufrêne, E., Kremer, A., Chuine, I. and Delzon, S., 2011. Assessing the effects of climate change on the phenology of European temperate trees. *Agricultural and Forest Meteorology*, 151(7), 969-980.

Wagle, P., Xiao, X., Kolb, T.E., Law, B.E., Wharton, S., Monson, R.K., Chen, J., Blanken, P.D., Novick, K.A., Dore, S. and Noormets, A., 2016. Differential responses of carbon and water vapor fluxes to climate among evergreen needleleaf forests in the USA. *Ecological Processes*, 5(1), 8.

Wang, J., Xiao, X., Wagle, P., Ma, S., Baldocchi, D., Carrara, A., Zhang, Y., Dong, J. and Qin, Y., 2016. Canopy and climate controls of gross primary production of Mediterranean-type deciduous and evergreen oak savannas. *Agric. For. Meteorol.*, 226, 132-147.

Warren, J.M., Norby, R.J. and Wullschleger, S.D., 2011. Elevated CO2 enhances leaf senescence during extreme drought in a temperate forest. *Tree Physiology*, *31*(2), 117-130.

Way, D.A. & Oren, R., 2010. Differential responses to changes in growth temperature between trees from different functional groups and biomes: a review and synthesis of data. *Tree Physiology*, 30(6), 669-688.

Weed, A.S., Ayres, M.P. and Hicke, J.A., 2013. Consequences of climate change for biotic disturbances in North American forests. *Ecological Monographs*, 83(4), 441-470.

White, M.A. & Nemani, R.R., 2003. Canopy duration has little influence on annual carbon storage in the deciduous broad leaf forest. *Global Change Biology,* 9(7), 967-972.

Wiken, E.D., Nava, F.J. and Griffith, G., 2011. North American Terrestrial Ecoregions—Level III. Commission for Environmental Cooperation, Montreal, Canada, 149.

Wofsy, S.C., Goulden, M.L., Munger, J.W., Fan, S.M., Bakwin, P.S., Daube, B.C., Bassow, S.L. and Bazzaz, F.A., 1993. Net exchange of CO2 in a mid-latitude forest. *Science*, 260(5112), 1314-1317.

Wolf, S., Eugster, W., Ammann, C., Häni, M., Zielis, S., Hiller, R., et al., 2013. Contrasting response of grassland versus forest carbon and water fluxes to spring drought in Switzerland. *Environ. Res. Lett.*, 8(3), 035007.

Wu, J., Jing, Y., Guan, D., Yang, H., Niu, L., Wang, A., et al., 2013. Controls of evapotranspiration during the short dry season in a temperate mixed forest in Northeast China. *Ecohydrology*, *6*(5), 775-782.

Xie, J., Chen, J., Sun, G., Chu, H., Noormets, A., Ouyang, Z., John, R., Wan, S. and Guan, W., 2014. Long-term variability and environmental control of the carbon cycle in an oak-dominated temperate forest. *Forest Ecology and Management*, 313, 319-328.

Xie, J., Chen, J., Sun, G., Zha, T., Yang, B., Chu, H., Liu, J., Wan, S., Zhou, C., Ma, H. and Bourque, C.P.A., 2016. Ten-year variability in ecosystem water use efficiency in an oak-dominated temperate forest under a warming climate. *Agricultural and Forest Meteorology*, 218, 209-217.

Yuan, W., Luo, Y., Richardson, A.D., Oren, R.A.M., Luyssaert, S., Janssens, I.A., Ceulemans, R., Zhou, X., Grünwald, T., Aubinet, M. and Berhofer, C., 2009. Latitudinal patterns of magnitude and interannual variability in net ecosystem exchange regulated by biological and environmental variables. *Global Change Biology*, 15(12), 2905-2920.

Zha, T., Barr, A.G., Black, T.A., McCaughey, J.H., Bhatti, J., Hawthorne, I., Krishnan, P., Kidston, J., Saigusa, N., Shashkov, A. and Nesic, Z., 2009. Carbon sequestration in boreal jack pine stands following harvesting. *Global Change Biology*, *15*(6), 1475-1487.

Table 4.1: Site characteristics of the deciduous (TPD) and coniferous (TP39) forest stands. The TP39 values in brackets indicate pre-thinning (2003 – 2011) values, prior to the period of focus.

	Turkey Point 1939 (TP39)	Turkey Point Deciduous (TPD)
	42.71°N, 80.357°W	42.635°N, 80.558°W
Stand	Afforested on oak savanna,	Naturally regenerated on
Previous Land Use	cleared for afforestation	abandoned agricultural land
Age (in 2017)	78 years	70 – 110 years
Elevation (m)	184	265
DBH (cm)	39.0 (37.2)	23.1
Density (trees ha^{-1})	321 (413)	504
Tree Height (m)	23.4 (22.9)	25.7
LAI (m^2 m^{-2})	5.3 (8.5)	8.0
Dominant Species	*Pinus Stobus L.*	*Quercus Alba*
Secondary & Understory	*Abies Balsamea, Q. Velutina, A. Rubrum, Prunus Serotina*	*Acer Saccharum, A. Rubrum, Fagus Grandifolia, Q. Velutina, Q. Rubra, Fraxinus Americana*
Ground	*M. Canadense, Rubus Spp., Rhus Radicans, Ferns, Mosses*	*Maianthemum Canadense, Aplectrum Hyemale, Equisetum*
Soil		
Drainage	Well-drained	Rapid to well-drained
Classification	Brunisolic grey brown luvisol	Brunisolic grey brown luvisol
Texture	Very fine sandy-loam	Predominantly sandy
Bulk Density ($kg\ m^{-3}$)	1.35 g m^{-3}	1.15 g m^{-3}

Table 4.2: The top section of the table contains the annual calculated phenological dates (reported as day of year) for both the evergreen conifer (TP39, **bolded C**) and deciduous broadleaf (TPD, *italicized D*) forests from year 2012 to year 2017. Phenological dates were calculated following Gonsamo et al. (2013) from eddy covariance measured GEP_{Max} data. Six-year mean values and standard deviations are included in the final column. The resulting phenological seasons and their duration in days are also shown, in the lower section of the table.

Phenology Transition Dates		**2012**	**2013**	**2014**	**2015**	**2016**	**2017**	**Mean**
Start of Season (SOS, bud-break)	**C**	**70**	**96**	**96**	**91**	**74**	**79**	**84 ± 12**
	D	*120*	*116*	*127*	*118*	*126*	*125*	122 ± 5
Mid of Greenup (MOG, fastest green-up)	**C**	**119**	**137**	**132**	**122**	**127**	**130**	**128 ± 7**
	D	*136*	*141*	*148*	*136*	*144*	*147*	*142 ± 5*
End of Greenup (EOG, end of leaf-out)	**C**	**147**	**160**	**153**	**140**	**158**	**159**	**153 ± 8**
	D	*145*	*155*	*160*	*146*	*154*	*159*	*153 ± 6*
Peak of Season (Midpoint between EOG & SOB)	**C**	**214**	**205**	**202**	**193**	**212**	**201**	**204 ± 8**
	D	*198*	*199*	*205*	*193*	*203*	*207*	*201 ± 5*
Start of Browndown (SOB, start of senescence)	**C**	**271**	**258**	**258**	**257**	**270**	**248**	**260 ± 9**
	D	*257*	*249*	*255*	*249*	*262*	*261*	*255 ± 6*
Mid of Browndown (MOB, fastest senescence)	**C**	**287**	**292**	**287**	**289**	**305**	**287**	**291 ± 7**
	D	*275*	*273*	*274*	*271*	*286*	*282*	*277 ± 6*
End of Season (EOS)	**C**	**314**	**351**	**338**	**345**	**366**	**354**	**345 ± 17**
	D	*306*	*314*	*307*	*309*	*328*	*318*	*314 ± 8*
Phenologically-Defined Seasons		**2012**	**2013**	**2014**	**2015**	**2016**	**2017**	**Mean**
Spring (EOG – SOS)	**C**	**78**	**64**	**58**	**48**	**84**	**80**	**69 ± 14**
	D	*25*	*39*	*34*	*28*	*28*	*34*	*31 ± 5*
Summer (SOB – EOG) (LOCC, Length of Canopy Closure)	**C**	**124**	**97**	**105**	**117**	**112**	**89**	**107 ± 13**
	D	*112*	*94*	*95*	*103*	*107*	*102*	*102 ± 7*
Autumn (EOS – SOB)	**C**	**43**	**94**	**80**	**89**	**96**	**106**	**85 ± 22**
	D	*49*	*65*	*52*	*61*	*67*	*57*	*58 ± 7*
Length of Growing Season (LOS)	**C**	**245**	**255**	**242**	**254**	**292**	**275**	**260 ± 19**
	D	*186*	*198*	*180*	*191*	*202*	*193*	*192 ± 8*

Table 4.3: Seasonal and annual sums of eddy covariance (EC) measured carbon (GEP, RE, and NEP, g C m^{-2} yr^{-1}) and water fluxes (ET, mm yr^{-1}) from 2012 to 2017 for both the conifer (TP39, **bolded C**) and deciduous (TPD, *italicized D*) forests. The phenologically-defined seasonal dates were calculated using the timing of transitions in phenological dates, outlined in Table 4.2. The six-year mean and standard deviations are also included for each row.

	Season		2012	2013	2014	2015	2016	2017	Mean
GEP Sum	Spring (SOS to EOG)	**C**	**308**	**306**	**279**	**213**	**359**	**418**	**314 ± 70**
		D	*104*	*197*	*165*	*117*	*129*	*174*	*148 ± 36*
	Summer (EOG to SOB)	**C**	**990**	**942**	**1070**	**1160**	**1014**	**930**	**1018 ± 86**
		D	*942*	*949*	*1023*	*1006*	*1084*	*1070*	*1012 ± 59*
	Autumn (SOB to EOS)	**C**	**132**	**264**	**265**	**340**	**249**	**377**	**271 ± 85**
		D	*147*	*239*	*200*	*240*	*219*	*213*	*210 ± 34*
	Annual	**C**	**1452**	**1501**	**1601**	**1701**	**1617**	**1709**	**1597 ± 104**
		D	*1198*	*1369*	*1382*	*1347*	*1420*	*1447*	*1360 ± 87*
RE Sum	Jan 1 to SOS	**C**	**66**	**83**	**78**	**79**	**82**	**81**	**78 ± 6**
		D	*167*	*107*	*129*	*109*	*163*	*170*	*141 ± 30*
	Spring (SOS to EOG)	**C**	**205**	**205**	**169**	**122**	**233**	**276**	**202 ± 53**
		D	*78*	*151*	*133*	*109*	*109*	*144*	*121 ± 27*
	Summer (EOG to SOB)	**C**	**908**	**718**	**809**	**790**	**888**	**735**	**808 ± 78**
		D	*500*	*672*	*581*	*714*	*684*	*700*	*642 ± 84*
	Autumn (SOB to EOS)	**C**	**142**	**272**	**269**	**310**	**302**	**434**	**288 ± 94**
		D	*138*	*269*	*196*	*259*	*266*	*252*	*230 ± 52*
	EOS to Dec 31	**C**	**77**	**14**	**33**	**39**	**--**	**13**	**35 ± 26**
		D	*82*	*64*	*84*	*110*	*55*	*65*	*77 ± 20*
	Annual	**C**	**1386**	**1282**	**1345**	**1328**	**1492**	**1525**	**1393 ± 96**
		D	*954*	*1250*	*1110*	*1283*	*1260*	*1317*	*1196 ± 138*
NEP Sum	Jan 1 to SOS	**C**	**-58**	**-74**	**-68**	**-73**	**-66**	**-66**	**-67 ± 6**
		D	*-117*	*-79*	*-88*	*-82*	*-129*	*-130*	*-104 ± 24*
	Spring (SOS to EOG)	**C**	**103**	**101**	**110**	**92**	**128**	**144**	**113 ± 19**
		D	*25*	*45*	*30*	*4*	*18*	*29*	*25 ± 14*
	Summer (EOG to SOB)	**C**	**80**	**223**	**262**	**374**	**127**	**196**	**210 ± 104**
		D	*442*	*276*	*441*	*288*	*398*	*371*	*369 ± 73*
	Autumn (SOB to EOS)	**C**	**-12**	**-5**	**-6**	**33**	**-48**	**-51**	**-15 ± 31**
		D	*16*	*-26*	*4*	*-18*	*-46*	*-37*	*-18 ± 24*
	EOS to Dec 31	**C**	**-35**	**-12**	**-30**	**-24**	**--**	**-12**	**-23 ± 10**
		D	*-68*	*-56*	*-79*	*-103*	*-51*	*-58*	*-69 ± 19*
	Annual	**C**	**76**	**228**	**263**	**395**	**139**	**208**	**218 ± 109**
		D	*292*	*156*	*305*	*90*	*185*	*169*	*200 ± 83*
ET Sum	Jan 1 to SOS	**C**	**22**	**23**	**11**	**19**	**13**	**15**	**17 ± 5**
		D	*56*	*28*	*33*	*24*	*39*	*44*	*37 ± 12*
	Spring (SOS to EOG)	**C**	**105**	**97**	**67**	**65**	**85**	**106**	**87 ± 18**
		D	*36*	*55*	*45*	*31*	*39*	*48*	*42 ± 9*
	Summer (EOG to SOB)	**C**	**315**	**277**	**260**	**286**	**249**	**210**	**266 ± 36**
		D	*283*	*231*	*213*	*219*	*266*	*237*	*242 ± 27*
	Autumn (SOB to EOS)	**C**	**43**	**73**	**82**	**67**	**64**	**97**	**71 ± 18**
		D	*45*	*63*	*50*	*66*	*69*	*64*	*60 ± 9*
	EOS to Dec 31	**C**	**15**	**2**	**6**	**4**	**--**	**3**	**6 ± 5**
		D	*14*	*9*	*12*	*14*	*11*	*15*	*12 ± 2*
	Annual	**C**	**495**	**468**	**421**	**436**	**408**	**424**	**442 ± 33**
		D	*428*	*381*	*350*	*349*	*417*	*403*	*388 ± 34*

Table 4.4: Linear relationships between total annual water (ET, mm yr^{-1}) and carbon (RE and NEP, g C m^{-2} yr^{-1}) flux measurements and both meteorological (i.e. VPD, Ta, $\theta_{0\text{-}30cm}$) and phenological (i.e. spring length, carbon uptake start) variables (annual or seasonal) from 2012 to 2017. In each section, the R^2 listed is for the relationship to the specified annual flux.

Conifer	**2012**	**2013**	**2014**	**2015**	**2016**	**2017**	**R^2**
Annual RE (g C m^{-2} yr^{-1})	1386	1282	1345	1328	1492	1525	--
Summer $\theta_{0\text{-}30cm}$ (m^3 m^{-3})	0.083	0.097	0.090	0.096	0.071	0.076	0.89
Annual NEP (g C m^{-2} yr^{-1})	76	228	263	395	139	208	--
Spring Length (Days)	78	64	58	48	84	80	0.75
Summer Ta (°C)	21.1	20.3	19.9	20.0	21.1	20.7	0.73
Summer NEP (g C m^{-2})	80	223	262	374	127	196	0.99
Deciduous	**2012**	**2013**	**2014**	**2015**	**2016**	**2017**	**R^2**
Annual ET (mm yr^{-1})	428	381	350	349	417	403	--
Annual Ta (°C)	11.8	9.2	8.0	9.2	10.6	10.0	0.84
Winter $\theta_{0\text{-}30cm}$ (m^3 m^{-3})	0.131	0.118	0.116	0.101	0.133	0.127	0.83
Annual RE (g C m^{-2} yr^{-1})	954	1250	1110	1283	1260	1317	--
Spring Ta (°C)	16.6	15.1	16.1	15.1	15.6	14.0	0.77
Annual NEP (g C m^{-2} yr^{-1})	292	156	305	90	185	169	--
Summer RE (g C m^{-2})	500	672	581	714	684	700	0.80

Table 4.5: The model-predicted scaling factors of meteorological variables (i.e. Ta, VPD, PAR, $\theta_{0\text{-}30cm}$) during the phenological summer (end of greenup to start of senescence) for the conifer and deciduous forests from 2012 to 2017. These normalized values show the cumulative effect of the meteorological variable in reducing GEP and RE from their theoretical maximum values. Higher values represent more favorable summer conditions for GEP and RE.

Conifer	**2012**	**2013**	**2014**	**2015**	**2016**	**2017**
GEP: Ta	0.994	0.990	0.987	0.981	1.00	0.997
GEP: VPD	0.939	1.00	1.00	0.981	0.914	0.975
GEP: PAR	0.949	0.950	0.946	0.956	1.00	0.950
GEP: $\theta_{0\text{-}30cm}$	0.956	1.00	0.998	0.993	0.976	0.973
GEP: All	0.846	0.941	0.932	0.914	0.892	0.899
RE: $\theta_{0\text{-}30cm}$	0.958	1.00	0.996	0.991	0.968	0.965

Deciduous	**2012**	**2013**	**2014**	**2015**	**2016**	**2017**
GEP: Ta	1.00	0.971	0.974	0.967	0.989	0.974
GEP: VPD	0.871	1.00	0.998	0.998	0.946	0.989
GEP: PAR	0.978	0.938	0.955	0.953	1.00	0.956
GEP: $\theta_{0\text{-}30cm}$	1.00	1.00	1.00	1.00	1.00	1.00
GEP: All	0.852	0.911	0.929	0.920	0.936	0.920
RE: $\theta_{0\text{-}30cm}$	0.976	1.00	0.997	1.00	0.965	0.992

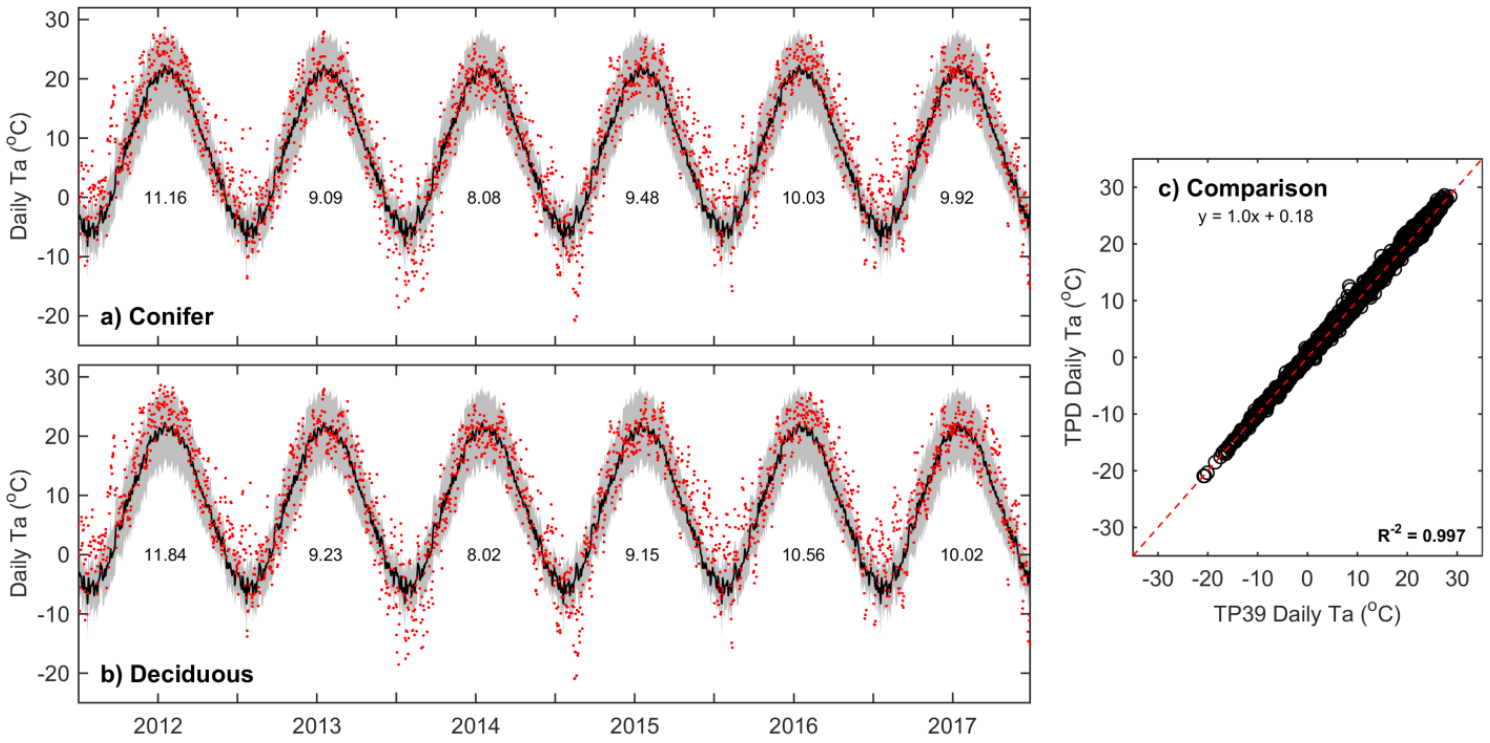

Figure 4.1: Daily above canopy air temperature (Ta, red dots) measured from 2012 to 2017 at the (a) conifer forest (TP39) and (b) deciduous forest (TPD), with the grey shading and black line corresponding to the 30-year Environment Canada (Delhi) minimum and maximum range of daily Ta and mean daily Ta, respectively. Values shown represent the annual mean Ta for each year of measurements. Also included is the (c) comparison of daily Ta at TP39 and TPD.

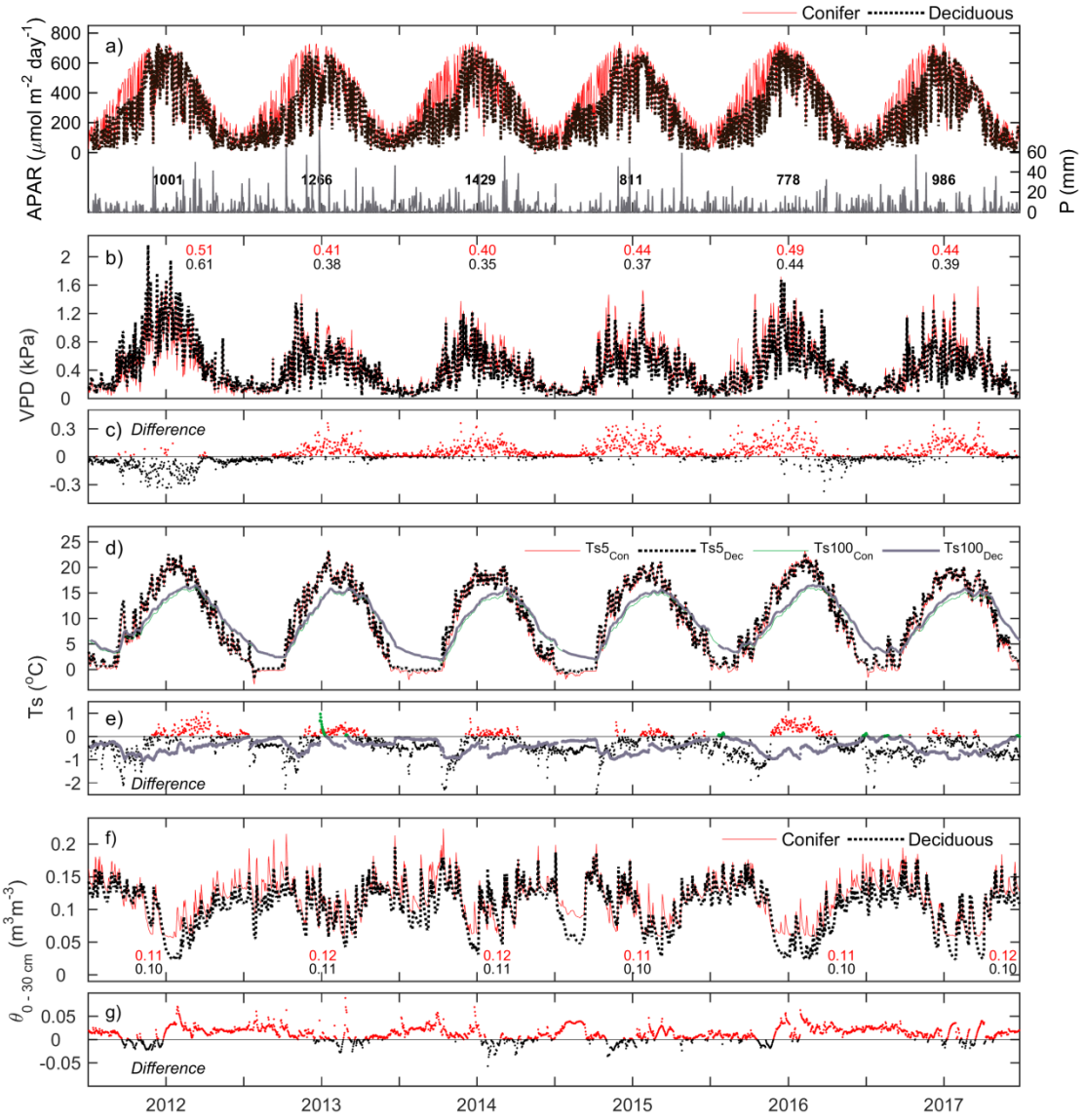

Figure 4.2: A daily time series of meteorological variables measured at the conifer (TP39, red line) and deciduous (TPD, black dashed line) forests from 2012 to 2017, including: (a, left) total absorbed photosynthetically active radiation (APAR), (a, right) total precipitation (P), (b) mean vapor pressure deficit (VPD), (c) the difference in VPD between the two forests (conifer – deciduous), (d) mean soil temperatures (Ts) at 5 cm and 100 cm depths, (e) the difference in Ts at both depths, (f) the mean soil volumetric water content from 0-30 cm depths ($\theta_{0\text{-}30cm}$), and (g) the difference in θ between the two forests.

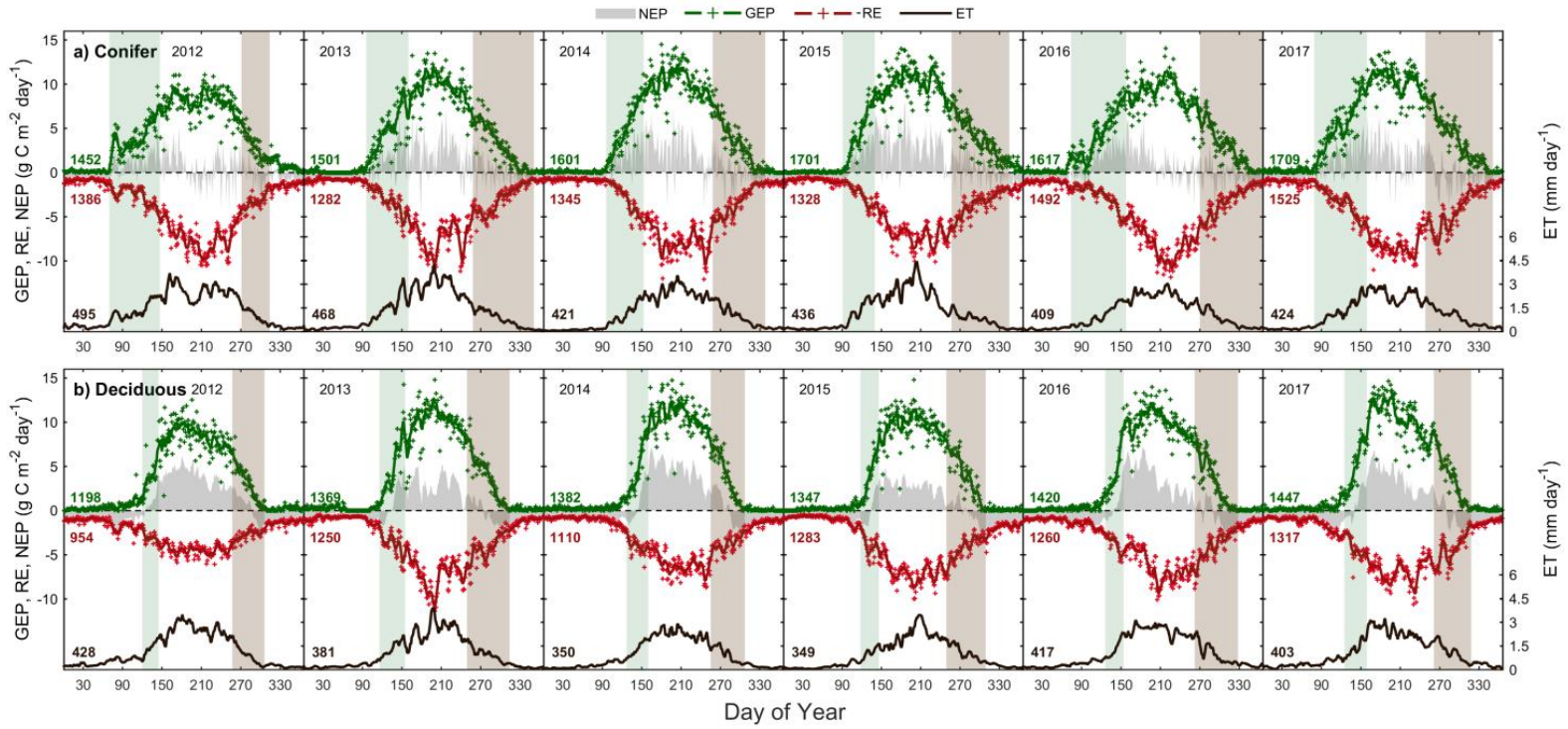

Figure 4.3: Time series from 2012 to 2017 of the daily total gross ecosystem productivity (GEP, green +), ecosystem respiration (RE, red +), net ecosystem productivity (NEP, grey shading), and evapotranspiration (ET, black [right]) for the (a) conifer forest (TP39), and the (b) deciduous forest (TPD). Solid lines of GEP, RE, NEP, and ET are derived from 5-day moving averages of the measured data, while the colored values for each year correspond to annual GEP (green), RE (red), and ET (black) for each site. The annual EC-derived phenological spring (green) and autumn (brown) are included for each site, and can be found in Table 4.2.

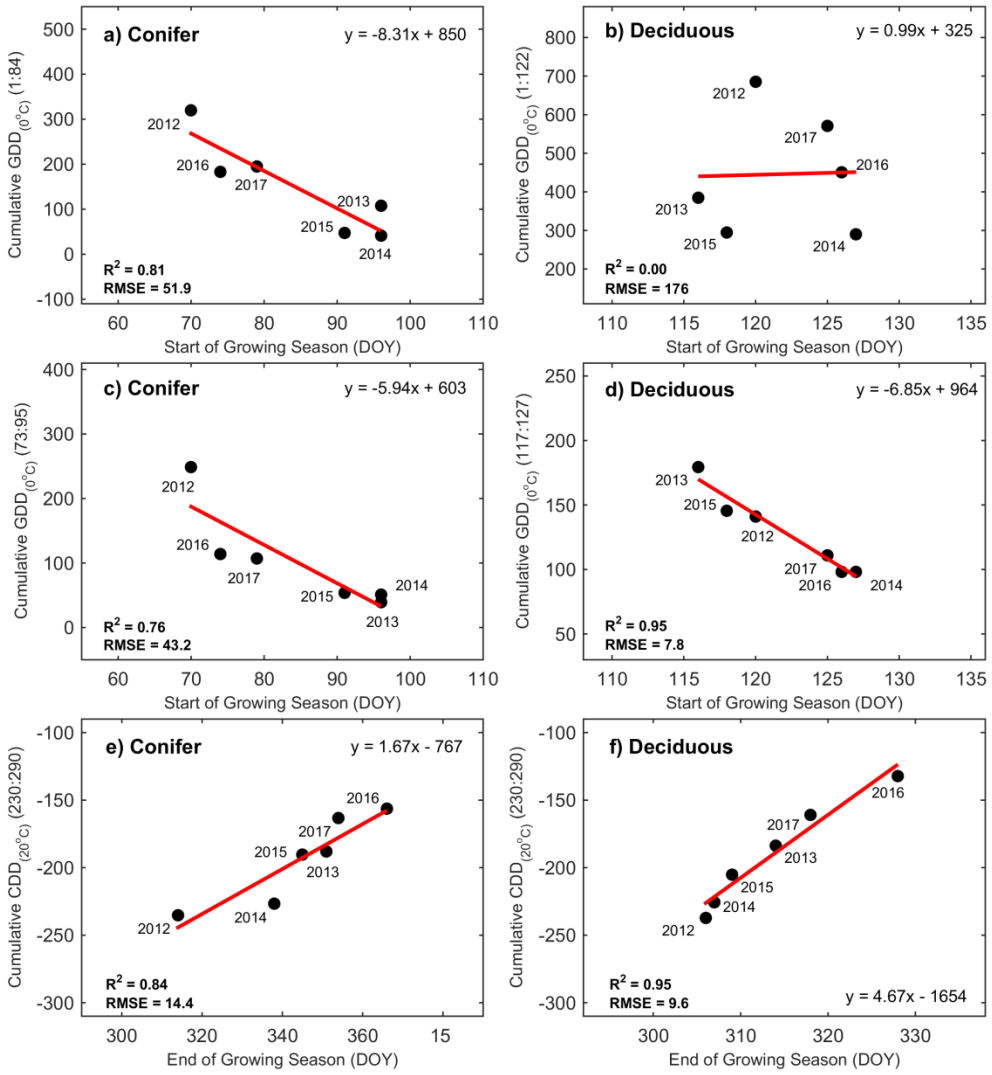

Figure 4.4: Correlations between growing degree days (GDD), cooling degree days (CDD) and and phenological start of the growing season (SOS) and end of the growing season (EOS) from 2012 to 2017 at both the conifer and deciduous forests. Shown are: (a) cumulative GDD from January 1st to the mean SOS at TP39 and (b) TPD, (c) cumulative GDD from the mean SOS ± standard deviation at TP39 and (d) TPD, and (e) the cumulative CDD from day of year 230:290 at TP39 and (f) TPD. Linear fit equations with R^2 and RMSE also included.

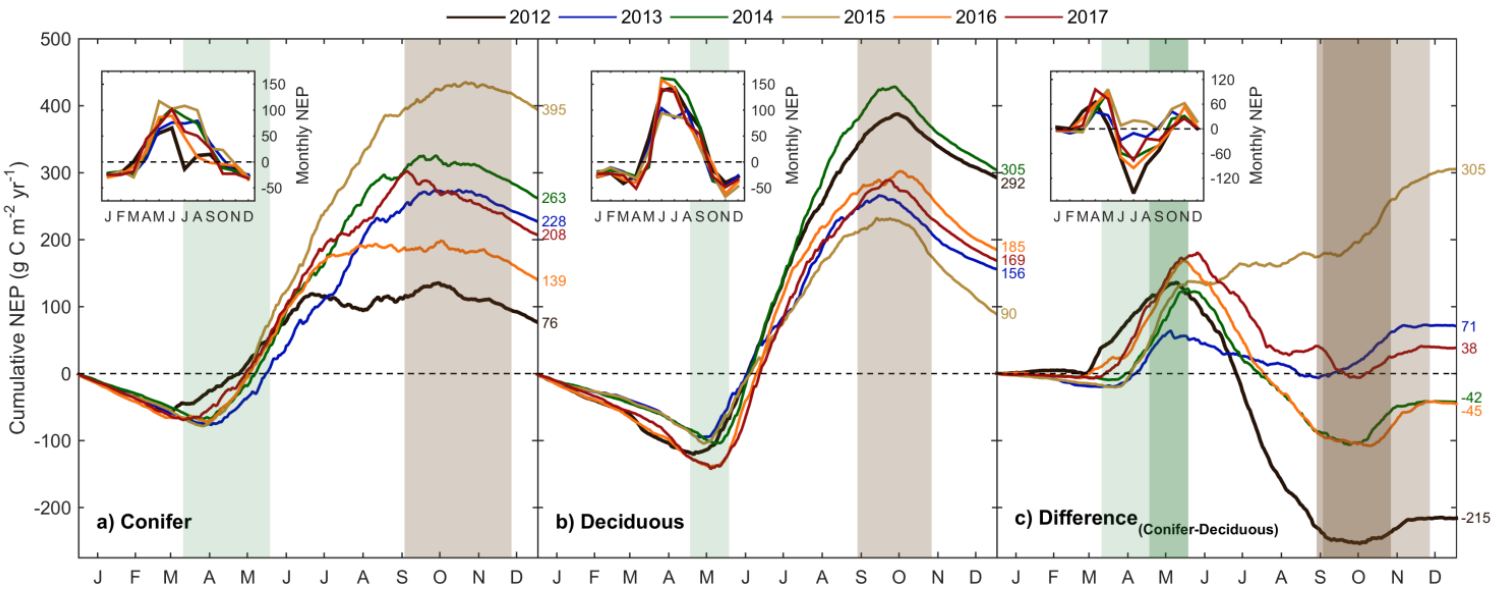

Figure 4.5: Cumulative daily sums of net ecosystem productivity (NEP) at the (a) conifer forest (TP39), the (b) deciduous forest (TPD), and (c) the cumulative difference (conifer – deciduous), with appropriate monthly NEP sums in each figure inset, from 2012 to 2017. Green shading in each panel corresponds to the site-specific 6-year mean phenological spring duration, while brown shading corresponds to the 6-year mean phenological autumn duration (Table 4.2). Dark shading in panel (c) represents the deciduous forest seasons overlaid on the conifer seasons. Cumulative annual values are shown for each site and year, with colors found in the key.

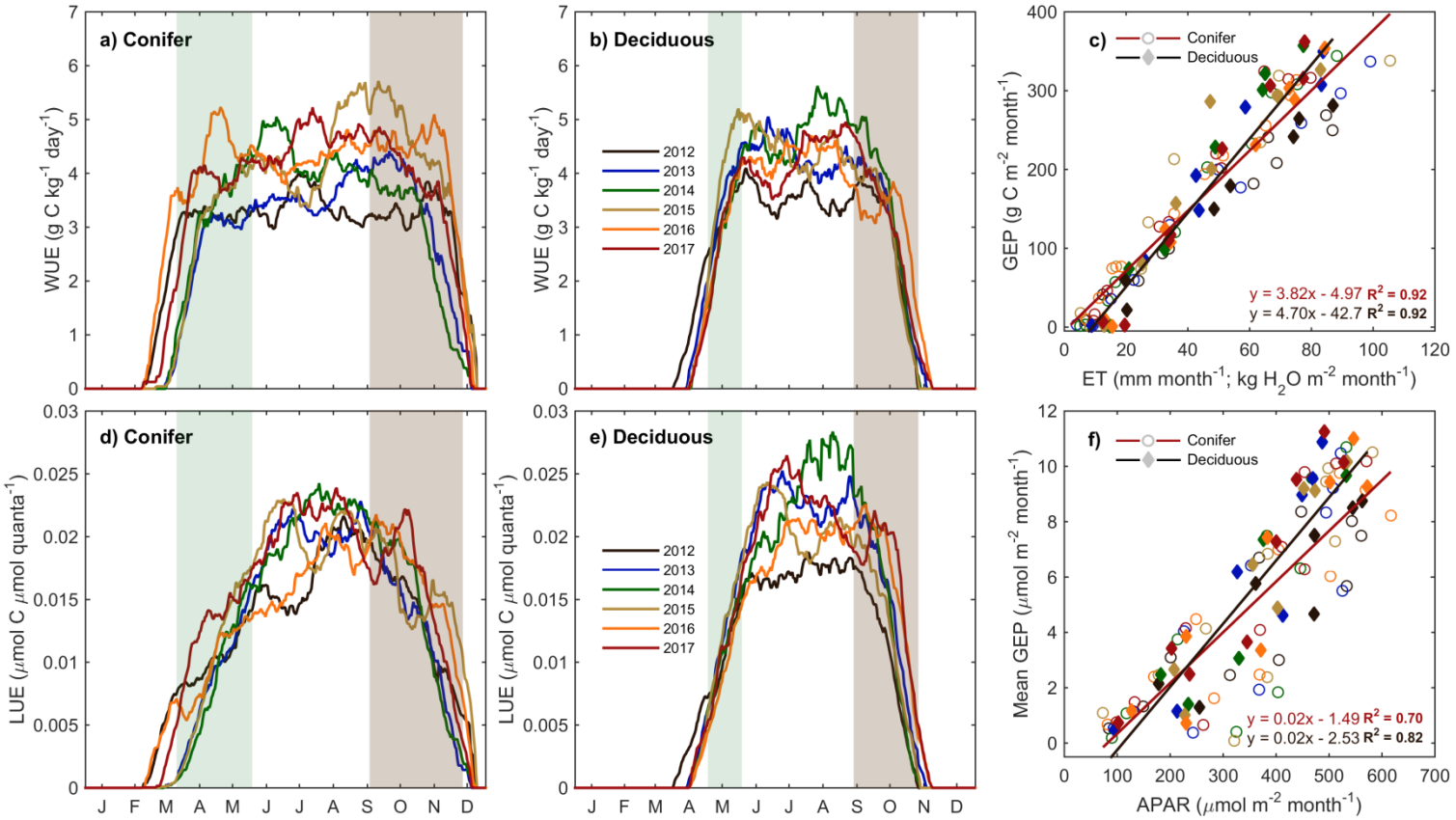

Figure 4.6: Annual smoothed (1-month moving average) time series of the (a) conifer (TP39) and (b) deciduous forest water use efficiency (WUE; GEP ET^{-1}), and (c) monthly linear relationships between GEP and ET at both sites from 2012 to 2017. Similarly, light use efficiency (LUE; GEP $APAR^{-1}$) calculations are shown for (d) the conifer forest and (e) deciduous forest, while linear relationships (f) of monthly GEP and APAR are also shown. The green and brown shading correspond to the site-specific 6-year mean phenological spring and autumn periods (Table 4.2), respectively. Linear fit equations and R^2 values are also shown (c & f).

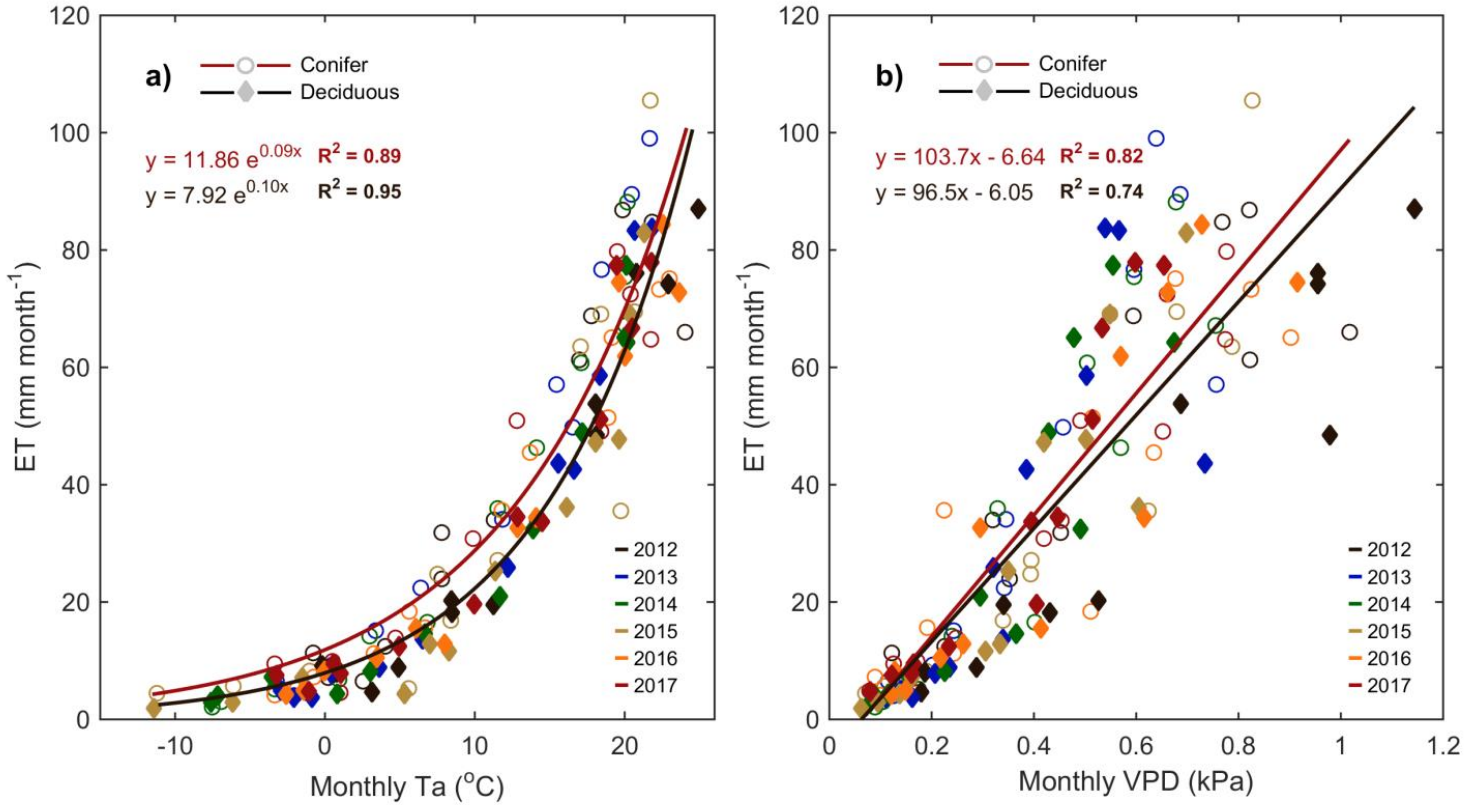

Figure 4.7: (a) Monthly exponential relationships between mean air temperature (Ta) and total evapotranspiration (ET) from 2012 to 2017 for the conifer (TP39, open circle) and deciduous (TPD, diamond) forests. Also shown are the six-year (b) monthly linear fits between mean vapor pressure deficit (VPD) and ET. Fit equations and R^2 also shown.

Table S4.1: Descriptions of the eddy covariance (EC) and meteorological instrumentation and sensors installed at both sites throughout the period of measurements (2012 to 2017). *Note: IRGA = infrared gas analyzer*

	Turkey Point 1939 (TP39)	Turkey Point Deciduous (TPD)
Canopy IRGA	LI-7000 (LI-COR)	LI-7200 (LI-COR)
Sonic Anemometer	CSAT3 (CSI)	CSAT3 (CSI)
Height	28 m (2003 – May 2016) 34 m (May 2016 – Present)	36 m (2012 – Present)
Orientation	Oriented west (270°)	Oriented west (270°)
Intake Tube	4 m long intake tube	1 m long intake tube
Flow	15 L/min	15 L/min
Mid-Canopy IRGA	LI-800 (LI-COR) Measured at 14 m height	LI-820 (LI-COR) Measured at 16 m height
Air Temperature (Ta) Relative Humidity (RH)	HMP45C (CSI)	HMP155A (CSI)
Wind Speed & Direction	Model 05103 (R.M. Young)	Model 85000 (2012 – 2015) Model 05013 (2015 – Present)
Photosynthetically Active Radiation (PAR)	PAR-Lite (Kipp & Zonen)	PQSI (Kipp & Zonen)
Net Radiation (Rn)	CNR1 (Kipp & Zonen)	CNR4 (Kipp & Zonen)
Soil Temperature (Ts)	107B (CSI)	107B (CSI)
Soil Water Content (θ)	CS615-L/CS616 (CSI)	CS650 (CSI)
Precipitation (P)	T-200B (GEONOR)	CS700H-L (CSI)

CHAPTER 5:

SEASONAL PATTERNS OF PHOTOSYNTHESIS CAPTURED BY REMOTE SENSING VEGETATION INDICES IN A TEMPERATE CONIFEROUS EVERGREEN AND DECIDUOUS BROADLEAF FOREST

5.1 Abstract

Remote sensing is a valuable tool used to accurately track seasonal changes in photosynthesis in an attempt to better predict carbon fluxes across a wide range of ecosystems. While conventional broad band vegetation indices (i.e. NDVI) derived from remote sensing have focused on changes in greenness through the seasonal adjustments in the structure of plant canopies, they failed to capture the more subtle photosynthetic changes typical of evergreen forests. Instead, more recent approaches look to track seasonal changes in fluorescence as well as chlorophyll and carotenoid pigment compositions, which have been shown to be effective in both evergreen and broadleaf forests. For that reason, this study examined the relative ability of different vegetative indices to track changes in photosynthetic phenology for two forests of differing leaf shapes and retention strategies (i.e. coniferous evergreen and deciduous broadleaf) in southern Ontario, Canada, by means of: (1) tower-based Automated Multiangular SPectro-radiometers for Estimation of Canopy reflectance systems (AMSPEC-III) operated during the 2016 growing season, and (2) satellite-based MODIS indices examined from 2012 to 2017. Carotenoid sensitive indices (photochemical

reflectance index [PRI] and chlorophyll/carotenoid index [CCI]) and the red-edge chlorophyll index (CIr) were shown to effectively capture seasonal (i.e. daily and 8-day) changes in photosynthesis of both forest stands during 2016. The Moderate Resolution Imaging Spectroradiometer (MODIS) gross primary productivity (GPP) and solar-induced fluorescence (SIF) via the Orbiting Carbon Observatory-2 (OCO-2) satellite showed strong positive correlations to annual measured eddy covariance based photosynthesis (gross ecosystem productivity) and meteorological controls at both forests from 2012 to 2017. While these relationships were similar to previous analyses, the observed interannual variability was likely a result of meteorological conditions or heterogeneous landscapes surrounding the forest stands. Based on these results, we found stand-level and satellite-based vegetative indices capable of monitoring photosynthetic phenology in a temperate deciduous and coniferous forest.

5.2 Introduction

In North America, temperate forests absorb significant amounts of atmospheric carbon dioxide (CO_2) emissions, storing carbon in biomass, soils, and other plant materials, often times storing several orders of magnitude more carbon than other vegetation types (Curtis et al., 2002; Pan et al., 2011; Gielen et al., 2013; Gough et al., 2016). While these forests are significant sinks of annual anthropogenic emissions, increasing temperatures in response to changing climates may negatively impact the magnitude of carbon being stored

(Kirschbaum, 2000; MacDonald, 2012; IPCC, 2013). Climate change may further impact a number of plant processes as shifts in the phenological growing season due to increasing temperatures will directly affect the timing and period of photosynthetic activity (Richardson et al., 2010; Estiarte & Peñuelas, 2015).

In temperate forests, tree species cycle between periods of growth and dormancy in response to physiological and climatic influences such as changing temperatures and photoperiod (Cleland et al., 2007; Korner & Basler, 2010). However, the responses to seasonal phenological variations may be different between diverse forest types (Springer et al., 2017). For deciduous species, the onset of photosynthetic development (bud-burst and leaf-out) is able to easily be observed, much like senescence and the changing of leaf color in autumn. Conifer species though see more subtle changes in leaf pigment composition that cannot be as readily observed (Bigras et al., 2001; Soolanayakanahally et al., 2013). These subtle changes include the hardening of needles in winter, acting to adjust chlorophyll and carotenoid contents in order to dissipate excess light energy during winter dormancy (Ottander et al., 1995; Demmig-Adams & Adams, 1996; Verhoeven, 2014). Such adjustments are reversed in spring with increasing temperatures and photoperiods (Wong & Gamon, 2014).

Similar modifications to needle pigment composition used by conifers in order to adjust the annual cycle of photosynthesis, are also used by deciduous leaves to regulate photosynthesis throughout the growing season (Lichtenthaler et al., 2007; Gamon et al., 2016). These seasonal changes in leaf pigments impact

leaf reflectance, fluorescence, and carotenoid chlorophyll ratios (Sims & Gamon, 2002; Junker & Ensminger, 2016). Fluorescence, capable of dissipating energy in a matter of seconds (Muller et al., 2001), operates much more rapidly than chlorophyll and carotenoid adjustments to pigment pool sizes, which may take hours to weeks (Wong & Gamon, 2015). The monitoring of such spectral and physiological adjustments throughout different forest communities is necessary to better understand the resulting changes in photosynthetic activity.

Conventionally, the normalized difference vegetation index (NDVI), through the detection of chlorophyll absorption and leaf scattering in the red and near-infrared (NIR) wavelengths, has been used to track vegetation greenness, representative of photosynthetic activity and growth (Peters et al., 2002; Park et al., 2008). In deciduous forests, NDVI effectively tracks seasonal phenological transitions (Gamon et al., 1995) and is commonly used as a proxy for the fraction of photosynthetically active radiation (FPAR) absorbed by the canopy (Nestola et al., 2016). In coniferous species, while NDVI can detect similar structural changes (i.e. FPAR), only minor deviations in greenness occur annually, making it less effective in detecting seasonal photosynthetic phenology in these ecosystems (Nagai et al., 2012).

In more recent years, the photochemical reflectance index (PRI), a suggested proxy for light-use efficiency (LUE), has displayed the ability to detect changes in photosynthetic activity that NDVI may often miss (Gamon et al., 1992; Hilker et al., 2008; Peñuelas et al., 2011; Wong & Gamon, 2015). On hourly to

daily time-scales, PRI responses are driven by changes in the xanthophyll cycle, while responses on seasonal time-scales reflect changes in chlorophyll and carotenoid pigment pool sizes (Sims & Gamon, 2002; Gamon et al., 2012; Fréchette et al., 2015). The chlorophyll carotenoid index (CCI) similarly tracks photosynthetic activity (Springer et al., 2017). Much like PRI, CCI is sensitive to seasonal changes in chlorophyll and carotenoid levels, especially in conifer species (Gamon et al., 2016). However, a reduced number of studies have examined the link between photosynthesis activity and CCI for deciduous species. Furthermore, red-edge vegetation indices (CI red edge; CIr), which correspond to an increase in reflectance between chlorophyll absorption in red wavelengths, and leaf scattering in NIR wavelengths, have been implemented in a limited number of studies in order to gain information on the estimation of photosynthetic activity (Gitelson et al., 2005; Gitelson et al., 2006; Wu et al., 2009).

Chlorophyll fluorescence may also provide information on photosynthetic activity (Baker et al., 2004; Springer et al., 2017), as satellite solar-induced fluorescence (SIF) has been shown to be closely linked to photosynthesis and gross primary productivity (GPP) (Joiner et al., 2014; Walther et al., 2016). However, current spatial and temporal resolutions of satellite-based SIF typically fail to resolve seasonal changes in pigment pool sizes and fluorescence (Gamon et al., 2019). Ultimately, the aforementioned vegetation indices derived from different remote sensing sources (i.e. proximal and satellite) can provide complementary information on the physiological and phenological responses of

ecosystems to changing meteorological conditions (Nestola et al., 2018). Furthermore, while the temporal dynamics of carbon storage are often measured by eddy covariance (EC) techniques (Baldocchi, 2003), the limited spatial extents of such studies may not be applicable for more broad scale remote sensing applications (Gamon et al., 2010; Chen et al., 2014). Therefore, studies using concurrent EC and remote sensing measurements are needed for a more accurate evaluation of changes in photosynthetic activity (Stylinski et al., 2002; Gamon et al., 2010; Coops et al., 2010).

This study considers multiple datasets of photosynthesis and the associated phenological responses for two geographically, climatically, and edaphically similar forests with different leaf retention and shape strategies (i.e. deciduous broadleaf and coniferous evergreen) in southern Ontario, Canada. In this study, we examined the relationships between EC photosynthesis (gross ecosystem productivity, GEP) and vegetation indices derived from two tower-based Automated Multiangular SPectro-radiometers for Estimation of Canopy reflectance systems (AMSPEC-III; Tortini et al., 2015). At both forest sites, the installation of an AMSPEC-III system during the growing season of 2016 allowed for the construction of stand-level vegetation indices (i.e. CCI, CIr, PRI, and NDVI). However, given the limited length of AMSPEC-III measurements, satellite remote sensing indices (i.e. Moderate Resolution Imaging Spectroradiometer (MODIS) and SIF) were also considered for comparison during the entire study period (2012 to 2017). Therefore, the objectives of this

study were to: (1) evaluate the effectiveness of tower-based and satellite-based remote sensing vegetation indices in tracking differences in photosynthetic phenology at each forest site; (2) investigate variations in the timing of phenological events for satellite-based indices; and (3) explore seasonal meteorological impacts on the dynamics of photosynthetic.

5.3 Materials and Methods

5.3.1 Study Area and Site Descriptions

This study was conducted from January 2012 until the end of December 2017 at two long-term eddy covariance (EC) forest carbon flux monitoring sites in southern Ontario, Canada (known as the Turkey Point Observatory). Located near Turkey Point Provincial Park and Long Point National Wildlife Area on the northern shores of Lake Erie (Figure 5.1), these forest sites are situated within an agriculturally dominated landscape, with roughly 18-25% of the total land area containing scattered temperate forests (Arain & Restrepo-Coupe, 2005).

This study focuses on two of the four Turkey Point Observatory forests; a 78-year old managed plantation coniferous evergreen forest (TP39, *42.71°N, -80.357°W*), and a roughly 90-year old (70 – 110 years old) naturally-regenerated deciduous broadleaf forest (TPD, *42.635°N, -80.558°W*). Planted in 1939, TP39 (CA-TP4), has a mean canopy height of 23.4 m, dominated (82%) by eastern white pine (*Pinus Strobus* L.), with balsam fir (*Abies balsamifera* L. Mill), black and white oak (*Quercus Velutina; Q. Alba),* and red maple (*Acer Rubrum)* trees

scattered throughout the flux tower footprint. The mixed-wood deciduous forest (CA-TPD) is located at the northernmost extent of the natural range of eastern deciduous forests. The forest has a mean canopy height of 25.7 m, and is dominated by white oak (*Quercus Alba*) and red maple (*Acer Rubrum*), with the remaining tree species including: black oak, red oak (*Q. Rubra*), American beech (*Fagus Grandifolia*), sugar maple (*A. Saccharum*) and white ash (*Fraxinus Americana*). The topography at both forest sites in generally flat, and given their close proximity (~20 km apart), they both experience similar meteorological conditions. The 30-year mean (1981 to 2010) annual air temperature (Ta) and total precipitation (P) measured at the Environment Canada Delhi CDA station (~25 km north of sites) was 8.0°C and 997 mm, respectively. Additional site details for TP39 and TPD can be found in Peichl et al. (2010) or in Beamesderfer et al. (2019a), respectively.

5.3.2 Eddy Covariance Measurements

Continuous, half-hourly fluxes of CO_2 (F_c) have been measured at both TP39 and TPD using closed-path eddy covariance (EC) systems since 2003 and 2012, respectively. Concurrent with the EC measurements, each forest is equipped with a suite of meteorological sensors located at the top of a scaffold flux tower (towers shown in Figure 5.1). Specific instrument details and information on the data processing and gap-filling methods implemented can be found in Arain & Restrepo-Coupe (2005), Peichl et al. (2010), or Beamesderfer et al. (2019a). In

short, half-hourly net ecosystem exchange (NEE, µmol m^{-2} s^{-1}) was calculated as the sum of the vertical CO_2 flux (F_c), and the rate of change in CO_2 storage (S_{CO2}) within the air column below the EC measurements at each site ($NEE = F_c + S_{CO2}$). Gross ecosystem productivity (GEP, µmol m^{-2} s^{-1}) was calculated as the difference between NEE and modelled daytime ecosystem respiration (RE). For this analysis, the daily maximum photosynthetic assimilation (GEP_{Max}) was calculated using non-gapfilled GEP found when half-hourly gapfilled NEE was equal to non-gapfilled NEE. This approach helped to remove any potential biases in GEP_{Max} due to meteorological responses found using gapfilled procedures. Half-hourly meteorological data (i.e. Ta, P, vapor pressure deficit (VPD), etc.) were analyzed to calculate daily, 8-day, and seasonal average values.

5.3.3 Proximal Remote Sensing Measurements and Corrections

A portable automated multi-angular spectro-radiometer (AMSPEC-III; Tortini et al., 2015) was installed on the top of the eddy-covariance (EC) fitted scaffold towers at each forest site (TP39 & TPD) from May 12th to October 22nd, 2016. The two AMSPEC-III systems used in the study included JAZ-COMBO (JC; Ocean Optics Inc.) portable spectro-radiometers fitted with upward-looking cosine diffusers (PP-Systems) which acted to correct sky irradiance at varying solar altitudes (Tortini et al., 2015). The systems also included pan-tilt units (PTU; Directed Perception Inc.) allowing the sensors to record data at various zenith and azimuth angles throughout the day. The moving sensor heads allowed

for bidirectional reflectance distribution function (BRDF) measurements to be made of the canopy reflectance (Hilker et al., 2008). Webcams (NetCam SC, StarDot), identical to each sites PhenoCams (Richardson et al., 2007), were used to concurrently capture phenological RGB images used to determine canopy shading. Together, the AMSPEC-III systems recorded solar irradiance, canopy irradiance, solar position, measurement time, and RGB phenological webcam images. Further AMSPEC-III specifications can be found in Tortini et al. (2015).

Measured canopy reflectance (ρ) was defined as the ratio of canopy radiance (upwelling) and solar irradiance (downwelling). The raw spectra acquired from the spectro-radiometers had a 0.145 nm spectral resolution (from 525 – 810 nm spectral range). Corrections were applied to raw measurements as the sensors observed the forest canopy under varying sun-view geometries, significantly impacting canopy spectra. A BRDF correction model normalizing canopy radiance was applied to the data following approaches used in past AMSPEC studies (Hilker et al., 2008; Tortini et al., 2015; Lin et al., 2019). The mean reflectance from 10:00am to 2:00pm (local time) was used in this analysis; representative of canopy-scale, noon-time BRDF corrected data. From these data, four unique vegetative indices were calculated daily for the 2016 growing season. The four indices include: (1) narrow-band Normalized Difference Vegetation Index (NDVI; $[(\rho_{780nm} - \rho_{650nm}) / (\rho_{780nm} + \rho_{650nm})]$), (2) the Photochemical Reflectance Index (PRI; $[(\rho_{531nm} - \rho_{570nm}) / (\rho_{531nm} + \rho_{570nm})]$), (3) the Chlorophyll/Carotenoid Index (CCI; $[(\rho_{531nm} - \rho_{645nm}) / (\rho_{531nm} + \rho_{645nm})]$), and (4)

the red-edge Chlorophyll Index (CIr; [((ρ_{740nm} − ρ_{705nm}) − 1)]). Due to the heterogeneity of the leaves at the deciduous forest during the autumn leaf-down season, the BRDF corrected CCI and CIr data were smoothed to represent a homogenous canopy.

5.3.4 Satellite Remote Sensing Measurements

Satellite solar-induced fluorescence (SIF) measurements for the same period (2012 to 2017) were obtained from the Orbiting Carbon Observatory-2 (OCO-2) SIF dataset (GOSIF) developed by Li and Xiao (2019). These data have finer spatial (0.05°, $1.3 \times 2.25\ km^2$) and temporal (8-day) resolutions than past SIF datasets (i.e. GOME-2: 40 × 40 km^2 (monthly); GOSAT: 10 km diameter (monthly) resolutions), however, currently are unable to provide similar spatial resolutions to that of other (i.e. AMSPEC-III, Landsat, MODIS, etc.) remote sensing vegetation indices (Sun et al., 2018; Li et al., 2018; Li & Xiao 2019). The GOSIF data were developed from global OCO-2 SIF soundings, MODIS data, and meteorological data from the Modern-Era Retrospective analysis for Research and Applications (MERRA-2). Grid points closest to the EC flux towers were chosen for this analysis. In each case, the GOSIF grid point was located in an agricultural field 1.8 km northeast of TP39 (*42.725°N, -80.35°W*) and in a similar section of deciduous forests 1.3 km southeast of TPD (*42.625°N, -80.55°W*). The 8-day GOSIF data (W m^{-2} μm^{-1} sr^{-1}) were downloaded from the Global Ecology

Group of the Earth Systems Research Center at the University of New Hampshire (http://data.globalecology.unh.edu/).

In addition to GOSIF measurements, vegetation indices from the MODIS-Aqua satellite were also incorporated into this study. A number of past studies have evaluated and validated these datasets, and in most cases, compared products derived from these satellites to EC flux tower measurements (i.e. Turner et al., 2006; Huete et al., 2010). This study examined three different datasets: (1) the Aqua MYD13A1 Version 6 Normalized Difference Vegetation Index (NDVI) produced at a 500 meter spatial resolution and 16 day temporal resolution (Huete et al., 1999), (2) the Aqua MYD15A2H Version 6 fraction of photosynthetically active radiation (FPAR) at a 500 meter spatial resolution and 8 day temporal resolution (Knyazikhin et al., 1999), and (3) the Aqua MYD17A2H Version 6 gross primary productivity (GPP; kg C m^{-2}) datasets at a similar 500 meter and 8 day spatial and temporal resolution, respectively (Running & Zhao, 2015). The GPP data is a cumulative 8-day composite, while FPAR and NDVI data integrate the use of an algorithm to choose the best available pixel within the 8-day and 16-day period, respectively. During this study, the same grid points were considered between the three datasets at each site due to the similar spatial resolutions (i.e. 500 m). For TP39, the nearest point was 100 m west of the tower (*42.7093°N, -80.3585°W*) within the forest footprint, and the nearest point at TPD was 300 m south of the tower (*42.6327°N, -80.5589°W*), similarly within the forest footprint. GPP, FPAR, and NDVI data were obtained using the USGS EarthExplorer

(earthexplorer.usgs.gov/). While not entirely identical, GEP and GPP are often used analogously to describe photosynthetic assimilation (Goulden et al., 1997), however, the usage of either term in our study is purely differentiated by the source of the measurement: EC (GEP) and MODIS (GPP).

5.3.5 Temporal Resolutions and Derivation of Phenological Periods

The outlined data were first analyzed at daily time scales to determine the effectiveness of AMSPEC-III and EC (GEP_{Max}) datasets in capturing the short term impacts of changes to canopy greenness and chlorophyll and carotenoid pigment pools. These data were then compared at 8-day time scales, equivalent to the typical temporal resolution of most satellite remote sensing vegetation indices. The linear correlations (R^2) between daily and 8-day mean indices (both proximal and satellite) and corresponding periods of EC GEP_{Max} measurements were calculated for each forest. Key annual relationships between EC GEP_{Max} and satellite indices were further identified from 2012 to 2017, and the indices with the highest annual linear fits were further considered for phenological modeling.

For EC daily maximum photosynthetic assimilation (GEP_{Max}) and estimates of satellite-based photosynthesis and fluorescence (i.e. GOSIF and MODIS; based on the methods described above) we calculated the timing of seasonal phenological events in spring and autumn transition periods, using a fitted double logistic function outlined by Gonsamo et al. (2013). This approach calculated phenological transition dates using first, second, and third derivatives

of the logistics curves. The second derivatives estimated the end of greenup (EOG) and the start of browndown (SOB, senescence), while the third derivatives calculated the start of the growing season (SOS) and the end of the growing season (EOS). The start of the growing season (SOS) marked the end of winter dormancy and the beginning of leaf emergence in the spring season (budburst and greenup). The phenological spring is defined as the period from SOS to EOG, the summer or peak carbon uptake period spans the period between EOG and SOB, while the autumn season considers the period from the SOB to the EOS, marking leaf senescence to abscission and the end of photosynthetic activity. The overall length of the phenologically-derived growing season (LOS) was calculated as the number of days between SOS and EOS. To identify the seasonal meteorological impacts on photosynthesis, the calculated transition dates were then compared to seasonal and annual meteorological variables measured at each tower.

5.4 Results

5.4.1 Seasonal Photosynthesis and Proximal Remote Sensing

The eddy covariance (EC) measured maximum daily photosynthetic assimilation, or maximum gross ecosystem productivity (GEP_{Max}), and the AMSPEC-III vegetation indices followed parallel seasonal patterns as temperature (grey) for the eastern white pine dominated coniferous evergreen and the white oak dominated deciduous broadleaf forests throughout the 2016 growing season (Figure 5.2). Spring activation began in March for the coniferous forest, with slow

increases in both photosynthesis and vegetation indices before reaching maximum summer values in July and August. Following the peak summer (calendar) period, a continued gradual decline in photosynthesis and a late winter downregulation (December) was observed for the coniferous forest. The deciduous forest displayed much more rapid photosynthetic changes as spring activation only occurred in early May, but maximum summer photosynthesis values were quickly reached in June and July. Similar rapid downregulation was experienced in autumn with the initiation of leaf senescence in mid-September, although unseasonably warm temperatures during that time helped to extend the overall growing season length within the deciduous forest (highlighted in Chapter 3).

For the evergreen conifer forest, AMSPEC-III CCI, CIr, and PRI had not adequately captured the seasonal variations in photosynthesis that roughly matched that of seasonal temperatures (Figure 5.2a-c). At all times during the measurement period, these vegetation indices effectively captured the overall dynamics (shape) of photosynthesis within the evergreen forest, but were unable to accurately capture day-to-day changes in GEP_{Max}, highlighted by the low R^2 values. NDVI was relatively constant throughout the measurement period, while seasonally higher values (~0.80) roughly coincided with maximum temperatures and photosynthesis in July and August (Figure 5.2d). For the deciduous broadleaf forest, all AMSPEC-III indices were able to capture similar variations in photosynthesis throughout the growing season (Figure 5.2e-h). CCI, CIr and PRI showed the strongest indications of seasonal changes in photosynthesis during the

measurement period (Figure 5.2 e-g). CCI accurately caught the timing of the spring transition, but soon after as chlorophyll began to decrease, so did CCI for the remainder of the summer (Figure 5.2e). Both CIr and PRI effectively followed the spring and autumn transitions, and the magnitude and shape of summer photosynthesis before similarly decreasing during the period of senescence and winter downregulation. Following a similar increase in spring, NDVI at the deciduous forest remained constant (~0.95) for the remainder of the summer.

While nearly every index indicated the ability to accurately capture broad patterns of photosynthesis within both forests, the resultant linear correlations (R^2: Figure 5.2) highlighted the relative difficulty of the indices in capturing day-to-day variations. When considering 8-day mean measurements (Figure 5.3), the seasonal patterns of the coniferous forest were nearly identical to that of the 8-day mean air temperature, while the delay in spring photosynthesis at the deciduous forest illustrated the physiological controls that help to control activation and leaf-out (bud-burst) even despite increasing spring temperatures. At these time scales, the effectiveness of the AMSPEC-III indices in capturing changes in photosynthesis during the spring and autumn transition seasons were highlighted (Figure 5.3a-c). The higher R^2 in each case reflects the abilities of the AMSPEC-III vegetation indices in accurately monitoring the larger deviations that may be missed at shorter (i.e. daily) time scales. With the exception of the spring timing (i.e. greenup) at the deciduous forest, NDVI again remained constant throughout the summer at both forests, emphasizing the relative inability of NDVI in

reproducing photosynthetic phenology (Figure 5.3d). Overall, each index responded better to the seasonal patterns of photosynthesis at the deciduous broadleaf forest as compared to that of the coniferous forest (R^2; Figure 5.3).

5.4.2 Satellite Remote Sensing Detection of Photosynthesis

The relationships between EC-measured maximum photosynthetic assimilation (GEP_{Max}) and vegetation indices were further explored at both sites over a longer study period (2012 to 2017). Without the proximal remote sensing (AMSPEC-III) measurements taking place outside of the summer of 2016, satellite based indices were instead considered. Satellite measurements included GOSIF (fluorescence), MODIS GPP and MODIS FPAR at 8-day temporal resolutions and MODIS NDVI at a 16-day temporal resolution. Much like 2016, all years showed similar timings of seasonal photosynthesis to that of temperature (Figure 5.4). Satellite fluorescence (GOSIF) was shown to be highly correlated to photosynthesis at both forests (Table 5.1). In the coniferous forest, seasonal patterns of photosynthesis were captured each year by the GOSIF data, but the timing of the spring and autumn transitions were delayed and advanced, respectively. Conversely, at the deciduous broadleaf forest, the timing of the spring and autumn transitions were nearly identical in each year, while the peak summer timing was often delayed in the GOSIF data (Figure 5.4a). Instead of correctly capturing peak photosynthesis in June and July like the AMSPEC-III indices, the GOSIF data for the deciduous forest peaked closer to August, similar to the conifer forest.

The seasonal dynamics of MODIS GPP were highly correlated to EC photosynthesis during the study period, although GPP often found difficulty in capturing photosynthesis in the summer at the coniferous forest (Figure 5.4b; Table 5.1). With nearly identical timing of the spring activation and winter downregulation at the conifer forest, the GPP underestimated summer photosynthesis in every year. On the other hand, seasonal GPP and EC photosynthesis at the deciduous broadleaf forest were comparable throughout each year, although large seasonal fluctuations in GPP likely resulting from unfavorable meteorological conditions (i.e. cloudy conditions), acting to reduce growing season correlations (Table 5.1). MODIS FPAR and NDVI have been suggested as alternatives for one another, highlighted by the similarities between seasonal measurements (Figure 5.4c-d). In both cases, FPAR and NDVI struggled to capture the seasonal changes in photosynthesis at the conifer forest, although NDVI often performed better, especially at the deciduous forest (Table 5.1). As the fraction of absorbed photosynthetically active radiation remained relatively constant within the coniferous forest, in most years FPAR mirrored seasonal changes in air temperature. Within the deciduous forest, FPAR and NDVI appeared to be able to depict changes in seasonal photosynthetic phenology. Both indices experienced similar rapid increases and decreases during the spring and autumn transition periods, representative of the changes in greenness and canopy structure (bud-burst and abscission).

5.4.3 Estimation of Photosynthetic Phenology

The photosynthetic activity measured by EC (GEP_{Max}) data and the satellite remote sensing vegetation indices were fitted using double logistic functions to determine phenological events such as the start of the growing season (SOS), end of the growing season (EOS), and overall length of the growing season (Table 5.2; Figure 5.5). The ability of these multiple satellite remote sensing datasets to similarly capture key photosynthetic phenological dates is essential for accurate estimates of annual forest carbon uptake.

For EC GEP_{Max} at the conifer forest, the start of the photosynthetic growing season (SOS) was effectively captured by the MODIS GPP in all years except for 2012. In 2012, increased air temperatures throughout the entire year (Table 5.3) advanced the SOS in every dataset, although MODIS GPP overestimated the advancement of spring activation. For GOSIF data, a delay in the SOS in some cases exceeded a month, highlighting the difficulty in tracking spring activation of the conifer forest by satellite fluorescence. In all years, the end of greenup (EOG) and the peak growing season timings were closely captured by GOSIF data, while GPP often measured earlier phenological dates. Following the peak growing season, the phenological dates of senescence marking the beginning of the winter downregulation, were much earlier for both GPP and GOSIF when compared to GEP_{Max} in all years. For the conifer forest, GPP was able to effectively capture the end of the growing season (EOS) in most years. Over the 6-year study period, the length of the growing season (LOS) was similar

between GEP_{Max} (260 ± 19 days) and GPP (269 ± 29 days), although significant differences existed interannually. Lastly, the GOSIF data often calculated a 2-3 month shorter overall growing season length (193 ± 10 days) than EC GEP_{Max}.

At the deciduous forest, GOSIF data accurately captured the SOS in all years, while MODIS GPP often overestimated an earlier SOS, likely resulting from the delayed onset of spring by the Oak (*Quercus*) dominated forest. While GPP effectively captured the rapid spring development of photosynthesis, a much slower spring response was seen by GOSIF, with EOG and peak season delayed in all years. The timing of senescence (SOB) was similar between both GOSIF and GPP, though in all years, this led to an earlier decline than what was measured at the forest (GEP_{Max}). However, while MODIS GPP often predicted an earlier onset of senescence, the timing was consistent in all years, making it highly correlated (R^2 = 0.93) to EC-measured GEP_{Max} SOB dates. A large difference was seen between GOSIF and MODIS GPP at the end of the growing season (EOS) at the deciduous forest. Much like GOSIF at the conifer forest, GOSIF again captured an earlier EOS, while MODIS GPP EOS was often later, comparable to that of the coniferous evergreen forest. During the 6-years of measurements, the length of the growing season captured by GOSIF data (171 ± 11 days) was slightly closer to that of EC-measured GEP_{Max} (192 ± 8 days), while earlier modeled early growing season dates (i.e. bud-burst) for GPP led to longer MODIS GPP predicted growing seasons (231 ± 18 days).

The relationships and the overall capabilities of these satellite vegetation indices in capturing changes in annual photosynthetic phenology were further analyzed to understand the role that large scale meteorological conditions may play on key dates. At both sites, the MODIS GPP start of browndown (SOB; senescence) exhibited a strong positive linear correlation with mean summer 0 to 30 cm soil volumetric water content (Table 5.3). In each case, dry conditions (i.e. lower $VWC_{0\text{-}30cm}$) acted to advance GPP senescence, although in these years (2012, 2016, and 2017), similar early senescence was not captured by EC $GEP_{Max.}$ Instead, while $VWC_{0\text{-}30cm}$ was likely depleted as a result of increased summer air temperatures, the higher temperatures helped to prolong the summer and delay GEP_{Max} senescence (Table 5.2 & 5.3). At the coniferous evergreen forest, the length of the GPP growing season showed a strong dependence on annual mean air temperature ($R^2 = 0.92$), which was not captured by GEP_{Max} dates.

5.5 Discussion

5.5.1 Seasonal Patterns of Stand-Level Photosynthesis

In this study we evaluated the effectiveness of stand-level remote sensing techniques in capturing the seasonal dynamics of photosynthetic phenology at a coniferous evergreen and a deciduous broadleaf forest. We implemented measurements of eddy covariance (EC) maximum photosynthetic assimilation (GEP_{Max}) as a proxy for site-specific photosynthetic phenology. The EC method has been well regarded by micrometeorologists as an effective tool in detecting

the CO_2 (photosynthesis and respiration) exchange between the atmosphere-forest canopy boundary (Baldocchi, 2003; Wohlfahrt & Gu, 2015). During the growing season of 2016, these GEP_{Max} measurements were compared to vegetation indices derived from similarly located, tower-based AMSPEC-III systems; providing cost-effective, portable detections of canopy photosynthesis (Tortini et al., 2015). The measured indices (CCI, CIr, PRI, and NDVI) captured clear responses to the seasonally changing air temperatures and EC measured photosynthesis within each forest.

Seasonal patterns of CCI closely followed gradual changes in temperature within the coniferous forest, while the deciduous forest CCI was less responsive to increasing temperatures throughout the summer. The cyclical response of the coniferous CCI results from the forests (*Pinus*) overwintering strategy. The downregulation of photosynthesis in autumn involves an increase (decrease) in carotenoid (chlorophyll) content in coniferous evergreen needles acting to enhance photoprotection, and thus reducing CCI (Adams et al., 2004; Ensminger et al., 2004). As coniferous evergreen needles annually retain most of their needles (and chlorophyll), this process is reversed during spring recovery as temperatures began to increase (Bowling et al., 2018). In the deciduous forest, with the development of new leaves in spring, chlorophyll pools begin to accumulate and peak during summer and often only decline during the initiation of senescence in autumn (Polgar & Primack, 2011; Vitasse et al., 2014). However, following the May peak, AMSPEC-III CCI at the deciduous forest

began to decline for the remainder of the summer, earlier than photosynthetic declines in GEP_{Max}. This decline in CCI could be linked to the meteorological conditions present during the warm and very dry summer of 2016, where studies suggest carotenoid levels increase when plants are exposed to environmental stressors (Peñuelas et al., 2013; Gamon et al., 2016).

The AMSPEC-III CIr and PRI were shown to be effective at capturing seasonal changes in EC GEP_{Max} at both forest sites. With air temperatures steadily increasing (decreasing) in the spring (autumn) transition season, coniferous CIr responded closely to both photosynthesis and temperature (similar to CCI and PRI), while deciduous CIr mirrored the dynamics of GEP_{Max}, not temperature. These trends in CIr during the 2016 growing season highlight the ability of red-edge indices in capturing seasonal photosynthetic phenology, parallel to previous studies (Zarco-Tajada et al., 2001; Gitelson et al., 2005). Furthermore, red-edge chlorophyll indices have been shown to accentuate altered plant physiological conditions (Cepl et al., 2018). Similar to Nestola et al. (2018), the higher correlations of CIr to changes in photosynthesis found in both our forests were likely improved due to unfavorable conditions (i.e. hot and dry), where shifts in pigment composition associated with stressed vegetation can be accurately detected by the red-edge index (Gitelson & Merzlyak, 1996; Zarco-Tajada et al., 2004). AMSPEC-III PRI responded similarly to CCI and CIr at both forests, reflecting seasonal changes in chlorophyll and carotenoid pigment pool sizes.

Similar to past studies, these results demonstrated the ability of PRI in tracking changes in photosynthesis (Sims & Gamon, 2002; Wong & Gamon, 2015).

Greenness indices (i.e. NDVI) have been widely used in the past in association with measurements of photosynthesis. For the deciduous forest, the timing of greenup (bud-burst and leaf-out) in spring was accurately captured by AMSPEC-III NDVI. Once summer began, NDVI in the deciduous forest remained largely unchanged for the rest of the growing season, much like the coniferous forest. At the coniferous forest, the lack of variation in NDVI reflected the similar consistency of chlorophyll content observed in coniferous species throughout the year (Gamon et al., 1995). Overall, NDVI did not capture plant physiological or phenological changes.

These results show that the chlorophyll red-edge index (CIr) was the best at capturing variations in photosynthesis for both a deciduous broadleaf forest and a coniferous evergreen forest during the 2016 growing season. While structural indices (i.e. NDVI) have been shown to be beneficial for global monitoring of forest canopies (Vescovo et al., 2012), chlorophyll indices (i.e. CCI, CIr, and PRI), in our study were shown to capture seasonal changes in photosynthesis. At both daily and 8-day time scales the effectiveness of most indices in capturing adjustments in seasonal pigment pool sizes for both plant functional types, highlights their ability in tracking stand-level photosynthetic phenology within the temperate forests of southern Ontario.

5.5.2 Satellite Representations of Photosynthesis

We further explored the seasonal changes in photosynthesis at the coniferous evergreen and deciduous broadleaf forests from 2012 to 2017 through the application of satellite remote sensing vegetation indices. Satellite measured solar-induced fluorescence (SIF) has been shown to provide an independent assessment of terrestrial photosynthesis necessary for phenological monitoring (Frankenberg et al., 2014; Li et al., 2018). SIF, emitted by chlorophyll after the absorption of solar radiation, is considered a proxy for terrestrial photosynthetic activity (Porcar-Castell et al., 2014; Zhao et al., 2018). These satellite-based data, along with MODIS GPP, FPAR, and NDVI allow for an introspective approach to vegetation satellite remote sensing.

Observing both forests, we found strong linear relationships (R^2) among eddy covariance (EC) measured GEP_{Max} and GOSIF and MODIS indices. The strongest relationships between the indices and seasonal photosynthetic variations were found annually for the GOSIF and MODIS GPP data at both sites, although significant relationships also existed for MODIS FPAR and NDVI at the deciduous forest. While GOSIF data often captured the seasonal dynamics of photosynthesis at each forest, the overall length and shape of the growing season often varied from GEP_{Max}. As strong seasonal patterns between SIF and changes in chlorophyll have been identified (Wittenberghe et al., 2013), and the relationships between stand-level chlorophyll and

GEP_{Max} were previously highlighted (AMSPEC-III indices) at both our forests, it is likely that the shorter coniferous growing season and irregularity of the deciduous spring are attributable to the coarse spatial resolutions of GOSIF data (Lu et al., 2018). GOSIF measurements are likely impacted by the significant landscape heterogeneity surrounding the forests, resulting from the agriculturally-dominated landscape. However, the annual relationships between SIF and EC GEP_{Max} at our forests (R^2 = 0.88 – 0.90) was similar to EC-comparative studies (Joiner et al., 2014; Yang et al., 2017; Li & Xiao, 2019).

The high spatial resolution (500 m) of MODIS GPP led to significant relationships with GEP_{Max} at both forests, though interannual deviations were more strongly found at the coniferous forest, despite higher annual linear correlations. Errors in GPP have previously been mentioned to result from meteorological conditions, primarily the estimation of VPD (Zhao et al., 2006; Coops et al., 2007). In years, with high VPD (i.e. 2012, 2016, and 2017), MODIS GPP at our coniferous forest was likely underestimated, similar to that experienced by Heinsch et al. (2006) and Zhao et al. (2006). These reductions (i.e. MODIS GPP) responded opposite to that of site temperature and GEP_{Max}. Instead, more climatically normal conditions (i.e. 2014), saw higher annual correlations between coniferous GEP and MODIS GPP. Similarly, MODIS GPP may also rely heavily on FPAR (Turner et al., 2003). With weak correlations between FPAR and GEP_{Max} at the coniferous forest in these high VPD years, and the strongest correlation between FPAR and GEP_{Max} found in 2014, it is likely that

meteorological conditions significantly influenced the GPP at the coniferous forest. Lastly, our results are similar to that of Yang et al. (2017) which found that the timing of FPAR and NDVI began before spring activation and ended after the start of winter downregulation. In this study, greenness indices (i.e. MODIS FPAR & NDVI) were shown to be able to track changes in the canopy structure and greenness at the deciduous site.

5.6 Conclusions

This study highlighted the relative ability of different vegetation indices in tracking changes in photosynthetic phenology for two forests of different leaf-strategies (i.e. coniferous evergreen and deciduous broadleaf) in southern Ontario, Canada. All proximal remote sensing indices (i.e. AMSPEC-III), with the exception of NDVI at the coniferous forest, demonstrated the capability of detecting changes in pigment pool size during the growing season of 2016. NDVI at the deciduous forest was sensitive to canopy structural changes associated with periods of leaf emergence, although no such changes were found for the coniferous site. At both sites, the chlorophyll red-edge index (CIr) showed the greatest capacity in estimating changes in photosynthetic phenology, likely resulting from the meteorological stress induced during the summer of the measurement period. These results highlight that red-edge chlorophyll and carotenoid sensitive indices strongly reflected changes in seasonal photosynthesis measured at the stand-level.

For satellite remote sensing measurements (i.e. GOSIF and MODIS) examined from 2012 to 2017, the seasonal absence of variations in chlorophyll content experienced in coniferous evergreen trees, led to the relative inability of FPAR and NDVI in capturing photosynthesis at the conifer forest. However, the strongest relationship between indices and photosynthesis at the conifer forest existed during a climatically normal year. For the deciduous broadleaf forest, much like AMSPEC-III NDVI, MODIS FPAR and NDVI only captured canopy structural changes due to annual leaf development and leaf senescence. GOSIF and MODIS GPP were highly correlated to EC GEP_{Max}, although significant deviations occurred, likely due to meteorological conditions or spatial heterogeneity. These results suggest the implementation of greater spatially resolved SIF products in the coming years will greatly benefit the tracking of photosynthesis by satellite.

5.7 Acknowledgements

This study was funded by the Natural Sciences and Engineering Research Council (NSREC), the Global Water Futures Program (GWF), and the Ontario Ministry of Environment, Conservation and Parks (MOECP). Funding from the Canadian Foundation of Innovation (CFI) through New Opportunity and Leaders Opportunity Fund and Ontario Research Fund of the Ministry of Research and Innovation is also acknowledged. In kind support from the Ontario Ministry of Natural Resources and Forestry (OMNRF). The St. Williams Conservation

Reserve Community Council and the Long Point Region Conservation Authority (LPRCA) are also acknowledged. The AMSPEC installation and operation was funded by the Natural Sciences and Engineering Research Council of Canada (NSERC) through a grant to Nicholas C. Coops. We are grateful to Prof. Andrew Black (Biometeorology Group, Faculty of Land and Food Systems, University of British Columbia) for his support in developing the AMSPEC system.

5.8 References

Adams, W.W., Zarter, C.R., Ebbert, V. and Demmig-Adams, B., 2004. Photo-protective strategies of overwintering evergreens. *Bioscience*, 54, 41-49.

Arain, M.A., & Restrepo-Coupe, N., 2005. Net ecosystem production in a temperate pine plantation in southeastern Canada. *Agricultural and Forest Meteorology*, 128, 223-241.

Baker, N.R. & Rosenqvist, E., 2004. Applications of chlorophyll fluorescence can improve crop production strategies: an examination of future possibilities. *Journal of Experimental Botany*, *55*(403), 1607-1621.

Baldocchi, D.D., 2003. Assessing the eddy covariance technique for evaluating carbon dioxide exchange rates of ecosystems: past, present and future. *Global Change Biology*, *9*(4), 479-492.

Beamesderfer, E.R., Arain, M.A., Khomik, M., and Brodeur, J.J., 2019a. How will the carbon fluxes within the northernmost temperate deciduous forests of North America fair under future climates?. *Journal of Geophysical Research: Biogeosciences*.

Beamesderfer, E.R., Arain, M.A., Khomik, M., Brodeur, J.J., Gonsamo, A., 2019b. The impact of spring and autumn seasons' timing and duration on the carbon uptake of a temperate deciduous forest in Eastern North America. *Agricultural and Forest Meteorology.*

Bigras, F.J., Ryyppö, A., Lindström, A. and Stattin, E., 2001. Cold acclimation and deacclimation of shoots and roots of conifer seedlings. In Conifer cold hardiness (57-88). *Springer*, Dordrecht.

Bowling, D.R., Logan, B.A., Hufkens, K., Aubrecht, D.M., Richardson, A.D., Burns, S.P., Anderegg, W.R., Blanken, P.D. and Eiriksson, D.P., 2018. Limitations to winter and spring photosynthesis of a Rocky Mountain subalpine forest. *Agricultural and Forest Meteorology*, 252, 241-255.

Čepl, J., Stejskal, J., Lhotáková, Z., Holá, D., Korecký, J., Lstibůrek, M., Tomášková, I., Kočová, M., Rothová, O., Palovská, M. and Hejtmánek, J., 2018. Heritable variation in needle spectral reflectance of Scots pine (Pinus sylvestris L.) peaks in red edge. *Remote Sensing of Environment*, *219*, 89-98.

Chen, B., Zhang, H., Coops, N.C., Fu, D., Worthy, D.E., Xu, G. and Black, T.A., 2014. Assessing scalar concentration footprint climatology and land surface impacts on tall-tower CO2 concentration measurements in the boreal forest of central Saskatchewan, Canada. *Theoretical and Applied Climatology*, *118*(1-2), 115-132.

Cleland, E.E., Chuine, I., Menzel, A., Mooney, H.A. and Schwartz, M.D., 2007. Shifting plant phenology in response to global change. *Trends in Ecology & Evolution*, 22(7), 357-365.

Coops, N.C., Black, T.A., Jassal, R.P.S., Trofymow, J.T. and Morgenstern, K., 2007. Comparison of MODIS, eddy covariance determined and physiologically modelled gross primary production (GPP) in a Douglas-fir forest stand. *Remote Sensing of Environment*, *107*(3), 385-401.

Coops, N.C., Hilker, T., Hall, F.G., Nichol, C.J. and Drolet, G.G., 2010. Estimation of light-use efficiency of terrestrial ecosystems from space: A status report. *BioScience*, 60(10), 788-797.

Curtis, P.S., Hanson, P.J., Bolstad, P., Barford, C., Randolph, J.C., Schmid, H.P. and Wilson, K.B., 2002. Biometric and eddy-covariance based estimates of annual carbon storage in five eastern North American deciduous forests. *Agricultural and Forest Meteorology*, *113*(1-4), 3-19.

Demmig-Adams, B. & Adams III, W.W., 1996. The role of xanthophyll cycle carotenoids in the protection of photosynthesis. *Trends in Plant Science*, *1*(1), 21-26.

Ensminger, I., Sveshnikov, D., Campbell, D.A., Funk, C., Jansson, S., Lloyd, J., Shibistova, O. and Öquist, G., 2004. Intermittent low temperatures constrain spring recovery of photosynthesis in boreal Scots pine forests. *Global Change Biology*, 10(6), 995-1008.

Estiarte, M. & Peñuelas, J., 2015. Alteration of the phenology of leaf senescence and fall in winter deciduous species by climate change: effects on nutrient proficiency. *Global Change Biology*, 21(3), 1005-1017.

Frankenberg, C., O'Dell, C., Berry, J., Guanter, L., Joiner, J., Köhler, P., Pollock, R. and Taylor, T.E., 2014. Prospects for chlorophyll fluorescence remote sensing from the Orbiting Carbon Observatory-2. *Remote Sensing of Environment*, 147, 1-12.

Fréchette, E., Wong, C.Y., Junker, L.V., Chang, C.Y.Y. and Ensminger, I., 2015. Zeaxanthin-independent energy quenching and alternative electron sinks cause a decoupling of the relationship between the photochemical reflectance index (PRI) and photosynthesis in an evergreen conifer during spring. *Journal of Experimental Botany*, 66(22), 7309-7323.

Gamon, J.A. & Berry, J.A., 2012. Facultative and constitutive pigment effects on the Photochemical Reflectance Index (PRI) in sun and shade conifer needles. *Israel Journal of Plant Sciences*, 60(1-2), 85-95.

Gamon, J.A., Penuelas, J. and Field, C.B., 1992. A narrow-waveband spectral index that tracks diurnal changes in photosynthetic efficiency. *Remote Sensing of Environment*, 41(1), 35-44.

Gamon, J.A., Field, C.B., Goulden, M.L., Griffin, K.L., Hartley, A.E., Joel, G., Penuelas, J. and Valentini, R., 1995. Relationships between NDVI, canopy structure, and photosynthesis in three Californian vegetation types. *Ecological Applications*, 5(1), 28-41.

Gamon, J.A., Coburn, C., Flanagan, L.B., Huemmrich, K.F., Kiddle, C., Sanchez-Azofeifa, G.A., Thayer, D.R., Vescovo, L., Gianelle, D., Sims, D.A. and Rahman, A.F., 2010. SpecNet revisited: bridging flux and remote sensing communities. *Canadian Journal of Remote Sensing*, *36(S2)*, S376-S390.

Gamon, J.A., Huemmrich, K.F., Wong, C.Y., Ensminger, I., Garrity, S., Hollinger, D.Y., Noormets, A. and Peñuelas, J., 2016. A remotely sensed pigment index reveals photosynthetic phenology in evergreen conifers. *Proceedings of the National Academy of Sciences*, 113(46), 13087-13092.

Gamon, J.A., Somers, B., Malenovský, Z., Middleton, E.M., Rascher, U. and Schaepman, M.E., 2019. Assessing vegetation function with imaging spectroscopy. *Surveys in Geophysics*, 40(3), 489-513.

Gielen, B., De Vos, B., Campioli, M., Neirynck, J., Papale, D., Verstraeten, A., Ceulemans, R. and Janssens, I.A., 2013. Biometric and eddy covariance-based assessment of decadal carbon sequestration of a temperate Scots pine forest. *Agricultural and Forest Meteorology*, *174*, 135-143.

Gitelson, A.A. & Merzlyak, M.N., 1996. Signature analysis of leaf reflectance spectra: algorithm development for remote sensing of chlorophyll. *J. Plant Physiol., 148*(3-4), 494-500.

Gitelson, A.A., Vina, A., Ciganda, V., Rundquist, D.C. and Arkebauer, T.J., 2005. Remote estimation of canopy chlorophyll content in crops. *Geophysical Research Letters*, *32*(8).

Gitelson, A.A., Viña, A., Verma, S.B., Rundquist, D.C., Arkebauer, T.J., Keydan, G., Leavitt, B., Ciganda, V., Burba, G.G. and Suyker, A.E., 2006. Relationship between gross primary production and chlorophyll content in crops: Implications for the synoptic monitoring of vegetation productivity. *Journal of Geophysical Research: Atmospheres, 111*(D8).

Gough, C.M., Curtis, P.S., Hardiman, B.S., Scheuermann, C.M. and Bond-Lamberty, B., 2016. Disturbance, complexity, and succession of net ecosystem production in North America's temperate deciduous forests. *Ecosphere*, 7(6), e01375.

Heinsch, F.A., Zhao, M., Running, S.W., Kimball, J.S., Nemani, R.R., Davis, K.J., Bolstad, P.V., Cook, B.D., Desai, A.R., Ricciuto, D.M. and Law, B.E., 2006. Evaluation of remote sensing based terrestrial productivity from MODIS using regional tower eddy flux network observations. *IEEE Trans. Geosci. Remote Sens., 44*(7), 1908-1925.

Hilker, T., Coops, N.C., Hall, F.G., Black, T.A., Wulder, M.A., Nesic, Z. and Krishnan, P., 2008. Separating physiologically and directionally induced changes in PRI using BRDF models. *Remote Sensing of Environment*, *112*(6), 2777-2788.

Huete, A., Justice, C. and Van Leeuwen, W., 1999. MODIS vegetation index (MOD13). Algorithm Theoretical Basis Document, 3.1, 213.

Huete, A., Didan, K., van Leeuwen, W., Miura, T. and Glenn, E., 2010. MODIS vegetation indices. In *Land remote sensing and global environmental change* (579-602). Springer, New York, NY.

IPCC, 2013: Climate Change 2013: The Physical Science Basis. Contribution of Working Group I to the Fifth Assessment Report of the Intergovernmental

Panel on Climate Change [Stocker, T.F., D. Qin, G.-K. Plattner, M. Tignor, S.K. Allen, J. Boschung, A. Nauels, Y. Xia, V. Bex and P.M. Midgley (eds.)]. Cambridge University Press, Cambridge, United Kingdom and New York, NY, USA, 1535.

Joiner, J., Yoshida, Y., Vasilkov, A.P., Schaefer, K., Jung, M., Guanter, L., Zhang, Y., Garrity, S., Middleton, E.M., Huemmrich, K.F. and Gu, L., 2014. The seasonal cycle of satellite chlorophyll fluorescence observations and its relationship to vegetation phenology and ecosystem atmosphere carbon exchange. *Remote Sens. Environ.*, 152, 375-391.

Junker, L.V. & Ensminger, I., 2016. Relationship between leaf optical properties, chlorophyll fluorescence and pigment changes in senescing Acer saccharum leaves. *Tree Physiology*, 36(6), 694-711.

Kirschbaum, M.U., 2000. Will changes in soil organic carbon act as a positive or negative feedback on global warming?. *Biogeochemistry*, 48(1), 21-51.

Knyazikhin, Y., Glassy, J., Privette, J.L., Tian, Y., Lotsch, A., Zhang, Y., et al., 1999. MODIS Leaf Area Index (LAI) and Fraction of Photosynthetically Active Radiation Absorbed by Vegetation (FPAR) Product (MOD15) Algorithm Theoretical Basis Document, 4, 130.

Körner, C. & Basler, D., 2010. Phenology under global warming. Science, 327(5972): 1461-1462.

Li, X. & Xiao, J., 2019. A Global, 0.05-Degree Product of Solar-Induced Chlorophyll Fluorescence Derived from OCO-2, MODIS, and Reanalysis Data. *Remote Sensing*, 11(5), 517.

Li, X., Xiao, J., He, B., Altaf Arain, M., Beringer, J., Desai, A.R., Emmel, C., Hollinger, D.Y., Krasnova, A., Mammarella, I. and Noe, S.M., 2018. Solar-induced chlorophyll fluorescence is strongly correlated with terrestrial photosynthesis for a wide variety of biomes: First global analysis based on OCO-2 and flux tower observations. *Global Change Biology*, 24(9), 3990-4008.

Lichtenthaler, H.K., Ač, A., Marek, M.V., Kalina, J. and Urban, O., 2007. Differences in pigment composition, photosynthetic rates and chlorophyll fluorescence images of sun and shade leaves of four tree species. *Plant Physiology and Biochemistry*, 45(8), 577-588.

Lin, S., Tortini, R., Coops, N.C., Jia, W., Nesic, Z., Beamesderfer, E., Arain, M.A., Jing, L., Qinhuo, L., 2019. How does stand age affect

photosynthetic light use efficiency? A remote sensing observational approach across a conifer chronosequence in southern Ontario, Canada. *ISPRS Journal of Photogrammetry and Remote Sensing*.

Lu, X., Liu, Z., Zhou, Y., Liu, Y., An, S. and Tang, J., 2018. Comparison of phenology estimated from reflectance-based indices and solar-induced chlorophyll fluorescence (SIF) observations in a temperate forest using GPP-based phenology as the standard. *Remote Sensing*, 10(6), 932.

MacDonald, G.M., 2010. Global warming and the Arctic: a new world beyond the reach of the Grinnellian niche?. *J. Exp. Biol.*, 213(6), 855-861.

Müller, P., Li, X.P. and Niyogi, K.K., 2001. Non-photochemical quenching. A response to excess light energy. *Plant Physiology*, 125(4), 1558-1566.

Nagai, S., Saitoh, T.M., Kobayashi, H., Ishihara, M., Suzuki, R., Motohka, T., Nasahara, K.N. and Muraoka, H., 2012. In situ examination of the relationship between various vegetation indices and canopy phenology in an evergreen coniferous forest, Japan. *International Journal of Remote Sensing*, 33(19), 6202-6214.

Nestola, E., Calfapietra, C., Emmerton, C., Wong, C., Thayer, D. and Gamon, J., 2016. Monitoring grassland seasonal carbon dynamics, by integrating MODIS NDVI, proximal optical sampling, and eddy covariance measurements. *Remote Sensing*, 8(3), 260.

Nestola, E., Scartazza, A., Di Baccio, D., Castagna, A., Ranieri, A., Cammarano, M., Mazzenga, F., Matteucci, G. and Calfapietra, C., 2018. Are optical indices good proxies of seasonal changes in carbon fluxes and stress-related physiological status in a beech forest?. *Science of the Total Environment*, *612*, 1030-1041.

Ottander, C., Campbell, D. and Öquist, G., 1995. Seasonal changes in photosystem II organisation and pigment composition in Pinus sylvestris. *Planta*, 197(1), 176-183.

Pan, Y., Birdsey, R.A., Fang, J., Houghton, R., Kauppi, P.E., Kurz, W.A., Phillips, O.L., Shvidenko, A., Lewis, S.L., Canadell, J.G. and Ciais, P., 2011. A large and persistent carbon sink in the world's forests. *Science*, *333*(6045), 988-993.

Park, T., Ganguly, S., Tømmervik, H., Euskirchen, E.S., Høgda, K.A., Karlsen, S.R., Brovkin, V., Nemani, R.R. and Myneni, R.B., 2016. Changes in

growing season duration and productivity of northern vegetation inferred from long-term remote sensing data. *Environ. Res.*, 11(8), 084001.

Peichl, M., Arain, M.A. and Brodeur, J.J., 2010. Age effects on carbon fluxes in temperate pine forests. *Agric. For. Meteorol.*, 150(7-8), 1090-1101.

Peichl, M., Arain, M.A., Ullah, S. and Moore, T.R., 2010. Carbon dioxide, methane, and nitrous oxide exchanges in an age-sequence of temperate pine forests. *Global Change Biology*, 16(8), 2198-2212.

Peñuelas, J., Garbulsky, M.F. and Filella, I., 2011. Photochemical reflectance index (PRI) and remote sensing of plant CO2 uptake. *New Phytologist*, 191(3), 596-599.

Peñuelas, J., Marino, G., LLusia, J., Morfopoulos, C., Farré-Armengol, G. and Filella, I., 2013. Photochemical reflectance index as an indirect estimator of foliar isoprenoid emissions at the ecosystem level. *Nature Communications*, 4, 2604.

Peters, A.J., Walter-Shea, E.A., Ji, L., Vina, A., Hayes, M. and Svoboda, M.D., 2002. Drought monitoring with NDVI-based standardized vegetation index. *Photogrammetric Engineering and Remote Sensing*, 68(1), 71-75.

Polgar, C.A. & Primack, R.B., 2011. Leaf-out phenology of temperate woody plants: from trees to ecosystems. *New Phytologist*, 191(4), 926-941.

Porcar-Castell, A., Tyystjärvi, E., Atherton, J., Van der Tol, C., Flexas, J., Pfündel, E.E., Moreno, J., Frankenberg, C. and Berry, J.A., 2014. Linking chlorophyll a fluorescence to photosynthesis for remote sensing applications: mechanisms and challenges. *Journal of Experimental Botany*, *65*(15), 4065-4095.

Richardson, A. D., Jenkins, J.P., Braswell, B.H., Hollinger, D.Y., Ollinger, S.V., and Smith, M.L., 2007. Use of digital webcam images to track spring green-up in a deciduous broadleaf forest. *Oecologia*, 152: 323–334.

Richardson, A.D., Black, T.A., Ciais, P., Delbart, N., Friedl, M.A., Gobron, N., Hollinger, D.Y., Kutsch, W.L., Longdoz, B., Luyssaert, S. and Migliavacca, M., 2010. Influence of spring and autumn phenological transitions on forest ecosystem productivity. *Philos. Trans. Royal Soc. London, Ser. B*, 365(1555), 3227-3246.

Running, S.W. & Zhao, M., 2015. Daily GPP and annual NPP (MOD17A2/A3) products NASA Earth Observing System MODIS land algorithm. MOD17 User's Guide, 3, 28.

Sims, D.A. & Gamon, J.A., 2002. Relationships between leaf pigment content and spectral reflectance across a wide range of species, leaf structures and developmental stages. *Remote Sensing of Environment*, 81(2-3), 337-354.

Soolanayakanahally, R.Y., Guy, R.D., Silim, S.N. and Song, M., 2013. Timing of photoperiodic competency causes phenological mismatch in balsam poplar (Populus balsamifera L.). *Plant, Cell & Environment*, 36(1), 116-127.

Springer, K., Wang, R. and Gamon, J., 2017. Parallel seasonal patterns of photosynthesis, fluorescence, and reflectance indices in boreal trees. *Remote Sensing*, 9(7), 691.

Stylinski, C., Gamon, J. and Oechel, W., 2002. Seasonal patterns of reflectance indices, carotenoid pigments and photosynthesis of evergreen chaparral species. *Oecologia*, 131(3), 366-374.

Tortini, R., Hilker, T., Coops, N. & Nesic, Z., 2015. Technological advancement in tower-based canopy reflectance monitoring: The AMSPEC-III system. *Sensors*, *15*(12), 32020-32030.

Turner, D.P., Ritts, W.D., Cohen, W.B., Gower, S.T., Zhao, M., Running, S.W., Wofsy, S.C., Urbanski, S., Dunn, A.L. and Munger, J.W., 2003. Scaling gross primary production (GPP) over boreal and deciduous forest landscapes in support of MODIS GPP product validation. *Remote Sensing of Environment*, *88*(3), 256-270.

Turner, D.P., Ritts, W.D., Cohen, W.B., Gower, S.T., Running, S.W., Zhao, M., Costa, M.H., Kirschbaum, A.A., Ham, J.M., Saleska, S.R. and Ahl, D.E., 2006. Evaluation of MODIS NPP and GPP products across multiple biomes. *Remote Sens. Environ.*, *102*(4), 282-292.

Verhoeven, A., 2014. Sustained energy dissipation in winter evergreens. *New Phytol*, 201, 57-65.

Vescovo, L., Wohlfahrt, G., Balzarolo, M., Pilloni, S., Sottocornola, M., Rodeghiero, M. and Gianelle, D., 2012. New spectral vegetation indices based on the near-infrared shoulder wavelengths for remote detection of grassland phytomass. *Int. J. Remote Sens.*, 33(7), 2178-2195.

Vitasse, Y., Lenz, A. and Körner, C., 2014. The interaction between freezing tolerance and phenology in temperate deciduous trees. *Frontiers in Plant Science*, 5, 541.

Walther, S., Voigt, M., Thum, T., Gonsamo, A., Zhang, Y., Köhler, P., Jung, M., Varlagin, A. and Guanter, L., 2016. Satellite chlorophyll fluorescence measurements reveal large-scale decoupling of photosynthesis and greenness dynamics in boreal evergreen forests. *Global Change Biology*, *22*(9), 2979-2996.

Wittenberghe, S.V., Alonso, L., Verrelst, J., Hermans, I., Delegido, J., Veroustraete, F., Valcke, R., Moreno, J. and Samson, R., 2013. Upward and downward solar-induced chlorophyll fluorescence yield indices of four tree species as indicators of traffic pollution in Valencia. *Environmental Pollution*, *173*, 29-37.

Wohlfahrt, G. & Gu, L., 2015. The many meanings of gross photosynthesis and their implication for photosynthesis research from leaf to globe. *Plant, Cell & Environment*, 38(12), 2500-2507.

Wong, C.Y. & Gamon, J.A., 2015. The photochemical reflectance index provides an optical indicator of spring photosynthetic activation in evergreen conifers. *New Phytologist*, 206(1), 196-208.

Wu, C., Niu, Z., Tang, Q., Huang, W., Rivard, B. and Feng, J., 2009. Remote estimation of gross primary production in wheat using chlorophyll-related vegetation indices. *Agric. For. Meteorol.*, *149*(6-7), 1015-1021.

Yang, H., Yang, X., Zhang, Y., Heskel, M.A., Lu, X., Munger, J.W., Sun, S. and Tang, J., 2017. Chlorophyll fluorescence tracks seasonal variations of photosynthesis from leaf to canopy in a temperate forest. *Global Change Biology*, 23(7), 2874-2886.

Zarco-Tejada, P.J., Miller, J.R., Noland, T.L., Mohammed, G.H. and Sampson, P.H., 2001. Scaling-up and model inversion methods with narrowband optical indices for chlorophyll content estimation in closed forest canopies with hyperspectral data. *IEEE Transactions on Geoscience and Remote Sensing*, 39(7), 1491-1507.

Zarco-Tejada, P.J., Miller, J.R., Morales, A., Berjón, A. and Agüera, J., 2004. Hyperspectral indices and model simulation for chlorophyll estimation in open-canopy tree crops. *Remote Sensing of Environment*, *90*(4), 463-476.

Zhao, M., Running, S.W. and Nemani, R.R., 2006. Sensitivity of Moderate Resolution Imaging Spectroradiometer (MODIS) terrestrial primary production to the accuracy of meteorological reanalyses. *Journal of Geophysical Research: Biogeosciences*, *111*(G1).

Zhao, F., Li, R., Verhoef, W., Cogliati, S., Liu, X., Huang, Y., Guo, Y. and Huang, J., 2018. Reconstruction of the full spectrum of solar-induced chlorophyll fluorescence: Intercomparison study for a novel method. *Remote Sense Environ.*, 219, 233-246.

Table 5.1: Annual linear relationships (R^2) between eddy covariance (EC) measured GEP_{Max} and satellite vegetation indices (illustrated in Figure 5.4). Given the temporal resolution of available data, GOSIF, GPP, and FPAR are considered at 8-day time scales, while NDVI was compared at a 16-day time scale. The 6-year mean annual (Ann) and growing season only (phenological start and end of the growing season; ***GS in bold and italics***) R^2 are also included. Growing season correlations were considered to reduce the temporal autocorrelation in winter.

Conifer (TP39)		**2012**	**2013**	**2014**	**2015**	**2016**	**2017**	**Mean**
GOSIF	Ann	0.872	0.887	0.882	0.885	0.856	0.880	0.877
	GS	***0.859***	***0.848***	***0.849***	***0.860***	***0.836***	***0.870***	***0.854***
MODIS GPP	Ann	0.841	0.784	0.923	0.904	0.814	0.856	0.854
	GS	***0.652***	***0.657***	***0.827***	***0.817***	***0.745***	***0.818***	***0.753***
MODIS FPAR	Ann	0.298	0.492	0.708	0.665	0.582	0.326	0.512
	GS	***0.073***	***0.366***	***0.448***	***0.475***	***0.630***	***0.320***	***0.385***
MODIS NDVI	Ann	0.316	0.616	0.645	0.466	0.545	0.317	0.484
	GS	***0.374***	***0.727***	***0.446***	***0.054***	***0.645***	***0.372***	***0.436***
Deciduous (TPD)		**2012**	**2013**	**2014**	**2015**	**2016**	**2017**	**Mean**
GOSIF	Ann	0.872	0.869	0.909	0.877	0.910	0.857	0.882
	GS	***0.724***	***0.762***	***0.809***	***0.720***	***0.827***	***0.719***	***0.760***
MODIS GPP	Ann	0.822	0.835	0.820	0.864	0.774	0.780	0.815
	GS	***0.596***	***0.693***	***0.598***	***0.657***	***0.563***	***0.571***	***0.613***
MODIS FPAR	Ann	0.795	0.773	0.646	0.651	0.714	0.651	0.705
	GS	***0.478***	***0.414***	***0.536***	***0.619***	***0.435***	***0.392***	***0.479***
MODIS NDVI	Ann	0.836	0.811	0.877	0.881	0.731	0.796	0.822
	GS	***0.841***	***0.782***	***0.855***	***0.850***	***0.809***	***0.820***	***0.826***

Table 5.2: Annual calculated phenological dates, reported as day of year, from 2012 to 2017. Dates were calculated following Gonsamo et al. (2013) for each year and dataset, including: eddy covariance measured GEP_{Max} (*italics*), GOSIF (**bold**), and MODIS GPP data. 6-year mean and standard deviations included.

Coniferous Forest (TP39)		**2012**	**2013**	**2014**	**2015**	**2016**	**2017**	**Mean**
Start of Season (SOS, bud-break)	*EC*	*70*	*96*	*96*	*91*	*74*	*79*	*84 ± 12*
	SIF	**99**	**103**	**116**	**105**	**112**	**110**	**107 ± 6**
	GPP	53	*83*	*89*	*88*	*82*	*83*	79 ± 13
End of Greenup (EOG, leaf-out end)	*EC*	*147*	*160*	*153*	*140*	*158*	*159*	*153 ± 8*
	SIF	**154**	**161**	**175**	**157**	**158**	**178**	***164 ± 10***
	GPP	143	126	146	134	145	159	142 ± 11
Peak of Season	*EC*	*214*	*205*	*202*	*193*	*212*	*201*	*204 ± 8*
	SIF	**202**	**202**	**207**	**196**	**188**	**206**	**200 ± 7**
	GPP	143	193	196	176	155	171	173 ± 20
Start of Browndown (SOB, senescence)	*EC*	*271*	*258*	*258*	*257*	*270*	*248*	*260 ± 9*
	SIF	**247**	**242**	**239**	**237**	**231**	**234**	***238 ± 6***
	GPP	184	264	250	238	202	203	224 ± 32
End of Season (EOS)	*EC*	*314*	*351*	*338*	*345*	*366*	*354*	*345 ± 17*
	SIF	**293**	**299**	**293**	**297**	**322**	**299**	**301 ± 11**
	GPP	366	324	323	356	366	355	348 ± 20
Length of Season (LOS, EOS – SOS)	*EC*	*245*	*255*	*242*	*254*	*292*	*275*	*260 ± 19*
	SIF	**194**	**196**	**178**	**192**	**210**	**189**	**193 ± 10**
	GPP	313	241	234	268	284	272	269 ± 29
Deciduous Forest (TPD)		**2012**	**2013**	**2014**	**2015**	**2016**	**2017**	**Mean**
Start of Season (SOS, bud-break)	*EC*	*120*	*116*	*127*	*118*	*126*	*125*	*122 ± 5*
	SIF	**104**	**136**	**121**	**118**	**119**	**113**	**118 ± 10**
	GPP	92	99	107	101	106	99	101 ± 5
End of Greenup (EOG, leaf-out end)	*EC*	*145*	*155*	*160*	*146*	*154*	*159*	*153 ± 6*
	SIF	**186**	**245**	**200**	**206**	**182**	**207**	**205 ± 22**
	GPP	130	128	139	132	142	141	135 ± 6
Peak of Season	*EC*	*198*	*199*	*205*	*193*	*203*	*207*	*201 ± 5*
	SIF	**220**	**239**	**228**	**221**	**207**	**230**	**224 ± 11**
	GPP	175	190	185	188	164	178	180 ± 10
Start of Browndown (SOB, senescence)	*EC*	*257*	*249*	*255*	*249*	*262*	*261*	*255 ± 6*
	SIF	**242**	**222**	**247**	**226**	**232**	**242**	**235 ± 10**
	GPP	235	260	242	254	218	230	240 ± 15
End of Season (EOS)	*EC*	*306*	*314*	*307*	*309*	*328*	*318*	*314 ± 8*
	SIF	**282**	**290**	**292**	**281**	**300**	**294**	**290 ± 7**
	GPP	333	318	315	327	366	334	332 ± 18
Length of Season (LOS, EOS – SOS)	*EC*	*186*	*198*	*180*	*191*	*202*	*193*	*192 ± 8*
	SIF	**178**	**155**	**170**	**163**	**181**	**181**	**171 ± 11**
	GPP	241	219	208	225	260	235	231 ± 18

Table 5.3: Site-specific annual meteorological (i.e. photosynthetically active radiation [PAR], air temperature [Ta], vapor pressure deficit [VPD], and volumetric water content [$VWC_{0\text{-}30cm}$]) and phenological summer (defined by GEP_{Max}) conditions from 2012 to 2017 for the conifer (**TP39, bold**) and deciduous (TPD) forests. The right half of the table includes linear correlations (R^2) between 6-year seasonal and annual meteorological values and phenological dates for the SIF and MODIS GPP data at both sites (Table 5.2).

Summer		**2012**	**2013**	**2014**	**2015**	**2016**	**2017**	***Coniferous (TP39)***		
Total PAR	**TP39**	**5501**	**4418**	**4764**	**5437**	**5382**	**4046**	GPP	Summer	0.616
(mol m^{-2})	TPD	4442	3402	3506	3911	4287	3783	SOB	VWC	
Mean Ta	**TP39**	**21.1**	**20.3**	**19.9**	**20.0**	**21.1**	**20.7**	GPP	Summer	0.777
(°C)	TPD	22.8	20.3	20.2	20.1	21.8	20.3	Peak	Ta	
Mean VPD	**TP39**	**0.82**	**0.64**	**0.65**	**0.70**	**0.74**	**0.73**	GPP	Annual	0.919
(kPa)	TPD	1.00	0.53	0.53	0.55	0.72	0.57	LOS	Ta	
Mean VWC	**TP39**	**0.08**	**0.10**	**0.09**	**0.10**	**0.07**	**0.08**	SIF	Annual	0.607
(m^3 m^{-3})	TPD	0.06	0.10	0.09	0.10	0.04	0.07	Peak	PAR	
Annual		**2012**	**2013**	**2014**	**2015**	**2016**	**2017**	***Deciduous (TPD)***		
Total PAR	**TP39**	**10918**	**10593**	**10906**	**11142**	**11291**	**10426**	GPP	Summer	0.901
(mol m^{-2} yr^{-1})	TPD	9071	8408	8845	8994	9088	8530	SOB	VWC	
Mean Ta	**TP39**	**11.2**	**9.1**	**8.1**	**9.5**	**9.9**	**9.9**	GPP	Summer	0.788
(°C)	TPD	11.8	9.2	8.0	9.2	10.6	10.0	LOS	VWC	
Mean VPD	**TP39**	**0.48**	**0.39**	**0.38**	**0.43**	**0.42**	**0.42**	SIF	Summer	0.760
(kPa)	TPD	0.57	0.35	0.33	0.35	0.42	0.36	LOS	VWC	
Mean VWC	**TP39**	**0.11**	**0.12**	**0.12**	**0.11**	**0.11**	**0.12**	SIF	Annual	0.788
(m^3 m^{-3})	TPD	0.10	0.11	0.11	0.10	0.10	0.10	Peak	PAR	

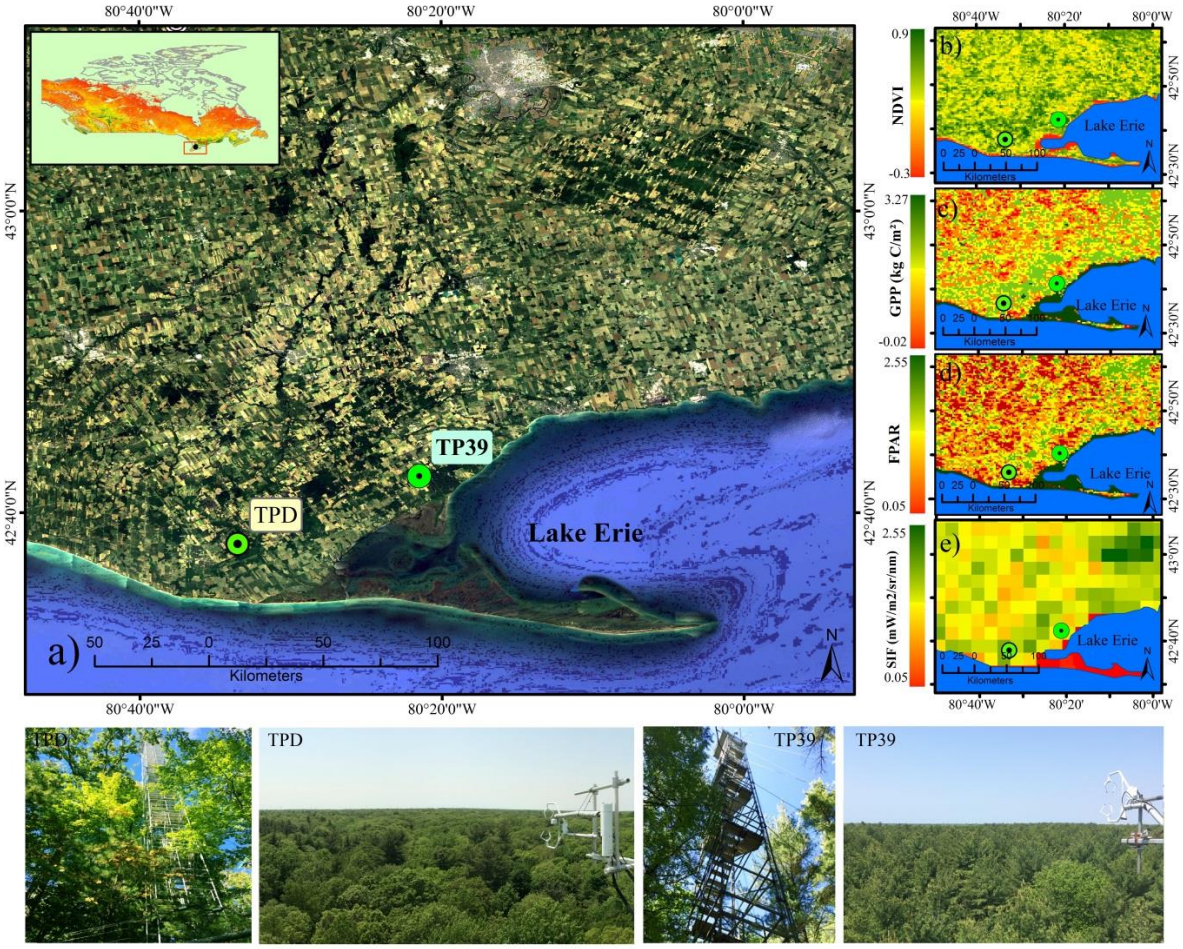

Figure 5.1: (a) Location of the deciduous broadleaf (TPD) and evergreen coniferous (TP39) forest sites in southern Ontario, Canada with images of the eddy covariance (EC) flux towers and forest canopies within each forest (bottom). Sample images of MODIS: (a) NDVI, (b) GPP, (c) FPAR, and also (d) OCO-2 SIF. All images are from 2017, with NDVI from day 137 (16-day resolution), while GPP, FPAR, and SIF are from day 145 (8-day resolutions).

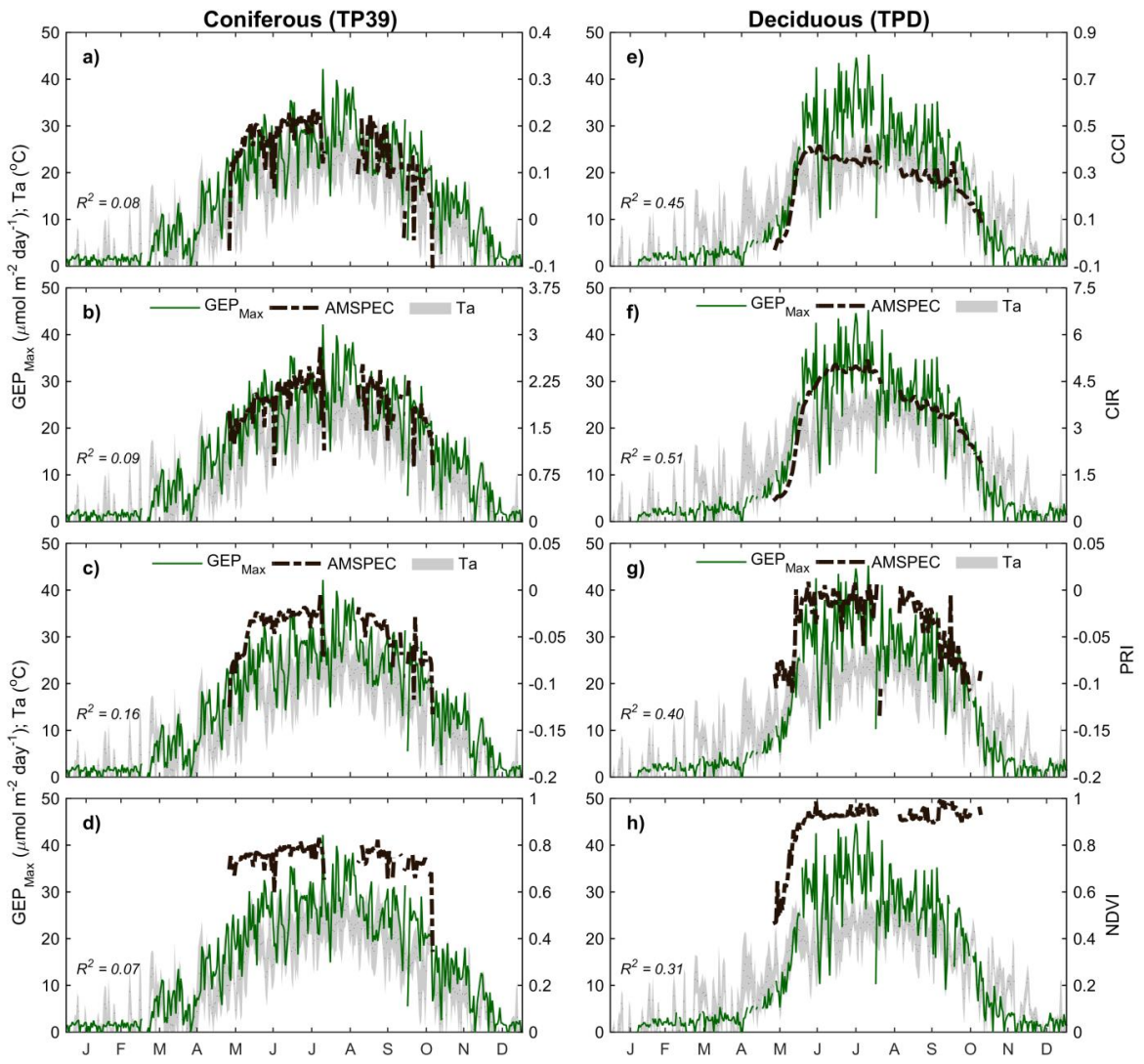

Figure 5.2: Daily patterns of eddy covariance (EC) maximum photosynthesis (GEP_{Max}; µmol m^{-2} day^{-1}; green) and AMSPEC-III (black) vegetation indices for the conifer (a – d) and deciduous (e – h) forests during the 2016 growing season. Indices include: (a & e) CCI, (b & f) CIr, (c & g) PRI, and (d & h) NDVI. Grey shading represents the daily range of air temperatures (Ta; °C) measured at the same height as EC and AMSPEC-III measurements. The linear correlations (R^2) between daily site-specific GEP_{Max} and each index are also shown. The reader should note the different scales for CCI and CIR between sites.

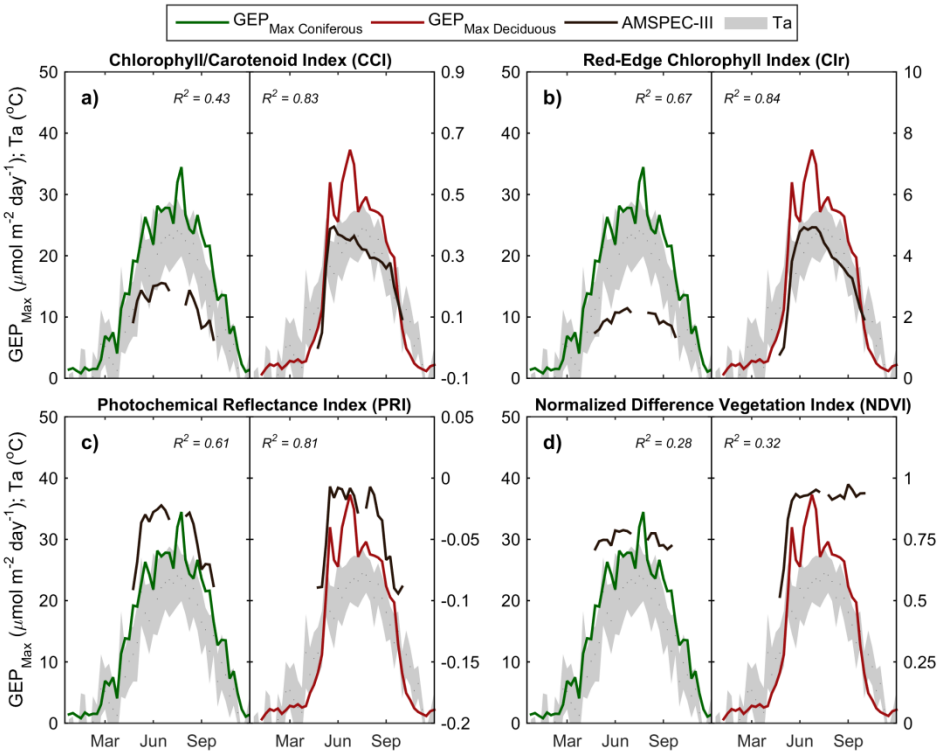

Figure 5.3: Patterns of the 8-day mean EC maximum photosynthesis (GEP_{Max}; µmol m^{-2} day^{-1}; left) and the 8-day mean AMSPEC-III (black; right) vegetation indices for the conifer (green) and deciduous (red) forests during 2016 growing season. Indices include (a) CCI, (b) CIr, (c) PRI, and (d) NDVI. Grey shading represents the daily range of air temperatures (Ta; °C) at each forest. The linear correlations (R^2) of the 8-day data are shown for each site and vegetation index.

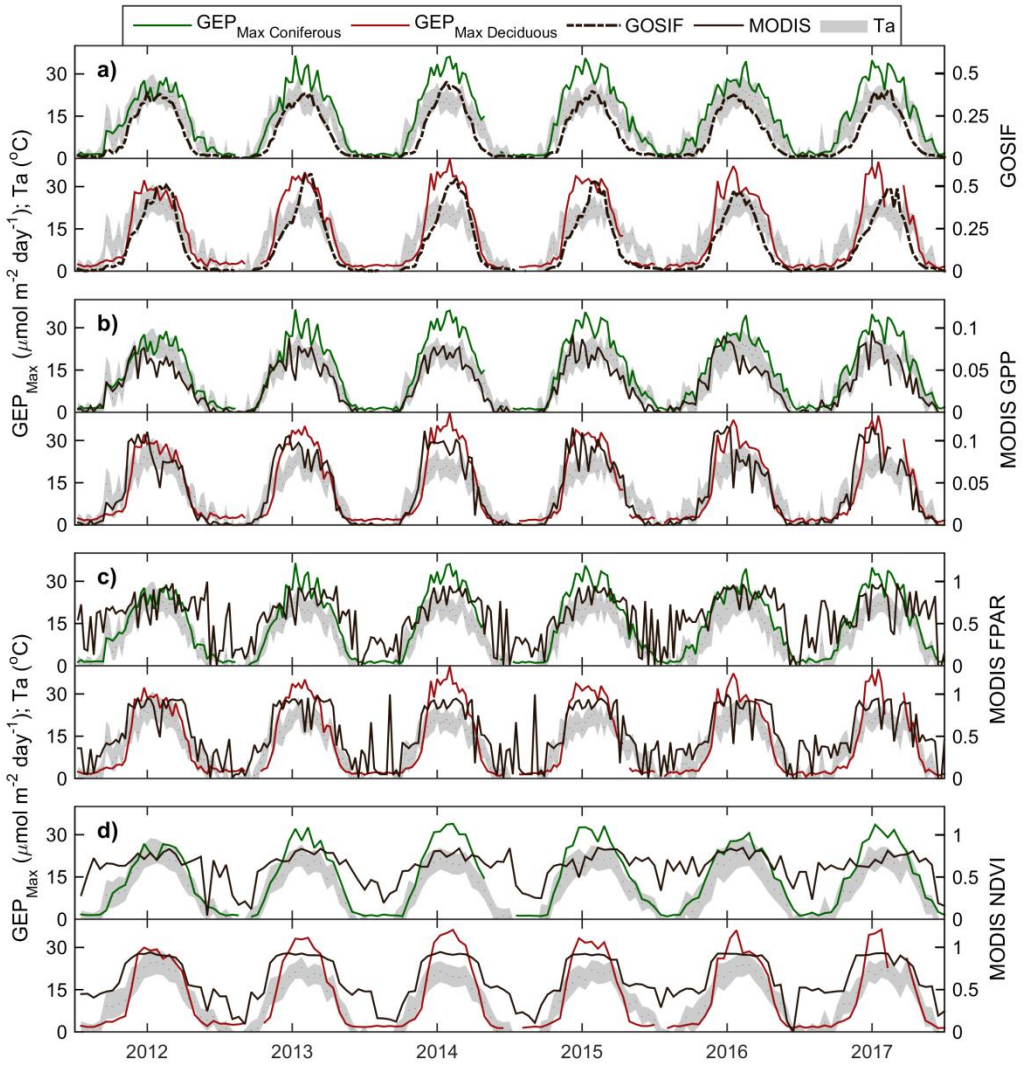

Figure 5.4: Seasonal dynamics of EC maximum photosynthetic assimilation (GEP_{Max}; µmol m^{-2} day^{-1}; left) satellite based vegetation indices (black; right) for the evergreen conifer (green) and deciduous broadleaf (red) forests from 2012 to 2017. Indices include: (a) GOSIF, (b) MODIS GPP, (c) MODIS FPAR, and (d) MODIS NDVI. Grey shading represents the range of Ta at each forest. The temporal resolution shown are (a – c) 8-day and (d) 16-day mean data.

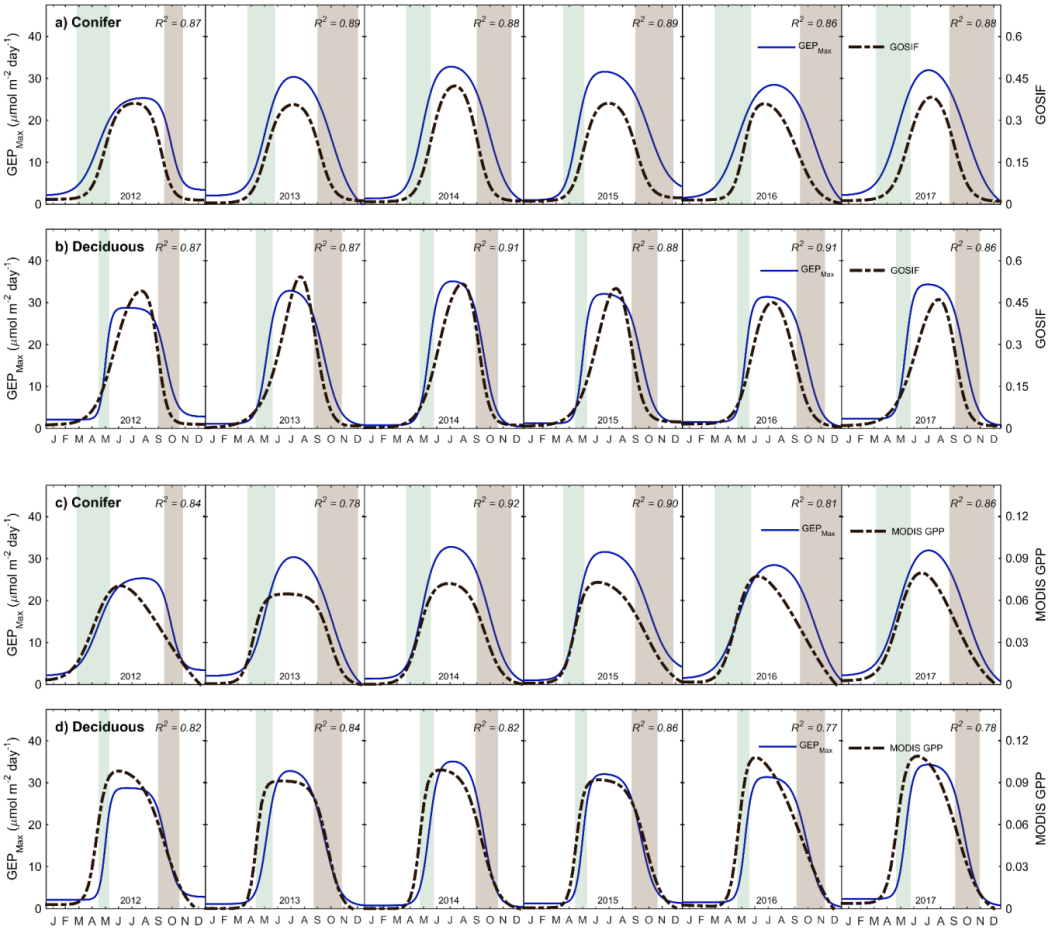

Figure 5.5: The seasonal course of the modeled phenological double logistic functions of EC maximum photosynthetic assimilation (GEP_{Max}; µmol m^{-2} day^{-1}; left) and (a & b) satellite based GOSIF (right) and (c & d) MODIS GPP for the (a & c) evergreen conifer and (b & d) deciduous broadleaf forests (both in blue) from 2012 to 2017. Green and brown shading represent the GEP_{Max} phenological spring and autumn periods, respectively. The resulting linear correlations (R^2) represent the annual relationships between 8-day GEP_{Max} and GOSIF or GPP.

CHAPTER 6:

SUMMARY AND CONCLUSIONS

6.1 Significance of Study

This dissertation will help to fill some gaps in the literature on studies of climatic impacts on carbon dynamics and photosynthetic phenology in forests growing in the temperate climate zone in the Great Lakes Region of northeastern North America. To date, few attempts have been made to quantify the annual atmosphere-canopy carbon exchanges in the geographically unique subset of deciduous forests in southern Ontario, Canada. The forests examined are managed for timber production, carbon sequestration, and sustain water resources in the region. This study was the first of its kind in providing annual long-term estimates of the magnitude of carbon sequestration of these forests. On average, the oak-dominated forest was a steady sink (200 ± 83 g C m^{-2} yr^{-1}) of atmospheric carbon, comparable (215 ± 107 g C m^{-2} yr^{-1}) to other similar deciduous forests in Eastern North America (Gough et al., 2013; Munger et al., 2017; Oishi et al., 2018; Lee et al., 2018). Nevertheless, understanding the effects of climate on shaping phenological events and carbon fluxes is necessary to evaluate the carbon sequestration potential of these forests under future climate warming. This study highlighted the importance of mid-summer meteorology in shaping annual sequestration. An interesting finding was that soil moisture was shown to have very little impact on photosynthesis, in contrast to an oak forest in Ohio, USA,

where soil moisture was a major determining factor for carbon uptake (Xie et al., 2014). Overall, the net annual carbon sequestration of the deciduous forest was shown to be limited by ecosystem respiration. This study further improved our understanding of the phenological impacts on carbon fluxes. Contrary to past studies (Goulden et al., 1996; Desai, 2010; Dragoni et al., 2011), our results suggest longer growing seasons may not lead to enhanced carbon sequestration. Instead, this work found that an extended growing season as a result of warming may be detrimental to carbon uptake, due to the relationship between temperature and ecosystem respiration.

A limited number of studies to date have compared the carbon and water fluxes of coniferous and deciduous forests under related climatic forcings. With over 400 eddy covariance sites measuring forest carbon and water exchange (Baldocchi, 2008), this study was unique in its ability to capture seasonal responses of these fluxes based solely on forest species composition. This dissertation assessed the impacts that plant functional types play in responding to variations in climate within the temperate forests of Canada. The key difference between forests was found in their sensitivities to drought, as carbon uptake was significantly reduced at the coniferous forest during hot and dry years. Lastly, this work attempted to bridge the gap between seasonal changes in photosynthesis captured by both remote sensing and eddy covariance measurements by means of variations to the start and end of the phenological growing seasons.

6.2 Summary of Results

Through the comparison of EC measured carbon fluxes and seasonal and annual meteorological data, the impacts of climate variations on the carbon sink capacity of a managed deciduous forest within the Great Lakes Region of southern Ontario, Canada, were studied from 2012 to 2017. This analysis provided insight into the dynamics of forest-atmosphere carbon exchanges and helped to better understand the role of climate on driving phenological variability, in particular in the spring and autumn seasons. This study helped to explore these processes in a nearby evergreen needleleaf plantation forest to highlight the role of different tree species and leaf-retention and shape strategies in shaping carbon and water dynamics for two forests growing under similar climatic and edaphic conditions. Furthermore, the seasonal patterns of photosynthesis were assessed by stand-level and satellite-based remote sensing vegetative indices at both forests. The main findings of this dissertation are outlined in each chapter, summarized below:

Chapter 2 concludes that the annual carbon sequestration of a mature temperate deciduous forest was greatly impacted by mid-summer meteorological conditions. Interannual temperature variability was highlighted as the dominant control on the length of the growing season and timing of carbon fluxes. Throughout the period of measurements, even during periods with heat and soil moisture limitations, the forest remained a reliable carbon sink. However, with largely consistent annual

gross ecosystem productivity (photosynthesis) across all years, seasonal increases in ecosystem respiration were shown to limit the amount of carbon sequestered.

Chapter 3 confirms that the phenological length of maximum canopy closure and peak photosynthetic activity was driven by seasonal air temperatures. Contrary to previous studies, earlier leaf-out in spring was not shown to lead to greater annual carbon sequestration. With greater variability in autumn phenological dates than that of spring, persistent warming in autumn acted to prolong the growing season length, negatively impacting annual carbon sequestration. During the period of measurements, the two most productive years (largest carbon sinks) experienced delayed starts to the growing season and shorter growing season lengths. These phenological trends were also compared to digital camera imagery, which found difficulty in capturing peak photosynthesis in summer, but accurately captured the changes in greenness associated with the spring and autumn transitional periods.

Chapter 4 compared the annual carbon and water dynamics within two temperate forests of different leaf-strategies. Expanding on Chapter 2, this work found that both forests were able to consistently sequester significant amounts of carbon. The key differences in carbon and water fluxes between forests resulted from their sensitivities to drought. While the deciduous forest was less responsive to reduced soil water availability, the same conditions negatively impacted the magnitude of sequestration in the conifer forest. These results suggest that future adjustments to

temperature and precipitation towards more frequent intermittent drought events may further impact the potential of carbon sequestration in the coniferous forest.

Chapter 5 demonstrated the ability of various remote sensing vegetation indices in tracking seasonal changes in photosynthetic phenology at both forests. Stand-level and satellite-based indices were able to detect changes in leaf pigment pool sizes and canopy structural changes, although irregularities in the satellite indices likely resulted from meteorological or landscape (land-use) differences between measurements. The findings highlighted the abilities and limitations of remote sensing indices in accurately capturing patterns of photosynthesis in our forests.

6.3 Suggestions for Future Research

The findings in this dissertation raised further questions that should be considered in future studies at the Turkey Point Observatory and the surrounding region. In this dissertation, annual photosynthetic phenology was calculated within similarly-aged forests. However, tree age may play an essential role in the timing and duration of photosynthesis and growth in coniferous species (Zheng et al., 2018; Albert et al., 2019). Given that the Observatory has an age-sequence of forest stands with 17 years of carbon flux measurements (from 2003 to 2019), the age-related responses of each forest to climate in terms of phenological variability should be assessed. Furthermore, the long-term datasets at each forest may be suitable for detecting variances or trends in phenology that may otherwise remain

unnoticed. For example, in the deciduous broadleaf forest, the practice of applying above-canopy measurements of photosynthesis for phenological applications results in the failure to partition the phenological impact of understory development. The spring leaf expansion of understory species may precede the canopy development, which may influence carbon fluxes (Augspurger et al., 2005; Vitasse, 2013). The implementation of an additional eddy covariance system in the forest understory, during the spring and autumn transition seasons, could provide innovative and interesting insights on the role of understory development in the carbon-sequestration capacity of the forest, and the differences in the timing of phenological events. Finally, the unique long-term data records at the mature forest stands, will allow the assessment of the potential response of carbon fluxes to future warmer climates in the region, through analysis of interannual variability of carbon fluxes and climatic variables. Such long-term datasets may help in the validation of biogeochemical models or remote sensing vegetation indices (Running et al., 1999; Baldocchi et al., 2003) in future studies. It would also be interesting to combine measured data with model simulations to test the future predictions for phenological variability in the region under changing climates and increased urban crawl.

6.4 References

Albert, L.P., Restrepo-Coupe, N., Smith, M.N., Wu, J., Chavana-Bryant, C., Prohaska, N., Taylor, T.C., Martins, G.A., Ciais, P., Mao, J. and Arain, M.A., 2019. Cryptic phenology in plants: Case studies, implications, and recommendations. *Global Change Biology*, *25*(11), 3591-3608.

Augspurger, C.K., Cheeseman, J.M. and Salk, C.F., 2005. Light gains and physiological capacity of understorey woody plants during phenological avoidance of canopy shade. *Functional Ecology*, 19(4), 537-546.

Baldocchi, D.D., 2003. Assessing the eddy covariance technique for evaluating carbon dioxide exchange rates of ecosystems: past, present and future. *Global Change Biology*, 9(4), 479-492.

Baldocchi, D., 2008. 'Breathing'of the terrestrial biosphere: lessons learned from a global network of carbon dioxide flux measurement systems. *Australian Journal of Botany*, 56(1), 1-26.

Desai, A.R., 2010. Climatic and phenological controls on coherent regional interannual variability of carbon dioxide flux in a heterogeneous landscape. *J. Geophys. Res. G: Biogeosci.*, 115(G3).

Dragoni, D., Schmid, H.P., Wayson, C.A., Potter, H., Grimmond, C.S.B. and Randolph, J.C., 2011. Evidence of increased net ecosystem productivity associated with a longer vegetated season in a deciduous forest in south-central Indiana, USA. *Global Change Biol.*, 17(2), 886-897.

Gough, C.M., Hardiman, B.S., Nave, L.E., Bohrer, G., Maurer, K.D., Vogel, C.S., Nadelhoffer, K.J. and Curtis, P.S., 2013. Sustained carbon uptake and storage following moderate disturbance in a Great Lakes forest. *Ecological Applications*, 23(5), 1202-1215.

Goulden, M.L., Munger, J.W., Fan, S.M., Daube, B.C. and Wofsy, S.C., 1996. Exchange of carbon dioxide by a deciduous forest: response to interannual climate variability. *Science*, 271(5255), 1576-1578.

Lee, M.S., Hollinger, D.Y., Keenan, T.F., Ouimette, A.P., Ollinger, S.V. and Richardson, A.D., 2018. Model-based analysis of the impact of diffuse radiation on CO2 exchange in a temperate deciduous forest. *Agricultural and Forest Meteorology*, 249, 377-389.

Munger, W. & Wofsy, S., 2017. Canopy-Atmosphere Exchange of Carbon, Water and Energy at Harvard Forest EMS Tower since 1991. Environmental Data Initiative. *Accessed Online June 2018.*

Oishi, A.C., Miniat, C.F., Novick, K.A., Brantley, S.T., Vose, J.M. and Walker, J.T., 2018. Warmer temperatures reduce net carbon uptake, but do not affect water use, in a mature southern Appalachian forest. *Agricultural and Forest Meteorology*, 252, 269-282.

Running, S.W., Baldocchi, D.D., Turner, D.P., Gower, S.T., Bakwin, P.S. and Hibbard, K.A., 1999. A global terrestrial monitoring network integrating tower fluxes, flask sampling, ecosystem modeling and EOS satellite data. *Remote Sensing of Environment*, *70*(1), 108-127.

Vitasse, Y., 2013. Ontogenic changes rather than difference in temperature cause understory trees to leaf out earlier. *New Phytologist*, *198*(1), 149-155.

Xie, J., Chen, J., Sun, G., Chu, H., Noormets, A., Ouyang, Z., John, R., Wan, S. and Guan, W., 2014. Long-term variability and environmental control of the carbon cycle in an oak-dominated temperate forest. *Forest Ecology and Management*, 313, 319-328.

Zeng, Q., Rossi, S. and Yang, B., 2018. Effects of age and size on xylem phenology in two conifers of Northwestern China. *Frontiers in Plant Science*, *8*, 2264.